

AD 688445

①

Bulletin 39  
Part 2  
(of 6 Parts)

# THE SHOCK AND VIBRATION BULLETIN

FEBRUARY 1969

A Publication of  
THE SHOCK AND VIBRATION  
INFORMATION CENTER  
Naval Research Laboratory, Washington, D.C.



Office of  
The Director of Defense  
Research and Engineering

Reproduced by the  
CLEARINGHOUSE  
for Federal Scientific & Technical  
Information Springfield Va. 22151

This document has been approved for public release and sale; its distribution is unlimited.

243

Part 2

Shock and Vibration Bulletin

February 1969

AD 388445

Bulletin 39

Part 2

(of 6 Parts)

# THE SHOCK AND VIBRATION BULLETIN

FEBRUARY 1969

A Publication of  
THE SHOCK AND VIBRATION  
INFORMATION CENTER  
Naval Research Laboratory, Washington, D.C.

The 39th Symposium on Shock and Vibration was held in Pacific Grove, California, on 22-24 October 1968. The U.S. Army was host.

Office of  
The Director of Defense  
Research and Engineering

### ANNOUNCEMENT

The Department of Defense has established a policy which will require the Shock and Vibration Information Center to make a charge for its publications and services. Pending a determination of prices, and methods of ordering and delivering the Center's publications, the 39th Bulletin is being distributed without charge as in the past. When costs and procedures have been determined, all addressees who have been receiving the Bulletin will be advised so that they may make arrangements to purchase future issues.

## CONTENTS

### PART 2

#### Vibration

ELECTRICAL GENERATION OF MOTION IN ELASTOMERS . . . . . S. Edelman, S. C. Roth and L. R. Grisham, National Bureau of Standards, Washington, D.C.	1
CONTROLLED DECELERATION SPECIMEN PROTECTION SYSTEMS FOR ELECTRODYNAMIC VIBRATION SYSTEMS . . . . . Lawrence L. Cook, Jr., NASA Goddard Space Flight Center, Greenbelt, Maryland	11
CONTROL TECHNIQUES FOR SIMULTANEOUS THREE-DEGREE-OF-FREEDOM HYDRAULIC VIBRATION SYSTEM . . . . . H. D. Cyphers and J. F. Sutton, NASA Goddard Space Flight Center, Greenbelt, Maryland	23
*INITIAL REPORT ON EQUIVALENT DAMAGE MEASUREMENT BY UTILIZING S/N FATIGUE GAGES . . . . . Thomas B. Cost, Naval Weapons Center, China Lake, California	35
HOLOGRAM INTERFEROMETRY AS A PRACTICAL VIBRATION MEASUREMENT TECHNIQUE . . . . . Cameron D. Johnson and Gerald M. Mayer, Navy Underwater Sound Laboratory, Fort Trumbull, New London, Connecticut	41
RESPONSE OF AN ELASTIC STRUCTURE INVOLVING CROSS CORRELATIONS BETWEEN TWO RANDOMLY VARYING EXCITATION FORCES . . . . . A. Razziano, Grumman Aircraft Engineering Corporation, Bethpage, New York, and J. R. Curreri, Polytechnic Institute of Brooklyn, Brooklyn, New York	51
AUTOMATIC NORMALIZATION OF STRUCTURAL MODE SHAPES . . . . . C. C. Isaacson and R. W. Merkel, Engineering Laboratories, McDonnell Aircraft Company, St. Louis, Missouri	63
*RESONANT BEAM HIGH "G" VIBRATION TESTING . . . . . B. A. Kohler, International Business Machines Corporation, Federal Systems Division, Owego, New York	71
THE USE OF LIQUID SQUEEZE-FILMS TO SUPPORT VIBRATING LOADS . . . . . Brantley R. Hanks, NASA Langley Research Center, Langley Station, Hampton, Virginia	77
POINT-TO-POINT CORRELATION OF SOUND PRESSURES IN REVERBERATION CHAMBERS . . . . . Charles T. Morrow, LTV Research Center, Western Division, Anaheim, California	87
ENVIRONMENTAL LABORATORY MISSILE FAILURE RATE TEST WITH AERODYNAMIC FUNCTION SIMULATION . . . . . Raymond C. Binder and Gerald E. Berge, Naval Missile Center, Point Mugu, California	99
APOLLO CSM DYNAMIC TEST PROGRAM . . . . . A. E. Chirby, R. A. Stevens and W. R. Wood, Jr., North American Rockwell Corporation, Downey, California	105
MODAL SURVEY RESULTS FROM THE MARINER MARS 1969 SPACECRAFT . . . . . R. E. Freeland, Jet Propulsion Laboratory, California Institute of Technology, Pasadena, California, and W. J. Gaugh, Northrop Systems Laboratories, Northrop Corporation, Hawthorne, California	123

\*This paper not presented at Symposium.



UPDATED SATURN : FULL SCALE DYNAMIC TEST CORRELATION . . . . .	135
Charles R. Wells and John E. Hord, Chrysler Corporation Space Division, New Orleans, Louisiana	
AN APPROACH FOR DUPLICATING SPACECRAFT FLIGHT-INDUCED BODY FORCES IN A LABORATORY . . . . .	147
S. M. Kaplan and A. J. Soroka, General Electric Company, Philadelphia, Pennsylvania	
FLEXURE GUIDES FOR VIBRATION TESTING . . . . .	157
Alexander Yorgiadis and Stanley Barrett, North American Rockwell Corporation, Downey, California	
A COMPRESSION-FASTENED GENERAL-PURPOSE VIBRATION AND SHOCK FIXTURE .	175
Warren C. Beecher, Instrument Division, Lear Siegler, Inc., Grand Rapids, Michigan	
VIBRATION EQUIVALENCE: FACT OR FICTION? . . . . .	187
LaVerne Root, Collins Radio Company, Cedar Rapids, Iowa	
PROVIDING REALISTIC VIBRATION TEST ENVIRONMENTS TO TACTICAL GUIDED MISSILES . . . . .	195
K. R. Jackman and H. L. Holt, General Dynamics, Pomona, California	
*THE REDUCTION OF THE VIBRATION LEVEL OF A CIRCULAR SHAFT MOVING TRANSVERSELY THROUGH WATER AT THE CRITICAL REYNOLDS NUMBER . . . . .	217
Irvin F. Gerks, Honeywell Inc., Seattle, Washington	
*ANALYSIS AND DESIGN OF RESONANT FIXTURES TO AMPLIFY VIBRATOR OUTPUT . . . . .	221
J. Verga, Hazeltine Corporation, Little Neck, New York	

#### PAPERS APPEARING IN PART 1

Part 1 - Classified  
(Unclassified Titles)

AN INTRODUCTION TO THE BASIC SHOCK PROBLEM F. Weinberger and R. Heise, Jr., Naval Ship Research and Development Center, Washington, D.C.
DESIGN INPUT DERIVATION AND VALIDATION R. O. Belsheim, G. J. O'Hara and R. L. Bort, Naval Research Laboratory, Washington, D.C.
SHOCK DESIGN OF NAVAL BOILERS D. M. Gray, Combustion Engineering, Inc., Windsor, Connecticut
MACHINERY DESIGN FOR SHIPBOARD UNDERWATER SHOCK G. W. Bishop, Bishop Engineering Company, Princeton, New Jersey
SHOCK DESIGN OF SHIPBOARD STRUCTURES R. J. Della Rocca and N. R. Addonizio, Gibbs and Cox, Inc., New York, New York
REVIEW AND APPROVAL OF DYNAMIC ANALYSIS M. J. Macy and L. A. Gordon, Supervisor of Shipbuilding, Conversion and Repair, USN, Brooklyn, New York
COMPUTER AIDED DESIGN - ANALYSIS FOR SHIPBOARD UNDERWATER SHOCK M. Pakstys, Jr., General Dynamics, Electric Boat Division, Groton, Connecticut
CURRENT NAVY SHOCK HARDENING REQUIREMENTS AND POLICY J. R. Sullivan, H. H. Ward and D. M. Lund, Department of the Navy, Naval Ship Systems Command Headquarters, Washington, D.C.
SHOCK DESIGN AND TEST QUALIFICATION OF SHIPBOARD SYSTEMS/COMPONENTS - PANEL SESSION
*HARDENING OF SURFACE SHIPS AND SUBMARINES FOR ADVANCED SEABASED DETERRENCE H. L. Rich, Naval Ship Research and Development Center, Washington, D.C.

\*This paper not presented at Symposium..

- TOWARD A MORE RATIONAL BLAST-HARDENED DECKHOUSE DESIGN  
Shou-Ling Wang, Naval Ship Research and Development Center, Washington, D.C.
- COMPUTATION OF THE MOBILITY PROPERTIES OF A UNIFORM BEAM FOUNDATION  
J. E. Smith and R. J. Hanners, Naval Ship Research and Development Center, Annapolis, Maryland
- AN ANALYTICAL INVESTIGATION OF THE DAMPING OF RADIAL VIBRATIONS OF A PIPE  
BY CONSTRAINED VISCOELASTIC LAYERS USING AXIAL STAVES  
R. A. DiTaranto, PMC Colleges, Chester, Pennsylvania, and W. Blasingame, Naval Ship Research and Development Center, Annapolis, Maryland
- \*DAMPED CYLINDRICAL SHELLS AND DYNAMIC SYSTEMS EFFECTS  
B. E. Douglas and E. V. Thomas, Naval Ship Research and Development Center, Annapolis, Maryland
- APPLICATION OF SPACED DAMPING TO MACHINERY FOUNDATIONS  
J. R. Hupton, General Dynamics, Electric Boat Division, Groton, Connecticut and H. T. Miller and G. E. Warnaka, Lord Manufacturing Company, Erie, Pennsylvania
- \*ROCKET SLED TESTS OF THE AGM-12 "BULLPUP" MISSILE  
Robert D. Kimsey, Naval Missile Center, Point Mugu, California
- AIM-4D FLIGHT MEASUREMENT PROGRAM  
R. P. Mandich and W. G. Spalthoff, Hughes Aircraft Company, Canoga Park, California
- \*AEROELASTIC ANALYSIS OF A FLEXIBLE RE-ENTRY VEHICLE  
H. Saunders and A. Kirsch, General Electric Company, Re-Entry Systems Department, Philadelphia, Pennsylvania

#### PAPERS APPEARING IN PART 3

##### Structural Analysis

- MODAL DENSITIES OF SANDWICH PANELS: THEORY AND EXPERIMENT  
Larry L. Erickson, NASA Ames Research Center, Moffett Field, California
- TURBINE ENGINE DYNAMIC COMPATIBILITY WITH HELICOPTER AIRFRAMES  
Kenneth C. Mard and Paul W. von Hardenberg, Sikorsky Aircraft Division of United Aircraft Corporation, Stratford, Connecticut
- SYNTHESIS OF RIGID FRAMES BASED ON DYNAMIC CRITERIA  
Henry N. Christiansen, Associate Professor, Department of Civil Engineering Science, Brigham Young University, Provo, Utah, and E. Alan Pettit, Jr., Engineer, Humble Oil Company, Benicia, California
- DYNAMIC RESPONSE OF PLASTIC AND METAL SPIDER BEAMS FOR 1/9TH SCALE SATURN MODEL  
L. V. Kulasa, KPA Computer Techniques, Inc., Pittsburgh, Pennsylvania, and W. M. Laird, University of New York, Fredonia, New York
- \*CHARTS FOR ESTIMATING THE EFFECT OF SHEAR DEFORMATION AND ROTARY INERTIA ON THE NATURAL FREQUENCIES OF UNIFORM BEAMS  
F. F. Rudder, Jr., Aerospace Sciences Research Laboratory, Lockheed-Georgia Company, Marietta, Georgia
- ACOUSTIC RESPONSE ANALYSIS OF LARGE STRUCTURES  
F. A. Smith, Martin Marietta Corporation, Denver Division, Denver, Colorado, and R. E. Jewell, NASA Marshall Space Flight Center, Huntsville, Alabama
- \*ESTIMATION OF PROBABILITY OF STRUCTURAL DAMAGE FROM COMBINED BLAST AND FINITE-DURATION ACOUSTIC LOADING  
Eric E. Ungar and Yoram Kadman, Bolt Beranek and Newman Inc., Cambridge, Massachusetts
- \*THE RESPONSE OF MECHANICAL SYSTEMS TO BANDS OF RANDOM EXCITATION  
L. J. Pulgrano and M. Ablowitz, Grumman Aircraft Engineering Corporation, Bethpage, New York

\*This paper not presented at Symposium.

- \*PREDICTION OF STRESS AND FATIGUE LIFE OF ACOUSTICALLY-EXCITED AIRCRAFT STRUCTURES**  
Noe Arcas, Grumman Aircraft Engineering Corporation, Bethpage, New York
- VIBRATION ANALYSIS OF COMPLEX STRUCTURAL SYSTEMS BY MODAL SUBSTITUTION**  
R. L. Bajan, C. C. Feng, University of Colorado, Boulder, Colorado, and I. J. Jaszlics, Martin Marietta Corporation, Denver, Colorado
- THE APPLICATION OF THE KENNEDY-PANCU METHOD TO EXPERIMENTAL VIBRATION STUDIES OF COMPLEX SHELL STRUCTURES**  
John D. Ray, Charles W. Bert and Davis M. Egle, School of Aerospace and Mechanical Engineering, University of Oklahoma, Norman, Oklahoma
- \*NORMAL MODE STRUCTURAL ANALYSIS CALCULATIONS VERSUS RESULTS**  
Culver J. Floyd, Raytheon Company, Submarine Signal Division, Portsmouth, Rhode Island
- COMPARISONS OF CONSISTENT MASS MATRIX SCHEMES**  
R. M. Mains, Department of Civil and Environmental Engineering, Washington University, St. Louis, Missouri
- MEASUREMENT OF A STRUCTURE'S MODAL EFFECTIVE MASS**  
G. J. O'Hara and G. M. Remmers, Naval Research Laboratory, Washington, D.C.
- SIMPLIFYING A LUMPED PARAMETER MODEL**  
Martin T. Solfer and Arlen W. Bell, Dynamic Science, a Division of Marshall Industries, Monrovia, California
- STEADY STATE BEHAVIOR OF TWO DEGREE OF FREEDOM NONLINEAR SYSTEMS**  
J. A. Padovan and J. R. Curreri, Polytechnic Institute of Brooklyn, Brooklyn, New York, and M. B. Electronics, New Haven, Connecticut
- THE FLUTTER OR GALLOPING OF CERTAIN STRUCTURES IN A FLUID STREAM**  
Raymond C. Binder, University of Southern California, Los Angeles, California
- \*AIRCRAFT LANDING GEAR BRAKE SQUEAL AND STRUT CHATTER INVESTIGATION**  
F. A. Biehl, McDonnell Douglas Corporation, Long Beach, California
- EXPERIMENTAL INVESTIGATION OF NONLINEAR VIBRATIONS OF LAMINATED ANISOTROPIC PANELS**  
Bryon L. Mayberry and Charles W. Bert, School of Aerospace and Mechanical Engineering, University of Oklahoma, Norman, Oklahoma
- \*STRUCTURAL DYNAMICS ANALYSIS OF AN ANISOTROPIC MATERIAL**  
S. K. Lee, General Electric Company, Syracuse, New York
- \*EXPERIMENTS ON THE LARGE AMPLITUDE PARAMETRIC RESPONSE OF RECTANGULAR PLATES UNDER IN-PLANE RANDOM LOADS**  
R. L. Silver and J. H. Somerset, Department of Mechanical and Aerospace Engineering, Syracuse University, Syracuse, New York
- \*RESPONSE OF STIFFENED PLATES TO MOVING SPRUNG MASS LOADS**  
Ganpat M. Singhvi, Schutte Mochon, Inc., Milwaukee, Wisconsin, and Larry J. Feeser, University of Colorado, Boulder, Colorado
- \*PARAMETRIC RESPONSE SPECTRA FOR IMPERFECT COLUMNS**  
Martin L. Moody, University of Colorado, Boulder, Colorado

#### PAPERS APPEARING IN PART 4

##### Damping

- \*APPLICATION OF A SINGLE-PARTICLE IMPACT DAMPER TO AN ANTENNA STRUCTURE**  
R. D. Roche, Hughes Aircraft Company, Fullerton, California, and S. F. Masri, University of Southern California, Los Angeles, California

**\*This paper not presented at Symposium.**

- A PROPOSED EXPERIMENTAL METHOD FOR ACCURATE MEASUREMENTS OF THE DYNAMIC PROPERTIES OF VISCOELASTIC MATERIALS**  
Kenneth G. McConnell, Associate Professor of Engineering Mechanics, Iowa State University, Ames, Iowa
- DAMPING OF BLADE-LIKE STRUCTURES**  
David I. G. Jones, Air Force Materials Laboratory, Wright-Patterson Air Force Base, Ohio, and Ahid D. Nashif, University of Dayton, Dayton, Ohio
- MULTI-LAYER ALTERNATELY ANCHORED TREATMENT FOR DAMPING OF SKIN-STRINGER STRUCTURES**  
Captain D. R. Simmons, Air Force Institute of Technology, Wright-Patterson Air Force Base, Ohio, J. P. Henderson, D. I. G. Jones, Air Force Materials Laboratory, Wright-Patterson Air Force Base, Ohio, and C. M. Cannon, University of Dayton, Dayton, Ohio
- AN ANALYTICAL AND EXPERIMENTAL INVESTIGATION OF A TWO-LAYER DAMPING TREATMENT**  
A. D. Nashif, University of Dayton, Dayton, Ohio, and T. Nicholas, Air Force Materials Laboratory, Wright-Patterson Air Force Base, Ohio
- DAMPING OF PLATE VIBRATIONS BY MEANS OF ATTACHED VISCOELASTIC MATERIAL**  
I. W. Jones, Applied Technology Associates, Inc., Ramsey, New Jersey
- VIBRATIONS OF SANDWICH PLATES WITH ORTHOTROPIC FACES AND CORES**  
Fakhruddin Abdulhadi, Reliability Engineering, IEM Systems Development Division, Rochester, Minnesota, and Lee P. Sapetta, Department of Mechanical Engineering, University of Minnesota, Minneapolis, Minnesota
- THE NATURAL MODES OF VIBRATION OF BORON-EPOXY PLATES**  
J. E. Ashton and J. D. Anderson, General Dynamics, Fort Worth, Texas
- \*NATURAL MODES OF FREE-FREE ANISOTROPIC PLATES**  
J. E. Ashton, General Dynamics, Fort Worth, Texas
- ACOUSTIC TEST OF BORON FIBER REINFORCED COMPOSITE PANELS CONDUCTED IN THE AIR FORCE FLIGHT DYNAMICS LABORATORY'S SONIC FATIGUE TEST FACILITY**  
Carl L. Rupert, Air Force Flight Dynamics Laboratory, Wright-Patterson Air Force Base, Ohio
- STRENGTH CHARACTERISTICS OF JOINTS INCORPORATING VISCOELASTIC MATERIALS**  
W. L. LaBarge and M. D. Lamoree, Lockheed-California Company, Burbank, California

#### Isolation

- RECENT ADVANCES IN ELECTROHYDRAULIC VIBRATION ISOLATION**  
Jerome E. Ruzicka and Dale W. Schubert, Barry Controls, Division of Barry Wright Corporation, Watertown, Massachusetts
- ACTIVE ISOLATION OF HUMAN SUBJECTS FROM SEVERE AIRCRAFT DYNAMIC ENVIRONMENTS**  
Peter C. Calcaterra and Dale W. Schubert, Barry Controls, Division of Barry Wright Corporation, Watertown, Massachusetts
- ELASTIC SKIDMOUNTS FOR MOBILE EQUIPMENT SHELTERS**  
R. W. Doll and R. L. Laier, Barry Controls, Division Barry Wright Corporation, Burbank, California
- COMPUTER-AIDED DESIGN OF OPTIMUM SHOCK-ISOLATION SYSTEMS**  
E. Sevin, W. D. Pilkey and A. J. Kalinowski, IIT Research Institute, Chicago, Illinois
- ANALYTIC INVESTIGATION OF BELOWGROUND SHOCK-ISOLATING SYSTEMS SUBJECTED TO DYNAMIC DISTURBANCES**  
J. Neils Thompson, Ervin S. Perry and Suresh C. Arya, The University of Texas at Austin, Austin, Texas
- GAS DYNAMICS OF ANNULAR CONFIGURED SHOCK MOUNTS**  
W. F. Andersen, Westinghouse Electric Corporation, Sunnyvale, California
- A SCALE MODEL STUDY OF CRASH ENERGY DISSIPATING VEHICLE STRUCTURES**  
D. J. Bozich and G. C. Kao, Research Staff, Wyle Laboratories, Huntsville, Alabama

\*This paper not presented at Symposium.

DESIGN OF RECOIL ADAPTERS FOR ARMAMENT SYSTEMS

A. S. Whitehill and T. L. Quinn, Lord Manufacturing Company, Erie, Pennsylvania

\*A DYNAMIC VIBRATION ABSORBER FOR TRANSIENTS

Dirse W. Sallet, University of Maryland, College Park, Maryland and Naval Ordnance Laboratory, White Oak, Silver Spring, Maryland

PAPERS APPEARING IN PART 5

Shock

DYNAMIC RESPONSE OF A SINGLE-DEGREE-OF-FREEDOM ELASTIC-PLASTIC SYSTEM  
SUBJECTED TO A SAWTOOTH PULSE

Martin Wohltmann, Structures and Mechanics Department, Martin Marietta Corporation,  
Orlando, Florida

\*TRANSIENT DYNAMIC RESPONSES IN ELASTIC MEDIUM GENERATED BY SUDDENLY  
APPLIED FORCE

Dr. James Chi-Dian Go, The Boeing Company, Seattle, Washington

IMPACT FAILURE CRITERION FOR CYLINDRICAL AND SPHERICAL SHELLS

Donald F. Haskell, Hittman Associates, Inc., Columbia, Maryland

\*THE EXCITATION OF SPHERICAL OBJECTS BY THE PASSAGE OF PRESSURE WAVES

Gordon E. Strickland, Jr., Lockheed Missiles and Space Company, Palo Alto, California

THE PERFORMANCE CHARACTERISTICS OF CONCENTRATED-CHARGE, EXPLOSIVE-  
DRIVEN SHOCK TUBES

L. W. Bickle and M. G. Vigil, Sandia Laboratories, Albuquerque, New Mexico

\*PRIMACORD EXPLOSIVE-DRIVEN SHOCK TUBES AND BLAST WAVE PARAMETERS IN  
AIR, SULFURHEXAFLUORIDE AND OCTOFLUOROCYCLOBUTANE (FREON-C318)

M. G. Vigil, Sandia Laboratories, Albuquerque, New Mexico

ZERO IMPEDANCE SHOCK TESTS, A CASE FOR SPECIFYING THE MACHINE

Charles T. Morrow, LTV Research Center, Western Division, Anaheim, California

SHOCK TESTING WITH AN ELECTRODYNAMIC EXCITER AND WAVEFORM SYNTHESIZER

Dana A. Regillo, Massachusetts Institute of Technology, Lincoln Laboratory,  
Lexington, Massachusetts

SLINGSHOT SHOCK TESTING

LaVerne Root and Carl Bohs, Collins Radio Company, Cedar Rapids, Iowa

SHOCK TESTING AND ANALYSIS: A NEW LABORATORY TECHNIQUE

J. Fagan and J. Sincavage, RCA Astro-Electronics Division, Princeton, New Jersey

\*INSTRUMENTATION FOR A HUMAN OCCUPANT SIMULATION SYSTEM

W. I. Kipp, Monterey Research Laboratory, Inc., Monterey, California

PAPERS APPEARING IN PART 6

Introductory Papers

THE IMPACT OF A DYNAMIC ENVIRONMENT ON FIELD EXPERIMENTATION

Walter W. Hollis, U.S. Army Combat Developments Command, Experimentation Command,  
Fort Ord, California

TRANSCRIPT OF PANEL DISCUSSION ON PROPOSED USASI STANDARD ON METHODS FOR  
ANALYSIS AND PRESENTATION OF SHOCK AND VIBRATION DATA

Julius S. Bendat, Measurement Analysis Corporation, Los Angeles, California, and Allen J. Curtis,  
Hughes Aircraft Corporation, Culver City, California

\*This paper not presented at Symposium.

#### Transportation and Packaging

THE BUMP TESTING OF MILITARY SIGNALS EQUIPMENT IN THE UNITED KINGDOM  
W. Childs, Signals Research and Development Establishment, Ministry of Technology,  
United Kingdom

NLABS SHIPPING HAZARDS RECORDER STATUS AND FUTURE PLANS  
Dennis J. O'Sullivan, Jr., U.S. Army Natick Laboratories, Natick, Massachusetts

NORMAL AND ABNORMAL DYNAMIC ENVIRONMENTS ENCOUNTERED IN TRUCK  
TRANSPORTATION  
J. T. Foley, Sandia Laboratories, Albuquerque, New Mexico

DEVELOPMENT OF A RAILROAD ROUGHNESS INDEXING AND SIMULATION PROCEDURE  
L. J. Pursifull and B. E. Prothro, U.S. Army Transportation Engineering Agency, Military  
Traffic Management and Terminal Service, Fort Eustis, Virginia

AN APPROXIMATE METHOD OF DYNAMIC ANALYSIS FOR MISSILE CONTAINER SYSTEMS  
Mario Paz, Associate Professor, and Ergin Citipitioglu, Associate Professor, University of  
Louisville, Louisville, Kentucky

SIMULATED MECHANICAL IMPACT TEST EQUIPMENT  
D. R. Agnew, Naval Air Development Center, Johnsville, Warminster, Pennsylvania

#### Environmental Measurements

SUCCESS AND FAILURE WITH PREDICTION AND SIMULATION OF AIRCRAFT VIBRATION  
A. J. Curtis and N. G. Tinling, Hughes Aircraft Company, Culver City, California

PHOENIX ENVIRONMENTAL MEASUREMENTS IN F-111B WEAPONS BAY  
T. M. Kiwior, R. P. Mandich and R. J. Oedy, Hughes Aircraft Company, Canoga Park, California

LUNAR ORBITER FLIGHT VIBRATIONS WITH COMPARISONS TO FLIGHT ACCEPTANCE  
REQUIREMENTS AND PREDICTIONS BASED ON A NEW GENERALIZED REGRESSION  
ANALYSIS  
Sherman A. Clevenson, NASA Langley Research Center, Langley Station, Hampton, Virginia

VIBRATION AND ACOUSTIC ENVIRONMENT CHARACTERISTICS OF THE SATURN V  
LAUNCH VEHICLE  
Clark J. Beck, Jr. and Donald W. Caba, The Boeing Company, Huntsville, Alabama

THE BLAST FIELD ABOUT THE MUZZLE OF GUNS  
Peter S. Westine, Southwest Research Institute, San Antonio, Texas

SPECIFICATIONS: A VIEW FROM THE MIDDLE  
T. B. Delchamps, Bell Telephone Laboratories, Inc., Whippany, New Jersey

# VIBRATION

## ELECTRICAL GENERATION OF MOTION IN ELASTOMERS

S. Edelman, S. C. Roth, and L. R. Grisham  
National Bureau of Standards  
Washington, D. C.

### ABSTRACT

Motion occurring in response to an applied electrical signal was studied in a number of elastomers. Motion at double the exciting frequency (electrostriction) was common. Linear response was found in a few materials. A few showed linear response in their original condition. Treatment with heat and intense electric fields caused linear response to appear or to increase in others. Superposition of a d.c. bias on the driving signal linearized the double frequency response and increased the linear response.

KEY WORDS: Elastomers, polymers, electrets, piezoelectricity, electrically controlled damping, vibration generation, electrostriction.

### INTRODUCTION

This is a preliminary report on a new investigation in the Instrumentation Applications Section of the National Bureau of Standards. The purpose of the investigation is to study those effects of electrical signals on the mechanical properties of elastomers which could lead to engineering applications.

The purpose of this paper is to call attention to the potential usefulness of this field of study. Accordingly, we emphasize results which seem promising for future improvement and application. In our view, the important finding of the exploratory study is the fact that some samples could be excited into significant motion electrically and that the response of some of them could be improved by treatment and electrical bias. It is less important that the magnitudes of the effects observed were in most cases insignificant or ambiguous.

The fact that this is an exploratory study is also responsible for the qualitative nature of the discussion. The equipment and techniques were chosen to allow a rapid but shallow survey. In this light, too much reliance should not be put on the numerical data in Table I. The measurements were reasonably stable when made but significant changes followed small changes in operating conditions.

### BACKGROUND

This investigation was suggested by experience during development of a set of piezoelectric shakers for calibrating vibration

pickups over a wide frequency range.<sup>1</sup> In this development, it was found possible to extend the working range of a piezoelectric shaker by using damping materials selectively to reduce the sharpness of particular resonances. At frequencies below 50 kHz, butyl rubber was used for damping. At higher frequencies piezoelectric ceramics were found to be more suitable. In addition to the inherent lossiness of the ceramics, it was found that their usefulness as damping material could be enhanced by exploiting their piezoelectric properties. This was done by connecting the electrodes through suitable impedances or by applying a portion of the driving signal through a suitable phasing circuit.

This development suggested that similar benefits might result at low frequencies from the use of damping material with piezoelectric properties. While rubber-like materials usually are not considered piezoelectric, there are some indications in the literature that long-chain polymers can have piezoelectric-like behavior. These are summarized by Guttman,<sup>2</sup> Johnson,<sup>3</sup> and Cady.<sup>4</sup> However, the work discussed in these references is concerned with d.c. effects and with the direct piezoelectric effect. Considering the small magnitudes involved and the fact that pressure applied to two charged surfaces will generate some voltage no matter what the intervening material, we thought it safer to restrict our study to vibration resulting from application of alternating voltages.

The technical literature contains a number of references to studies of the properties of polymers using alternating voltages.<sup>5</sup> However,

it is difficult to use this material to determine the suitability of a material for an engineering application or to determine the effectiveness of bias and treatment in improving the activity of available materials.

#### PREPARATION OF SPECIMENS

Procedures used to prepare materials for test followed those used to prepare electrets. As a heuristic device we assumed that the material contained electrical dipoles. We attempted to align these to some extent by reducing the viscosity of the material, applying as intense a constant electric field as the material would support without arcing, and allowing the material to solidify under the field.

The first specimens were prepared by evaporating a volatile solvent from a solution of the material while the field was applied. This seemed to show some promise but it was a slow process and required leaving an intense field on the specimen overnight while the laboratory was unattended. After a number of near accidents and a fire we abandoned the use of volatile solvents and simply heated solid materials. Some of the materials could be completely or nearly liquified and some were only heated and allowed to cool under the field. Heat was applied with an electrical hot plate at first. Later, specimens were heated in a furnace. Figure 1 shows the configuration used to apply the field while the specimen was on the hot plate and Figure 2 shows the corresponding setup used in the furnace. The samples were heated as near as

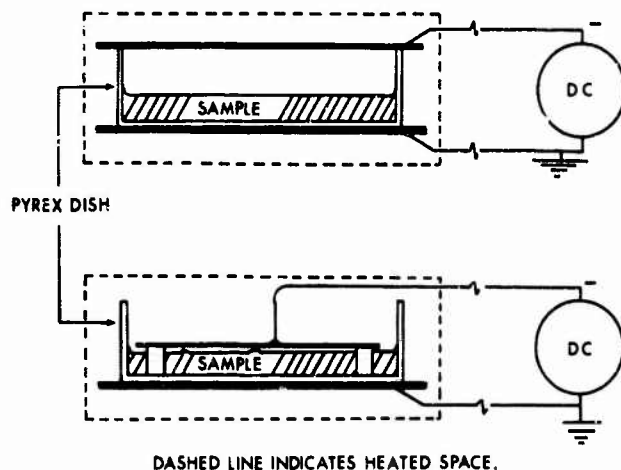
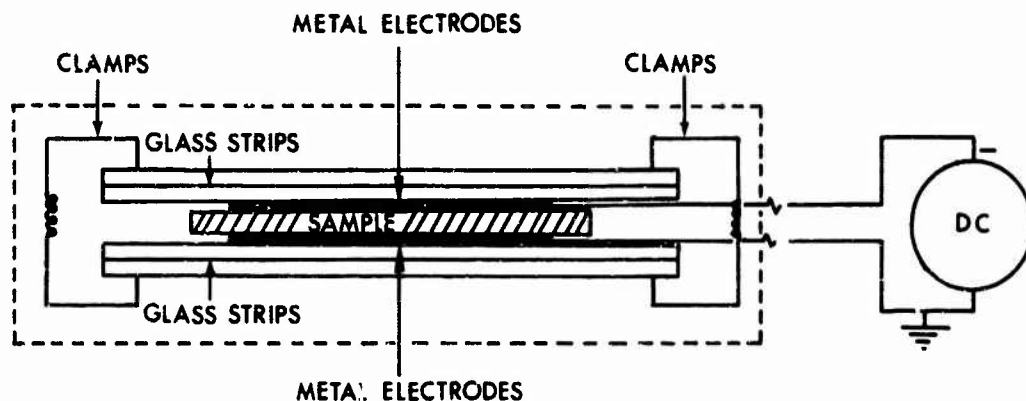


Figure 1: Sample with applied electric field heated on hot plate



Glass strips clamped together to hold electrodes and sample in place.

Figure 2: Sample with applied electric field heated in furnace  
Dashed line indicates portion heated.  
Temperature monitored by thermocouple in furnace.



possible to the melting point without causing perceptible changes in composition, discoloration, bubbles, change in translucence, etc.

The electric field across the samples was maintained just below the magnitude at which arcing occurred. Usually, the field could be increased as the material cooled, often reaching the 30,000 V limit of the power supply by the time the sample had cooled to about 30°C, the usual point at which the treatment ended.

All of the test elements consisted of disks cut from the sheets of material by suitable tools. Cork borers were used for soft materials, hole cutters in a drill press for

most hard plastics, and a brass cylinder with carborundum powder for glass and a few very hard plastics.

Each test element was made of two disks put together so that the adjacent faces in the test assembly had been oriented similarly before the disks were cut from the treated samples. The outer faces were both connected to ground and the test signal was applied between ground and the common face in the center. With this orientation and connection, the grounded outer electrodes provided some shielding while both disks responded similarly to the applied signal. A typical test element is shown in Figure 3.

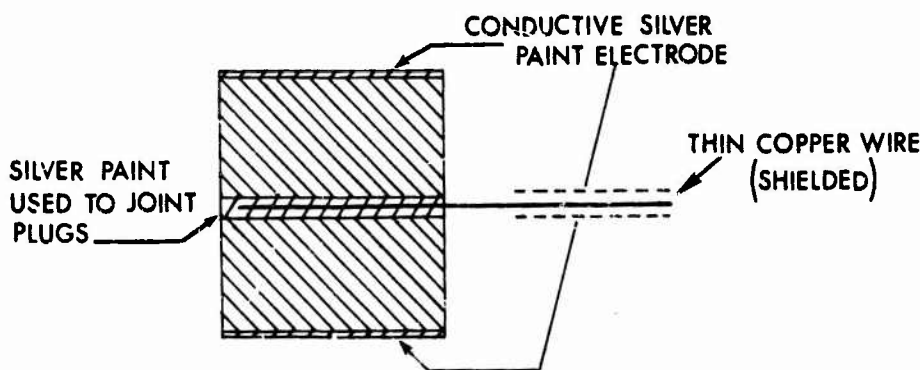


Figure 3: Test element construction

#### TESTS

The circuit used for testing is shown schematically in Figure 4. Three different oscillators were used, in some cases with an external transformer to match the input impedance of the test element. The voltage applied to the specimen varied in different cases but all of the results presented in Table I are normalized for an input of 400 V. Within the sensitivity of our measurements for these cases, the activity was linear with applied signal.

The voltage divider reduced the trace showing the driving signal to manageable levels and the capacitor allowed a d.c. bias to be applied to the test element without affecting the a.c. portion of the circuit. The d.c. power supply was also used to provide the field in preparing the material. The accelerometer was a piezoelectric type with a sensitivity of about 50 mV/g at the frequencies reported in Table I. The accelerometer signal was measured at the oscilloscope. The sensitivity of its beam was usually set at 200  $\mu$ V per cm.

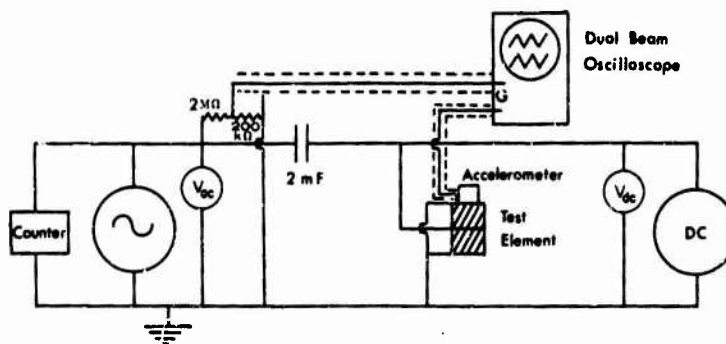


Figure 4: Circuit used for testing

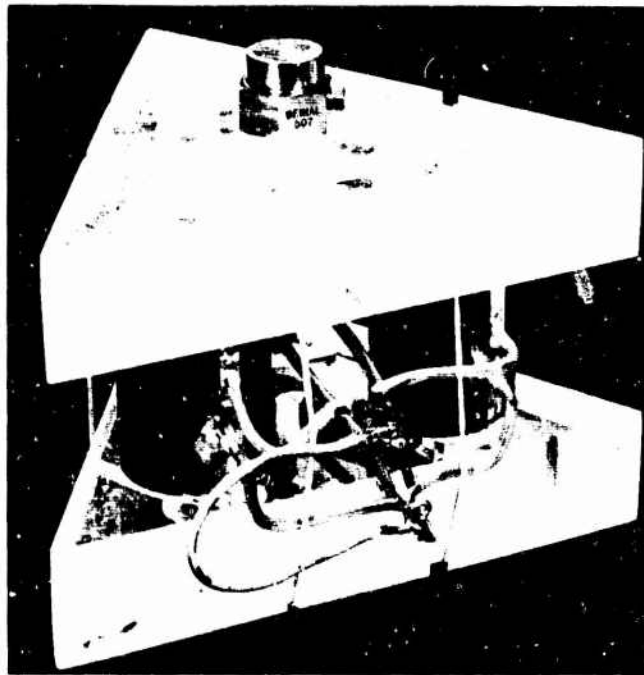


Figure 5: Triangular test fixture

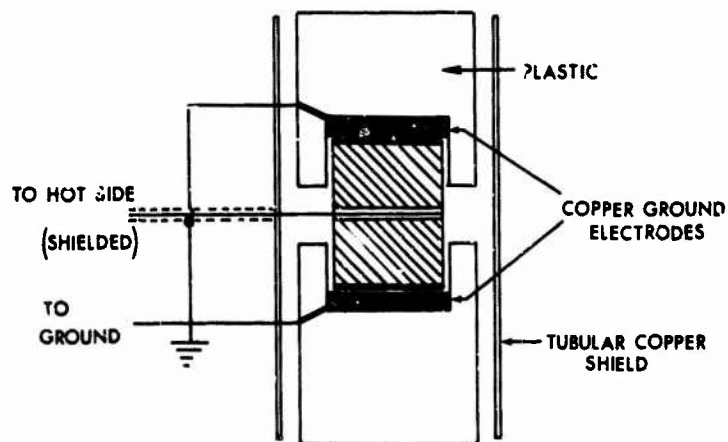


Figure 6: Test element in triangular fixture

A number of arrangements of the test element were used but only two contributed enough to be worth reporting. The first used a triangular fixture shown in Figure 5. Three test elements were used, one in each of the legs separating

two plastic triangles. Figure 6 shows the arrangement of a test element in one of the plastic legs. Figure 7 shows the lower of the two triangular plates and Figure 8 shows a complete assembly with an accelerometer in place.

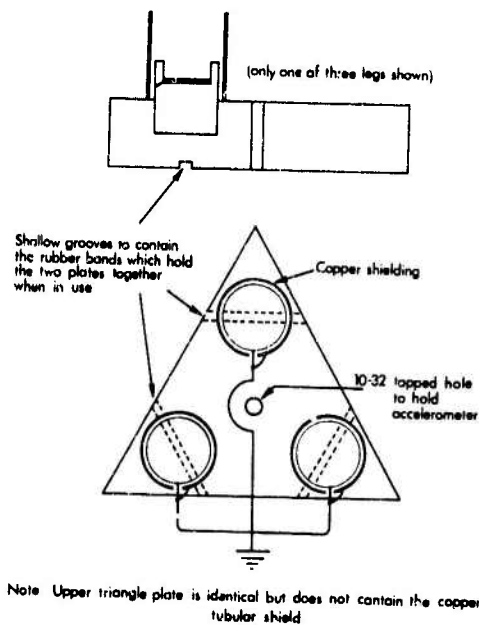


Figure 7: Lower plate of triangular fixture

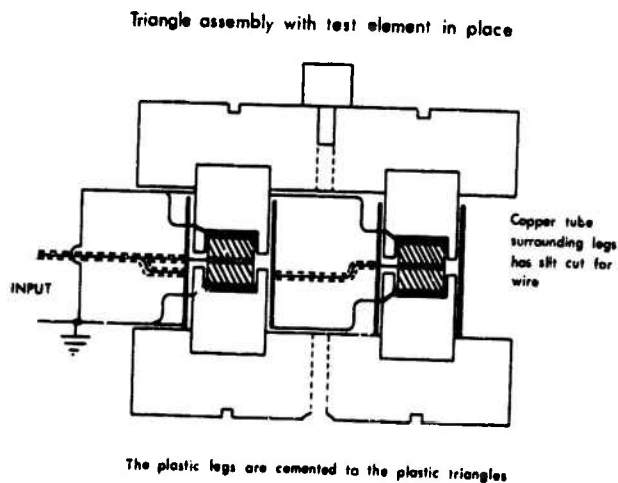


Figure 8: Triangular fixture assembled

Only one of the experiments performed on the triangular fixture is reported here. With the lower triangle clamped to a heavy steel block, the system was driven at a resonance by a loudspeaker. The signal from the accelerometer on the upper triangle was displayed on the oscilloscope. The signal disappeared if the upper triangle was clamped, ensuring that the signal was not due to microphonic action in the accelerometer. A signal from another oscillator tuned nearly to the frequency of the speaker was applied to the test elements in the legs of the fixture. After adjustment of the ampli-

tudes of the two signals, the oscilloscope trace showed the typical pattern of a modulated sine wave with an envelope at the beat frequency. Adjusting the frequencies of the two signals nearly to coincidence gave a slow beat with long periods when the signal was essentially nulled. It seemed likely that if some of the speaker signal could have been applied to the test elements in the proper phase, the motion of the upper plate could have been stopped. Unfortunately, a suitable phase shifter was not available.

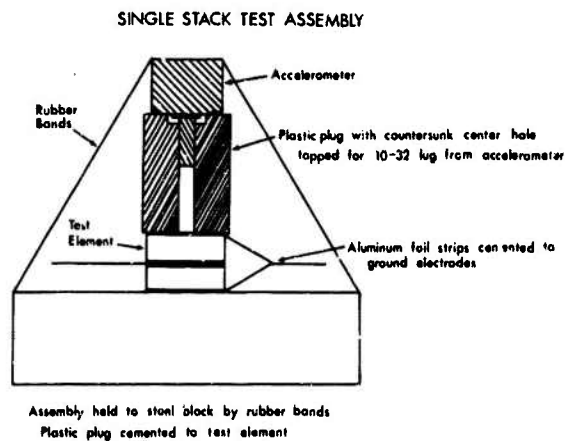


Figure 9: Plastic plug test fixture



Figure 10: Plastic plug test fixture

The fixture used for the measurements reported in Table I is pictured in Figure 9 and shown schematically in Figure 10. This arrangement was found to be simple and rapid to set up, free of electrical pickup, and quite satisfactory for the kind of survey we conducted.

#### MEASUREMENTS

The measurement procedure consisted of

connecting the test element in the circuit shown in Figure 4, setting the d.c. bias for those cases when it was used, setting the amplitude of the a.c. signal across the test element, sweeping the oscillator through the frequency range from 10 to 10k Hz, stopping at frequencies where the accelerometer signal peaked, and recording frequency and amplitude. The frequencies at which the accelerometer signal peaked appeared to be resonances of the

structure consisting of the sample, the plastic plug, and the accelerometer. Some interesting results were found at frequencies above 10 kHz but they are not reported here because of uncertainty about the sensitivity of the accelerometer and the high frequency behavior of the mount and the electronic equipment. It seems likely that the use of proper equipment will yield useful information at high frequencies.

Our early optimism about the benefits of the heat and electric field treatment used in preparing the material was shaken when we found that in many cases, untreated material responded to the signal as well as treated samples. This discovery led to testing similar elements of treated and untreated samples of the same material. In many cases the treatment had little or no effect. However, as shown in Table 1, there were a number of cases in which the treatment did have a beneficial effect. The effect of the d.c. bias was also beneficial. As well as we could measure, the activity increased linearly with bias and added linearly to the effect present without bias. For the measurements in Table 1 each material was tested four times, an untreated sample with and without bias and a treated sample, with and without bias.

Only peak signals with good wave shape were recorded. In many cases a poor signal was caused by distortion in the driving signal. This was obviously the case when a distorted signal was found at a subharmonic of a strong resonance. All such cases, from a small perturbation of the sinusoidal accelerometer signal to apparent responses at several times the driving frequency, were eliminated.

Another kind of unwanted response was caused by electrostriction.<sup>6</sup> This can be thought of as due to the attraction between unlike charges on opposite faces of the material and thus occurs twice in each cycle of the driving signal. When this effect occurs alone it can be distinguished from distortion, since the double frequency effect diminishes with the use of d.c. bias and disappears when the bias equals the driving amplitude. In a number of cases the material seemed to respond at both the driving frequency and double that frequency when there was no harmonic distortion. These cases are not reported but will be investigated further.

In addition to good wave shape at the driving frequency, the responses included in the table had to meet two other criteria. The accelerometer had no output when there was no mechanical connection with the sample when it was driven at the frequency of peak response and a signal did appear when the accelerometer touched the sample, with the electrical connections remaining unchanged. There was a phase shift between the accelerometer signal and the oscillator signal as the frequency was swept through the resonance.

The material designations in Table 1 are broad and intended only to separate the samples.

We used materials available in the NBS storeroom which the literature on electrets indicated might respond favorably. Accurate designation, based on formulation and measurement of physical and electrical properties would be out of place for this preliminary survey. The dimensions are nominal. Some of the treated samples warped and were machined flat. The kind of preparation applied to the treated samples is summarized in Table 11. The d.c. bias applied to the samples was chosen for convenience since its effect was linear. The frequencies were read on an electronic counter. The measured values seemed stable and reproducible. The values of activity are nominally related to the acceleration generated by a 400 V input signal. However, we consider it better to treat them as figures of merit by which different samples can be compared.

#### CONCLUSIONS

Detailed results, summarized in Table 1, are the measurements which remain after all doubtful cases have been eliminated. We are reasonably confident that the deductions to be obtained from intercomparison of the activities shown by the various samples is qualitatively correct. Uncertainty about the quantitative results arise from the mathematical manipulation in normalizing, from the lack of definite identification of the materials, from the variation in the heat and electric field applied to the samples during preparation, and from the changes in techniques and instrumentation which occurred as the tests progressed.

In spite of these uncertainties, the results in the table do allow some definite conclusions to be drawn.

1. Some elastomers have a linear mechanical response to an electrical signal.
2. In all the cases listed the response was accentuated by the use of a d.c. bias.
3. In the cases of fluorocarbon and polystyrene, the treatment with heat and high voltage left a residual effect which had not been found in the untreated material. In the cases of polymeric amide and phenolic resins the treatment enhanced the response.
4. The response varies greatly in different materials so that proper choice or special formulation may lead to improved response.

In most cases the same samples showed responses at frequencies other than those listed and samples of the same materials with different dimensions had a different pattern of response. However, the results shown in the table are typical of a large number of the measurements.

The results obtained with glass deserve special mention. They are not included in the table because only response at double the driving frequency was found and because glass is not an elastomer. It was tested because some

TABLE I  
Motion Generated at Selected Resonances

Material	Dimensions		Condition		Frequency of Resonance Hz	Activity *
	Diam.	Thickness	Preparation	Bias Volts		
Flouorocarbon	3/4"	1/16"	None	None	None	-----
			None	3150	None	-----
			Treated	None	4141	1.3
			Treated	3150	4433	4.0
Polymeric Amide	3/4"	1/8"	None	None	2431	0.16
			None	3150	2216	3.0
			None	3150	2383	2.9
			Treated	None	4632	0.67
			Treated	3150	4416	5.0
Polystyrene	5/8"	3/32"	None	None	None	-----
			None	2100	None	-----
			Treated	None	3343	0.32
			Treated	2100	3297	1.1
Filled Phenolic Resin	3/4"	1/8"	None	None	6315	0.32
			None	3150	6052	2.8
			Treated	None	4660	4.0
			Treated	3150	4670	14.7
Epoxy Resin	3/4"	1/8"	None	None	3681	0.24
			None	3150	3568	0.90
			Treated	None	3176	0.36
			Treated	None	4963	0.25
			Treated	3150	3173	1.2
			Treated	3150	5250	0.99
Natural Rubber	5/8"	3/32"	None	None	None	-----
			None	2100	537	3.1
			Treated	None	290	0.58
			Treated	2100	553	2.42

\*Arbitrary Units

TABLE II  
Treatment of Samples

Material	During Heating			During Cooling	
	Temperature °C	Volts	Time Hours	Volts	Time Hours
Flouorocarbon	80-150	15000	25	15-16000	18
Polymeric Amide	Low Heat on Hot Plate	4-6000	1/2	63-18000	--
Polystyrene	100	15000	6	15000	16
Filled Phenolic (Treated) (Twice)	Low Heat	6000	1	28000	--
	Medium	5000	2 1/2	16000	--
Epoxy	No Heat Applied	----	---	1200-30000	6 1/2
Natural Rubber	Low Heat	9000	1/2	9000-29000	--

disks were available, having been made for face plates on the test elements to provide better mechanical coupling. However, the response of glass was larger than any of those in the table by a factor of nearly 20 and the use of d.c. bias increased it and converted it to a linear response. Similar but smaller results were found with acrylic resin and butyl rubber.

Promising avenues for future development appear to be development of more effective methods of treating materials and developing a systematic means for finding more active material. A better understanding of the mechanism of response to electrical signals on a molecular level is basic to both developments. Even without such knowledge, variations of the methods of treatment we used could be tried as well as others that have been suggested. We expect favorable results from more experimentation with epoxies, polyesters, and other resins which solidify from a liquid during polymerization. The epoxy entry in Table 1 is not particularly impressive but others eliminated by our rigid criteria for inclusion in the table were more promising. Development of a rational method for finding more responsive materials guided by properties such as dielectric constant, elastic moduli, and density and by composition and molecular structure can be expected to be fruitful. Eventually such a search might lead to special formulation of materials.

The principal conclusion of this paper is that further investigation of the mechanical response of elastomers to electrical stimulus should be pursued.

#### ACKNOWLEDGEMENTS

The suggestion that piezoelectric-like properties of rubber-like materials would be worth investigating came from Dr. A. T. McPherson, retired Associate Director of the National Bureau of Standards. Useful comments

and suggestions were made by Leon Horn, Joshua Stern, J. F. Mayo-Wells, Paul Lederer, John Hiltner, and Earle Jones. The last four provided most of the equipment for the study. Leslie P. Parker and Joseph P. Nobel were very helpful in building and assembling the various special fixtures. Paul D. Freeze guided our use of the furnace for heat treatment.

#### BIBLIOGRAPHY

1. Piezoelectric Shakers for Wide-Frequency Calibration of Vibration Pickups, E. Jones, W. B. Yelon, and S. Edelman, J. Acoust. Soc. Am. (to be published).
2. The Electret, F. Guttman, Rev. Mod. Phys., 20, #3, 463 (1948).
3. Electrets: Part 1, A State of the Art Survey, Virginia Ann Johnson, Harry Diamond Laboratories, Army Materiel Command, TR-1045, 31 Aug 1962, Part 11, A Bibliography, TR-1074, 30 Sept 1962.
4. Piezoelectricity, W. G. Cady, p. 233, McGraw Hill Book Co., New York, 1946.
5. N. G. McCrum, B. E. Read, and G. Williams, Anelastic and Dielectric Effects in Polymeric Solids, John Wiley & Sons, London, 1967, Chapter 7.
6. W. G. Cady, *ibid.* p. 198.

After this paper was submitted our attention was called to U.S. Patent No. 3,365,593. L. B. Roof and G. Halklades of the Phillips Petroleum Company describe the use of thin sheets of piezoelectric polymers for microphones, speakers, and vibration pickups. They name several kinds of suitable polymers.

#### DISCUSSION

Mr. Naylor (Defence Research Est., Suffield, Alberta, Canada): Did you try carnauba wax? This has been used as an electret.

Mr. Edelman: No, we did not. Our treatment is obviously inspired by the kind of treatment that is used to create electrets. We were

looking for a rubbery material. This project started with a real practical need, and carnauba wax would not be suitable. People have reported a dc piezo-electric effect in wax and others have said they could not find it. But we did not try it.

CONTROLLED DECELERATION SPECIMEN PROTECTION SYSTEMS  
FOR ELECTRODYNAMIC VIBRATION SYSTEMS

Lawrence L. Cook, Jr.  
NASA, Goddard Space Flight Center  
Greenbelt, Maryland

Electrodynamic vibration systems are usually equipped with a means of terminating a test very rapidly in case of an operator error, equipment malfunction, or a power outage. The device used to implement this protection is known as an armature protector or an amplitude protector. The armature protector discharges the energy stored in the power amplifier and short-circuits the armature. Its function is to protect the shaker moving element or armature by preventing it from hitting the mechanical stops; however, it was not designed to protect the test specimen. In fact, when the protector is initiated, the specimen is subjected to possible damage due to the high deceleration levels generated when the armature is suddenly stopped. In order to prevent specimen damage, additional protection devices were needed.

Accordingly, two Controlled Deceleration Specimen Protection Systems were developed to Goddard Space Flight Center specifications by two different manufacturers. The object of this paper is to describe these two systems and show typical response data during their operation. These specimen protection systems were designed to limit the high deceleration level consistent with specimen safety limits.

The method used to effect controlled deceleration is to automatically insert a variable damping resistance across the armature. In practice, fixed parallel resistances are inserted in the armature circuit in the proper sequence so that the total armature resistance decreases incrementally with time. Thus, the resistance of the armature path is continuously decreased as needed in order to maintain the deceleration at or below a selected level.

A test program was conducted to evaluate both Controlled Deceleration Specimen Protection Systems. The test results, block diagrams, and time histories of the decelerations due to dynamic braking are included in the paper.

INTRODUCTION

One of the most undesirable occurrences in the field of vibration testing, when operating an electrodynamic exciter, is a shutdown due to the firing of an armature protector because of operator error, equipment malfunction, or power outage. The armature protector was designed to

protect the moving element (armature) of the shaker by preventing it from hitting the mechanical stops. This is accomplished by electronically shorting the energy in the amplifier to ground and short-circuiting the armature. Unfortunately, the sudden dynamic braking, due to short-circuiting the armature, generates large accelerations which have caused



the spacecraft or specimen to be subjected to excessive levels and possibly be damaged.

The firing of an armature protector or "shaker dump" is of particular significance at Goddard Space Flight Center because one "dump" could destroy a spacecraft valued at more than \$1,000,000 or reduce the reliability in the specimen to a point where it would cause a costly delay in the launch of a spacecraft. The purpose of this paper is to describe the two specimen protections systems that were developed for Goddard, and to present and discuss results from typical operational tests of each.

#### DESCRIPTION OF DECELERATION SYSTEMS

##### Mathematical Treatment

The mechanism for dynamically braking the armature as smoothly as possible so that no damage is incurred by the test specimen is described by the following equation:

$$(1) -a = B_0^2 d + 2\alpha v$$

where:  $v$  is the velocity and  $d$  is the displacement of the armature at the time shutdown is initiated and  $-a$  is the maximum deceleration level reached during shutdown.

This relationship is a combination of electrical and mechanical parameters as developed by their mathematical analogies. The parameter  $\alpha$  is the shunting resistance in the armature circuit, and the parameter  $B_0^2$  is a function of the flexure stiffness and armature mass. Further treatment is presented in Appendix A as established by (1), (2) and (3). It is by virtue of the second term of equation (1),  $2\alpha v$ , and solely through this term, that the dynamic braking effect occurs.

Control of deceleration by means of armature resistance is dominated by the first term of the equation (1). This term,  $B_0^2 d$ , is a function of the flexure stiffness, displacement, and armature mass, and is completely independent of the resistance. Any

acceleration due to  $B_0^2 d$  has to be allowed for and cannot be adjusted. This effect is particularly noticeable at low frequencies and large displacements under conditions of light load.

The major component common to each of the two deceleration systems (one designated type A, the other type B) is the dynamics computer. These computers are designed to perform the following functions:

1. To monitor certain significant parameters and initiate a controlled deceleration of the armature whenever these parameters exceed preset safety limits.
2. To dynamically brake the armature to a stop by causing successive damping resistance to be switched across the armature circuit in such a way as to avoid large deceleration peaks.

##### Type A

Figure 1 shows a block diagram of an MB C126 (10,000 lb. force) vibration system that incorporates the Type A deceleration system. The system consists of a relative displacement transducer, deceleration dynamics computer, deceleration level controller, acceleration limiter, ignitron, dynamic braking chassis and a status display panel.

The displacement transducer, mounted on the shaker, and attached to the armature, generates a signal proportional to the position of the armature, relative to the exciter field body. The displacement transducer responds from DC to 200 Hz and senses the static as well as the dynamic position of the armature. The instantaneous displacement signal from the transducer is fed to the dynamics computer, which determines the instantaneous deceleration required to bring the armature to rest in a given distance. If the computed deceleration equals or exceeds a prescribed level, the dynamics computer commands system shutdown by triggering the level controller. The level controller triggers the ignitron; thereby shorting electrical energy in the

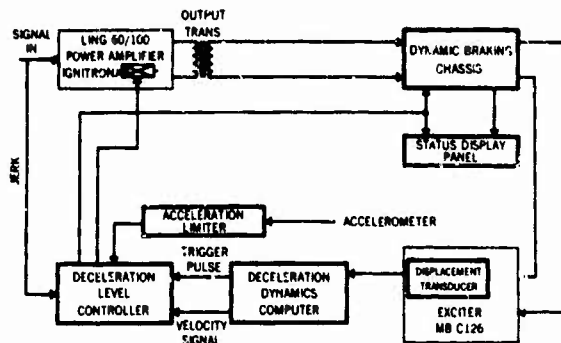


Figure 1. MB C126 Exciter with the Type A Deceleration System

amplifier to ground, and after a slight delay, on the order of micro-seconds, provides control signals to the dynamic braking chassis. The level controller monitors the armature velocity as computed by the dynamics computer, and, as this velocity decreases, causes the dynamic braking chassis to automatically switch in progressively smaller resistors in the armature circuit. The number and sequence of level controller command signals, and the number of dynamic braking resistors inserted by the dynamic braking chassis, are indicated on the Status Display Board.

This deceleration system may also be initiated by: (1) excessive acceleration level, preset from 3 to 300 g's, (2) a transient input or "jerk", and (3) loss of AC power to the system. An acceleration limiter monitors the input or control accelerometer and when preset level is exceeded, the acceleration limiter triggers the deceleration level controller to initiate a controlled deceleration. A differentiator built into the deceleration level controller determines the jerk magnitude by monitoring the amplifier input signal and similarly initiates deceleration. A level detector is also built into the deceleration level controller to monitor AC power and initiate deceleration when power is lost.

#### Type B

Figure 2 is a block diagram showing the type B deceleration system, integrated with an MB C210 (28,000 lb. force) vibration system currently in use at Goddard. The deceleration system consists of a computer control chassis and a cabinet containing an ignitron, thyratrons, and damping resistors, needed to carry out the dynamic braking action.

The sensing signal for the type B system uses the armature terminal voltage as a measure of velocity. An integrator is used to compute the armature displacement and a prediction circuit computes the increment of displacement required to shutdown at a preset test level. The sum of the final computer displacements (armature plus increment) is used to initiate shutdown whenever the absolute value approaches the maximum amplitude excursion of the exciter. When the dynamic braking operation is initiated, a resistance is immediately switched through the first thyatron across the exciter armature. At the same time, the power amplifier driving the exciter is shutdown, via the ignitron. After a short delay of about 20 microseconds, the control chassis is free to permit the second, third, fourth, and fifth resistor, in sequence, to be switched via the appropriate thyatron. The

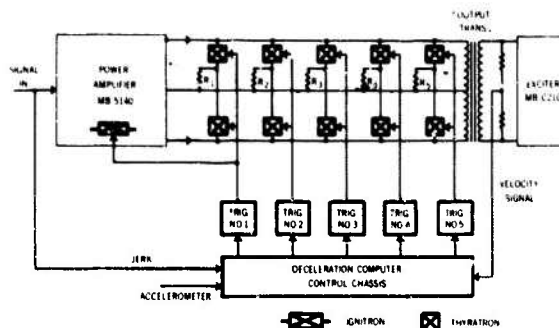


Figure 2. MB C210 Exciter with the Type B Deceleration System

control chassis using the armature voltage as a measure of velocity, computes the displacement, and continuously for each resistor, computes the acceleration as if that resistor were switched in. When the computation indicates that the acceleration would be at a safe level if that resistor were switched in, the appropriate thyatron is fired, and the resistor is then activated. Triggering of this system may also be initiated by: (1) jerk at the amplifier input, and (2) excessive acceleration level, preset from 3 to 300 g's.

#### TEST RESULTS

Time histories of decelerations on the type A (MB C126 exciter, 10,000 lb. force) and on the type B (MB C210 exciter, 28,000 lb. force) systems were recorded on an oscillograph using a piezoelectric accelerometer mounted on the exciter armature (bare table).

Figure 3 shows the acceleration response of an MB C126 exciter vibration system caused by initiating the standard amplitude protector system. This system does not have the type A deceleration capability and is presented to show a typical shaker dump as a reference. Exciter operating conditions during this time period were 5 Hz and 0.5 inches double amplitude displacement (equivalent to  $\pm 0.64$  g-peak). The amplitude protector was

fired close to the peak of the acceleration waveform and the amplitude of the resulting transient was 12 g-peak. Figure 4 shows the acceleration response entirely due to table mass and flexures at low frequencies under a condition of a light load without amplitude protector or type A deceleration systems. The MB C126 exciter was operated at 5 Hz,  $\pm 0.64$  g-peak, and then the power amplifier was turned off near the peak of the acceleration waveform. The resultant transient due to the effect of the table mass and flexures was 10 g-peak.

Figure 5 shows the shutdown transient using the type A deceleration system. The exciter was operated at 5 Hz,  $\pm 0.64$  g-peak and the type A system was triggered near the peak of the acceleration waveform. The resultant transient was 8.5 g-peak.

Figures 6, 7, and 8 illustrate the action of the type A system when initiated at different frequencies and on a random basis. Figure 6 shows a shutdown when operating the exciter at 10 Hz,  $\pm 2.5$  g-peak. The system was triggered near the peak of the acceleration waveform and the resultant transient was 12.4 g-peak. Figure 7 illustrates a shutdown at 20 Hz and  $\pm 8.2$  g-peak with the system triggered between maximum velocity and maximum acceleration. The deceleration transient was 24 g-peak. Figure 8 shows a shutdown at  $\pm 18$  g-peak and 50 Hz with

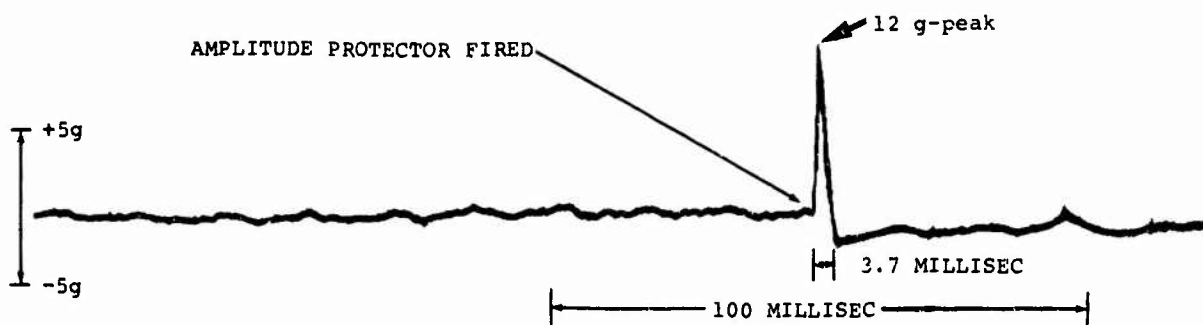


Figure 3. Standard Amplitude Protector Shutdown of the MB C126 Vibration System

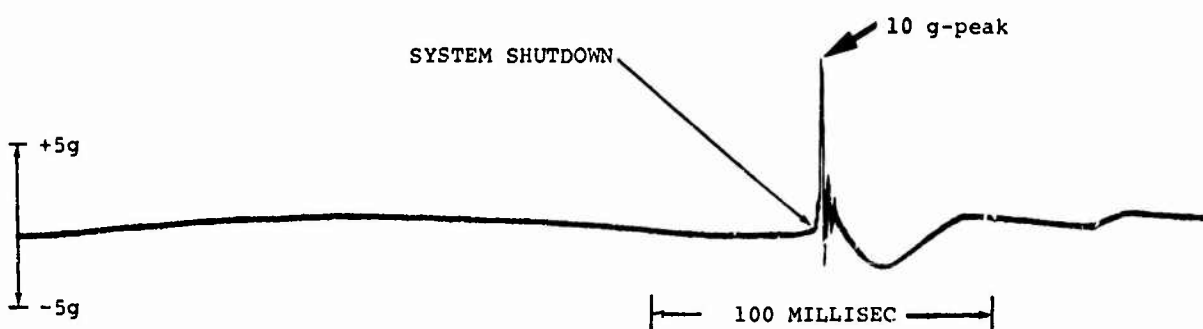


Figure 4. Resultant Transient Due to the Effect of the Table Mass and Flexures of a MB C126 Exciter

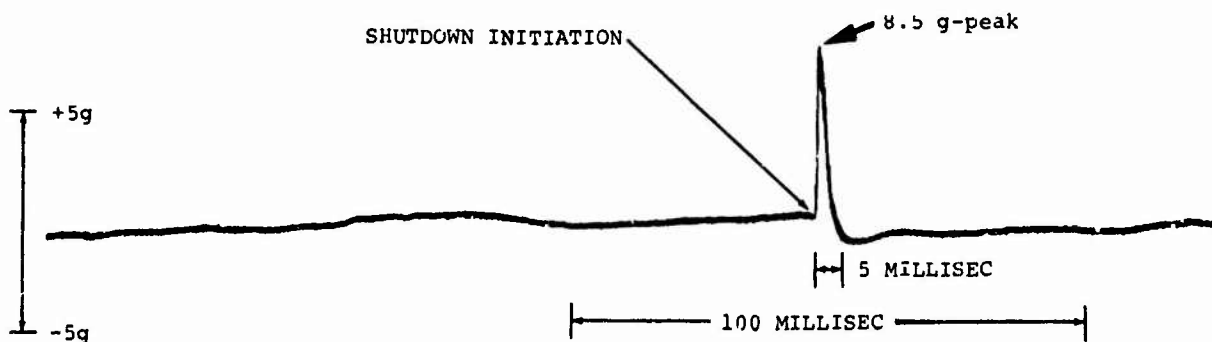


Figure 5. Type A Deceleration System Shutdown Transient at 5 Hz,  $\pm 0.64$  g-peak

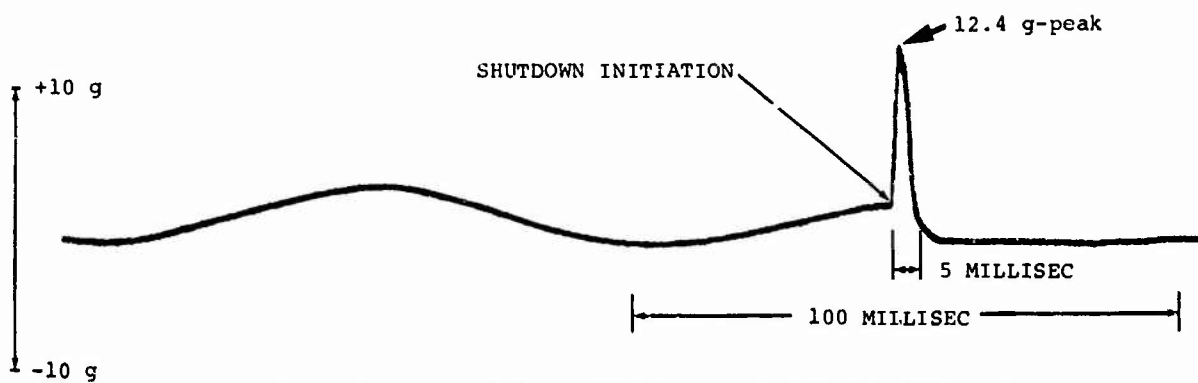


Figure 6. Type A Deceleration System Shutdown Transient at 10 Hz,  $\pm 2.5$  g-peak

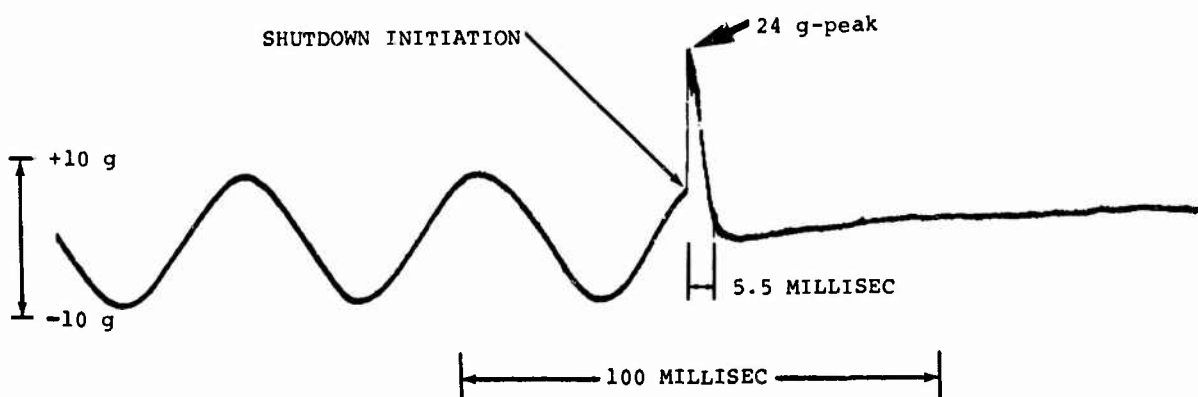


Figure 7. Type A Deceleration System Shutdown Transient at 20 Hz,  $\pm 8.2$  g-peak

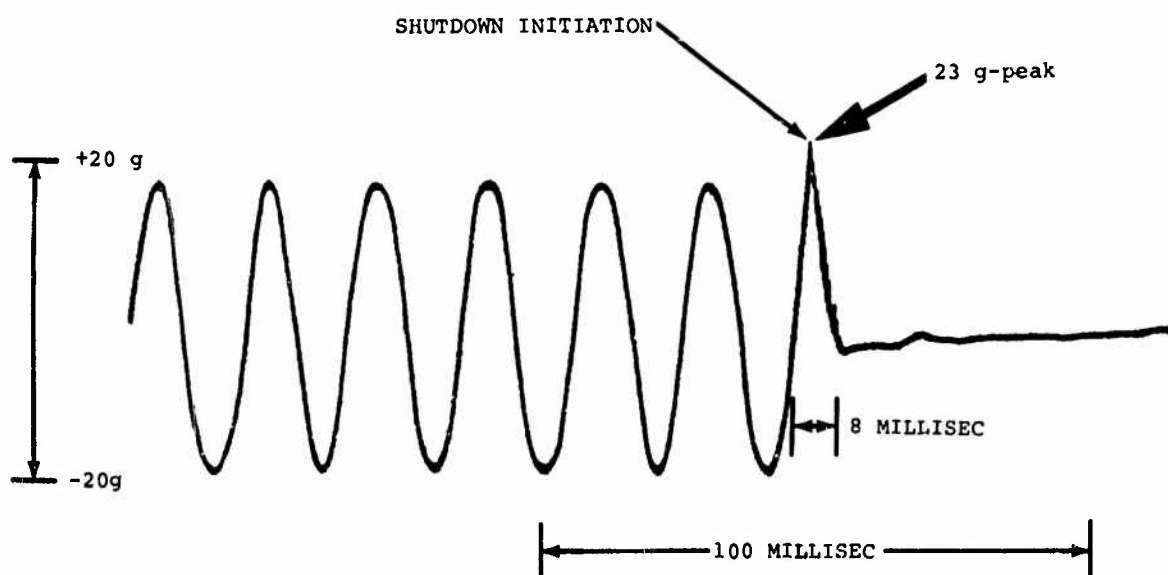


Figure 8. Type A Deceleration System Shutdown Transient at 50 Hz,  $\pm 18$  g-peak

the shutdown initiated at maximum acceleration. The deceleration transient was 23 g-peak.

Figure 9 illustrates the effect of a shutdown amplitude protector on a MB C210 exciter. The exciter was operated at 5 Hz,  $\pm 0.8$  g-peak, bare table. The amplitude protector fired at the peak of the acceleration waveform and the transient exceeded 10 g-peak.

Figure 10 shows the effect of the C210 table mass and flexures while the exciter was operating at 5 Hz,  $\pm 0.5$  g-peak and then disconnected from the amplifier, so as to eliminate armature braking, at the peak of the acceleration waveform. The resultant transient was 3.6 g-peak.

Figures 11 through 14 illustrate the action of the type B deceleration system on the C210 shaker system under a variety of conditions. Figure 11 shows a shutdown transient at 5 Hz,  $\pm 0.64$  g-peak. The system was triggered at the peak of the acceleration waveform and the resultant transient was 12 g-peak. The ringing on the waveform is probably due to the ignitron firing and exciting the armature resonance. The undamped oscillations

after deceleration are caused by the thyratrons which extinguish themselves when the AC voltage goes to zero and the armature sees an open circuit. When this happens, the armature will oscillate at its mass resonance until damped out. Figure 12 illustrates a shutdown when the exciter is operated at a frequency of 10 Hz, and a level of  $\pm 2.5$  g-peak. The deceleration transient was at the peak of the deceleration waveform with a level of 13 g-peak. Figure 13 shows a deceleration transient when the system was operated at 20 Hz and  $\pm 8.2$  g-peak. The system was triggered near maximum velocity and zero acceleration. The resultant transient was 11.4 g-peak with armature ringing and oscillations. Figure 14 illustrates a shutdown transient when the exciter was operated at 50 Hz,  $\pm 18$  g-peak. The system was triggered between maximum velocity and maximum acceleration. The resultant transient was 24 g-peak.

For clarification purposes, Table 1 summarizes the shutdown transients of the type A deceleration system. The shutdown transient was computed for each of the test runs and compared to the actual shutdown transient. It can be seen by the table that there is close agreement between the computed and actual shutdown transients.

Table 1 - Type A Shutdown Transient Data

Test Level	Shutdown Transient	
	Computed *	Actual
5 Hz, $\pm 0.64$ g-peak	11.6 g-peak	8.5 g-peak
10 Hz, $\pm 2.5$ g-peak	13.5 g-peak	12.4 g-peak
20 Hz, $\pm 8.2$ g-peak	24 g-peak	24 g-peak
50 Hz, $\pm 18$ g-peak	21 g-peak	23 g-peak

$$*a = B_0^2 d + 2\omega v$$

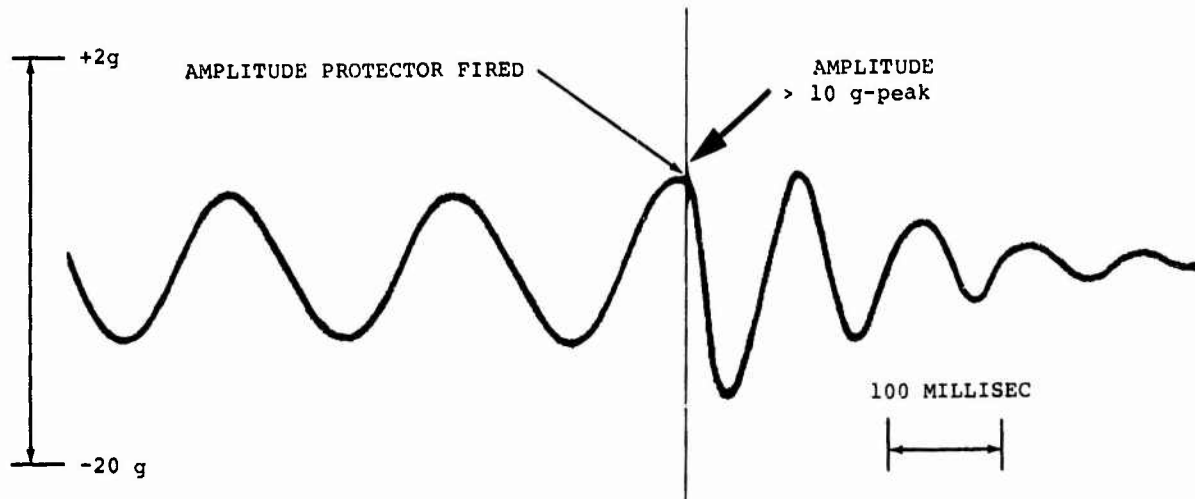


Figure 9. Standard Amplitude Protector Shutdown of the MB C210 Vibration System

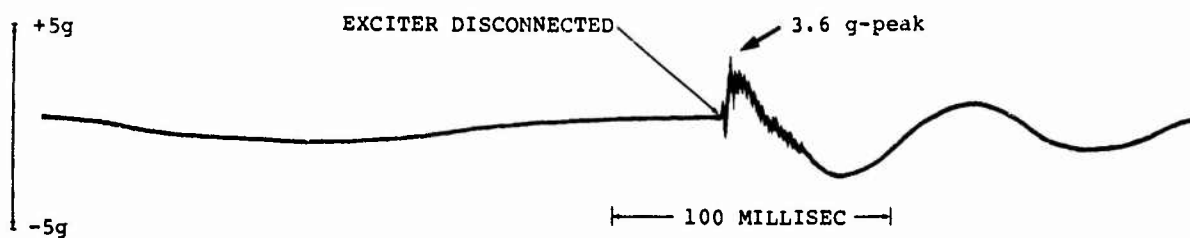


Figure 10. Resultant Transient Due to the Effect of the Table Mass and Flexures of a MB 210 Exciter

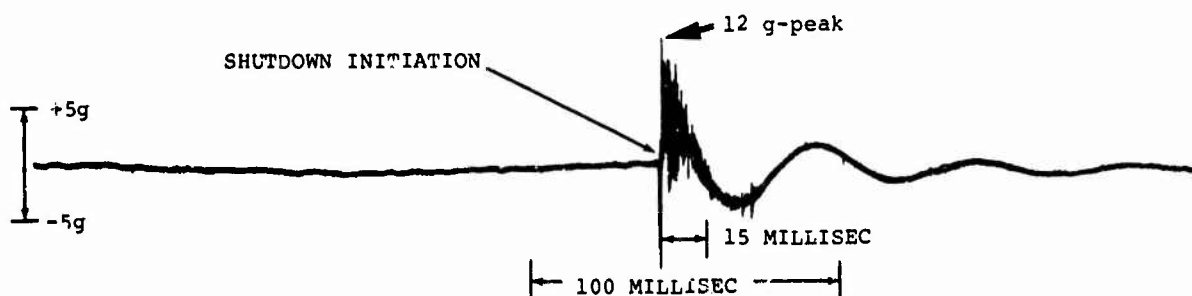


Figure 11. Type B Deceleration System Shutdown Transient at 5 Hz,  $\pm 0.64$  g-peak

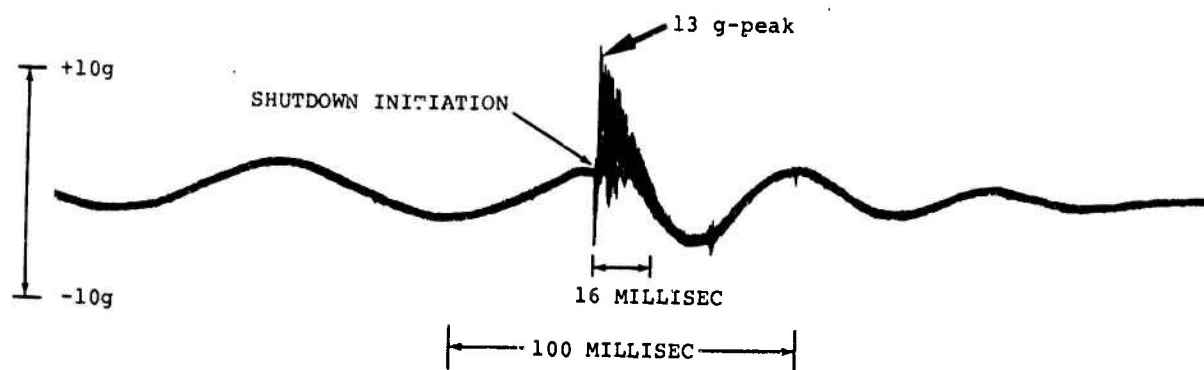


Figure 12. Type B Deceleration System Shutdown Transient at 10 Hz,  $\pm 2.5$  g-peak

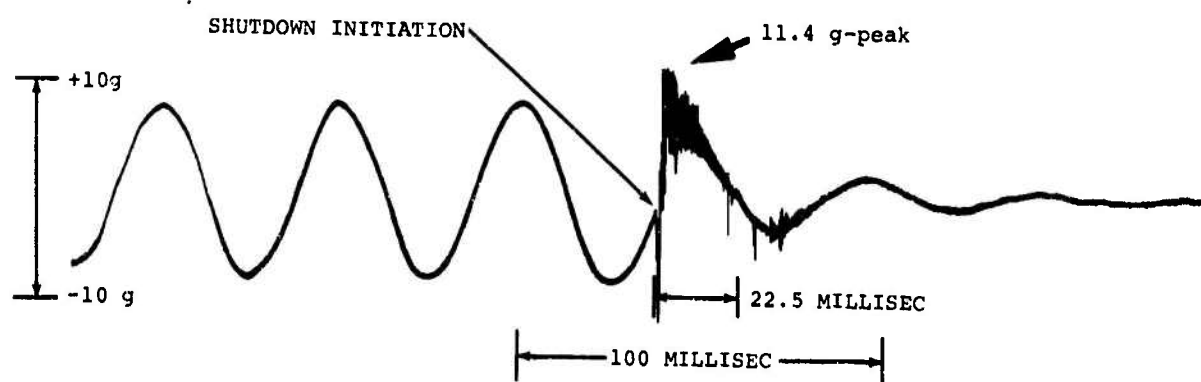


Figure 13. Type B Deceleration System Shutdown Transient at 20 Hz,  $\pm 8.2$  g-peak

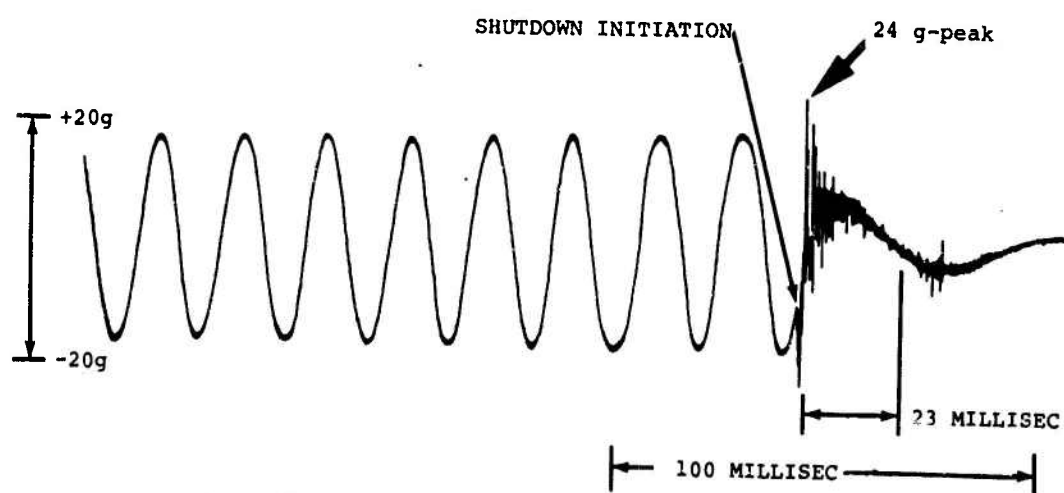


Figure 14. Type B Deceleration System Shutdown Transient at 50 Hz,  $\pm 18$  g-peak



Table 2 - Type B Shutdown Transient Data

Test Level	Shutdown Transient	
	Computed *	Actual
5 Hz, $\pm 0.64$ g-peak	6.2 g-peak	12 g-peak
10 Hz, $\pm 2.5$ g-peak	8.1 g-peak	13 g-peak
20 Hz, $\pm 8.2$ g-peak	3.8 g-peak	11.4 g-peak
50 Hz, $\pm 18$ g-peak	2.4 g-peak	24 g-peak

$$*-a = B_o^2 d + 2\alpha v$$

Table 2 summarizes the shutdown transient of the type B deceleration system. The actual shutdown transient is compared to the computed transient. The computed transients are lower in value because of the armature ringing and undamped armature oscillations generated by the actual shutdown event.

#### CONCLUDING REMARKS

One of the specification requirements for the deceleration systems was that the deceleration should not exceed the test level. It has been shown that under conditions of light loads, low frequencies and large displacements, that this is not possible with either type A or type B systems. With an understanding of the transient effect of the table mass and flexures, it can be said that the deceleration systems are quite successful in reducing deceleration transients to a safe controllable level.

#### APPENDIX A

Mobility Analog Formulas for the Vibration Exciter (1), (2) and (3).

$$(1) -a = B_o^2 d + 2\alpha v$$

where: a, d and v are the instantaneous values of acceleration, displacement and velocity at the time of shutdown.

$$(2) B_o^2 = \frac{1}{LC}$$

$$L \text{ (Henries)} = \frac{.113\mu^2}{K_f}$$

$K_f$  = flexure spring constant, lb/in.

$\mu = \frac{F}{I}$  = generated force to driver coil current, lb/amp.

$$C \text{ (farads)} = \frac{2.29 \times 10^{-2} W}{\mu^2}$$

$$W = W_{\text{table}} + W_{\text{coil}} + W_{\text{load}}, \text{ lbs.}$$

$$(3) \alpha = \frac{1}{2RC}$$

$R$  (ohm) = the total damping resistance,  $\frac{.113\mu^2}{D}$

$D$  = mechanical damping constant, lbs/in/sec

#### REFERENCES

1. Harris and Crede; Shock and Vibration Handbook, Volume 2, Chapter 25, Vibration Testing Machines, Carl Unholtz.
2. Engineering Report No. 27 (unpublished), February 28, 1968, Dr. A. G. Ratz, MB Electronics, New Haven, Conn.
3. Electro Mechanical Analogs, Ling Electronics, Anaheim, California.

#### DISCUSSION

Mr. Mutter (Boeing Co.): Can this process be used on a random signal as well as on a sinusoidal test?

Mr. Cook: Yes, it can.

Mr. Mutter: How can it work on a random signal, if control is mainly on displacement? How do you distinguish the level through the frequency spectrum on a random test?

Mr. Cook: The system looks at the velocity and at the displacement when using the random signal. It was designed to do this. We have not done much testing on the system with random signals. But it was designed to decelerate under a random input.

Mr. Meza (IBM Corp.): What about the reliability of the overall system? We are hanging x number of more chassis on that amplifier.

Mr. Cook: So far it has been fair. These number one systems are more or less prototype, and reliability should improve as further systems are manufactured.

Mr. Meza: You have used the system with random though?

Mr. Cook: Yes, we have used them with random.

CONTROL TECHNIQUES FOR SIMULTANEOUS  
THREE-DEGREE-OF-FREEDOM HYDRAULIC VIBRATION SYSTEM

H. D. Cyphers and J. F. Sutton  
NASA, Goddard Space Flight Center  
Greenbelt, Maryland

A new combined environment test facility known as the Launch Phase Simulator (LPS), is now in operation at the Goddard Space Flight Center. Included in the facility is a vibration system designed to simulate the low frequency mechanical vibrations experienced by spacecraft during the launch phase of flight. The system is capable of operation both on the end of a large centrifuge arm and as a conventional shaker system mounted on a fixed reaction mass.

This paper discusses the operation and control of the vibration system, problems relating to phase and amplitude control of the shakers for sinusoidal and random inputs, and several advanced control techniques which are presently under study.

The vibration system consists of five electro-hydraulic actuators mounted in a configuration which permit three-degree-of-freedom motion, corresponding to a combination of longitudinal, yaw, and lateral vibration. The three types of motion can be applied independently or in any combination. This system employs multiple-loop feedback servo controllers for actuator control and completely automated input functions which enable one person to operate the complete system. Input sources include tape recordings of actual flights, an automatic random equalizer, and sinusoidal generators.

The input control system uses the latest techniques for automatic amplitude, phase, and cross coupling control. It features automatic displacement and acceleration level control and a unique shaker galling circuit designed to detect breakdown of the moving actuator lubricating oil film. This circuit shows promise as an aid in detecting this galling phenomenon which has long plagued hydraulic shaker designers and users.

#### INTRODUCTION

The dynamic environment to which a spacecraft is exposed can, in general, be divided into three categories: the prelaunch or ground handling environment, the launch environment, and the orbital environment. During launch, the most severe environmental loading conditions often occur simultaneously. In the past, simultaneous reproduction of all of these conditions has not been attempted because the required facilities and techniques

didn't exist. Spacecraft design philosophies, therefore, have been limited to single environment test conditions, resulting in hardware tailored to the simulated test conditions rather than to the real environmental conditions.

During launch of a space vehicle, the severity of acoustic noise-induced vibration is at its greatest. At the same time, the liftoff accelerations are of an appreciable magnitude, as are other effects such as pressure and temperature variations. The combination

of mechanical vibration and static (non-vibratory) acceleration in a laboratory test is especially difficult and was formerly avoided because of the complex nature of the facility required. We are now approaching a sophistication in the design of spacecraft and vehicles such that the specific effects of combining static acceleration, mechanical and acoustic vibration, and pressure can no longer be ignored in evolving efficient and reliable designs for spacecraft structures, subassemblies and components. Significant effects can be produced by a combination of stresses resulting from such factors as steady-state structural deformations which modify vibration response characteristics, binding or friction in mechanisms causing erratic responses under vibration, and additive static and vibratory acceleration causing overstressing of structures and components. To complicate matters further, additional combinations of environmental stresses such as those produced by temperature and pressure can increase the physical effects that must now be considered in simulating the launch environmental conditions.

An advanced combined environmental test facility designated as the Launch Phase Simulator (LPS) is now operational at the Goddard Space Flight Center [1]. The LPS is capable of simultaneously reproducing the major launch environmental conditions; i.e., static acceleration, acoustic noise, pressure profile (vacuum), and mechanical vibration (low frequency). Presented here is a detailed description of the environmental capabilities of the three-degree-of-freedom mechanical vibration system which forms a part of the LPS test facility.

#### System Capabilities

The LPS Vibration System produces three-degree-of-freedom motion (longitudinal, lateral, and yaw) from 0.5 to 200 Hz with both sinusoidal and random capability. The three types of motion can be applied independently or in any combination. This system is capable of operation on the centrifuge arm or on a seismic reaction mass located off of the arm (offboard) (Fig. 1). The maximum sinusoidal and random vibration capabilities of this system are as follows:

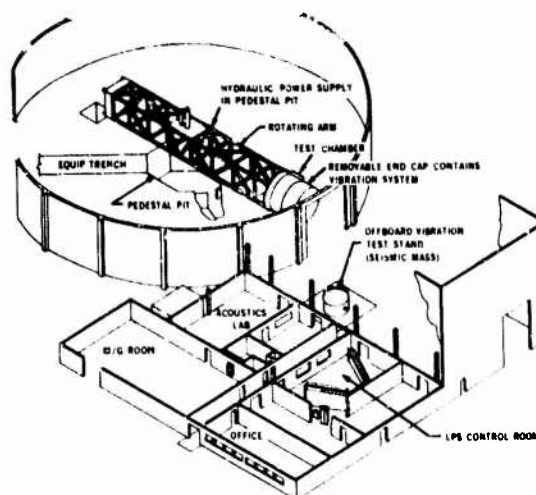


Figure 1. LPS Facility Including Overall Building Arrangement

#### Sinusoidal Vibration

Longitudinal:  $+4g$ , 1 in. double amplitude.  
 Lateral:  $+2g$ , 1 in. double amplitude.  
 Yaw:  $+10 \text{ rad/sec}^2$  angular acceleration  
 0.015 radians double amplitude.

#### Random Vibration

Longitudinal: 2.8 g-rms, 1 in. double amplitude.  
 Lateral: 1.4 g-rms, 1 in. double amplitude.  
 Yaw:  $7 \text{ rad/sec}^2$  rms angular acceleration, 0.015 radians double amplitude.

Design capabilities of the vibration system when mounted on the seismic reaction mass are identical to those for the system when mounted on the centrifuge arm except for the frequency range which is  $1/2 - 200 \text{ Hz}$  for the former condition and  $5 - 100 \text{ Hz}$  for the latter condition. The system can simulate the actual environmental conditions in real time and can be operated either automatically or manually.

The facility can accommodate a payload or spacecraft configuration that weighs up to 5000 lb. and is contained in an envelope 10 ft. in diameter and

15 ft. long. This spacecraft size was based on the dimensions of the second generation or observatory class of unmanned spacecraft.

#### Detailed Description

The vibration system consists of a configuration of five electro-hydraulic actuators interconnected with two structural tables, such that three-degree-of-freedom motion is possible. This system is completely housed in a structure known as the end cap. The end cap is the removable part of the test chamber which is located on the end of the rotating arm structure. Figure 2 illustrates the operation of loading the end cap end on the test chamber structure. The hydraulic power supply required for this system is located in the pedestal pit beneath the center of the arm. Hydraulic power requirements for maximum force output with simultaneous motion in the three-degrees-of-freedom is 300 gpm at 3000 psi. The hydraulic fluid is transferred from the power supply to the system through a hydraulic rotary joint at the center of rotation of the arm structure and is routed along the arm through piping to the vibration system for on-board operation. For offboard operation, the hydraulic piping is routed to the seismic reaction mass from the hydraulic power supply via an equipment trench.

The multi-axis motion of this system on the centrifuge arm is defined in Figure 2 as follows: (a) longitudinal motion is rectilinear motion along the x-axis or thrust axis (longitudinal axis of test chamber and spacecraft); (b) lateral is rectilinear motion along the z-axis; and (c) yaw is rotary motion in the horizontal (x-z) plane about the vertical axis. The motions for the system when oriented on the seismic mass are identical except that they are in a vertical plane rather than the horizontal plane. Explanation of the motion capability requires a description of the shaker arrangements: four actuators are mounted at 90 degree intervals around the periphery of the interior of the end cap structure. There is a lower vibration table which is attached to the moving elements (pistons) of these actuators. When these four actuators are operating in phase, longitudinal or thrusting motion is produced. When two opposite actuators

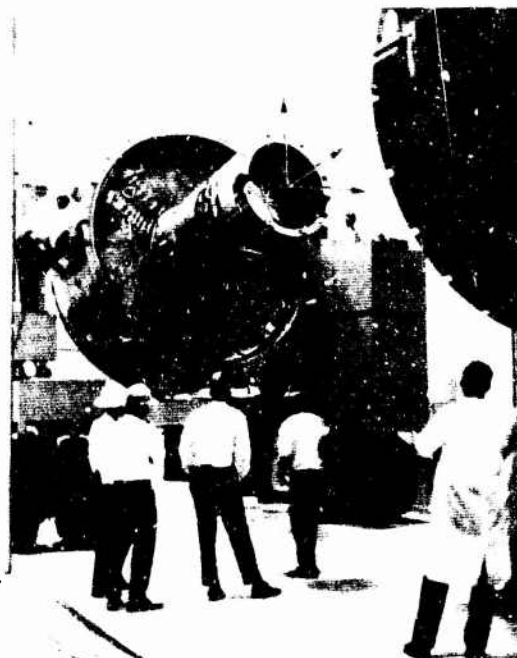
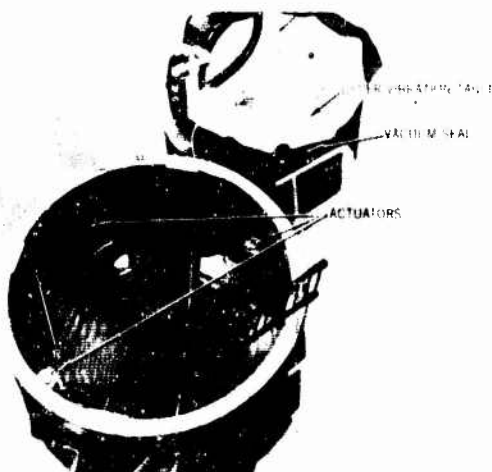
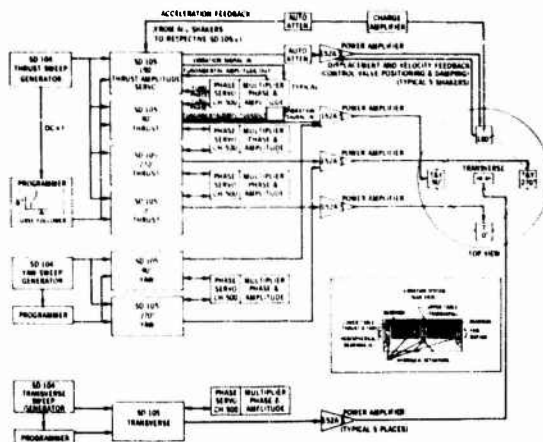
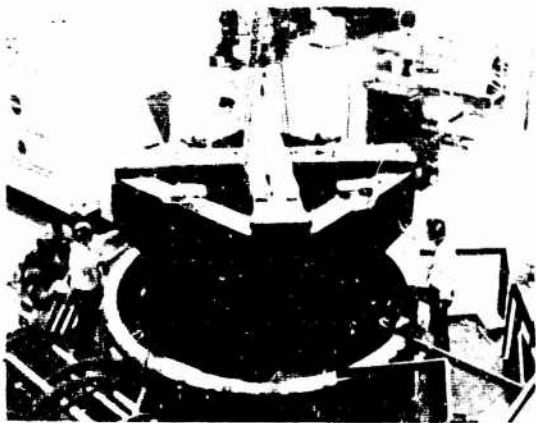


Figure 2. Applications Technology Satellite During Test Chamber Loading Operation

of this system are operating 180 degrees out of phase, yawing motion is produced. An upper vibration table structure is mounted to the lower vibration table through a series of hydrostatic bearings and moves relative to the lower table by virtue of imposed motion from the fifth actuator located within the lower table. When lateral motion is not required, the upper table is held stationary by means of a position feedback loop. The lower table has a mechanical locking feature which secures the table during mounting of the test specimen and subsequent transportation from the offboard seismic mass to the onboard (on arm) configuration. Figure 3 depicts the end cap (on the seismic mass) with the lower vibration table being lowered into place and shows the coordinate system with x-axis vertical for this orientation. Shown in Figure 4 is the end cap with lower vibration table removed and upper vibration table adjacent to the end cap. Note three of the four thrust-yaw system actuators and the vacuum seal (or "boot") attached to the upper table structure.



## CONTROL SYSTEM

## Design Considerations

The overall design of the LPS Vibration Input Control System is shown schematically in Figure 5, and embodies the results of extensive model studies performed at Goddard [2] as well as the techniques developed and used by other test facilities [3]. Because of the

three-fold increase in control complexity over conventional single degree-of-freedom multi-shaker systems, a completely automatic system was developed for control of the shakers. The vibration system must also operate in conjunction with three other environmental control systems, i.e., steady-state acceleration, vacuum (pressure profile) and acoustic noise, to produce a real-time simulation of the launch environment. As a result, these factors added much to the complexity of the design requirements for the control system.

The following typical operational sequence illustrates the programming capability that is required: At  $T=0$  the thrust system frequency starts sweeping at a given sweep rate. Simultaneously, at  $T=0$  or at later (preprogrammed) times the yaw and lateral systems begin similar preprogrammed test sequences. (Note: the yaw and lateral sweep rates and amplitude variations may or may not be the same as the thrust system sweep rates and amplitude variations.) Time  $T=0$  is dictated by the time of occurrence of the specified vibration in the overall combined environmental test. This may correspond to liftoff, max Q, transonic buffeting, or engine firings in space.

The input control parameters are most often defined in terms of vibratory acceleration levels obtained at interfaces between major structural elements. A simulation of the flight environment can be obtained by applying vibrational excitation to the structure at these interfaces and controlling the levels at these points to match those encountered in flight. With this in mind some of the practical limitations in achieving true flight vibration simulation should be pointed out:

1. Control systems are generally limited to a specific number of control sensor points. The behavior of the specimen between these points is dependent upon fixture and table design and selection of the control points. By choosing these points through both analytical and empirical means, the vibration between the control points will be somewhat predictable.
2. Hydraulic actuators are inherently non-linear devices with frequency, load, and time dependent phase shift characteristics.
3. Whenever multiple shaker excitation is used, energy crossfeed between shakers can cause control problems at some frequencies. This occurs due to the fact that at certain frequencies the specimen and/or fixture will tend to vibrate in its natural mode shape in violation of the specification test levels and phase relationships. Trouble occurs whenever the coupled vibration from one driven point to another exceeds the level desired at the second point.
4. The shaker-plus-fixture system usually presents a mechanical impedance very different from that of the interfacing launch vehicle. In the case of the LPS system, a large table mass of 8000 lb. compared to a maximum payload mass of 5000 lb. combined with the inherent stiffness of a hydraulic shaker system present an extremely high impedance to the specimen.

In view of the above factors, the design goal was to develop a control system which would: (a) permit selection of one or more control points; (b) compensate for the load and frequency dependent characteristics of the actuators; and (c) employ cross-coupling control techniques in order to minimize interaction of the extremely close-coupled system. The resultant system should provide a well controlled input with a very high impedance at the plane of the spacecraft attachment interface.

#### GENERAL DESCRIPTION

The vibration input control system as shown schematically in Figure 5 generates sinusoidal voltages and receives signals proportional to accelerations and displacements of the actuators. In addition, it accepts external signals from either a tape recorder or random equalizer. The system consists of Spectral Dynamics (SD) amplitude control and Chadwick-Helmuth (C-H) phase control equipment. This combination was chosen because it lends itself to complete automation, incorporation of the necessary protective features and provides maximum control loop stability. The signal input source (tape, sine, or random) is selected by means of a patch panel. From there the signal goes through the master control panel which contains automatic level controls, individual actuator level controls, and a master control. The automatic level controls allow any number of actuators to be brought on line slowly to a level 40 db down from the operating level. This point permits the control loop to be established (in compression) and all the pertinent parameters to be checked immediately prior to testing. At test initiate the automatic level control will bring all controllers out of compression simultaneously at a controlled rate. The system is then ready to accept amplitude control signals.

#### Amplitude Control

Once the operating level is reached, the sinusoidal signal generator frequency sweep circuits are energized. The frequency analog output of the generators in turn

drives the level programmers. The same sequence is repeated for each of the three axes. The Model SD104 sine generator controls the duration of the test for all input sources (tape, sine, or random) since it drives the x-axis of the level programmers.

The block diagram of Figure 5 shows a total of seven SD104 servo controllers. One is for control of the lateral or transverse actuator, four are for thrust control, and the remaining two are for yaw control. All control is done on the fundamental frequency component of the control signal.

A typical normalized accelerometer feedback signal from a charge amplifier receives some amplification in the SD105, it is then routed to the Model CH500 Phase and Amplitude multiplier chassis. The Model CH500 extracts the fundamental acceleration signal by analog multiplication techniques. A voltage proportional to the fundamental amplitude is applied directly to the SD105 compressor (amplitude servo) to maintain the vibration level constant and independent of distortion components. Note that the amplitude controls employ signals which have been effectively filtered by use of analog multiplication. If narrow bandwidth tracking filters had been employed instead of the multipliers, additional time constants equal to the reciprocal of the filter bandwidth would have been added to the system. This could cause instability under certain conditions.

The fundamental yaw acceleration component is detected by the multipliers from the accelerometer signals obtained from the 90° and 270° hydraulic actuators which excite both yaw and thrust motion. The yaw signal is then controlled for amplitude and phase separately and summed with the thrust signal at the power amplifier input. The thrust signal components are handled in similar fashion.

Level programmers control the scale factors applied to the accelerometer signals for each axis and thus determine, together with the SD105 settings, the vibration level for each axis. Displacement control is obtained either by double integration of the accelerometer signal or by using displacement signals which are generated by transducers mounted directly on the actuators. This actuator displacement signal and an additional slave feedback signal are normally used only in instantaneous servo loops for actuator positioning and servo valve damping.

#### Phase Control

The desired phase relationships among all actuators are controlled automatically by the Model CH 500-7AS Phase Control System. Phase sensing is accomplished by analog multiplication of the accelerometer signal and the undistorted reference sine wave at the generator frequency. This analog multiplication gives a control voltage proportional to the phase

TABLE I  
RATE OF PHASE SHIFT FOR STRUCTURAL RESONANCES

Time to Sweep 20-2000 cps	Generator Sweep Rate Degrees/Min.	(Phase Shift Degrees/Second)				
		Q=5	Q=10	Q=20	Q=50	Q=100
29 min.	5	1.7	3.3	6.7	17	33
14 min.	10	3.3	6.7	13.0	33	65
7 min.	20	6.7	13.0	27.0	65	133
4 min.	40	13.0	27.0	53.0	133	270*
2 min.	80	27.0	53.0	110.0	270*	540*

\* Too fast for 180°/second maximum speed of 500 systems



(out of phase component) of the two signals with rejection of harmonics, noise, hum, or other signals not at or very near the shaker frequency. This control voltage is used as an error signal by the phase servo. The servo then shifts the phase of the fundamental drive frequency to the actuator in the proper direction to bring the actuator into the desired phase relationship with the others. Front panel adjustments allow the actuators to operate in phase, or permit selecting any desired phase offset, relative to the reference actuator motion. For each actuator, a phase error meter indicates any deviation from the desired phase. Table I shows rates of phase shift for structural resonances and the control capability of the phase control system.

#### Random Control

Present plans for the provision of random control equipment for the LPS vibration system include an 80-channel automatic random equalization system and a multi-channel random averager. This equipment will be operated in conjunction with the sinusoidal control system to average the four thrust accelerometer signals and feed the average PSD spectrum and level data into the automatic equalizer. The random console adjusts the input signal to provide proper equalization of accelerometer signal levels within each filter band as required by the test specification. The overall random drive to each shaker is controlled by a Data-trak-SD105 combination in the same manner as are the sine inputs. (See Figure 6). (Note: The Data-trak is essentially a device for following a pre-plotted curve.)

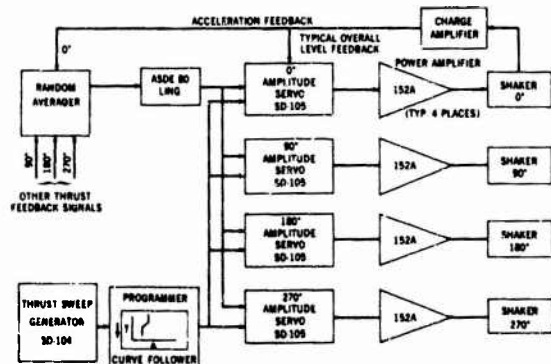


Figure 6. Present Random Control System

#### Cross-Coupling Compensation

Both amplitude and phase control can be defeated by high-Q resonances in the structure between the drive points. For instance, with resonance amplification of input from the principal or master shaker, a greater "g" level than desired may appear at the drive point of a particular slave actuator. This condition depends on the mechanical impedances of the test structure and fixture, and of the shaker table. Should resonances occur, the compressor circuit at the slave actuator can decrease drive to zero. The test objective for "g" input, then, cannot be met, and phase control is also lost since there is no slave actuator drive to control.

One (impractical) solution to this problem is to control manually through the resonant frequencies. The operator adjusts the amount of drive from the oscillators (compressor off), and the phase of drive from the phase control unit (servo off) until return to automatic control is possible.

Another solution is to study the structural behavior at the resonant frequencies, determine "cause and effect" paths (e.g. drive at actuator "a" causes largest response at shaker "b" accelerometer), and program for exchange of accelerometer signals and control channels at these frequencies. This approach works well with a two-channel system, but for a more complex system, the exchange becomes very complicated and impractical to program.

One general approach toward stabilization of an "N" channel system is to generate "N" bias "test frequency" signals which are directly applied to the drive signal input for each channel, (i.e., not through the phase and amplitude control system). These bias signals are approximately the electrical equivalent to (but opposing) the structural cross coupling between drive points. Operation of the Model CH532 Cross Coupling Compensator is based upon this general approach, but with an added practical advantage of very uncritical bias value (amplitude and phase). This advantage is a result, in part, of the use of multipliers for detection of vibration amplitude and phase (in-phase and out-of-phase components rather than magnitude and phase angle.)

The LPS control system contains two model CH532 cross-coupling compensation systems; a four-channel unit for thrust interactions and a two-channel unit to correct for yaw interactions.

#### Safety Features

The testing of expensive spacecraft hardware requires that every precaution be exercised in order to insure that environmental tests are performed correctly. Therefore, it is necessary to ascertain that the setup prior to test is correct and that once the test is begun, any malfunctions will subject the specimen to levels lower than the specification levels. The input control system has several modes of operation. A brief description of these is given below:

Pretest checkout of the vibration input control system is accomplished by means of a Preset Mode. In this mode, the control loop is connected directly from the servo controller (SD105) output to the accelerometer input. This permits checking the input control system from Initiate through Shut Down. The control system is interlocked so that prior to selecting Operate Mode all gain settings, program limits, pressures, etc., must be established. In the Operate Mode, just prior to test initiation, the system is placed in automatic operation and a signal is inserted which will hold the system approximately 40 db. below the preset test level. This condition allows the table and specimen to be centered and the control feedback loops to be closed.

There are several circuits which are designed to protect the spacecraft once the test is initiated. Shutdown of the compressors at a predetermined rate will occur if: (1) there is a loss of any accelerometer control signal; (2) a switch is changed; (3) a component fails; or (4) a preset level of acceleration is exceeded. In addition, emergency stop buttons located at various points in the system are available to initiate smooth, rapid, automatically sequenced, transient free shutdown of the entire facility.

Because the LPS vibration system is completely enclosed with the end cap with all actuators permanently connected to the tables, a means of detecting incipient galling (breakdown of the lubricating oil film between moving parts) was developed.

This system consists of accelerometers mounted on the hydraulic actuators, amplifiers, monitoring loud-speakers, and oscilloscopes. The system detects the high frequency (greater than 500 Hz) noise which is typical of increased friction between parts and gives a visual and audible warning of light galling allowing immediate shutdown for prevention of costly severe galling.

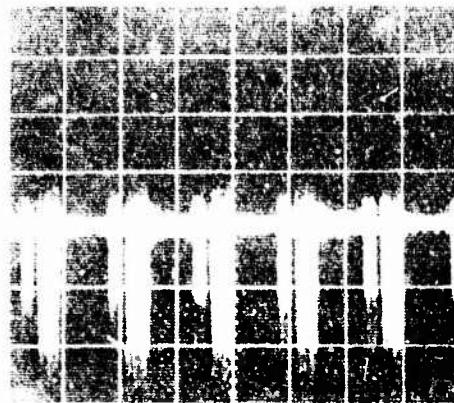


Figure 7. Acceleration Time History of Galling Response

Figure 7 is a photograph of the output of an accelerometer mounted directly on a hydraulic actuator during a 2 Hz sinusoidal dwell. The plots of Figures 8 and 9 show the Fourier spectrum power spectral density (PSD) and probability density (PDA) of the galling and non-galling portions of a cycle. Note the relative magnitudes of the Fourier and PSD plots. For quick detection of incipient galling, such data analysis is not necessary. The characteristic rasping sound heard when the signal is reproduced via a loudspeaker is very effective for this purpose. The skewness of the PDA and the "one-sided" characteristics of Figure 7 are due to data recording problems.

#### PLANS FOR FUTURE DEVELOPMENT

Such techniques as control from points on the spacecraft above the table level, improved random control, impedance control, automatic cross-coupling compensation, and

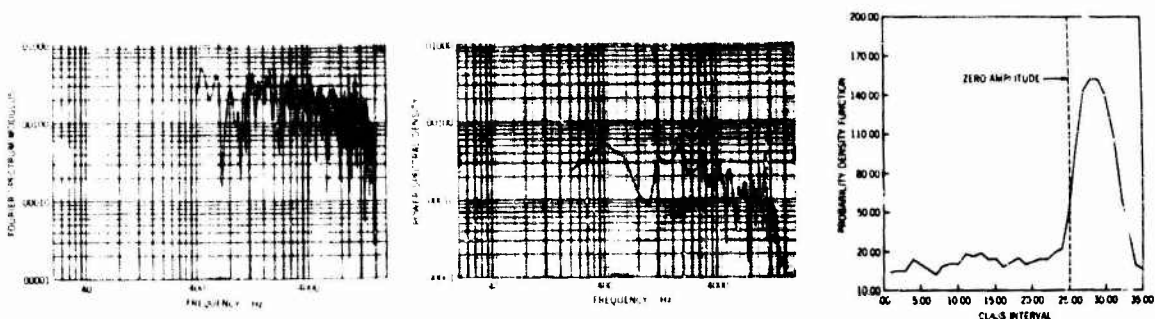


Figure 8. Fourier Spectrum, Power Spectral Density, Probability Density Analysis of Galling Response

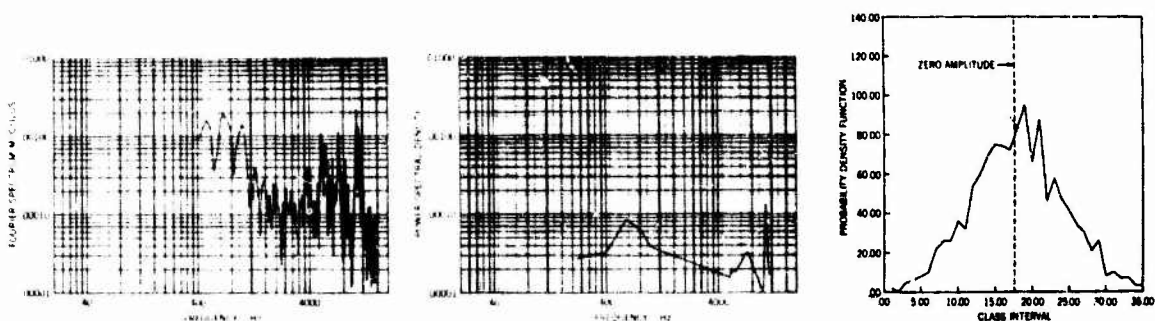


Figure 9. Fourier Spectrum, Power Spectral Density, Probability Density Analysis of Non-Galling Response

digital computer control are under consideration.

#### Spacecraft Control Points

Provisions have been made in the present system to permit control of the acceleration level at points on the spacecraft other than at the interface. This type of control will consist of selecting one or more points to be controlled on the spacecraft structure, feeding signals obtained at these points into a phase insensitive multi-channel averager and then introducing the resulting average signal into the control system via a variable gain amplifier. This signal will be introduced in a manner which will enable the system to control to the required amplitude level on the spacecraft and yet maintain the proper phase and amplitude relationships at the interface.

#### Random Phase Control

Preliminary studies at Goddard and elsewhere [5] indicate a need for phase control of random signals applied to multiple-shaker systems because hydraulic actuators are non-linear devices with phase shift characteristics which are apparently functions of temperature, contamination of the hydraulic fluid, and of specimen mechanical impedance. In the case of a common random input to two or more shakers, a condition could exist in which one actuator would be moving up when another would be moving down. In multiple-shaker configurations such performance could cause large stresses on fixtures and introduce undesirable yaw components into pure thrust tests.

The random excitation control system under consideration consists of a modified 80-channel automatic

equalizer. This modified system provides five independent automatic equalizer and analyzer controls, each covering a 200 Hz bandwidth. This arrangement will provide 16 filters, each having a 12.5 Hz bandwidth. This modification, to incorporate phase control, may take the form of a set of variable delay lines or employ the use of heterodyne techniques. Operation of one possible phase control system (Figure 10) is as follows: Wide band random noise is fed to a balanced modulator where it is modulated by a 100 kHz carrier. The resulting signal is passed through a bank of narrow bandwidth filters and demodulated again. In the demodulation process, however, voltage-variable crystal controlled oscillators are used so that servo-controlled phase shift may be introduced into the forward signal path of each narrow band of noise. The demodulated signals are recombined and fed to the actuators. The feedback accelerometer signals are heterodyned with the 100 kHz carrier and narrow band filtered so that the average phase angle between the two 10 Hz components, the two 20 Hz components, etc., can be measured. The resulting DC signals are used to close the phase control loops.

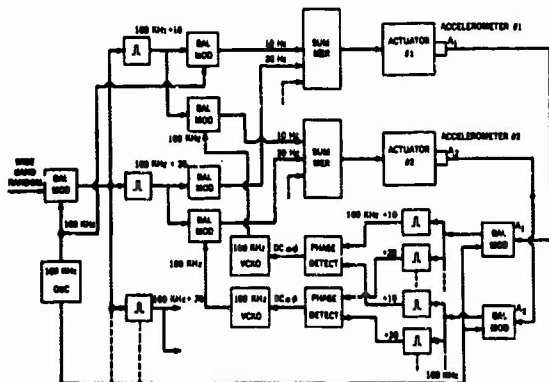


Figure 10. Block Diagram of Proposed Random Phase Control System

"Phase" in the application discussed here refers to the phase angles between the outputs of two nearly identical narrow bandwidth filters. For random noise inputs, the narrow band random outputs have the appearance of randomly amplitude-modulated sinusoids. The "frequency" of the output signal is well enough defined so that DC "average" phase can be derived. Figure 11 depicts

the appearance of two nearly identical narrow-band signals maintained approximately at  $0^\circ$ ,  $90^\circ$ , and  $180^\circ$  relative phase angle. In the two-actuator system described here, if the two 10 Hz components, the two 20 Hz components, etc., are all maintained in phase in pairs, then the net result when the two complete sets of narrow band signals are recombined will be "in phase" i.e., both actuators will move up and down in unison.

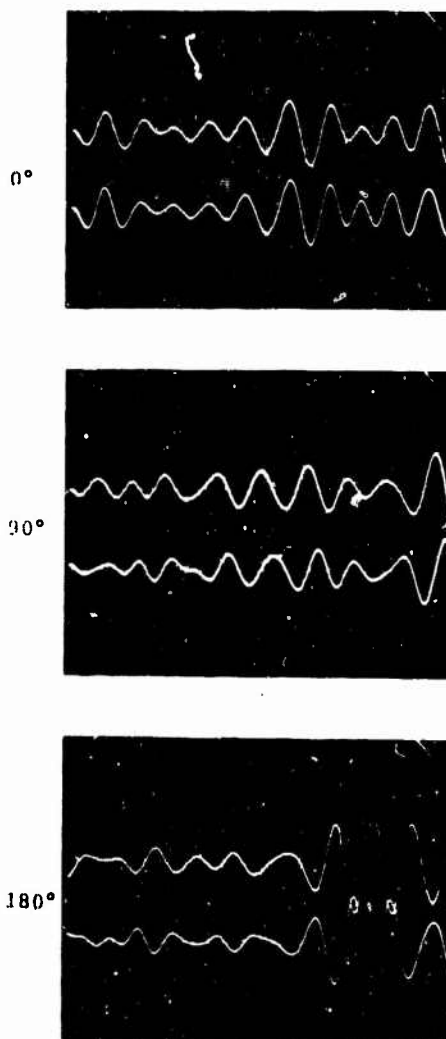


Figure 11.  $0^\circ$ ,  $90^\circ$ ,  $180^\circ$  Phase Relationships of Random Signals

## Impedance Control

In most practical situations, the impedance at a point is a complicated function of frequency, with resistive and reactive effects becoming dominant alternately in continuing succession as the frequency is increased. To date, most impedance control work has been done using sinusoidal inputs. A technique which holds promise for impedance control with random inputs consists of adding a force gage signal in a parallel feedback path with an accelerometer signal. When this force signal is fed to individual phase and amplitude weighting controls and then summed with the accelerometer signal, the random equalizer is able to adjust the acceleration spectrum as required by the interaction of the test specimen with the interface impedance. This argument is developed in greater detail in Reference 5.

As the mechanical impedance problems involved in a multi-degree-of-freedom vibration simulation problem are more complicated than those for a single-degree-of-freedom situation, this technique will probably not be applied to the LPS until it has been successfully applied to simpler systems.

## CONCLUDING REMARKS

This vibration control system: (1) permits selection of any desired control point or point; (2) compensates for the load and frequency dependent

characteristics of the individual actuators; (3) employs advanced cross-coupling control techniques to minimize shaker interaction; and (4) incorporates all necessary protective features along with completely automated control. Thus, the resultant system provides a well-controlled three-degree-of-freedom input motion at the plane of the spacecraft attachment.

## REFERENCES

1. Edward J. Kirchman and Charles J. Arciles, "Advanced Combined Environmental Test Facility," Shock and Vibration Bulletin No. 37, Part 3, pp. 175-191, January, 1968.
2. Edwin J. Skolka, "Hydraulic Exciter Combined Environment Tests," Shock and Vibration Bulletin No. 36, Part 3, pp. 119-138, January, 1967.
3. Richard A. Arone and Paul A. Brock, "Control Techniques for Multi-Shaker Vibration Systems," Shock and Vibration Bulletin No. 36, Part 3, January, 1967.
4. N. F. Hunter, Jr. and J. G. Helmuth, "Control Stabilization for Multiple Shaker Tests," Shock and Vibration Bulletin No. 37, Part 7, pp. 155-162, January, 1968.
5. Alfred G. Ratz, "An Impedance Compensated Random Equalizer," M. B. Electronics, New Haven, Connecticut.

## DISCUSSION

Mr. Otts (Sandia Corp.): What type averager did you use?

Mr. Cyphers: This is an Unholtz-Dickie.

Mr. Otts: With random signals on two axes, have you considered the use of dual equalization? In other words, equalizing one axis with one equalizer, the other axis with the other?

Mr. Cyphers: Yes. The paper discusses in some detail a system in which we are very much interested, which would take a conventional 80 channel system, divide it into 5 separate random equalization systems, each containing 16 filters at 12-1/2 cycle bandwidths, up to 200 cycles. This would provide all the capability of a single system for each actuator.

Mr. Otts: Are you going to equalize one channel at a time with the others down, or are you going to attempt to equalize simultaneously?

Mr. Cyphers: I think on this closely coupled system we would have to do it mostly simultaneously. They are solidly attached to each other as you saw by the lower table and they would have to be done in conjunction with one another.

Mr. Otts: Then you are just going to live with the cross coupling and in certain frequencies you are going to be out of spec, is this true?

Mr. Cyphers: We have not even thought about cross coupling under random control yet.

INITIAL REPORT ON EQUIVALENT DAMAGE MEASUREMENT  
BY UTILIZING S/N FATIGUE GAGES\*

Thomas B. Cost  
Naval Weapons Center  
China Lake, California

Code 5517, Quality Engineering Division, Central Engineering Test Branch, Naval Weapons Center, China Lake, California, has successfully utilized S/N Fatigue Gages for ascertaining structural degradation induced in missile body structures during road transportation tests and cross country transportation tests. The results indicate a reliable and simplified method for correlating field induced damage to laboratory-controlled equivalent damage tests can be developed by utilizing fatigue gages.

INTRODUCTION

The purpose of this paper is to describe a method that was recently used by personnel at NWC, China Lake, California for determining the amount of structural damage incurred by the Chaparral missile during road tests on the XM-370 self propelled launcher at Aberdeen Proving Ground, Aberdeen, Maryland. The results of this investigation indicate that the measurement of field incurred fatigue damage can be achieved by the utilization of fatigue gages and this damage can be related to laboratory induced fatigue damage. The utilization of this uncomplicated method of fatigue damage measurement opens a new dimension in equivalent damage test design and test evaluation.

THE S/N FATIGUE GAGE

Heretofore, the determination of accumulated fatigue damage has been largely speculative in nature due to the lack of an effective, uncomplicated, and reliable method of fatigue damage measurement that would lend itself to practical application outside the laboratory. A good deal of fatigue damage investigation has been done with methods using ultra-sonic devices,

eddy current devices, and magnetic devices. These are, for their purposes, quite often very useful. They are, however, somewhat complicated, require some rather sophisticated electronics, and can be rather difficult to utilize under field conditions.

The fatigue gage discussed in this paper was developed by Mr. Darrel R. Harting of the Boeing Aircraft Company in 1964 and is, in essence, a strain gage that develops an irreversible resistance change directly correlated to fatigue damage when it is subjected to cyclic strains. Although resistance changes occur in the gage at strain levels below 800 or 900  $\mu$ in, these changes are very small and the gage appears to "saturate" or fail to change resistance when subjected to these low strains. As the strain levels increase, the resistance changes also increase. These resistance changes can be directly correlated to the induced pre-crack fatigue damage in a specimen. The resistance change for a particular fatigue gage is a function of the strain level environment experienced by the gage. The results from tests with cyclic strain about a zero mean strain are essentially the same as those from tests with cyclic strain levels above zero

\*Paper not presented at Symposium.

mean strain. A complete and detailed evaluation of these and other characteristics of this type of fatigue gage are found in references 1 and 2 and need not be reiterated here. It should be stated, however, that these gages, unlike conventional strain gages, do not require continuous monitoring. The gages may be monitored periodically during a test and resistance changes can be detected by resistance sensing devices with resolutions of 0.01 to 0.001 ohm. Because the S/N fatigue gage possesses these attributes together with the ease of application and relatively low cost found in most strain gages, it was selected by Code 5517, Central Engineering Test Branch, Quality Engineering Division, NWC China Lake for measuring the fatigue damage incurred by the Chaparral missile while transported on the XM 370 self propelled launcher.

#### TEST PHILOSOPHY

Theoretical structural analysis of the Chaparral missile, as described in reference 3, together with structural load tests conducted by Code 5517 NWC, described in reference 4, disclosed that if a serious structural problem existed on the Chaparral missile, it would be at the motor tube-warhead interface. Fig. 1 shows the warhead motor tube interface. This enlarged cross-section view of the warhead and motor tube clamp ring grooves shows how possible stress concentrations could exist at the radius on the bottom of the grooves. These data predicated the location of the gages as shown in fig. 1.

#### FATIGUE GAGE LOCATIONS DURING APG 5,000 (+ 1,600) MILE ROAD TEST

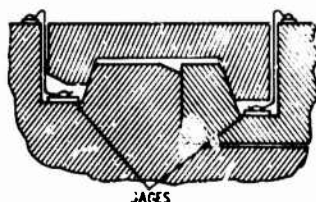


Figure 1. Chaparral Missile  
With Cross-Section View of  
Warhead-Motor Tube Interface

It was postulated that even though a fatigue gage could not be mounted on the radius at the bottom of the clamp ring grooves, a gage could be mounted immediately adjacent to the radius and would be in a relatively high strain field if such a field existed at the radius. A correlation could then be achieved between the resistance changes incurred during the transportation tests and those incurred during fatigue tests to failure that could be conducted in the laboratory.

#### ROAD AND CROSS COUNTRY TESTS

Twelve Chaparral missiles were instrumented as follows for the road and cross country tests: Two each FNA-06 fatigue gages were mounted on the bottoms of the clamp ring grooves at positions  $\pm 90^\circ$  from the hangers whereby the gages would see maximum strains either in compression or in tension. Two each FNA-02 fatigue gages were mounted on the outside of the motor tube-warhead-clamp ring at similar positions relative to the hangers as those on the bottom of the grooves. The backing on the gages used on the bottom of the grooves was trimmed as close as possible to the grid in order to permit locating the gage adjacent to the sharp radius at bottom of the grooves.

The Chaparral missiles were then loaded on the XM-370 self propelled launcher with four missiles loaded on the launcher rails and eight missiles loaded in the storage compartments. The missiles were changed from storage rack to launcher rails at periodic intervals during the test to equalize input vibration loadings on each missile. The self propelled launcher completed 5000 miles of road transportation plus 1600 miles of cross country transportation at Aberdeen Proving Ground, Aberdeen Maryland.

#### LABORATORY TESTS TO FAILURE

The laboratory fatigue tests to failure were conducted on 5 standard motor tubes sections and inert warheads and on 3 modified motor tube sections and inert warheads. The standard and modified motor tubes are compared in figure 2. The sharp radius at the base of the motor tube clamp ring groove has been removed in the modified tubes.

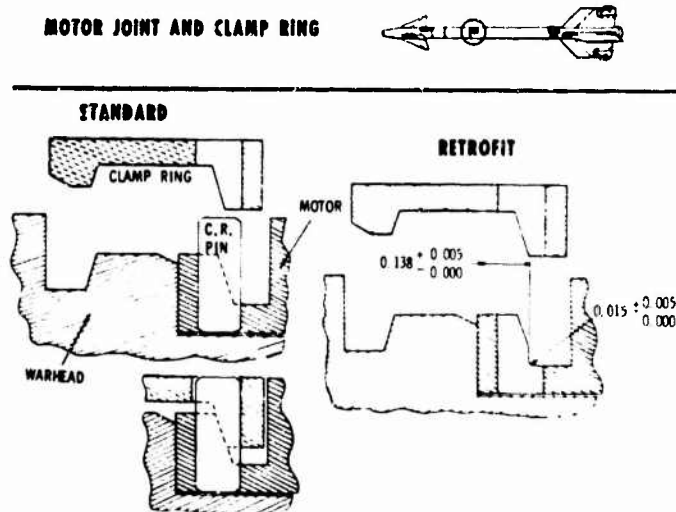


Figure 2. Comparison Between Standard and Modified Motor Tube Grooves



Data acquisition instrumentation for these test specimens consisted of a strain gage and an FNA-06 fatigue gage mounted at the bottom of the clamp ring groove on each warhead. These gages were located on the specimens to respond to the maximum induced strain. The warhead-motor tube specimens were mounted in a restraining bracket and attached via a drive rod and collar to an electro-dynamic vibration exciter. This test set-up is shown in figure 3. Data acquisition and test monitoring equipment is shown in figure 4. These instruments consisted of: (a) A force gage, (b) A signal amplifier, (c) An oscilloscope, (d) A counter for counting loading cycles, and (e) A resistance reading device.

The test parameters consisted of a sinusoidally varying load of 1000 pounds peak force applied to the specimen at 30 cycles per second in such a manner as to introduce a 15000 inch-pound moment at the warhead-motor tube clamp ring grooves. This sinusoidal moment loading, corresponding to that induced by an 11.6g pulse, produced strain levels of  $\pm 1500$  u-in/in the bottom of the motor tube clamp ring grooves and  $\pm 100$  to  $\pm 200$  u-in/in strains in the bottom of the warhead clamp ring grooves. These parameters were applied until failure occurred in the motor tube clamp ring grooves.

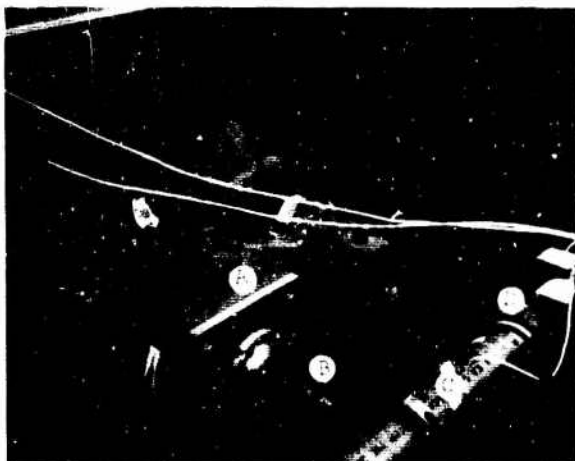


Figure 3 (Left)

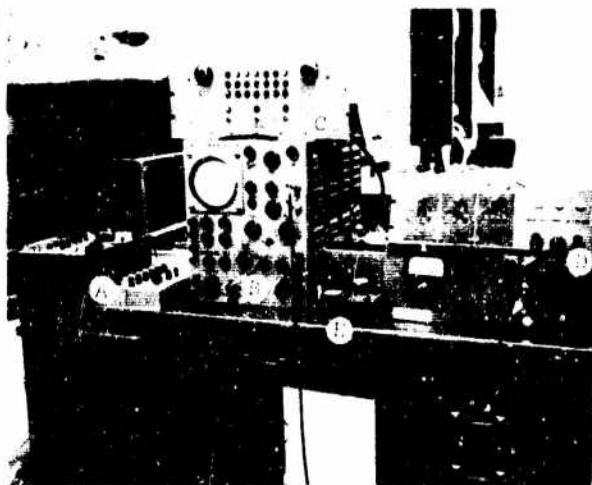
Test Set-Up

- A. Vibration Exciter
- B. Force Gage
- C. Motor Tube and Warhead
- D. Restraining Bracket

Figure 4 (Right)

Data Acquisition and  
Test Monitoring  
Instrumentation

- A. Strain Gage Signal  
Conditioning System
- B. Oscilloscope
- C. Counter
- D. Force Signal Amplifier
- E. Resistance Meter



## TEST RESULTS

The fatigue gage data for the warhead-motor tube joint collected during the road tests are shown in figure 5. These are frequency distribution plots of the resistance changes for the fatigue gages located in the motor tube clamp ring grooves and in the warhead clamp ring grooves. As can be seen, the resistance changes are low in magnitude. The average resistance change in the gages on the motor tubes is 0.116-ohm and the average resistance change on the warheads is 0.096 ohms.

The  $\pm 100$  to  $\pm 200$  u-in/in strain on the warheads in the laboratory tests was too low to induce detrimental fatiguing. The gages on these warheads "saturated" or stabilized very early in the tests with resistance changes of 0.04 to 0.20-ohms which compare favorably with the data from the road tests.

The fatigue gage data for the gages on the standard motor tubes are displayed in graphical form in figure 6 as resistance change versus cycles to failure.

### RESISTANCE CHANGES DURING APG 5,000 MILE (+ 1,600 MILES) ROAD TEST

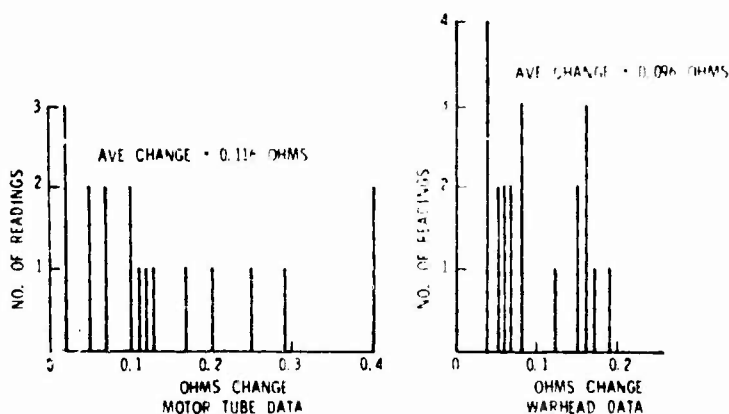


Figure 5 (left)  
Resistance Changes  
on Motor Tube and  
Warhead Clamp Ring  
Grooves.

### MOTOR TUBE FATIGUE GAGE DATA WHEN TESTED USING 15,000 IN.-LB BENDING MOMENT AT WH-MTR JOINT

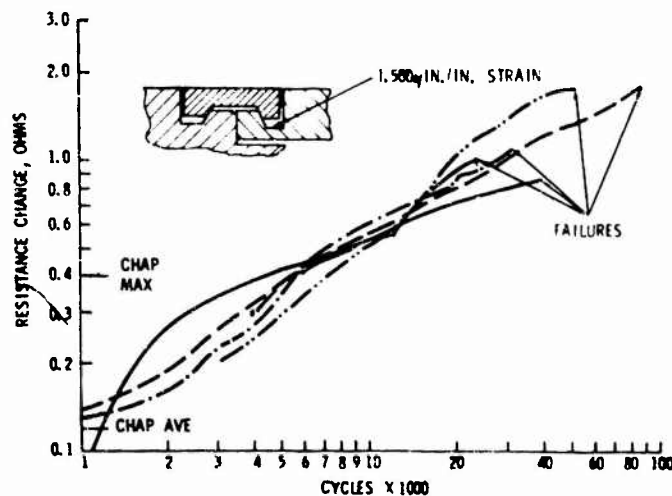


Figure 6 (right)  
Resistance Changes  
From Fatigue Tests  
on Motor Tubes.

There is a spread of resistance changes from 0.85-ohm at 38,000 cycles to failure to 1.7-ohms at 82,000 cycles to failure.

The three modified motor tubes withstood 180,000, 325,000 and 417,000 cycles to failure. Unfortunately, only one of these, the 180,000 cycles to failure specimen, had a fatigue gage on it. This gage had a resistance change of 2.48 ohms.

#### CONCLUSIONS

There are three conclusions that can be made from these data. These are:

1. The resistance changes in the fatigue gages on the 12 Chaparral missiles used during the road and cross-country tests are negligible compared to the total resistance changes to failure incurred in the laboratory specimens. The 12 missiles were not structurally degraded during the road and cross country tests as is confirmed by these data.
2. The modification of the motor tubes represents a marked improvement in the fatigue life of the motor tube
3. The use of S/N fatigue gages can be used to accurately determine the equivalent structural degradation between field induced damage and laboratory induced damage. The question of over- or under-testing can essentially be eliminated.

Certain precautions are in order, however, before blindly applying fatigue gages to a specimen. The proper use of fatigue gages is predicated on the same engineering principles as the use of any other data transducer. The proper installation of the gages at the correct points on the specimen implies that stress-strain peculiarities of the specimen must be examined by the application of brittle coating, strain gage, or photo-elastic techniques, or through the knowledge of previous failures before instrumentation is begun.

Also, absolute control of the test operation and data acquisition must be attained. This precludes the introduction of spurious parameters which can compromise test results.

#### REFERENCES

1. Applications Manual for the S/N Fatigue Life Gage, Micro-Measurements Inc., August 1966.
2. Proceedings of Technical Committee on Strain Gages. Society for Experimental Stress Analysis, May 16, 1967.
3. G. Maki and P. Soresen, "Worst Case Mechanical Tolerance Analysis of the Warhead Case and Motor Tube Interface for The Chaparral Missile System" ARINC Research Corporation Publication W7-408-TN031-1, April 19, 1967.
4. T. B. Cost "Chaparral Motor Tube/Warhead Interface Structural Testing Report "NavWpnsCen Report of 2 July 1968 (Code 5517).

## HOLOGRAM INTERFEROMETRY AS A PRACTICAL VIBRATION MEASUREMENT TECHNIQUE

Cameron D. Johnson and Gerald M. Moyer  
U. S. Navy Underwater Sound Laboratory  
Fort Trumbull, New London, Connecticut 06320

Hologram interferometry, a technique that has been described primarily in the optical literature, is an eminently practical means of measuring mechanical vibrations. The process uses coherent illumination to produce an optical interference pattern on the surface of a vibrating object. Qualitative and quantitative information is readily obtained from the interference pattern. Unlike conventional interferometry, this technique is simple and straightforward and does not require an optically polished specimen. An example in which hologram interferometry was used to study the vibration behavior of two plate specimens is presented. The mode shapes of 36 discrete resonant modes were photographed and used to draw conclusions concerning boundary conditions, assembly procedures, and material properties. It is concluded that the time has come for mechanical engineers to start taking advantage of this new area of optical technology.

### INTRODUCTION

Hologram interferometry as a vibration measurement technique was introduced by Powell and Stetson<sup>1</sup> in December 1965. Although their work has vast potential application in the field of mechanics, most of the subsequent papers dealing with the topic have appeared in the optical literature. It is the intent of this paper to discuss the practical applications of the technique and to encourage its use by those engaged in measuring mechanical vibrations.

### THE HOLOGRAPHY PROCESS

Holography is a specialized photographic process for recording the interaction of two coherent light fields on high resolution film plates. The necessary equipment for making a hologram is shown in Fig. 1. The output from the helium-neon laser is divided by a beam splitter into a reference beam and an object beam. The reference beam is expanded and directed onto a photographic plate, and the object beam is expanded and directed onto the object to be photographed. The photographic plate then records the interaction of the reference beam and the light scattered from the object.

Since the photographic plate is a record of light fields rather than images, the finished plate appears to be merely a light-fogged plate containing no useful information. It is not possible to deduce the subject of a hologram by examining the plate under normal room-lighting conditions. However, since coherent light was used in the recording process, the hologram contains not only the amplitude information

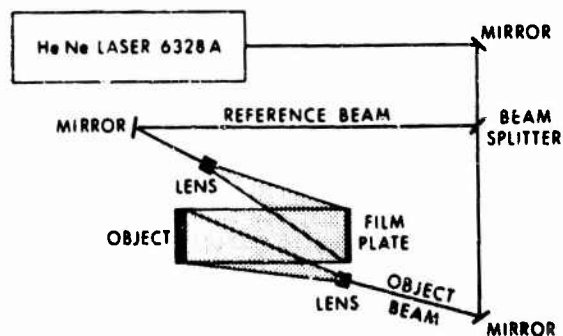


Fig. 1 - Holography Apparatus

found on a normal photograph but also phase information. The hologram is viewed by illuminating it with a coherent light source and looking through the plate exactly as if looking through a window. The original object is then visible in a perfect three-dimensional image having exactly the same spatial orientation that it had when the hologram was exposed. The three-dimensional property has caused a great deal of speculation about the feasibility of three-dimensional television, motion pictures, and training devices, and a host of other glamorous applications. A somewhat more prosaic application, but one which offers immediate technical rewards, is the measurement of mechanical vibrations.

### HOLOGRAM INTERFEROMETRY

Holography is in itself an interferometric process, with interference occurring, on a microscopic scale, between the reference and object beams. The interference phenomenon of interest in engineering measurements, however, is the macroscopic interference between two images in double or multiple exposures with a small change in object position occurring between exposures. Fringes will appear on the surface of the object at intervals corresponding to changes in the pathlength of light in one-wavelength increments. The most significant advantage of hologram interferometry over conventional interferometry is that no special surface preparation is required. Conventional interferometry requires an optically perfect surface to work from, whereas any diffusely reflecting surface will produce good results with hologram interferometry. This characteristic makes it possible to use hologram interferometry to measure surface deformations of engineering structures of practical interest.

Hologram interferometry may be used for static or dynamic measurements, and in both cases it offers significant advantages over other available techniques. It is a non-contact measurement and therefore does not in any way load the structure to be measured. More significantly, it is a continuous measurement that provides detailed information on the deformation of all points on the surface simultaneously.

Hologram interferometry is accomplished by making a double exposure of the object and introducing a surface deformation between exposures. The resulting hologram will contain two nearly identical images that differ only by the deformation introduced between exposures. If the surface deformation is in the order of several wavelengths of the light used for illumination, the object will have superimposed on it a number of interference fringes that accurately describe the nature of the deformation. The fringes are then read exactly like a contour map, with the fringes representing lines of constant displacements that have caused changes in the pathlength of the object beam in one-wavelength

increments. From a practical standpoint, deformations ranging from  $10 \times 10^{-6}$  to  $500 \times 10^{-6}$  inches may be conveniently observed. Techniques are available, at some sacrifice in convenience, for extending the range to several thousandths of an inch.

The application of hologram interferometry to vibrating surfaces is accomplished by a method similar to that described above, except that only one exposure is made and the object is vibrated during the exposure. Because the object is continually vibrating, the fringe pattern is continually changing, and the resultant hologram contains the superposition of an infinite number of positions. Since the photographic emulsion integrates the incident light during the exposure, the resultant fringe pattern is related to the probability density function of the amplitude, which, for sinusoidal vibration, results in comparison between positions near the positive and negative peaks.

The occurrence of fringes for sinusoidal vibration may be described by Eq. (1),

$$I = J_0^2 \left[ \frac{2\pi}{\lambda} (\cos \phi_1 + \cos \phi_2) \delta \right] I_{ST} \quad (1)$$

where  $I$  is the intensity of the image,  $I_{ST}$  is the intensity of the image if the object were stationary,  $J_0$  is the zero-order Bessel function,  $\lambda$  is the wavelength of the coherent illumination,  $\phi_1$  and  $\phi_2$  are the angles between the object beam and the normal to the vibrating surface and between the axis of observation and the normal to the vibrating surface, respectively, and  $\delta$  is the displacement. A plot of the square of the zero-order Bessel function is shown in Fig. 2. It can be seen that the maximum value of  $J_0^2 [\xi]$  occurs when  $[\xi] = 0$ . Since that condition exists only when the displacement is equal to zero, nodal regions are easily identified in the holo-

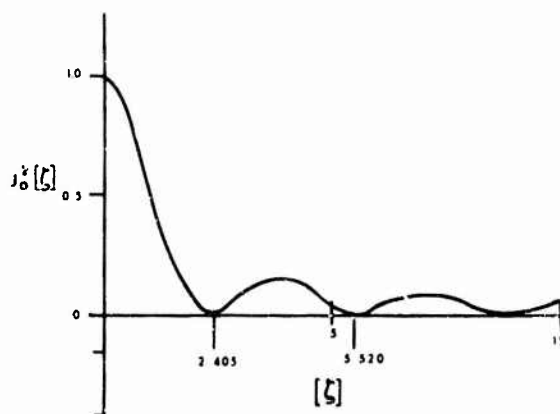


Fig. 2 -  $J_0^2 [\xi]$  Bessel Function

gram by their high relative intensity. Dark fringes occur at the tangent points of the Bessel function with the zero axis. The amplitude associated with each fringe may then be calculated by equating the argument of the Bessel function in Eq. (1) to the numerical value of  $J_0$  at the tangent points and solving for  $\delta$ .

#### APPLICATION TO VIBRATION MEASUREMENT

A good example of the value of hologram interferometry is a study of the vibration response of two plate models used in a hydrodynamic research project at the Underwater Sound Laboratory. The plate specimens were of stainless steel, 5 in. x 7 in. x .031 in. thick. They were soldered or cemented to a rectangular stainless steel frame made of 1/2-in.-square material having outside dimensions of 5 in. by 7 in.; thus, a 4-in. by 6-in. area of the plate was left free to vibrate and an approximation of a clamped boundary condition for the plate was established. The plates were cut from commercial rolled stainless steel stock and were sandblasted after assembly.

The holography study had the following objectives:

1. Determine whether the 1/2-in.-square frame provided a suitable approximation of a clamped boundary condition,
2. Determine whether cementing was a suitable assembly procedure for attaching the plate to the frame,
3. Determine whether anisotropic material properties due to the preferred grain orientation resulting from the rolling process had an appreciable effect on the resonant modal structure of the plate,
4. Identify the frequency and mode shape of as many resonant modes as possible.

The basic work table was a 4-ft. by 8-ft. by 10-in.-thick granite toolroom inspection plate mounted on a three-point low-frequency air-servo suspension system. A helium-neon laser, the optical elements, and the test specimen were mounted on the granite slab. The excitation was provided by air-coupling by placing an 8-in. loudspeaker behind the plate specimen and driving it with the amplified output from an audio-frequency oscillator. An electronic counter was used for precise frequency determination.

The hologram recordings were made by the conventional two-beam process, in which the laser output is split into reference and object beams, which are expanded and directed on the photographic plate and the test specimen, respectively. Kodak type 649-F high resolution spectroscopic film plate was used for all holograms. No special precautions other than

providing inherent stability by means of the air-mounted granite slab were necessary.

All holograms were of the time-averaged type, in which the nodal regions are readily apparent from their high relative brightness and the fringes are read like a contour map. An example of this physical interpretation is shown in Fig. 3 for one of the higher-order modes, for which the reconstructed image of the hologram and the corresponding model of the deformed surface are shown side by side.

The specimen subjected to the most intensive analysis was one in which the plate was silver-soldered to the frame. A resonance study of this plate was made with the plate standing upright on one of its 7-in. sides and with no additional support provided. Resonance frequencies were tuned by detecting maximum displacement with a non-contact fiber-optic-probe sensing device. Holograms were exposed at each resonance detected. A total of 36 discrete modes were identified in this manner and were used as the basis of comparison for all other phases of the investigation. The modes are characterized by essentially rectangular nodal patterns and are catalogued by a two-number system in which the first number designates the number of vertical nodal lines and the second number the number of horizontal nodal lines. Thus, by this convention, the primary mode is designated (0,0), and the (2,3) mode is that which has 12 regions of vibration separated by a nodal matrix having two vertical and three horizontal nodal lines. The 36 modes detected are shown in Figs. 4 through 6.

The modes shown do not represent all the resonant modes present in the frequency range examined, as several were not excited to a sufficient amplitude to permit a hologram to be made. They do, however, contain sufficient information to accurately predict the frequency and shape of many of the missing modes. A convenient graphical representation may be made by holding one mode number constant and plotting the other mode number against frequency. In the resulting family of curves, typical curves represent all modes having zero horizontal nodal lines, one horizontal nodal line, two horizontal nodal lines, etc. A representative curve, then, contains the (0,0), (1,0), (2,0), (3,0), (4,0), (5,0), (6,0), and (7,0) modes. Intermediate modes, i.e., those at frequencies between the highest and lowest recorded on any given curve, can be predicted with precision, and a good approximation of modes of higher frequency may be made by extrapolation. This was, in several instances, demonstrated in the resonance study by predicting the location of a missing mode and obtaining a hologram at the predicted frequency. The family of modal curves for this plate is given in Fig. 7.

It is interesting to note the comparative ease with

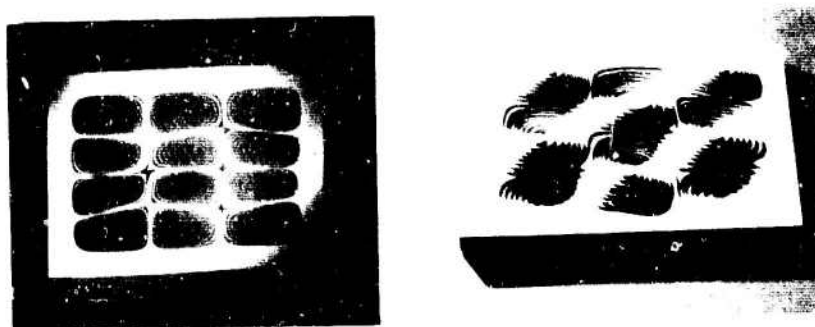


Fig. 3 - Physical Interpretation of Representative Mode of Vibration

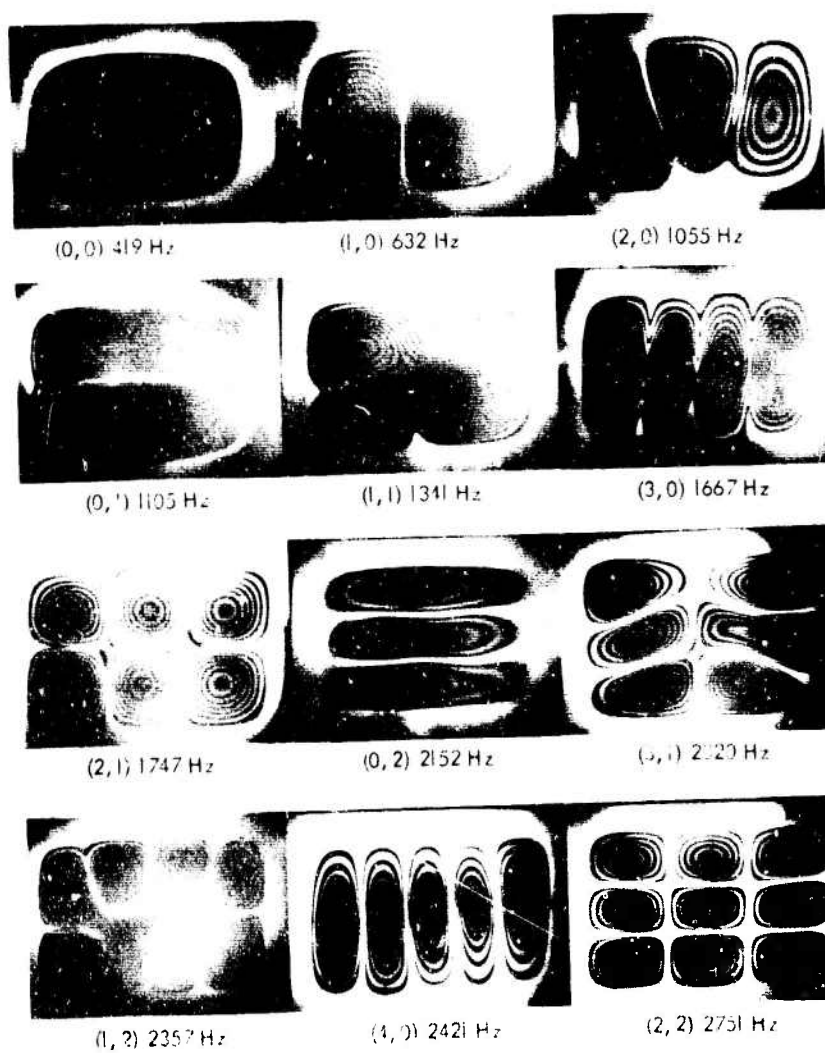


Fig. 4 - Vibration of Flow Noise Plate for Modes 1 through 12

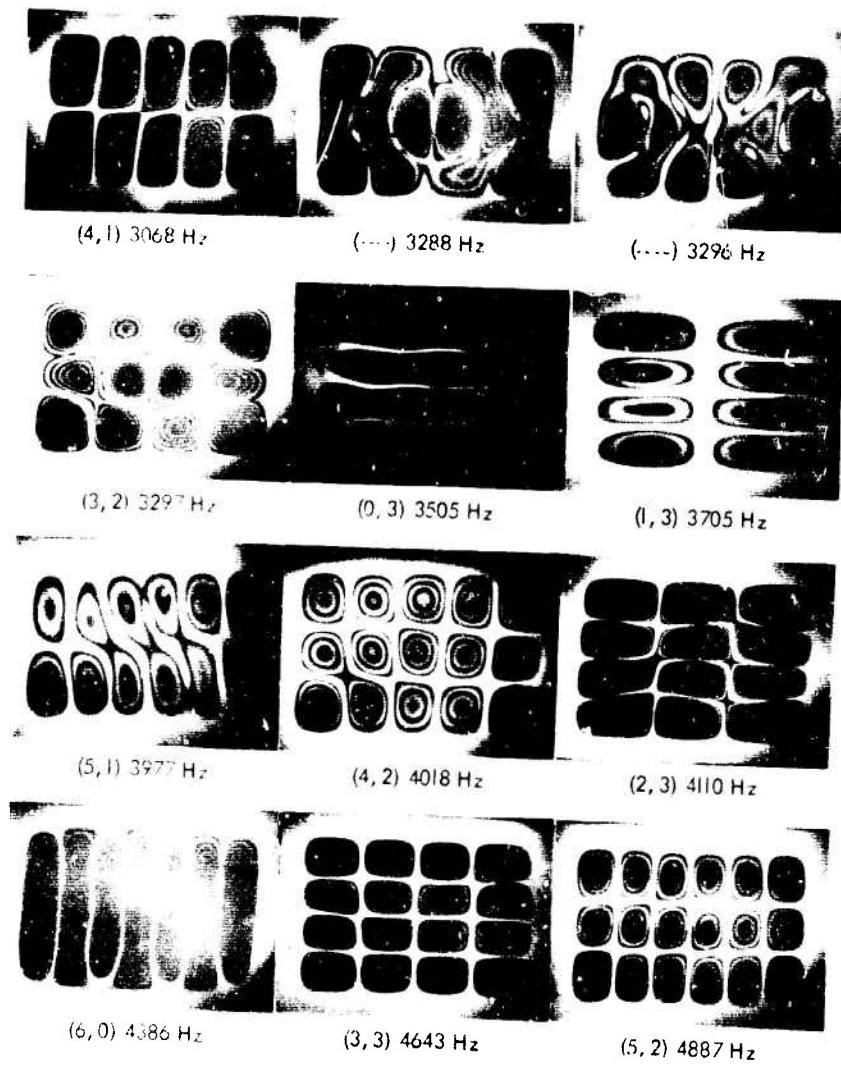


Fig. 5 - Vibration of Flow Noise Plate for Modes 13 through 24



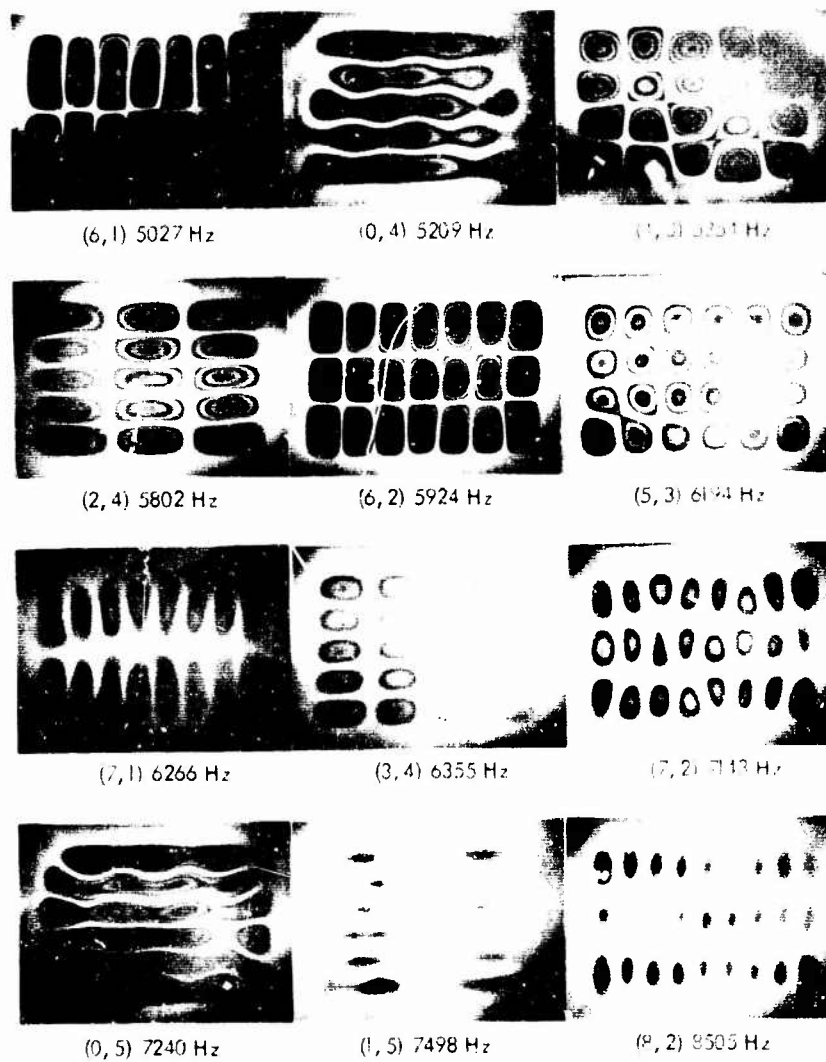


Fig. 6 - Vibration of Flow Noise Plate for Modes 25 through 36

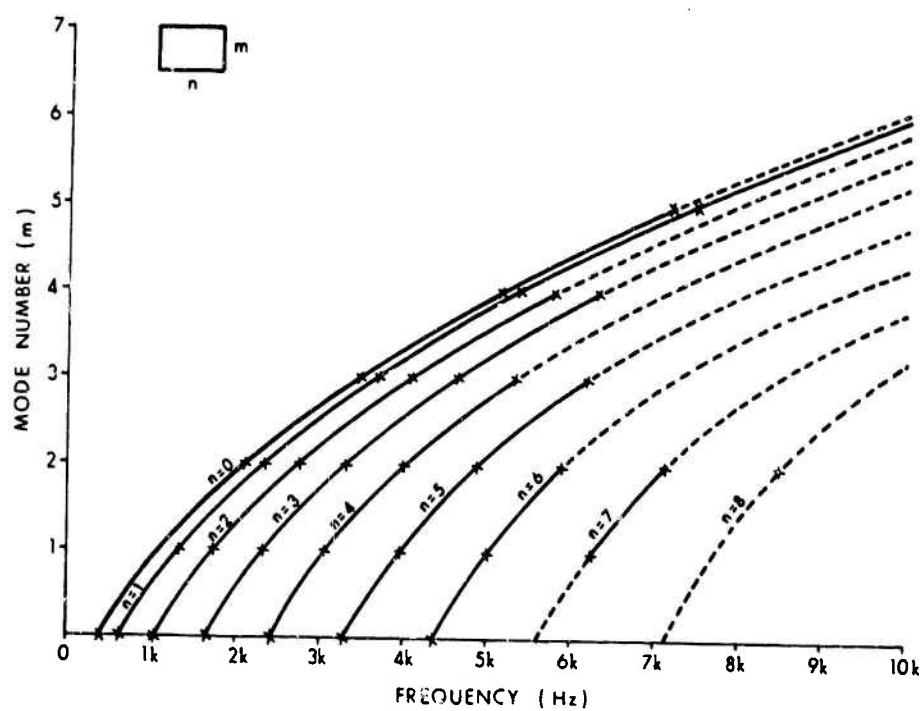


Fig. 7 - Characteristic Frequency Curves of Flow Noise Plate

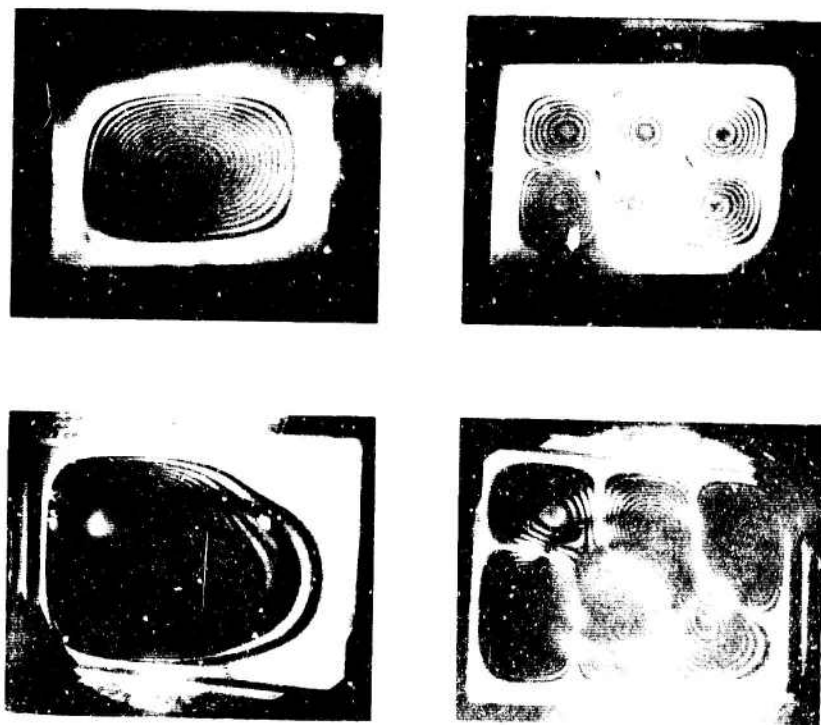


Fig. 8 - Effect of Additional Restraints on Plate Boundary

which such a resonance study was accomplished with holography. Although it is certainly possible to identify resonance frequencies with a point measuring device such as a fiber optic probe, the number of point measurements required to identify each particular mode is prohibitive for all but the first few mode shapes.

The other objectives were accomplished by comparing the results of other selected test conditions with the results of the basic resonance study. The assumption of a fixed boundary condition for the plate was disproved by examining the first several modes of the same plate with additional restraints placed on

the boundary. The additional restraints severely distorted the nodal patterns, as shown in Fig. 8. Additional restraints would have had no effect on the mode shapes if the 1/2-in.-square framework had been sufficiently stiff to establish the desired fixed boundary condition by itself.

The suitability of cementing rather than soldering as a means of attaching the plate to the framework was examined by making holograms of a cemented plate and comparing the mode shapes to those obtained with the soldered plate. A sampling of some of the corresponding modes is shown in Fig. 9. It was concluded from this study that cementing is a suitable method of

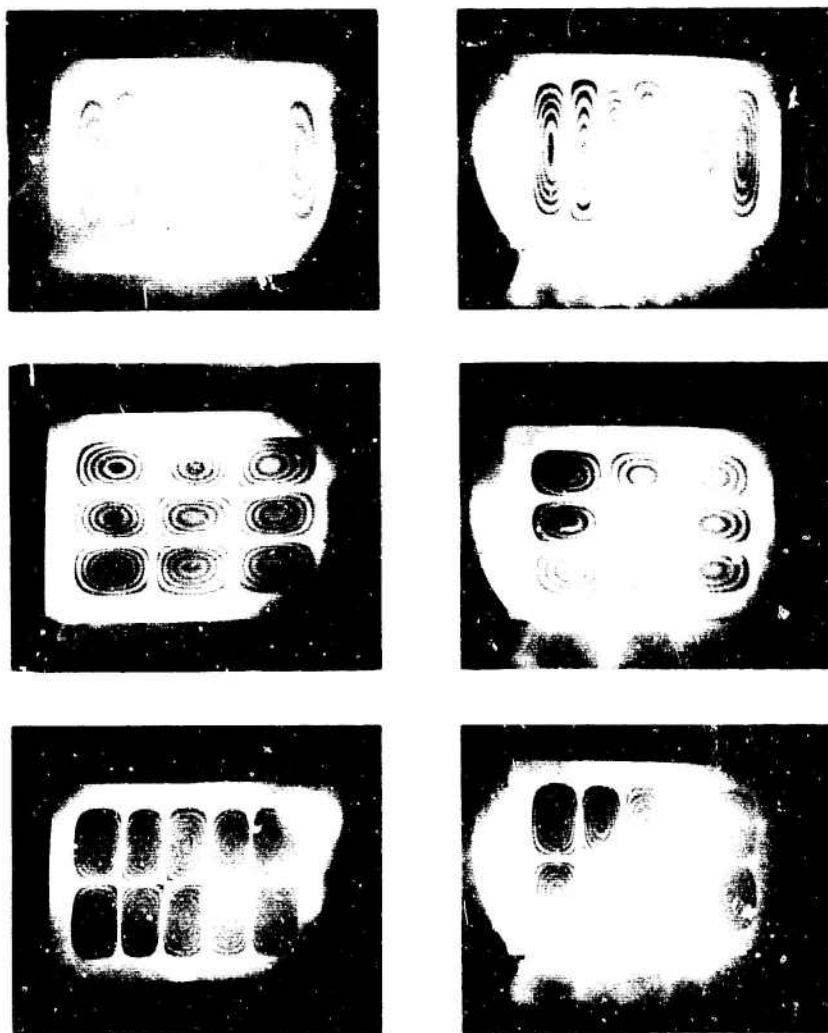


Fig. 9 - Comparison of Representative Modes of Cemented and Soldered Plates

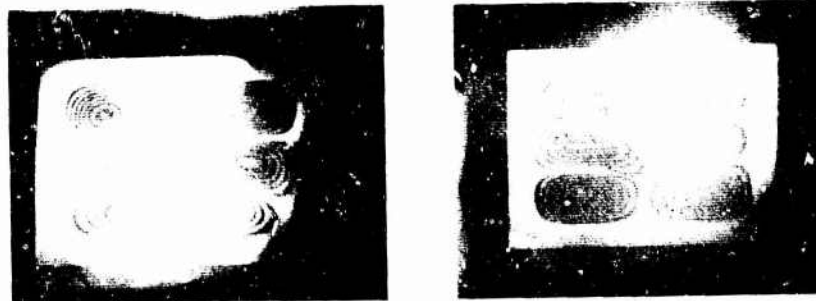


Fig. 10 - Mode Distortion Due to Anisotropic Material

attaching the plate to its supporting structure.

That the anisotropic material properties have an effect on the model structure is evident from the distortions observed in the (1,2) mode. A comparison of the behavior of the soldered and cemented plates reveals that the distortion is unchanged; this is to be expected as the specimens were cut from the same piece of stock. The comparison suggests that the distortion is independent of the manner in which the plates are secured to the framework and also that it is not due to an effect introduced by heating one of the plates in the soldering process. As a final check to preclude the possibility that the distortion was due to the manner in which the plate was driven, the plate was inverted and another hologram was exposed. The fact that the resulting distortion was also inverted indicates that it was due to an inherent characteristic of the plate material rather than to the method of mounting or driving. The above comparisons are shown in Fig. 10.

## CONCLUSIONS

In the example stated above, hologram interferometry was used to analyze the vibration characteristics of plate specimens to an extent that would have been impractical with conventional vibration measurement techniques. Hologram interferometry is a simple, straightforward procedure and is well within the technical capability and financial means of most research laboratories. The time has come to stop thinking of holography as an interesting optical curiosity and to start exploiting its potential in the mechanical measurements laboratory.

## REFERENCE

1. R. L. Powell and K. A. Stetson, "Interferometric Vibration Analysis by Wavefront Reconstruction," *J. Opt. Soc. Am.*, Vol. 55, No. 12, pp. 1593-1598, Dec. 1965.

## DISCUSSION

**Mr. Jackman (General Dynamics/Pomona):** This was a very interesting paper. The thing that intrigued me most was the three dimensional or isometric view that you showed. The one that shows the depth and the two outer phase conditions. How was that obtained?

**Mr. Johnson:** This was simply made by taking a picture of the hologram which you saw previously and making a model by cutting layers. Each layer was a piece of 1/16-inch balsa wood, and the layers were just stacked up according

to the fringes - cut out along the fringes from the picture.

**Mr. Miller (Itek Corp.):** Have you used ruby lasers in your holographic setups to measure transient vibrations?

**Mr. Johnson:** We have not done it ourselves, however, some very fine work has been done in this area by Worker of TRW and some work has been done on particle analysis in fog and, as I said, oxidation in rocket engines.

RESPONSE OF AN ELASTIC STRUCTURE INVOLVING  
CROSS CORRELATIONS BETWEEN TWO RANDOMLY VARYING EXCITATION FORCES

A. Razziano  
Grumman Aircraft Engineering Corporation  
Bethpage, New York

and

J. R. Curreri  
Polytechnic Institute of Brooklyn  
Brooklyn, New York

This paper presents the results of an investigation to show the importance of considering cross correlations between shaker inputs in environmental vibration tests. General responses to two random loadings that are uncorrelated, directly correlated, and having various time lags are determined. The general equations were then applied to a simply supported beam, and response curves plotted for a point on the beam for the three random input cases. The beam response at the prescribed location will then obviously be the input to any piece of equipment mounted at that point. These response curves reveal the magnitude of errors involved when cross correlation between the two shaker inputs is not taken into consideration.

INTRODUCTION

Effects of cross correlation between two shaker random excitations in the field of environmental testing has not been to date taken into consideration. It is the intent of this report to reveal the necessity to do so by analyzing three cases, uncorrelated, directly correlated, and various time lags between random inputs to a simply supported beam with motion input. The beam responses for each case will indicate that cross correlation between the inputs and its time position on the time scale of the correlation function has a real importance and that neglecting it would lead to an erroneous response spectrum, and in turn an erroneous input environment to equipment mounted on the beam.

A literature search revealed that work had been performed in the area of cross correlated excitations. M. Trubert (1) published a report on investigation in determining the response of a linear continuous structure (cantilever beam) to random loadings of various correlations by a semi-experimental method. Transfer functions were determined and the natural frequency was chosen high enough so that only the first mode was involved in the investigation. Similar work was reported by H. Kizner (2) which involved an experimental determination of transfer functions of beams and plates by cross correlation techniques. Again, a cantilever

beam was used for the model, and only the first mode was used in the investigation. In both investigations reported excitation forces were applied directly to the beam, and both noted the effects of cross correlation of two excitation forces on the response of the beam.

In the analytical investigation reported herein, the model is a simply supported beam with two input excitations at the supports. This was done to simulate typical spacecraft environmental tests. General theory was found in the text written by J. Robson (3) and applied to our model beam. This model was selected so that effects of the first three modes could be investigated. Aside from this being a typical case, the author wanted to determine effects of cross correlations on combined symmetrical and unsymmetrical modes. It should be made clear that the transfer functions used in the random response analysis is obtained as a result of a sinusoidal input. The functions are then shaped by random spectral density inputs which includes uncorrelated and cross correlated terms, and are statistical in nature.

GENERAL RESPONSE TO TWO RANDOM LOADINGS  
(Effect of Cross Correlation of Two Random Force Inputs on the General Response)

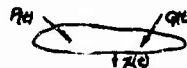


Figure 1 - Response of Elastic Structure to Two Loads

$P(t)$  and  $Q(t)$  = two random loadings acting simultaneously, but at different points.

$x(t)$  = resulting displacement of a given point in a given direction.

The spectral density of  $x(t)$  can be expressed in terms of the spectral densities of  $P(t)$  and  $Q(t)$  by means of the autocorrelation functions.

Let the autocorrelation function of  $x(t)$ ,  $P(t)$  and  $Q(t)$  be  $R_x(\tau)$  and  $R_q(\tau)$ .

$R_x(\tau) = \langle x(t) x(t + \tau) \rangle$  where the brackets represent a mean value (2.1)

$$= \left\langle \int_0^\infty \int_0^\infty W_{xp}(\tau_1) P(t - \tau_1) + W_{xq}(\tau_1) Q(t - \tau_1) \right. \\ \left. d\tau_1 \int_0^\infty [W_{xp}(\tau_2) P(t - \tau_2 + \tau) + W_{xq}(\tau_2) Q(t - \tau_2 + \tau)] d\tau_2 \right\rangle$$

where the above integral is known as Duhamel's integral, or the convolution integral and  $W_{xp}(t)$  and  $W_{xq}(t)$  = weighting functions giving the response to a unit impulse.

$\alpha_{xp}$  and  $\alpha_{xq}$  = receptance for harmonic excitation

$$R_x(\tau) = \int_0^\infty \int_0^\infty W_{xp}(\tau_1) \left[ \int_0^\infty W_{xp}(\tau_2) \langle P(t) \right. \\ \left. P(t + \tau_1 - \tau_2 + \tau) \rangle d\tau_2 \right] d\tau_1 \\ + \int_0^\infty \int_0^\infty W_{xp}(\tau_1) \left[ \int_0^\infty W_{xp}(\tau_2) \langle P(t) \right. \\ \left. Q(t + \tau_1 - \tau_2 + \tau) \rangle d\tau_2 \right] d\tau_1 \\ + \int_0^\infty \int_0^\infty W_{xp}(\tau_1) \left[ \int_0^\infty W_{xp}(\tau_2) \langle Q(t) \right. \\ \left. P(t + \tau_1 - \tau_2 + \tau) \rangle d\tau_2 \right] d\tau_1 \\ + \int_0^\infty \int_0^\infty W_{xp}(\tau_1) \left[ \int_0^\infty W_{xp}(\tau_2) \langle Q(t) \right. \\ \left. Q(t + \tau_1 - \tau_2 + \tau) \rangle d\tau_2 \right] d\tau_1 \quad (2.2)$$

The mixed quantities in the first and last terms are simply autocorrelation functions and may be written as  $R_p(\tau_1 - \tau_2 + \tau)$ ,  $R_q(\tau_1 - \tau_2 + \tau)$ . The corresponding quantities in the second and third terms are cross correlations functions as defined by;

$$R_{pq}(\tau) = \langle P(t) Q(t + \tau) \rangle \quad (2.3)$$

They can be written as follows:

$$R_{pq}(\tau_1 - \tau_2 + \tau) \text{ and } R_{qp}(\tau_1 - \tau_2 + \tau)$$

The autocorrelation function of the response is therefore;

$$R_x(\tau) = \int_0^\infty \int_0^\infty W_{xp}(\tau_1) \left[ \int_0^\infty W_{xp}(\tau_2) R_p \right. \\ \left. (\tau_1 - \tau_2 + \tau) d\tau_2 \right] d\tau_1 \\ + \int_0^\infty \int_0^\infty W_{xp}(\tau_1) \left[ \int_0^\infty W_{xq}(\tau_2) R_{pq} \right. \\ \left. (\tau_1 - \tau_2 + \tau) d\tau_2 \right] d\tau_1 \\ + \int_0^\infty \int_0^\infty W_{xq}(\tau_1) \left[ \int_0^\infty W_{xp}(\tau_2) R_{qp} \right. \\ \left. (\tau_1 - \tau_2 + \tau) d\tau_2 \right] d\tau_1 \\ + \int_0^\infty \int_0^\infty W_{xq}(\tau_1) \left[ \int_0^\infty W_{xq}(\tau_2) R_q \right. \\ \left. (\tau_1 - \tau_2 + \tau) d\tau_2 \right] d\tau_1 \quad (2.4)$$

By using the Fourier transform relationship between  $S_x(f)$  and  $R_x(\tau)$  we have

$$S_x(f) = 2 \int_0^\infty R_x(\tau) e^{-i 2\pi f \tau} d\tau \quad (2.5)$$

by substituting Equation (2.4) into Equation (2.5) results in the following;

$$S_x(f) = \alpha_{xp}^* \alpha_{xp} S_p(f) + \alpha_{xp}^* \alpha_{xq} S_{pq}(f) \\ + \alpha_{xq}^* \alpha_{xp} S_{qp}(f) + \alpha_{xq}^* \alpha_{xq} S_q(f) \quad (2.6)$$

where the cross spectral density  $S_{pq}(f)$  is given by:

$$S_{pq}(f) = 2 \int_0^\infty R_{pq}(\tau) e^{-i 2\pi f \tau} d\tau \quad (2.7)$$

So the spectral density of the response cannot be determined from knowledge only of the spectral densities  $S_p(f)$  and  $S_q(f)$  of the applied forces; a knowledge of the two cross spectral densities  $S_{pq}(f)$  and  $S_{qp}(f)$  is also necessary.

The effect of cross correlation can be illustrated by determining the combined responses due to two randomly varying forces,  $P(t)$  and  $Q(t)$ , considering these to be first uncorrelated, and then to be correlated in such a way that  $P(t)$  and  $Q(t)$  have a constant ratio.

#### Case I

For no correlation between force inputs  $P(t)$  and  $Q(t)$

If  $P(t)$  and  $Q(t)$  arise from quite independent sources - the cross-correlation functions  $R_{pq}(\tau)$  and  $R_{qp}(\tau)$ , and so the

cross spectral densities  $S_{pq}(f)$  and  $S_{qp}(f)$ ,

will be zero. It is assumed, unless the opposite is obviously implied, that all randomly varying quantities have zero mean value. Equation (2.6) then reduces to

$$S_x(f) = |\alpha_{xp}|^2 S_p(f) + |\alpha_{xq}|^2 S_q(f) \quad (2.8)$$

The response spectral density in this case is thus simply the sum of the two response spectral densities obtained with the forces acting separately.

#### Case II

If  $P(t)$  and  $Q(t)$  are directly correlated so that  $Q(t) = kP(t)$  where  $k$  is a constant, then

$$R_{pq}(\tau) = \langle P(t) \cdot k P(t + \tau) \rangle = k R_p(\tau)$$

$$R_{qp}(\tau) = \langle k P(t) \cdot P(t + \tau) \rangle = k R_p(\tau)$$

$$R_q(\tau) = \langle k P(t) \cdot k P(t + \tau) \rangle = k^2 R_p(\tau)$$

Using the known relations between correlation functions and spectral densities we have:

$$S_{pq}(f) = k S_p(f), S_{qp}(f) = k S_p(f), S_q(f) = k^2 S_p(f)$$

Equation (2.6) now gives the following:

$$S_x(f) = \alpha_{xp}^* \alpha_{xp} S_p(f) + \alpha_{xp}^* \alpha_{xq} k S_p(f)$$

$$+ \alpha_{xq}^* \alpha_{xp} k S_p(f) + \alpha_{xq}^* \alpha_{xq} k^2 S_p(f)$$

$$S_x(f) = (\alpha_{xp}^* + k \alpha_{xq}^*) (\alpha_{xp} + k \alpha_{xq}) S_p(f)$$

$$S_x(f) = |\alpha_{xp} + k \alpha_{xq}|^2 S_p(f)$$

The spectral density of the response now depends on the modulus of a vector sum of two receptances and so on the relative phase of the two receptances.

#### Case III

Consider the case where the spectral densities of the two loadings are identical; that is where

$$S_p(f) = S_q(f) = S(f)$$

If the forces are uncorrelated, we see from Equation (2.8) that

$$S_x(f) = [|\alpha_{xp}|^2 + |\alpha_{xq}|^2] S(f) \quad (2.9)$$

whereas,

If the forces are directly correlated, for  $S_p(f) = S_q(f)$  implies that  $k = 1$  we have

$$S_x(f) = |\alpha_{xp} + \alpha_{xq}|^2 S(f) \quad (2.10)$$

Equation (2.10) may be written as

$$S_x(f) = \left[ |\alpha_{xp}|^2 + |\alpha_{xq}|^2 + 2|\alpha_{xp}||\alpha_{xq}| \cos \phi \right] S(f) \quad (2.11)$$

where  $\phi$  is the phase difference between the two receptances at the particular frequency  $f$ , and in this form it is more easily compared with Equation (2.9). Clearly the result for the uncorrelated loadings given by Equation (2.9) will only be equal to that for the correlated loadings given by Equation (2.11) when  $\cos \phi = 0$  that is when  $\phi = \pm \frac{\pi}{2}$ . For other values of  $\phi$  the spectral density in the correlated case may have any value between  $[|\alpha_{xp}| - |\alpha_{xq}|]^2 S(f)$  and  $[|\alpha_{xp}| + |\alpha_{xq}|]^2 S(f)$  depending on the values of  $\cos \phi$ . If  $\alpha_{xp} = -\alpha_{xq}$  at some frequency, the spectral density at that frequency in the correlated case will be zero. For any frequency at which  $\alpha_{xp} = \alpha_{xq}$ , the spectral density with correlation will be twice that obtained without it.

These last results could have been inferred without using Equation (2.6) by considering the discrete frequency response to in-phase and out-of-phase loadings at the two excitation points.

#### Case IV

When  $Q(t)$  reproduces  $P(t)$  after a lag of  $\tau_0$  so that  $Q(t) = P(t + \tau_0)$ .

In this case

$$R_{PQ}(\tau) = \langle P(t) P(t + \tau_0 + \tau) \rangle = R_P(\tau_0 + \tau)$$

Using Equation (2.7)

$$\begin{aligned} S_{PQ}(f) &= 2 \int_0^\infty R_P(\tau_0 + \tau) e^{-2\pi i f \tau} d\tau \\ &= 2e^{-2\pi i f \tau_0} \int_0^\infty R_P(\tau) e^{-2\pi i f \tau} d\tau \\ &= e^{-2\pi i f \tau_0} S_P(f) \end{aligned}$$

As  $S_{QP}(f)$  and  $S_{PQ}(f)$  are complex conjugates, we have also  $S_{PQ}(f) = e^{-2\pi i f \tau_0} S(f)$

and obviously  $S_Q(f) = S_P(f)$

Equation (2.6) now becomes

$$S_x(f) = \left[ \alpha_{xp}^* \alpha_{xp} + e^{-2\pi i f \tau_0} \alpha_{xp}^* \alpha_{xq} + e^{-2\pi i f \tau_0} \alpha_{xq}^* \alpha_{xq} \right] S(f) \quad (2.12)$$

#### General Determination of the Receptance (Transfer Function) To A Point Force Loading

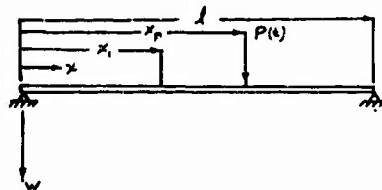


Figure 2 - General Response of a Beam

Consider a beam of length  $l$  as shown with a transverse point load  $P(t)$  acting at  $x = x_p$  and consider in particular the transverse displacement  $w(x_1, t)$  at  $x = x_1$ . To obtain the response to random  $P(t)$  we must obtain the relevant receptance  $\alpha_{1p}$ , which defines the response at  $x = x_1$  due to harmonic excitation

of unit amplitude at  $x_p$ . To do this, therefore, we determine the response when

$P(t) = P_0 e^{i\omega t}$ . We must first set up the equations of motion of the system. The displacement at any point,  $w(x, t)$ , may be expressed in terms of the normal modes of the beam as

$$w(x, t) = \sum_r w_r(x) \xi_r(t) \quad (2.13)$$

where  $w_r(x)$  represents the  $r^{\text{th}}$  normal mode of the beam and  $\xi_r(t)$  are the normal coordinates.

Damping can also be included, either by adding a further term proportional to  $\dot{\xi}_r$ , or, when considering sinusoidal motion, by including an imaginary part in the stiffness term. (It is assumed that the damping is small, and that there is no coupling between the modes due to damping). We shall use the latter because hysteretic damping gives a good approximation to the behavior of an actual system. The exciting force is represented by generalized forces  $\Xi_r$ . The equation of motion in the  $r^{\text{th}}$  mode is

$$M_r \ddot{\xi}_r + M_r \omega_r^2 (1 + i \eta_r) \xi_r = \Xi_r$$

The generalized force  $\Xi_r$  corresponding to  $\xi_r$  is obtained by considering the work done,  $\delta w$ , in a virtual displacement  $\delta w(x)$ . Thus for



$$\begin{aligned}
P(t) &= P_0 e^{i\omega t} \\
\delta w &= P_0 e^{i\omega t} \delta w(x_p) \\
&= P_0 e^{i\omega t} \sum_r w_r(x_p) \delta \xi_r \\
\xi_r &\text{ must be such that } \delta w = \sum_r \xi_r \delta \xi_r \\
\xi_r &= w_r(x_p) P_0 e^{i\omega t}
\end{aligned}$$

The equations of motion may then be written

$$\begin{aligned}
M_r \ddot{\xi}_r + \omega_r^2 (1 + i\eta_r) M_r \xi_r &= \\
w_r(x_p) P_0 e^{i\omega t} \quad (r = 1, 2, \dots) \quad (2.14)
\end{aligned}$$

Solving Equation (2.14)

$$\xi_r = \frac{w_r(x_p) P_0 e^{i\omega t}}{M_r (\omega_r^2 - \omega^2 + i\eta_r \omega_r^2)}$$

Using Equation (2.13) yields

$$w(x_1, t) = P_0 e^{i\omega t} \sum_r \left[ \frac{w_r(x_1) w_r(x_p)}{M_r} \right]$$

$$\left( \frac{1}{\omega_r^2 - \omega^2 + i\eta_r \omega_r^2} \right)$$

$w(x_1, t)$  is therefore proportional to  $e^{i\omega t}$

let  $w(x_1, t) = w_0(x_1) e^{i\omega t}$

$$\begin{aligned}
\alpha_{lp} &= \frac{w_0(x_1)}{P_0} = \sum_r \left[ \frac{w_r(x_1) w_r(x_p)}{M_r} \right] \\
&\left( \frac{1}{\omega_r^2 - \omega^2 + i\eta_r \omega_r^2} \right) \\
\alpha_{lp} &= \sum_r \left[ \frac{w_r(x_1) w_r(x_p)}{M_r} \frac{(\omega_r^2 - \omega^2) - i\eta_r \omega_r^2}{(\omega_r^2 - \omega^2)^2 + \eta_r^2 \omega_r^4} \right] \quad (2.15)
\end{aligned}$$

The receptance in terms of frequency is

$$\begin{aligned}
f_r &= \frac{\omega_r}{2\pi} \\
\alpha_{lp} &= \sum_r \mu_r (X_r - iY_r) \quad (2.16)
\end{aligned}$$

where

$$\begin{aligned}
\mu_r &= \frac{w_r(x_1) w_r(x_p)}{M_r} \\
X_r &= \frac{f_r^2 - f^2}{4\pi^2 [(f_r^2 - f^2)^2 + \eta_r^2 f_r^4]} \\
Y_r &= \frac{\eta_r f_r^2}{4\pi^2 [(f_r^2 - f^2)^2 + \eta_r^2 f_r^4]}
\end{aligned}$$

When there is random excitation  $P(t)$ , the spectral density  $S_1(f)$  of the motion  $x_1$  is related to the spectral density  $S_p(f)$  of  $P(t)$ , at any frequency, by

$$S_1(f) = |\alpha_{lp}|^2 S_p(f) \quad (2.17)$$

From Equation (2.16)

$$|\alpha_{lp}|^2 = \sum_r \mu_r^2 X_r^2 + \sum_r \mu_r^2 Y_r^2 \quad (2.18)$$

$$= \sum_r \sum_s \mu_r \mu_s X_r X_s + \sum_r \sum_s \mu_r \mu_s Y_r Y_s$$

$$= \sum_r \sum_s \mu_r \mu_s (X_r X_s + Y_r Y_s)$$

$$|\alpha_{lp}|^2 = \sum_r \mu_r^2 (X_r^2 + Y_r^2) + \sum_{r \neq s} \mu_r \mu_s (X_r X_s + Y_r Y_s) \quad (2.19)$$

If the damping of the system is small, the peaks will be pronounced, and provided that the natural frequencies are well separated, the response in vicinity of the resonant frequency will be dominated by a single term of the summation. It follows that the product terms will be small relative to one single  $(X_r^2 + Y_r^2)$  term. Away from a resonance this will not be so, but in these regions some inaccuracy can be permitted because, as the magnitudes are so much smaller, such frequencies play little part in random vibration. Equation (2.19) therefore, reduces to the following:

$$|\alpha_{lp}|^2 = \sum_r \mu_r^2 (X_r^2 + Y_r^2) \quad (2.20)$$

substituting  $X_r^2$  and  $Y_r^2$  gives

$$|\alpha_{lp}|^2 = \frac{\mu_r^2}{16\pi^4 [(f_r^2 - f^2)^2 + \eta_r^2 f_r^4]}$$

If only a single term is important near any one peak, Equation (2.20) need not be written as a series. The response depends on two factors,  $\mu_r$ , which depends on the positioning of loading and measurement points with respect to the normal modes, and the magnitude of  $X_r, Y_r$  at the particular frequency. If, for any  $r$ ,  $w_r(x_1)$ , or  $w_r(x_p)$  is zero, that is if the loading or measuring device is situated at a node of any normal mode then  $\mu_r$  for that  $r$  is zero, and there is no response in that mode. For  $f$  close to any  $f_r$ , the corresponding mode will be greatly emphasized.

#### DETERMINATION OF THE RECEPTANCE TO A MOTION INPUT FOR A SIMPLY SUPPORTED BEAM

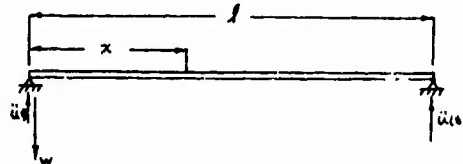


Figure 3 - Response of a Simply Supported Beam

As shown before the equation of motion in the  $r^{\text{th}}$  normal mode is as follows:

$$M_r \ddot{\xi}_r + M_r \omega_r^2 (1 + i\eta_r) \xi_r = \xi_r$$

$$\text{Let } \ddot{\xi}_r = -\omega_r^2 \xi_r$$

$M_r = \int_0^l w_r^2(x) m(x) dx$  is the generalized mass where  $m(x)$  = mass per unit length and is constant. (2.22)

and  $\ddot{\Xi}_r = \int_0^l w_r(x) m \ddot{u}(t) dx$  is the generalized forcing function. (2.23)

where  $\ddot{u}(t)$  is a sinusoidal input

$$M_r \ddot{\xi}_r - \frac{M_r \omega_r^2 (1 + i \eta_r) \xi_r}{\omega^2} = \ddot{\Xi}_r$$

$$\ddot{\xi}_r = \frac{\ddot{\Xi}_r}{M_r - \frac{M_r \omega_r^2 (1 + i \eta_r)}{\omega^2}}$$

The displacement of the beam at any point as expressed in terms of the normal modes is:

$$\ddot{w}(x, t) = \sum_r \frac{w_r(x)}{\omega_r^2} \ddot{\xi}_r$$

$$w(x, t) = \sum_r \frac{w_r(x) \ddot{\Xi}_r}{M_r - \frac{M_r \omega_r^2 (1 + i \eta_r)}{\omega^2}} \quad (2.24)$$

For a simply supported beam let the normal mode shape be expressed as follows;

$$w_r(x) = \sin \frac{r\pi x}{l} \text{ for } (r = 1, 2, 3, \dots) \quad (2.25)$$

substitute equation (2.25) into (2.22).

$$M_r = \int_0^l \sin^2 \frac{r\pi x}{l} dx$$

but due to orthogonality

$$\int_0^l \sin \frac{r\pi x}{l} \sin \frac{n\pi x}{l} dx = 0$$

if  $r \neq n$

$$\therefore M_r = m \int_0^l \left( \frac{1}{2} - \frac{1}{2} \cos \frac{2r\pi x}{l} \right) dx$$

$$M_r = m \frac{l}{2} \quad (2.26)$$

Substitute Equation (2.25) into (2.23)

$$\begin{aligned} \ddot{\Xi}_r &= \int_0^l w_r(x) m \ddot{u}(t) dx \\ &= m \ddot{u}(t) \int_0^l \sin \frac{r\pi x}{l} dx \\ &= -m \ddot{u}(t) \frac{2l}{r\pi} \end{aligned} \quad (2.27)$$

Substitute Equations (2.25), (2.26), and (2.27) into (2.24)

$$\ddot{w}(x, t) = -\sum_r \frac{\sin \frac{r\pi x}{l} m \ddot{u}(t) \frac{2l}{r\pi}}{m \frac{l}{2} \left( 1 - \frac{\omega_r^2 (1 + i \eta_r)}{\omega^2} \right)}$$

$$\ddot{w}(x, t) = \ddot{u}(t) \sum_r \frac{4 \sin \frac{r\pi x}{l}}{r\pi} \left( \frac{\omega^2}{\omega_r^2 - \omega^2 + i \eta_r \omega_r^2} \right) \quad (2.28)$$

This is the acceleration at any point along the beam due to a motion input at the two supports.

The receptance is obtained from Equation (2.28) as follows:

$$\alpha_{x,0,l} = \frac{\ddot{w}(x, t)}{\ddot{u}(t)} = \sum_r \frac{4 \sin \frac{r\pi x}{l}}{r\pi} \left( \frac{\omega^2}{\omega_r^2 - \omega^2 + i \eta_r \omega_r^2} \right) \quad (2.29)$$

$$\alpha_{x,0,l} = \sum_r \frac{4 \sin \frac{r\pi x}{l}}{r\pi} (X_r - i Y_r)$$

and as previously shown

$$|\alpha_{x,0,l}|^2 = \sum_r \frac{4 \sin^2 \frac{r\pi x}{l}}{r^2 \pi^2} (X_r^2 + Y_r^2)$$

$$|\alpha_{x,0,l}|^2 = \sum_r \frac{16 \sin^2 \frac{r\pi x}{l}}{r^2 \pi^2} \left( \frac{f^4}{(f_r^2 - f^2)^2 + \eta_r^2 f_r^2} \right) \quad (2.30)$$

where  $f = \frac{\omega}{2\pi}$

Equation (2.29) is the receptance at  $x$  due to motion input at  $x = 0$  and  $x = l$ .

The receptance forms which are needed in Equations (2.9), (2.10), and (2.11) are as follows:

$\alpha_{x,l}$  = receptance at  $x$  due to input at  $x=l$

$\alpha_{x_1,l}$  = receptance at  $x$  due to input at  $x_1=l$

To find  $\alpha_{x,l}$  the generalized forcing function changes to the following:

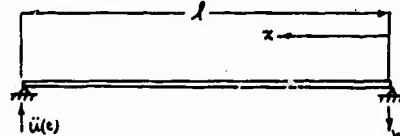


Figure 4 - Simply Supported Beam with Input at Left Support

$$\ddot{\Xi} = \int_0^l \left( \frac{x}{l} \right) w_r(x) m \ddot{u}(t) dx$$

where  $\frac{x}{l}$  is the rigid body mode shape

$$\ddot{\Xi} = \frac{m \ddot{u}(t)}{l} \int_0^l x \sin \frac{r\pi x}{l} dx$$

where the integral is of the form

$$\begin{aligned} \int_0^l x \sin ax dx &\text{ when } a = \frac{r\pi}{l} \\ &= \left[ \frac{1}{a^2} \sin ax - \frac{1}{a} x \cos ax \right]_0^l \end{aligned}$$

Therefore;

$$\ddot{u} = \frac{m \ddot{u}(t)}{r \pi} \quad \text{for } r = 1, 3, 5, \dots$$

$$\ddot{u} = \frac{m \ddot{u}(t)}{r \pi} \quad (r = 1, 3, 5, \dots) \quad (2.31)$$

and

$$\ddot{u} = -\frac{m \ddot{u}(t)}{r \pi} \quad (r = 2, 4, 6, \dots) \quad (2.32)$$

Substitute Equation (2.31) into (2.28)

$$\ddot{w}(x, t) = \sum_{r=1,3,5,\dots} \frac{\frac{m \ddot{u}(t)}{r \pi} \sin \frac{r \pi x}{l}}{\frac{m}{2} \left( \frac{\omega^2}{\omega_r^2 - \omega^2 + i \eta_r \omega_r^2} \right)}$$

$$\ddot{w}(x, t) = \sum_{r=1,3,5,\dots} \frac{2 \ddot{u}(t) \sin \frac{r \pi x}{l}}{r \pi}$$

$$\text{and,} \quad \left( \frac{\omega^2}{\omega_r^2 - \omega^2 + i \eta_r \omega_r^2} \right) \quad (2.33)$$

$$\ddot{w}(x, t) = \sum_{r=2,4,6,\dots} \frac{-2 \ddot{u}(t) \sin \frac{r \pi x}{l}}{r \pi}$$

$$\left( \frac{\omega^2}{\omega_r^2 - \omega^2 + i \eta_r \omega_r^2} \right) \quad (2.34)$$

and the receptance becomes

$$\alpha_{x,l} = \frac{\ddot{w}(x, t)}{\ddot{u}(t)} = \sum_{r=1,3,5,\dots} \frac{2 \sin \frac{r \pi x}{l}}{r \pi}$$

$$\left( \frac{\omega^2}{\omega_r^2 - \omega^2 + i \eta_r \omega_r^2} \right) \quad (2.35)$$

and

$$\alpha_{x,l} = -\sum_{r=2,4,6,\dots} \frac{2 \sin \frac{r \pi x}{l}}{r \pi}$$

$$\left( \frac{\omega^2}{\omega_r^2 - \omega^2 + i \eta_r \omega_r^2} \right) \quad (2.36)$$

similarly;

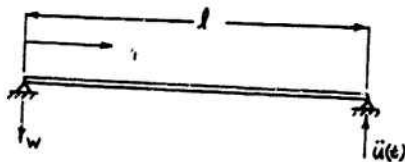


Figure 5 - Simply Supported Beam with Input at Right Support

$$\alpha_{x,l} = \sum_{r=1,3,5,\dots} \frac{2 \sin \frac{r \pi x}{l}}{r \pi}$$

$$\frac{\omega^2}{\omega_r^2 - \omega^2 + i \eta_r \omega_r^2} \quad (2.37)$$

$$\alpha_{x,l} = -\sum_{r=2,4,6,\dots} \frac{2 \sin \frac{r \pi x}{l}}{r \pi} \left( \frac{\omega^2}{\omega_r^2 - \omega^2 + i \eta_r \omega_r^2} \right) \quad (2.38)$$

Equations (2.35), (2.36), (2.37), (2.38) may be written in terms of  $f$  by just replacing  $\omega$  by  $f$ .

$$\alpha_{x,l} = \sum_{r=1,3,5,\dots} \frac{2 \sin \frac{r \pi x}{l}}{r \pi} \left( \frac{f^2}{f_r^2 - f^2 + i \eta_r f_r^2} \right) \quad (2.35)$$

$$\alpha_{x,l} = -\sum_{r=2,4,6,\dots} \frac{2 \sin \frac{r \pi x}{l}}{r \pi} \left( \frac{f^2}{f_r^2 - f^2 + i \eta_r f_r^2} \right) \quad (2.36a)$$

and

$$\alpha_{x,l} = \sum_{r=1,3,5,\dots} \frac{2 \sin \frac{r \pi x}{l}}{r \pi} \left( \frac{f^2}{f_r^2 - f^2 + i \eta_r f_r^2} \right) \quad (2.37a)$$

$$\alpha_{x,l} = -\sum_{r=2,4,6,\dots} \frac{2 \sin \frac{r \pi x}{l}}{r \pi} \left( \frac{f^2}{f_r^2 - f^2 + i \eta_r f_r^2} \right) \quad (2.38a)$$

$$\alpha_{x,l}^2 = \sum_{r=1,2,3,\dots} \frac{4 \sin^2 \frac{r \pi x}{l}}{r^2 \pi^2} \left( \frac{f^4}{(f_r^2 - f^2)^2 + \eta_r^2 f_r^4} \right) \quad (2.39)$$

$$\alpha_{x,l}^2 = \sum_{r=1,2,3,\dots} \frac{4 \sin^2 \frac{r \pi x}{l}}{r^2 \pi^2} \left( \frac{f^4}{(f_r^2 - f^2)^2 + \eta_r^2 f_r^4} \right) \quad (2.40)$$

$$\alpha_{x,l}^* = \sum_{r=2,4,6,\dots} \frac{2 \sin \frac{r \pi x}{l}}{r \pi} \left( \frac{f^2}{f_r^2 - f^2 - i \eta_r f_r^2} \right)$$

$$\alpha_{x,l}^* = \sum_{r=1,3,5,\dots} \frac{2 \sin \frac{r \pi x}{l}}{r \pi} \left( \frac{f^2}{f_r^2 - f^2 - i \eta_r f_r^2} \right)$$

As shown before;

Case I - For no correlation between the two

motion inputs;

$$S_x(f) = |\alpha_{x,l}|^2 S_L(f) + |\alpha_{x,l}|^2 S_R(f)$$

where  $S_x(f)$  is the power spectral density of the response at the point  $x$ .

$S_L(f)$  and  $S_R(f)$  are the power spectral densities of the input at the left support and right supports respectively.

Case II - If there is direct correlation between the two motion inputs;

$$S_x(f) = |\alpha_{x,l} + k \alpha_{x,l}|^2 S_R(f)$$

Case III - If the two spectral density inputs are identical;

$$S_L(f) = S_R(f) = S(f)$$

so that for Case I

$$S_x(f) = [|\alpha_{x,l}|^2 + |\alpha_{x,l}|^2] S(f)$$

and for Case II

$$S_x(f) = [|\alpha_{x,l} + \alpha_{x,l}|^2] S(f)$$

which may be written

$$S_x(f) = [|\alpha_{x,l}|^2 + |\alpha_{x,l}|^2 + 2|\alpha_{x,l}||\alpha_{x,l}| \cos \phi] S(f)$$

Case IV - When one input reproduces the other after a lag of  $\tau_0$

$$S_x(f) = (\alpha_{x,l}^* \alpha_{x,l} + e^{i 2 \pi f \tau_0} \alpha_{x,l}^* \alpha_{x,l} + e^{-i 2 \pi f \tau_0} \alpha_{x,l} \alpha_{x,l}^*) S(f)$$

at  $x = \frac{l}{4}$

where  $\alpha_{x,l}^*$  is the complex conjugate of  $\alpha_{x,l}$

and  $\alpha_{x,l}^*$  is the complex conjugate of  $\alpha_{x,l}$

### 3. The Model Beam

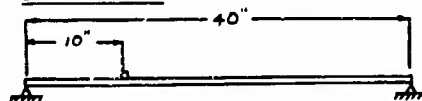


Figure 6

The model is a simply supported steel beam 40 inches long, 2 inches square and a weight of 48 pounds. The first three natural frequencies of the beam are as follows;

$$f_r = \frac{a_n}{2\pi} \sqrt{\frac{EI}{m l^4}}$$

where  $a_1 = \pi^2$

$$a_2 = 4\pi^2$$

$$a_3 = 9\pi^2$$

$l$  = length of the beam = 40 inches

$$m = \text{mass per unit length} = \frac{\text{weight}}{g l} = .0031 \frac{\text{lb. sec}^2}{\text{in.}}$$

$EI$  = bending stiffness of the section =  $40 \times 10^6 \text{ lb. in.}^2$

$$f_1 = \frac{\pi^2}{2\pi} \frac{40 \times 10^6}{.0031 (256 \times 10^4)} = 114 \text{ cps}$$

$$f_2 = 448$$

$$f_3 = 1008 \text{ cps}$$

The P.S.D. (power spectral density) response of the beam will be found at a point 10 inches from the left end. Assume  $\eta$  for this beam is 0.1.

### 4. Conclusions

In comparing the response plots for uncorrelated (Figure 8) and directly correlated (Figure 9) cases it can be seen that the difference between them is quite dramatic. Symmetrical first and third modes of directly correlated responses are twice that of the uncorrelated case. This is due to the additive phasing relationship between cross terms. The opposite is true for unsymmetrical second mode where in the directly correlated case phasing of the cross terms have a canceling effect causing us to lose this mode, but conversely, phasing is such that it is retained in the uncorrelated response. For simplicity spectral density inputs  $S(f)$  at the supports were chosen to be  $1.0 g^2/\text{cps}$ .

Responses with time delays between the inputs, as expected, reduced to the directly correlated response for a zero time delay. Reduction to the uncorrelated case obviously occurs when the cross terms are zero (Figure 8)

Dramatic results were obtained for arbitrarily chosen time delays of one half, one, and two milliseconds. For a one-half

millisecond delay, (Figure 11) we find the unsymmetrical second mode that was lost in the directly correlated case reappears, and with a response equal to that of the uncorrelated case. The first mode is retained, but the third mode is lost as a result of cross terms completely canceling the pure terms.

When the time delay is increased to one millisecond (Figure 12) the third mode reappears but not to its highest level and width. The second mode is drastically reduced, but the first mode remains unchanged.

A further increase in delay to two milliseconds (Figure 13) drastically reduces the first mode width and peak. Phasing of cross terms also causes the third mode width to decrease, and distorts the second mode shape.

These results show clearly that the cross correlation between the inputs has a real importance and that neglecting it would lead to an erroneous response spectrum. The response curves also show that not only the maximum of the cross correlation is important, but also its time position on the time scale of the correlation function plays a determinant role.

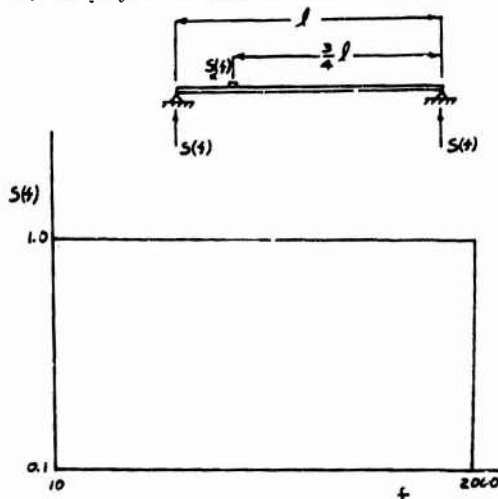


Figure 7 - Spectral Density of Random Inputs at Supports

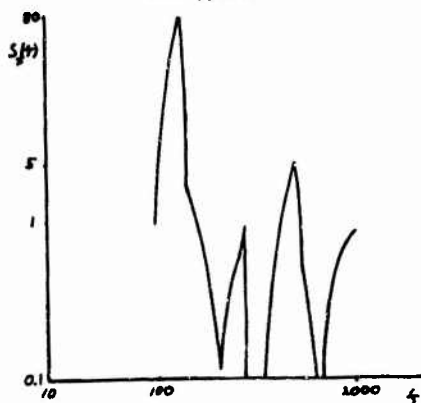


Figure 12 - Spectral Density of Correlated Response with a Time Lag between Inputs of  $\tau_0 = 1.0$  millisecond.

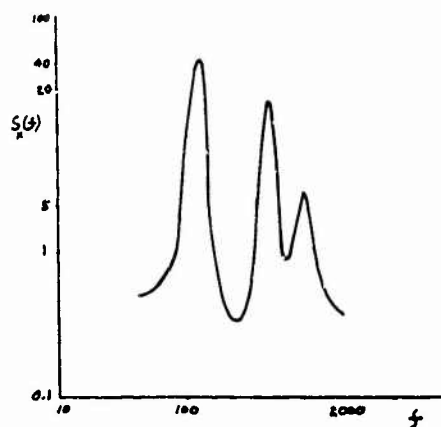


Figure 8 - Uncorrelated Response Spectral Density

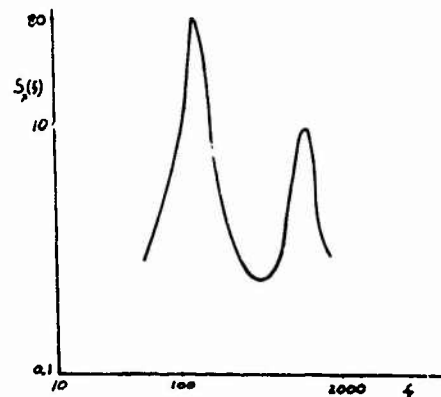


Figure 9 - Correlated Response Spectral Density

Figure 10 - Spectral Density of Correlated Response with a Time Lag Between Inputs of  $\tau_0 = 0$  sec.

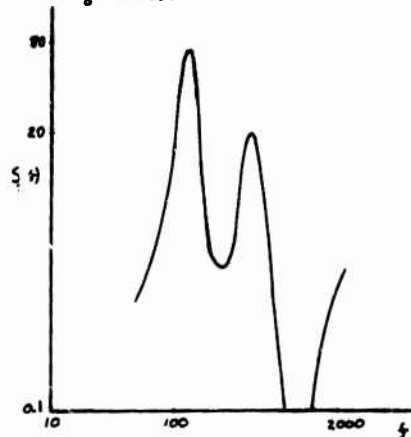


Figure 11 - Spectral Density of Correlated Response with a Time lag Between Inputs of  $\tau_0 = 0.5$  milliseconds

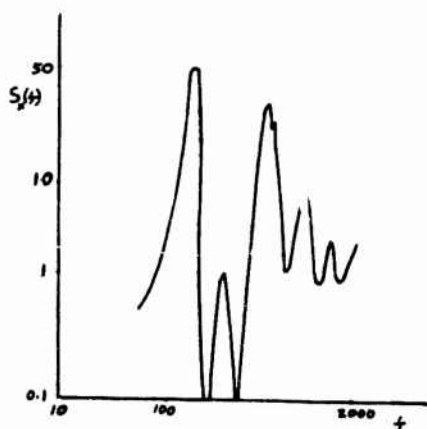


Figure 13 - Spectral Density of Correlated Response with a Time Lag Between Inputs of  $\tau_0 = 2.0$  milliseconds

#### LIST OF SYMBOLS

- $E$  = modulus of elasticity
- $g$  = acceleration of gravity
- $I$  = moment of inertia
- $i = \sqrt{-1}$
- $k$  = constant
- $l$  = length
- $M_r$  = generalized mass
- $m(x)$  = mass per unit length
- $n = (1, 2, 3, \dots)$
- $P(t)$  = random loading on left side of elastic structure
- $Q(t)$  = random loading on right side of elastic structure
- $R_p(\tau)$  = autocorrelation function of  $P(t)$
- $R_q(\tau)$  = autocorrelation function of  $Q(t)$
- $R_x(\tau)$  = autocorrelation function of  $x(t)$
- $R_{pq}(\tau)$  = cross correlation function between the loadings  $P(t)$  and  $Q(t)$
- $t$  = time
- $\ddot{u}(t)$  = sinusoidal excitation
- $w_{p_x}(t)$  = weighting function giving the response to a unit impulse at  $P(t)$
- $w_{q_x}(t)$  = weighting function giving the response to a unit impulse at  $Q(t)$
- $w_r(x)$  = normal mode shape
- $w(x,t)$  = displacement of the beam at any point
- $x(t)$  = displacement of a given point in a given direction

- $\alpha_{xp}$  = receptance at  $x$  due to harmonic input at  $P(t)$
- $\alpha_{xq}$  = receptance at  $x$  due to harmonic input at  $Q(t)$
- $\xi_r$  = normal mode
- $\theta$  = phase angle of receptance
- $\Xi_r$  = generalized forces
- $\gamma$  = damping factor
- $\tau_0$  = time delay
- $\phi$  = difference of phase angles between receptances
- $\omega$  = excitation frequency
- $\omega_r$  = natural frequency of  $r^{\text{th}}$  mode
- $*$  = denotes complex conjugate

#### REFERENCES

- (1) Marc R. P. Trubert, "Response of Elastic Structure to Random Excitations," AF-AFOSR-62-313, August, 1963
- (2) H. G. Kizner, "Experimental Determination of Transfer Functions of Beams and Plates by Cross-Correlation Techniques," 67-373, June, 1962.
- (3) J. D. Robson, "An Introduction to Random Vibration," University Press and Elsevier Publishing Company, 11964).

## DISCUSSION

Mr. Edgington (White Sands Missile Range, N.M.): Considering a two-body system would you recommend testing with two completely noncoherent random inputs without any correlation or any given time lag?

Mr. Razziano: Yes, in order to excite all the modes you would want to have uncorrelated inputs.

Mr. Bendat (Measurement Analysis Corp.): I think that your application of cross correlation and spectral analysis techniques is very interesting but some of those curves look pretty theoretical. In actual measurements there are lots of errors that are introduced as a result of the record length, the frequency ranges and the methods of analysis. What did you actually do about the error analysis question?

Mr. Razziano: I have some test results I would be glad to show them to you, if you would like.

Mr. McConnell (Naval Ship R&D Center): Have you looked into the fact that when tau becomes of the order of one millisecond you are getting into the frequency range of your input. How does this relate to suppressing certain parts of the input. When tau is zero there is no effect and when tau is one this corresponds to a thousand cps. It appeared that the notch was at about a thousand cps. When tau was two there appeared to be a big notch at about 500. Have you looked at the effect of this time in terms of any particular frequencies that could be suppressed by the time delay?

Mr. Razziano: No, as I showed you in, I think, the third slide the power spectral density input was flat across  $s(f)$  and was a constant in the entire analysis. In other words, in each frequency band there is exactly  $1 \text{ g}^2/\text{cps}$  put in at the two shaker locations.

## AUTOMATIC NORMALIZATION OF STRUCTURAL MODE SHAPES

C. C. Isaacson

R. W. Merkel

Engineering Laboratories  
McDonnell Aircraft Company  
St. Louis, Missouri

Two basic problems have been encountered in the measurement and plotting of vibration mode shapes of large structures. First, application of hand-held vibration probes to the structure sometimes causes a small amount of damping and may distort the indicated mode shape. Second, data from each test station must be manually divided by a reference value in order to plot the normalized mode shape. In order to minimize these problems, an instrument, developed and evaluated in the laboratory, is used to normalize data outputs to a reference transducer on the structure, thereby cancelling the small damping effect and providing a normalized ratio indication.

The instrument, designed primarily for use during aircraft ground vibration testing, processes output signals from the velocity pickups which are used to map the vibratory mode shapes of the aircraft. A normalized mode shape graph is subsequently obtained by plotting the output readings of the normalizer. Modular operational amplifiers were used in a "building block" fashion in the signal normalizer design because of their versatility in performing the various computing functions required.

Diagrams of the instrument's operational circuits are presented with complementary descriptions of operations including the mathematical computations performed in each module. System evaluation includes an analysis of performance data curves.

### INTRODUCTION

An electronic normalizing device was recently designed and built in the Engineering Laboratories of the McDonnell Aircraft Company to be used in ground vibration tests on aerospace structures. The normalizer's function is to produce an output voltage which is indicative of the relative amplitude between the maximum amplitude reference point and other points on a vibrating structure. These relative amplitudes are tabulated and then plotted to obtain a graphic representation of the vibration mode shape at a particular normal mode frequency. This paper discusses the operational details of the normalizer and presents performance curves for the instrument.

### BACKGROUND

Data handling is a tedious, time consuming process when performing ground vibration tests on aircraft and spacecraft. Mapping a vibration mode shape requires recording the response of a large number of data points in order to accurately define the motion of the structure.

Since most of our ground vibration testing is usually performed at sites remote from the laboratory, it is impractical to utilize the Central Data Acquisition System of the laboratories. Special efforts have therefore been made to develop equipment and techniques to expedite testing and data processing.

A mapping layout, illustrated in Figure 1A, is usually employed by our Structural Dynamics testing group on ground vibration tests of flight aircraft where fixed pickup locations and roving hand-held pickups are utilized. In the normalizing process, the point of maximum deflection must first be identified and then followed by the response from each of the remaining data points expressed as a percentage of this maximum deflection. The relative phase of each response point is also tabulated with respect to the input force to the structure. A typical wing-bending mode shape describing the motion of the wing when it is excited in its first asymmetric bending mode is presented in Figure 1B.



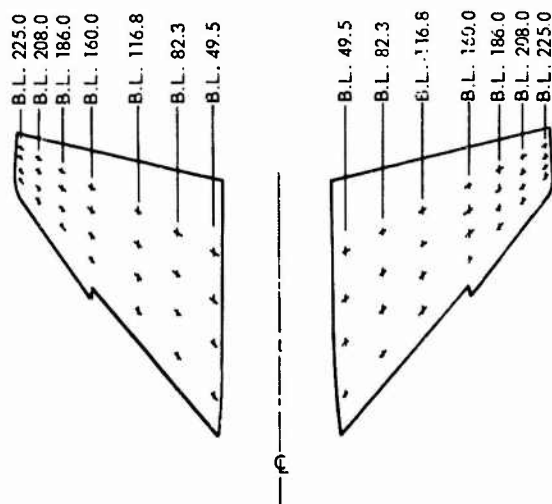


Figure 1A - Mode Shape Mapping Locations

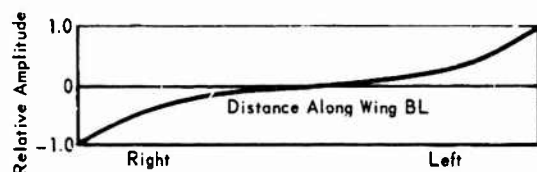


Figure 1B - Typical Mode Shape and Mapping Locations

In mapping a mode, the roving pickup is held on the structure at each station while the response amplitude and relative phase are tabulated. The data is then normalized and plotted. One of the early attempts to expedite this process by automatic normalization involved the use of a potentiometer as a dividing element, illustrated in Figure 2. The pickup with the maximum deflection was switched into a potentiometer which was adjusted for a reading of 1.0 volts on a vacuum tube voltmeter. Each response point was then measured through the same potentiometer setting which normalized each reading.

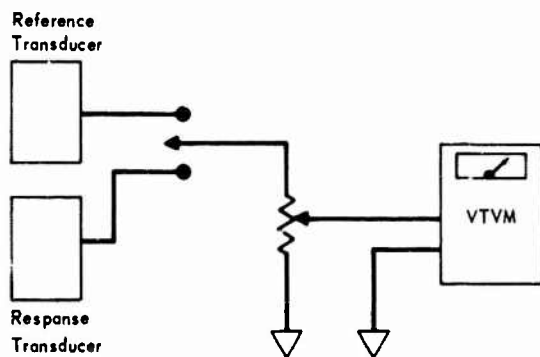


Figure 2 - Potentiometric Normalizing System

One of the problems encountered when measuring mode shapes with a hand-held probe is that the motion of the structure may be damped slightly with the application of the probe. To overcome this problem, the operator of the normalizing potentiometer had to monitor the reference point before each reading was taken and had to confirm that it was remaining on 1.0 volts. However, this monitoring required much time and presented questions as to the advantages of this method of normalization. A program was initiated to obtain an instrument that would simultaneously compare the response amplitude with the reference amplitude. The basic requirements for the normalizer were that it have the following characteristics:

- a high input impedance,
- a frequency response from 1 to 1000 Hz,
- an output voltage proportional to input voltage ratios from .01 to 10,
- minimum operator adjustments,
- good voltage sensitivity, and
- reliability.

After intensive investigation, it was established that an "off the shelf" instrument that would meet our objectives was not available. Thus a decision was made to develop a normalizer utilizing operational amplifiers which resulted in the instrument shown in Figure 3.



Figure 3 - Front View of Complete Unit

#### GENERAL DESCRIPTION

The basic enclosure for the normalizer is a Barr-Brown Model 1600-16R Rack Adapter. It contains the three modules which make up the normalizer circuitry, a plus and minus 15-volt power supply and the external BNC cable connectors. The computing circuitry of the instrument is composed of twelve operational amplifiers chosen as the basic elements because of the ease of wiring them for various required computing functions. Other advantages of the op-amps are their accuracy, small physical size, and low power requirements.

The basic mathematical operations performed in the new electronic normalizer unit are logarithmic conversion, subtraction and antilogarithmic conversion. The principle of logarithmic division is used to produce the ratio indication. Voltages proportional to the logarithms of the two input and scaling voltages are produced by three matched log

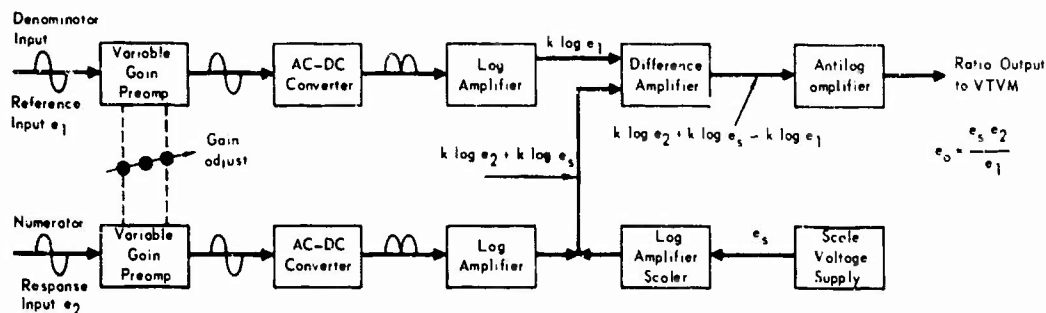


Figure 4 - Normalizer Computing Circuits

converters. These three logarithmic voltages are then subtracted and the antilogarithm of the difference voltage is taken. The antilog voltage is then displayed on a DC vacuum tube voltmeter and read out as the ratio of the two input signals. A block diagram of this normalizing unit is in Figure 4.

#### CIRCUIT DESCRIPTION

The first module of the normalizer contains six operational amplifiers which make up a dual channel preamplifier and precision full-wave rectifier. A circuit schematic of the unit is presented in Figure 5 and a linearity plot is shown in Figure 6.

The preamplifier is of the non-inverting configuration which presents a very high input impedance to the transducer amplifiers. The numerator (response pickup) and the denominator (reference pickup) signals are fed through identical circuitry. The circuit draws very small currents and therefore has no loading effect on the input instrumentation. The gain switch is ganged so that both the numerator and denominator channels are switched simultaneously. The full-wave precision rectifier is required to provide a positive voltage for the logarithmic conversion amplifiers when an alternating signal from a vibration pickup is applied to the input terminals. The gain of the rectifier circuit is adjustable by a trimpot in the feedback loop.

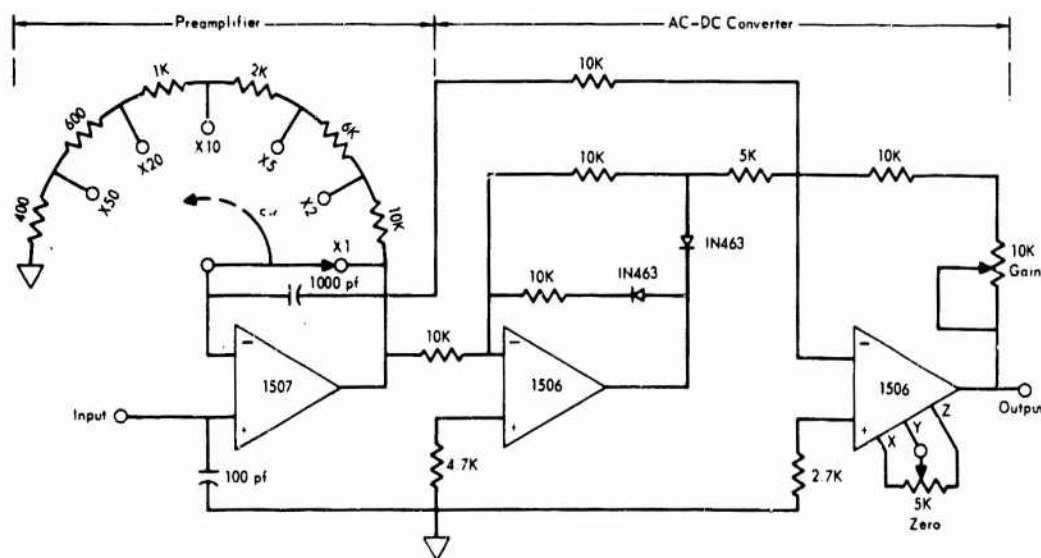
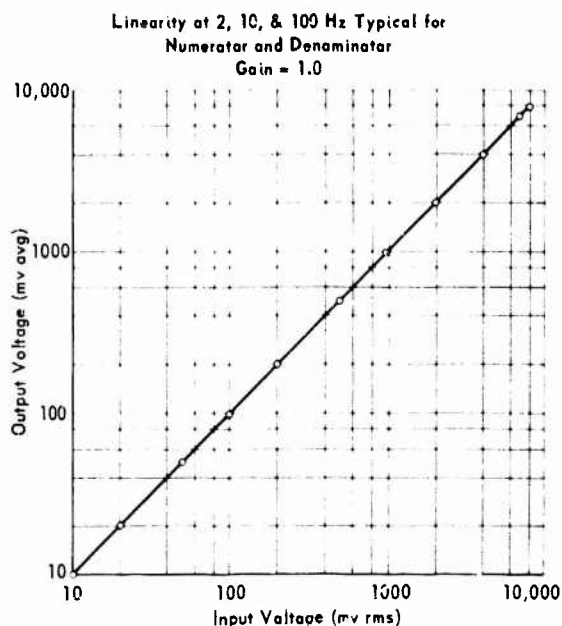


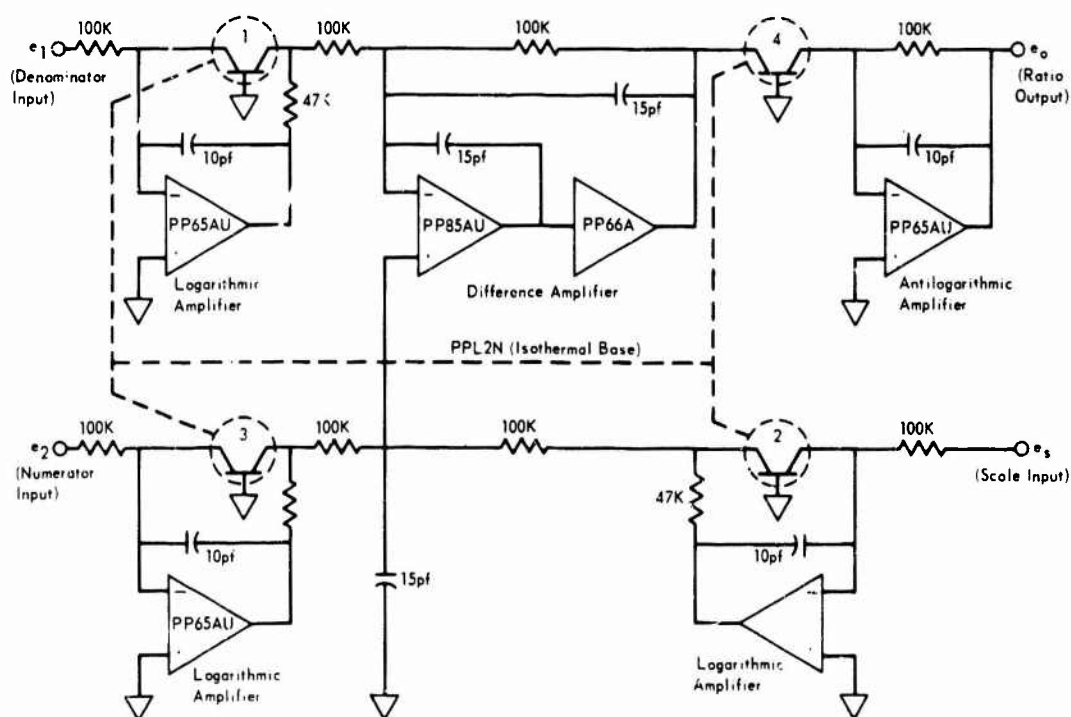
Figure 5 - Typical Preamplifier/AC-DC Converter Channel



**Figure 6 - Preamplifier/AC-DC Converter**

The logarithmic divider module (Figure 7) contains five operational amplifier circuits consisting of three logarithmic amplifiers, a difference amplifier and an antilogarithmic amplifier. Logarithmic conversion is accomplished by inserting a transistor in the feedback loop of an operational amplifier. In this case the logarithmic elements are included in a Philbrick-Nexus model PPL2N transconductor containing four closely matched transistors.

A logarithmic amplifier conditions the numerator signal, the denominator signal, and the scale voltage. These three logarithmically varying voltages are then fed into the difference amplifier which produces an output voltage proportional to the logarithm of the scale voltage multiplied by the quotient of the numerator and denominator signals. This voltage is then fed through the antilog amplifier which produces an output that varies linearly with the quotient of the input voltages. The linear output is read on a DC logarithmic voltmeter which permits a reading of a wide range of ratios with no scale switching. The linearity of the two logarithmic amplifiers is shown in Figure 8.



**Figure 7 - Logarithmic Divider**

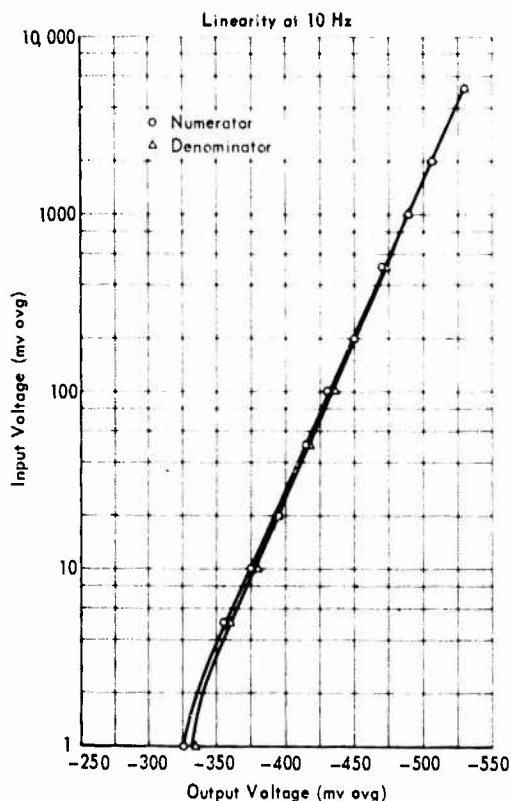


Figure 8 - Logarithmic Amplifier

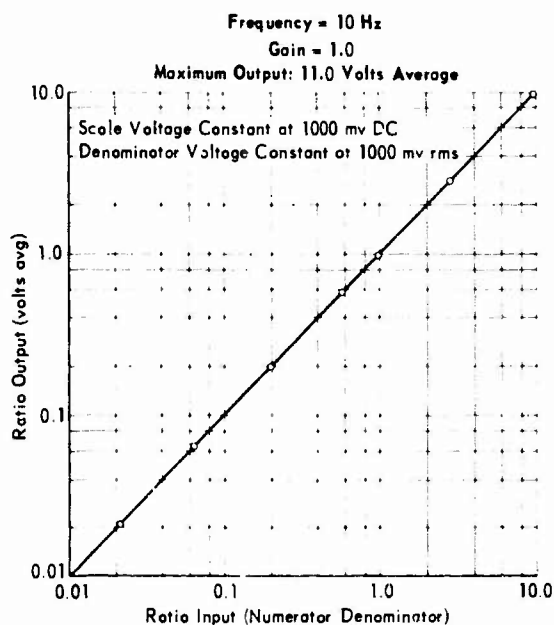


Figure 9 - Normalizer Overall Linearity

The remaining module contains a single non-inverting voltage-follower amplifier that provides a stable scale-voltage source. This voltage is passed through a logarithmic amplifier and added to the non-inverting input of the difference amplifier. The result is a unipolar input voltage required by the antilogarithmic amplifier for normalizer input voltage ratios from .01 to 10. The scale voltage is adjusted to provide a normalizer output range of 1.0 volt with an input voltage ratio of 1.0.

#### PERFORMANCE CHARACTERISTICS

The output voltage of the normalizer is linear for input voltage ratios from .01 to 10.0. A curve describing the linearity of the normalizer (Figure 9) was generated with the reference voltage held constant at 1.0 volt rms while the numerator voltage was varied from 10 millivolts to 10 volts. A frequency response curve of the normalizer, presented in Figure 10, indicates an essentially flat response from 0 to 10 KHz.

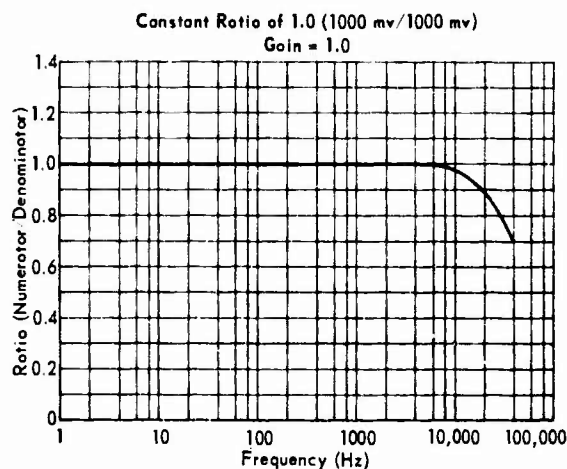


Figure 10 - Normalizer Frequency Response

A block diagram in Figure 11 illustrates the normalizer and associated equipment as used on a ground vibration test. A typical mode shape plot made by utilizing the normalizer is presented in Figure 12. Experimentation on the normalizer and other projects utilizing solid-state operational amplifiers as the basic circuit element has been performed in our laboratory during the past several years. This work has been directed mainly toward improving methods of processing vibration data. The advent of solid-state and integrated circuit operational amplifiers has made experimentation in these problem areas much less complicated.

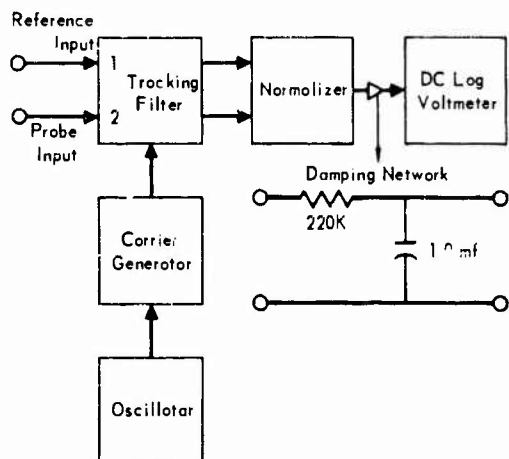


Figure 11 - Normalizer in Test Setup

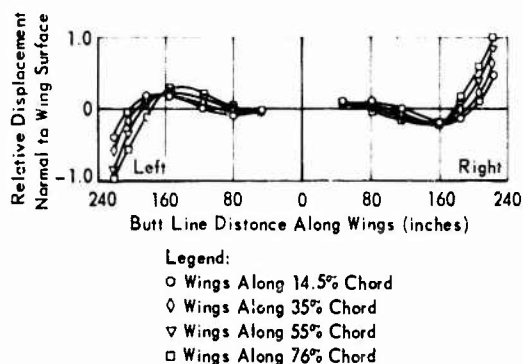


Figure 12 - F-4 Aircraft Asymmetrical Mode

One of the "spin-offs" from the development of the electronic normalizer is an instrument designated as the logarithmic ratio computer which performs the very important function for the dynamics test engineer of providing a plot of vibration transmissibility. Figure 13 shows a block diagram of the logarithmic ratio computer and a linearity plot of the unit is shown in Figure 14.

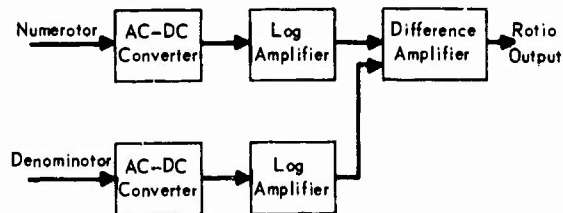


Figure 13 - Block Diagram Logarithmic Ratio Computer

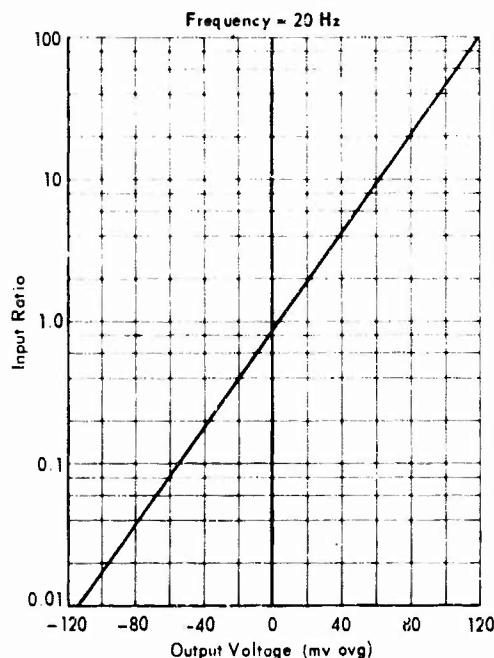


Figure 14 - Logarithmic Ratio Computer Linearity

The circuit of the logarithmic ratio computer is very similar to that of the normalizer with the exception of the antilog and scale voltage stages. The output voltage of the difference amplifier is plotted directly on logarithmic graph paper which is calibrated in units of acceleration transmissibility or "g per g". A block diagram of a typical transmissibility system is presented in Figure 15. A typical transmissibility plot is presented in Figure 16.

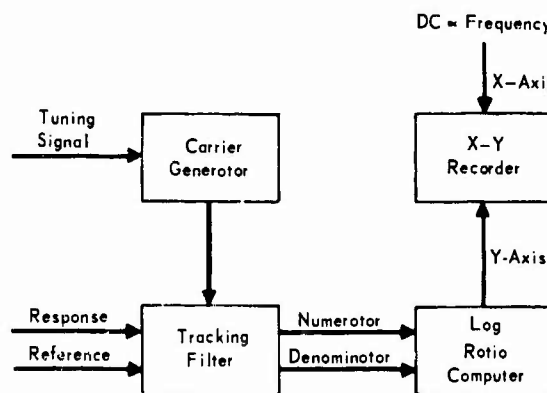


Figure 15 - Typical Transmissibility Plotting System

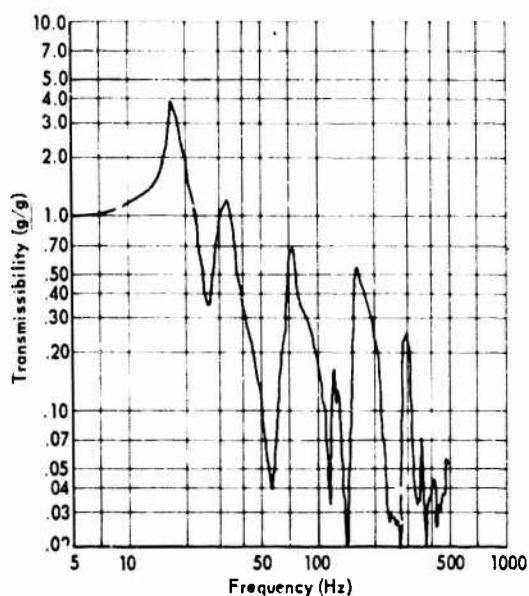


Figure 16 - Acceleration Transmissibility

#### SUMMARY

For two years the two described units have been advantageously used by the test engineers in our Dynamics Laboratory. The normalizer eliminates previous errors and promotes direct plotting of the mode shape without correcting the data. The logarithmic ratio computer permits the plotting of transmissibility data during the sinusoidal-sweep cycling portion of the qualification and developmental vibration tests. In addition to the assets of the instruments, the immediate acquisition of on-site test data available from the described methods of plotting decreases the time and increases the efficiency of tests.

#### REFERENCES

1. Handbook of Operational Amplifier Applications, Barr-Brown Research Corporation, 1963.
2. "Applications Manual for Operational Amplifiers", Engineering Staff, Philbrick/Nexas Research, 1968.

## RESONANT BEAM HIGH "G" VIBRATION TESTING\*

B. A. Kohler  
International Business Machines Corporation  
Federal Systems Division  
Owego, New York

Response data from early development vibration tests on the Saturn Switch Selector (a small unit that routes and controls command signals in the Saturn V booster) indicated that the internal components were exposed to 250-g acceleration levels in the 200- to 700-Hz frequency range. These g levels were higher than any levels previously experienced at IBM Owego, and they far exceeded the levels to which component suppliers were expected to guarantee their product. As a result, IBM began a comprehensive component qualification program to assure that components selected for the unit would operate in the high g-level vibration environment.

Part of the qualification program called for simulation of the high acceleration levels, so a special resonant beam fixture was designed and built to extend the capabilities of existing vibration equipment. This report covers the design, development, and fabrication of the resonant beam fixture that allowed vibration tests up to 250 g at varying frequencies.

### INTRODUCTION

Tests conducted on a Saturn Switch Selector disclosed that 25-g vibration inputs to the housing subjected electronic circuitry within the unit to vibration levels up to 250 g. These components -- transistors, capacitors, diodes, and relays -- were packaged into modules and then filled with encapsulant.




Most component procurement specifications require that the component function successfully when vibrated to 30 g from 20 to 2,000 Hz. A survey of approximately 50 component test reports at IBM Owego disclosed that 33 percent of the small components were vibration tested to levels of 30 g or less; 90 percent of the test levels were 50 g or less; 10 percent were within a range of 50 to 90 g, and none were tested at over 90 g. Exploratory vibration tests on potted Saturn Switch Selector components showed that they could withstand vibration levels up to 250 g. Although the components functioned satisfactorily, the question

of fatigue and how much vibration the components could withstand, still remained.

A vibration analysis was performed to establish the fragility level of the components. The analysis was performed, using the IBM 7090 computer program for vibration and stress analyses, to determine the acceleration level where the components ceased to function properly. The flexible elements within the components were analyzed for natural frequencies and for responses under a forced vibration input up to 2,100 Hz. Table 1 shows the results. These data indicate that the components were capable of withstanding extremely high vibration levels. The relays had the lowest fragility level and provided the least margin of safety. When vibrations were applied along the relay's sensitive axis, the minimum fragility level was caused by contact chatter. The level was above 200 g from 20 to 1,000 Hz, but it gradually dropped to 30 g as the forcing frequency approached the natural frequency of 2,006 Hz.

\*This paper not presented at Symposium.

TABLE 1  
Component Failure Levels

Component	Natural Frequency cps	Minimum Fragility Level - G Peak	Failure Mode	Criteria for Failure
Relay  Latch Position	$f_x = f_y = 2,006$ $f_z = 1,885$	Y direction - 275 g, 20-100 Hz 260 g at 400 Hz 200 g at 1,000 Hz 125 g at 1,500 Hz 30 g at 2,008 Hz	Contact Chatter	Deflection of moveable contact at stationary contact exceeds .00055 in.
S-IN645 Diode 	$f_x = f_y = 54,451$ $f_z = 74,333$	X Direction - 8250 g, 20-2,100 Hz	Changes in electrical characteristics	Preload of whisker on semi-conductor chip reduced by 1 ounce.
IN 753A Diode 	$f_x = f_y = 52,248$ $f_z = 101,755$	Z Direction - 40,300 g, 20-2,100 Hz	Failure in whisker to chip board	Shear stress in bond exceeds the 300 psi lap shear strength of the adhesive at 100° C.
Transistor 5972-SM 2928	193,823	68,000 g, 20-2,100 Hz	Mechanical fatigue	Stress in aluminum lead exceeds 4000 psi.
Transistor 5970-SM 6409	14,149	2 560 g, 20-2,100 Hz	Mechanical	Stress in gold lead exceeds 6,000 psi.
Transistor 5969-SM 6408	22,914	4,220 g, 20-2,100 Hz	Mechanical fatigue	Stress in gold lead exceeds 8,000 psi.
Transistor 5971-SM 2929	142,315	23,300 g, 20-2,100 Hz	Mechanical fatigue	Stress in gold lead exceeds 8,000 psi.
Capacitor 350 D	40,878	8,480 g, 20-2,100 Hz	Mechanical fatigue	Stress in solder joint exceeds 8,000 psi.

#### RESONANT BEAM DESIGN

The first step in the resonant beam design was to determine its physical size. Calculations based on vibration table size, encapsulated cube dimension, concentrated beam load, and vibration frequency bandwidth were used in beam natural frequency formulas; the results indicated a variable length beam 14 by 1.875 by 0.187 inches. By using a variable length, the beam natural frequencies could be excited from 100 to 1,500 Hz.

Initial design concepts included an automatic beam adjustment with the vibration machine operating automatically in the sweep frequency test range. Further study indicated that a simpler design with fewer parts would be more reliable and cost less. The final beam configuration, shown in Fig. 1, included a hold-down clamp for the encapsulated test component, adjustable beam clamps, and a clamp base to attach the beam to the vibration table.

The end clamps allow manual adjustment of the beam's length. Experimental vibration runs through the test frequency range indicated where graduations should be marked along the clamping base. With five clamping adjustments, vibration performance could be monitored from 100 to 1,500 Hz. The lowest resonant beam frequency and corresponding maximum beam length allowed the vibration inputs to stabilize at 100 g while sweeping a 100-through 200-Hz bandwidth. At the high end, a sweep frequency band between 700 and 1,500 Hz can be covered with the clamped beam setting fixed. Fig. 2 shows the clamping intervals during the vibration test profile.

#### BEAM TESTING AND VIBRATION RESULTS

Initial beam evaluation included a test to indicate operational vibration input/output levels. The beam material for this test was 2024-T4 aluminum 0.185 inch thick. Peak resonance was maintained constant at 430 Hz with an effective beam length of 6.25 inches.



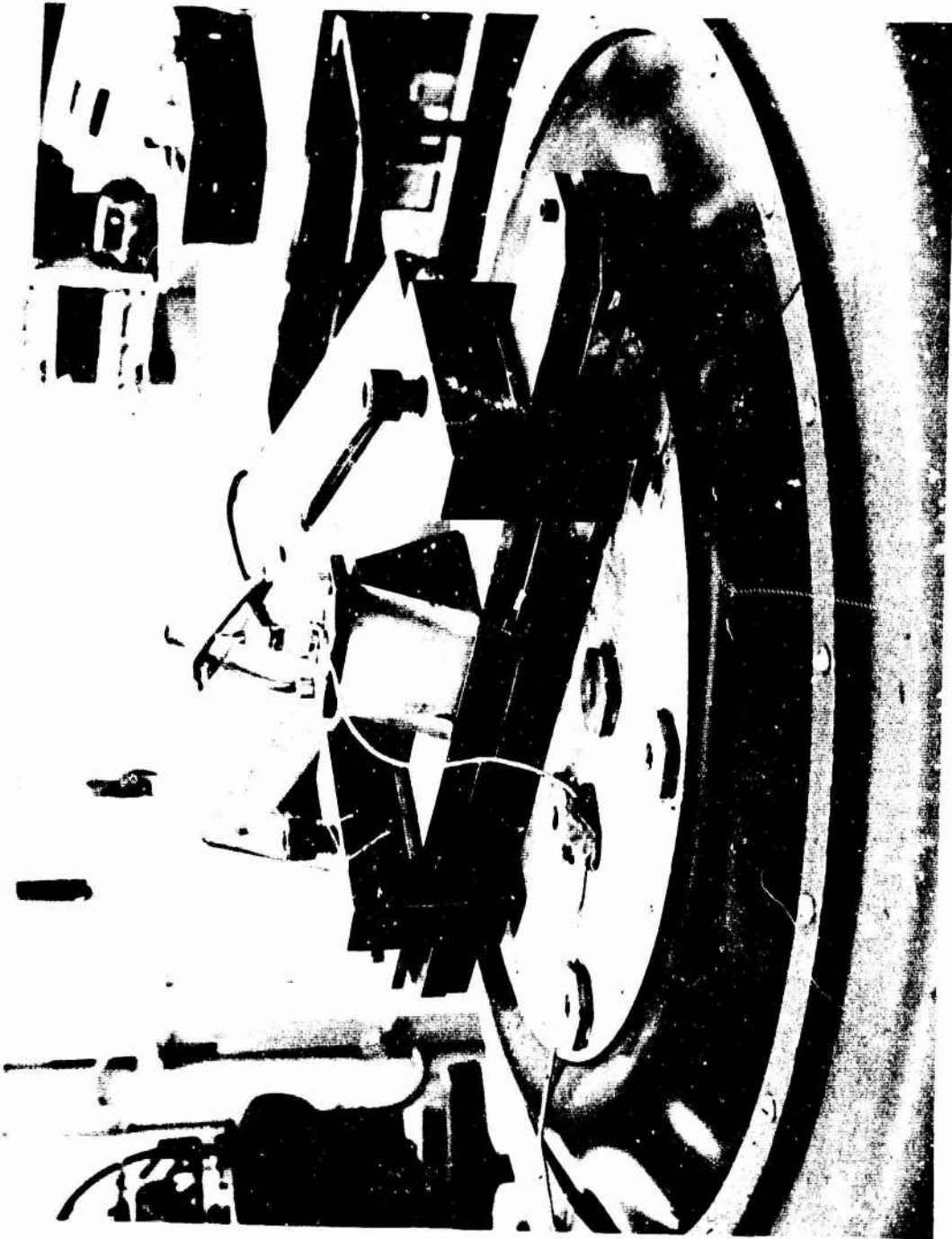


Fig. 1 Resonant beam for high g vibration testing

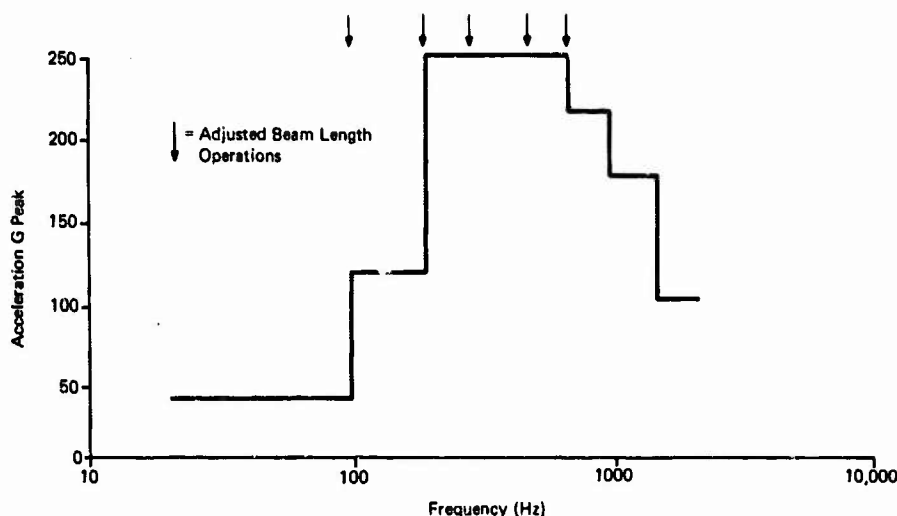


Fig. 2. Test profile

A 2-inch cube of encapsulant mounted at the center of the beam weighed 0.3 pound. The results in Fig. 3 indicate a beam acceleration performance exceeding the maximum g test requirement of 250 g.

During continuous operation at 250 g, a decreasing transmissibility ratio indicated beam fatigue. Therefore, life tests were performed on beams of various material: aluminum, stainless steel, and steel. Stainless steel was selected. Test conditions and results are shown in Fig. 4.

Further evaluation established stainless steel beam vibration capabilities when the beam was clamped at maximum and minimum effective lengths. With the beam clamped at a maximum effective length of 14 inches, peak resonance occurred at 95 Hz and the beam acceleration reached 140 g with a 2-g exciter input. When the beam was clamped at a minimum effective length of 3.25 inches, peak resonance occurred at 1,400 Hz and the beam acceleration reached 20 g with a 2-g exciter input. Different beam frequencies can be obtained by changing the beam thickness.

Loading at the beam center included the test component, encapsulant cube, accelerometer, and clamping hardware as shown in Fig. 5. Individual test components embedded in a cube of encapsulant simulated actual assembly holding conditions. Wiring attached to

each component extended through the encapsulant cube to accept test equipment inputs during vibration testing.

The cube configuration allowed the encapsulated component to be clamped to the beam in each of the three vibration axes. Tests conducted with accelerometers in the centers of different types of encapsulants indicated little or no vibration damping, and the encapsulants themselves endured high g loading when clamped to the resonant beam. These tests to determine mechanical transmissibility were performed with an accelerometer embedded in Stycast 1090, Koldmount, epolene wax, and a 1/8-inch jacket of epolene wax in Koldmount. The encapsulated accelerometers were subjected to the following vibration levels: 100 Hz at 14 g peak; 200, 400, 500, and 700 Hz at 250 g peak; 800 and 1,000 Hz at 215 g peak; 1,000, 1,200, and 1,500 Hz at 175 g peak; and 1,700 and 2,000 Hz at 100 g peak.

Fig. 6 shows the output g level deviation in the encapsulants from the input g level for five frequency bands.

An analysis of the point-to-point g level measurements for the encapsulant, excluding epolene wax, showed that all levels were within +6 percent and -10.7 percent of the input levels. Some support problems occurred with the epolene wax because of its extreme brittleness. However, the maximum percent

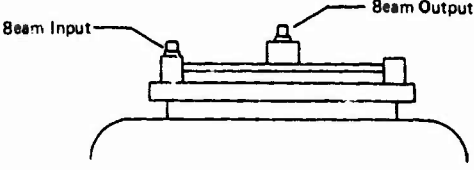
Beam Input G-RMS	Beam Output G-RMS	Test Configuration Accelerometer Locations
1	80	
2	140	
3	160	
4	170	
6	200	
8	240	
10	280	

Fig. 3. Beam acceleration output at 430 Hz peak resonance

Material	Thickness (Inches)	Length (Inches)	Freq (Hz)	Accel G-Peak	Time to Fail (Minutes)
Aluminum 2024-T4	.250	13.94	105	250	20
Stainless Steel 304	.250	13.94	170	250	94
Steel 1020	.250	13.94	162	250	45

Fig. 4. Beam vibration fatigue

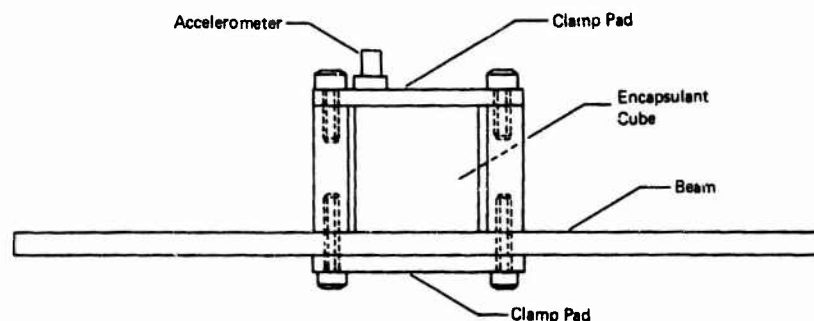


Fig. 5. Clamping configuration

variation in the wax was 13.9 percent. The average transmissability of the encapsulants up to 1,500 Hz was basically unity. Beyond 1,500 Hz, a maximum deviation of -10.7 percent could be expected.

Beam fatigue failure was the most significant problem during the component vibration qualification program. However, a total running time test log was maintained so that beams could be replaced before failure. Spare beams supplied in advance allowed continuous testing with minimum delay.

## CONCLUSIONS

High g level vibration testing can be accomplished by using resonant beams in conjunction with existing vibration exciters. The specific stainless steel beam used in the Saturn Switch Selector vibration tests performed to a stepped vibration profile requiring a maximum 250-g level. Small test components embedded in the center of a cube of encapsulant and clamped to a resonant beam remained practically undamped during high g-level vibration and functioned properly during vibration levels as high as 250 g.

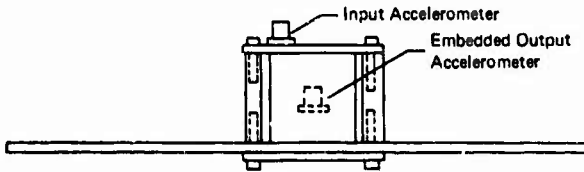
Frequency (Hz)	9 Deviation Input G/Output G			
	Stycast 1090	0.12 Inch Jacket Epolene Wax in Koldmount	Koldmount	Epolene Wax
100-200	+2.1	+0.7	+0.2	-8.3
200-700	-1.3	-2.5	+2.7	-1.5
700-1,000	-1.5	-1.2	+1.2	-1.0
1,000-1,500	+2.0	-1.5	-1.0	-5.5
1,500-2,000	-5.0	-3.0	-8.0	-9.0
Accelerometer Locations				
 <p>The diagram illustrates the placement of two accelerometers on a rectangular device. An 'Input Accelerometer' is shown mounted on the top surface of the device. An 'Embedded Output Accelerometer' is shown as a small square symbol within the device's footprint. The device is mounted on a horizontal base plate.</p>				

Fig. 6. Encapsulant vibration response

## THE USE OF LIQUID SQUEEZE-FILMS TO SUPPORT VIBRATING LOADS

By Brantley R. Hanks  
NASA Langley Research Center  
Langley Station, Hampton, Va.

An analytical and experimental investigation was conducted to determine the bond strength of liquid squeeze-films subjected to oscillating loads normal to the plane of the film. A mass with a flat circular bottom was placed on a rigid flat base covered with a thin layer of liquid. A sinusoidal oscillation was then imparted to the base, and the acceleration level necessary to break the bond of the liquid film was measured under both atmospheric and vacuum ambient pressure conditions. The effects of a number of variables, in particular the mass, contact area, oscillatory frequency, fluid vapor pressure, viscosity, and surface tension, were considered. Results indicated that liquid squeeze-films can be used to support vibrating loads of considerable magnitude, even in a vacuum environment. The limiting factor on the bond strength was found to be the fluid cavitation pressure which can be negative. An analysis was developed based on Reynolds lubrication theory and was found to predict the basic trends of the data.

### INTRODUCTION

The launch of spacecraft substructures which are very sensitive to deflection, such as large diffraction-limited telescope mirrors, presents problems in securing the substructure to the spacecraft. Launch vibrations can damage the structure so as to reduce or destroy its usefulness. Liquid squeeze-films, that is, thin liquid films loaded normal to the plane of the film, may offer advantages for the support of such structures during launch. A thin film of fluid separating two parallel surfaces offers considerable resistance to forces which tend to push the surfaces together or pull them apart provided the load is not applied for a long period of time. Therefore, a squeeze-film may be applicable for the attachment of substructures to a launch vehicle during the vibratory load periods of launch. For a deflection-sensitive structure such as a telescope mirror, this method of attachment offers several potential advantages including (1) a continuously distributed load, hence, negligible stress concentrations (2) evenly distributed heat transfer between the mirror and supports and (3) easy release of the mirror for positioning once the launch period has passed by either applying a very small static load for a long time or by permitting the fluid to evaporate into the vacuum of outer space.

The load-supporting capacity of liquid squeeze-films is of primary importance in lubrication theory. The basic analysis of this capacity was first presented by Reynolds in reference 1 in 1886. His work included studies of flat and curved surfaces moving both vertically and horizontally with respect to a thin fluid film. Generally, the load-supporting capacity of a thin liquid film is considered for application to dynamic bearings of all types. However, the hydrostatic capacity of such films has also received some attention. For example, the resistance of a fluid to being squeezed from beneath flat plates of various geometries is discussed in reference 2, and force-time values for the thickness of such a film are presented in reference 3. The actual use of this squeeze-film load capacity for other than lubrication purposes has received only limited attention. The use of a squeeze-film as a high-force vibration damper was hypothesized in reference 4 but was never actually applied to dynamic problems. A brief experiment was mentioned in reference 5 in which an oil film was used to attach a mass to a vibrating table, but results were nonconclusive. There is a brief discussion of using a squeeze-film as a bond in reference 7, and random localized cavitation is mentioned as the limiting bond strength factor for impact-loaded squeeze-films.

The purpose of the investigation reported herein was to explore the feasibility of using

thin liquid squeeze-films to support vibrating loads and to obtain information about the tensile failure loads of such films. The vibratory acceleration necessary to cause detachment of a mass held to a vibrating base by a fluid film was measured as affected by the following variables: load per unit contact area, ambient pressure, fluid vapor pressure, and oscillatory frequency. A modified version of the Reynolds theory was developed for the prediction of the failure load, and a comparison between theory and experiment is made.

## THEORY

The behavior of thin viscous fluid films being squeezed from between parallel or nearly parallel surfaces was first treated theoretically by Reynolds in reference 1 and is discussed in detail in modern text books on lubrication. Since the general theory is well known, only the specific case of interest, that of a flat disc vibrating against a fluid-covered flat surface, will be considered here. Application of the basic theory to the case of a mass bonded to a vibrating base by a thin liquid film will then be discussed.

### Basic Equations

The configuration considered is shown in figure 1. It consists of a rigid disc of radius  $R$  separated from a surface by a thin fluid film of instantaneous thickness  $h$  and moving with instantaneous velocity  $V$  relative to the surface.

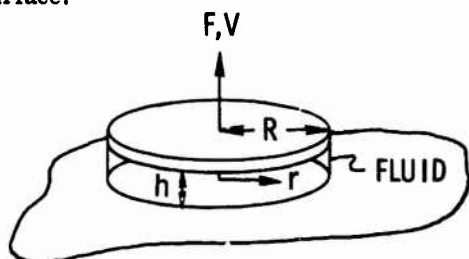


Figure 1.- Basic configuration for analysis. Considering this as a hydrostatic problem Reynolds determined the pressure  $p$  at any radius  $r$  in the fluid to be

$$p = p_a - \frac{3\mu V}{h^3} (R^2 - r^2) \quad (1)$$

where  $p_a$  is the ambient pressure of the environment and  $\mu$  is the viscosity of the fluid. The derivation of this equation is based upon the assumptions that viscous forces predominate over acceleration forces in the fluid and that the pressure is constant across the film thickness. The equation is generally used to demonstrate the resisting force produced by a fluid being squeezed from between two closely spaced parallel surfaces

(i.e.,  $V$  is negative). However, if the plate is being pulled away from the surface ( $V$  positive), the film can exert a large hold-down force. This can be shown by examining a cross section of the pressure distribution on the top and bottom of the plate as shown in figure 2.

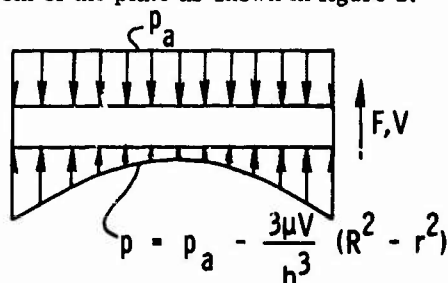


Figure 2.- Pressure distribution on plate.

The force  $F$  on the plate required to produce the velocity  $V$  is calculated by integrating the difference in pressure over the area, that is,

$$F = - \int_A \left\{ -p_a + \left[ p_a - \frac{3\mu V}{h^3} (R^2 - r^2) \right] \right\} dA = \frac{3\pi\mu VR^4}{2h^3} \quad (2)$$

If the film thickness is small compared to the plate radius ( $h \ll R$ ), the velocity  $V$  will be small unless the force  $F$  is extremely high. In cases where the velocity is small, it seems reasonable to assume that equation (2) holds when  $F$  is time varying. When  $F$  is a known applied force,  $h$  can be calculated as a function of time from the equation since  $V = \frac{dh}{dt}$ . Assuming  $F = F_0 \sin \omega t$  and an initial film thickness of  $h_0$ , integration of (2) yields

$$h(t) = h_0 \left[ \frac{1}{1 - \frac{4F_0 h_0^2}{3\pi\mu R^4 \omega} (1 - \cos \omega t)} \right]^{1/2} \quad (3)$$

The maximum thickness  $h_{\max}$  occurs at  $t = \frac{(2n-1)\pi}{\omega}$  and is given by

$$h_{\max} = h_0 \left[ \frac{1}{1 - \frac{8F_0 h_0^2}{3\pi\mu R^4 \omega}} \right]^{1/2} \quad (4)$$

For the thickness to increase to a point where the fluid offers little resistance to the plate

motion, the term  $\frac{8F_0 h_0^2}{3\pi\mu R^4 \omega}$  must be equal to

almost one. For example, if this term has a value of 0.99, the film thickness will increase by a factor of ten which would change an  $h_0$  of 0.01 cm to an  $h_{\max}$  of 0.1 cm. Therefore, the condition for viscous failure of the fluid film bond may be written

$$\frac{F_0}{f} \approx \frac{3\pi^2 \mu R^4}{4h_0^2} \quad (5)$$

where  $f \left( f = \frac{\omega}{2\pi} \right)$  is the frequency of the vibrating force. Obviously, if  $h_0$  is small compared to  $R$ , the force  $F_0$  must be extremely high or the frequency must be extremely low to result in a flow failure of the bond.

#### Cavitation and Liquid Tension

It is likely that instead of viscous flow failure of a squeeze-film bond taking place, cavitation will occur in the fluid and equation (5) will not be applicable to predicting bond failure. The pressure distribution in the fluid is given by equation (1). During upward motion of the plate, the minimum pressure will occur at  $r = 0$  and is given by

$$p_{\min} = p_a - \frac{3\mu VR^2}{h^3} \quad (6)$$

Rewriting equation (2) as

$$\frac{3\mu VR^2}{h^3} = \frac{2F}{\pi R^2}$$

and substituting in (6) gives

$$p_{\min} = p_a - \frac{2F}{\pi R^2} \quad (7)$$

Substituting the cavitation pressure  $p_c$  of the fluid for  $p_{\min}$  in (7) and rearranging gives the force to produce cavitation as

$$F = \frac{\pi R^2}{2} (p_a - p_c) \quad (8)$$

Substituting (8) for  $F_0$  in equation (5) and rearranging yields

$$f \approx \frac{2h_0^2}{3\pi\mu R^2} (p_a - p_c) \quad (9)$$

for the approximate transition frequency above which cavitation occurs before a flow failure can take place. For very thin films the failure mechanism will usually be cavitation rather

than flow except at very low frequencies. In elementary fluid mechanics, cavitation is assumed to occur when the pressure at some point in the fluid becomes equal to the vapor pressure of the fluid. However, theoretical studies (ref. 6) and experimental tests (ref. 7) have shown that, because of Van der Waal-type molecular forces, a liquid can sustain a tensile force of large magnitude (i.e., the pressure in the liquid state cannot only be less than the vapor pressure but can actually become negative). In practice, this tensile capacity is a function of the cleanliness and absence of gas bubbles in the fluid (refs. 9-11). Generally, small impurities and gas bubbles exist in the fluid and cavitation occurs around these nuclei. Even when such nuclei are present, the pressure must be low enough to overcome surface tension around the nucleus and/or the low pressure application time must be long enough for absorbed gases to come out of solution around the nucleus before cavitation can occur. This means that liquid tension can be obtained in impure liquids and, in the case of pressure cycling, may be frequency dependent. Therefore, even if the ambient pressure is negligible, as in outer space, a thin fluid film can be capable of supporting a vibrating load provided that the frequency of the load does not permit separation by flow as governed by equation (9) and provided some device is employed to prevent vaporization under static conditions. The magnitude of this load will depend on the absence of impurities or gas bubbles of appreciable size in the fluid. If the fluid can be kept absolutely free of cavitation nuclei, a bond of significant dynamic strength may be realized. Characteristics of this type bond are that freedom of side movement would be maintained, the load is distributed over a large area rather than concentrated at points, and release by flow can be attained by applying a small static load. Such a bond could be of use in securing space vehicle components during the vibrations of launch and yet permit easy release and/or positioning once the critical dynamic loading period has passed. A typical application would be in launch of large telescope mirrors into orbit since critical optical figure requirements preclude "point load" clamps on such mirrors. On the earth where a large ambient pressure gives high bond strength, possible applications are for temporary attachment of objects to vibrating bases and prevention of "hop" of vibrating machinery where reasonable portability must be maintained.

Once a bubble has formed and started to grow, some additional load may be required to cause actual separation of the two plates. Calculation of this load is a complex problem involving bubble growth rate and rate of change of viscous forces. A simplified treatment of this problem in reference 12 showed that, once the bubble starts to grow, it can grow to considerable size with no increase in applied force. Simultaneously, the thickness of the film is increasing resulting in a decrease in the

viscous force in the fluid. These phenomena are possibly dependent on time, surface tension, and viscosity. Hence, separation may not occur at the instant bubble growth begins but will probably occur as loads and frequencies very near those which initiate bubble growth.

#### Mass on a Vibrating Base

The motion of a mass bonded to a vibrating base by a squeeze-film is governed by a non-linear differential equation having a force term proportional to the inverse cube of displacement. The utility of a solution to the equation is far outweighed by its complexity since for very thin films, the motion of the mass will be nearly the same as that of the base. This can be seen by assuming that the base is moving in some manner which produces a sinusoidal acceleration of the mass. Equation (2) is then, since  $F = nmg \sin \omega t$ ,

$$\frac{dh}{dt} = \frac{2 nmg h^3}{3\pi\mu R^4} \sin \omega t \quad (10)$$

where  $m$  is the mass and  $n$  is the peak acceleration of the mass in earth gravity units. Differentiation of this equation gives

$$\frac{d^2h}{dt^2} = \frac{2 nmg h^3}{3\pi\mu R^4} \left[ \omega \cos \omega t + \frac{2 nmg h^2}{\pi\mu R^4} \sin^2 \omega t \right] \quad (11)$$

for the relative acceleration of the mass with respect to the moving base where  $h$  is given by equation (4). If the film thickness is small with respect to the disc radius and other variables, then the peak relative acceleration between the mass and base will be negligible compared the peak absolute acceleration,  $ng$ , of the mass. The same is true of velocity as can be seen in equation (10). Obviously, the motion of the mass and the base will be virtually the same and a transmissibility of one can be assumed through the squeeze-film.

Assuming a sinusoidal input and a transmissibility of one, the peak force on the squeeze-film during a cycle is equal to the mass times the acceleration or  $nmg$ . Therefore, the minimum input acceleration in earth gravity units to cause cavitation is given by

$$n = \frac{\pi R^2}{2mg} (p_a - p_c) \quad (12)$$

which comes from substituting for the force in equation (8).

Some difficulty is encountered in applying equation (12) because of the unknown variable  $p_c$ . The approach used in this paper is to present experimental data and determine from the data the magnitude and trends of the liquid tension forces. Equation (12) with the

cavitation pressure assumed to be the fluid vapor pressure  $p_v$  ( $p_c = p_v$ ), that is

$$n = \frac{\pi R^2}{2mg} (p_a - p_v) \quad (13)$$

was used as a basis; and the difference between this calculated value of  $n$  and the actual test value was treated as tension.

#### APPARATUS AND TEST PROCEDURE

The experimental configuration used to investigate liquid film bond strength was basically two parallel discs separated by a thin fluid film. A dynamic excitation was imparted to one disc, and the other was free to move as the fluid permitted. The actual test apparatus, shown schematically in figure 3, consisted of a cylindrical mass standing on end in a rigid base which was, in turn, attached to an electro-magnetic shaker.

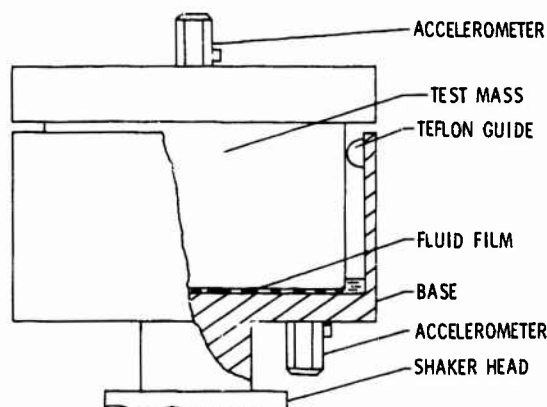


Figure 3.- Sectioned schematic of basic test apparatus.

A thin fluid film separated the two adjoining surfaces, and a small reservoir of fluid was maintained around the mass by walls on the base. Clearance between the sides of the mass and base was sufficiently large to eliminate shear effects and teflon guides prevented side slippage of the mass. An accelerometer was attached to each mass, as shown, to monitor the vertical accelerations. The mass and base were machined from 6061 aluminum alloy, and the contact surfaces were finished to 1.6 microns rms. Three cylindrical mass configurations were used to study the effects of mass and contact area. Masses of 1767 gr, 4020 gr, and 13,600 gr with a 12.7 cm contact surface diameter and 3730 gr with a 7.62 cm contact surface diameter were tested giving area loadings of 1365, 3105, 10 500, and 8020  $N/m^2$ , respectively. A photograph showing the base mounted to the shaker and two of the mass configurations is shown in figure 4.



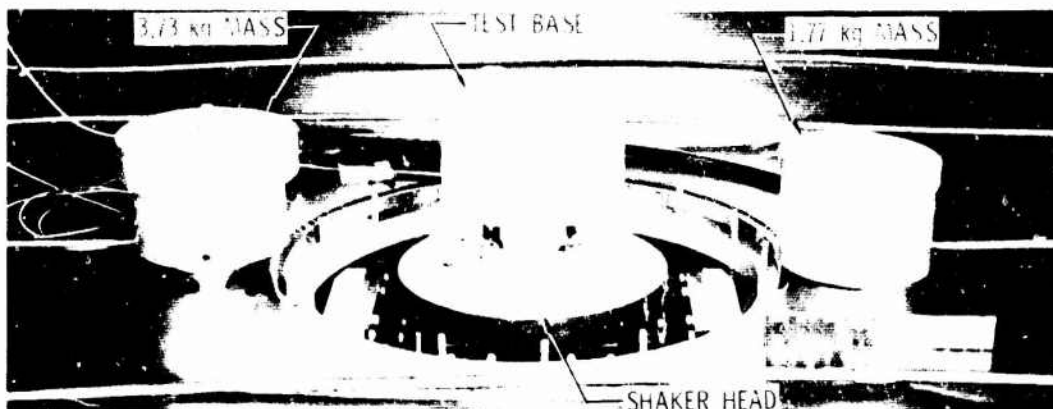


Figure 4.- Test base mounted to shaker head and two of the test mass configurations.

Three different fluids - tap water, acetone, and silicone oil - were tested in order to study the effects of vapor pressure and viscosity. The properties of these fluids are shown in table I.

The tests were conducted in a combined environments test chamber. It is a double-walled cylinder with a 1.8-m internal diameter test section and an electromagnetic shaker rigidly mounted to a foundation beneath the chamber. The shaker head extends through the wall of the vacuum chamber and is sealed by a thin rubber diaphragm. The environmental chamber was used to produce a moderate vacuum (5 torr) for the squeeze-film tests.

A block diagram of the instrumentation used to control the shaker and obtain data is shown in figure 5. A servo-controlled oscillator was used to control the input frequency and amplitude to the shaker. Small, matched-output, piezoelectric crystal accelerometers monitored the motion of the mass and base. The accelerometers were coupled through battery-operated power supply units to a dual-beam oscilloscope and to two rms voltmeters.

The output of the base accelerometer was also used to operate a protection circuit in the oscillator which deenergized the shaker when a large instantaneous amplitude increase occurred. This automatically shut off the shaker when the test mass detached from the base. The automatic shut-off circuit could be bypassed when desired. An electronic frequency counter was used to monitor the vibration frequency.

The vibratory force required to break the fluid bond between the mass and base plate was measured for a range of ambient pressures, vibration frequencies, and fluid properties. For a particular ambient pressure, fluid, and input frequency, the vibration level was increased manually until the mass detached from the base. The vibration level at which separation occurred was read visually from the rms voltmeter displaying the output of the base plate accelerometer. During each test, a constant comparison of the two accelerometer outputs was made to determine transmissibility. Generally, two minutes time for the mass to settle was allowed between tests to obtain the same approximate film thickness from test to

TABLE I. - TEST FLUID PROPERTIES AT 20° C

Fluid	Density, $\rho$ , gr/cm <sup>3</sup>	Viscosity, $\mu$ , cp	Surface tension, $\sigma$ , dynes/cm	Vapor pressure, $P_v$ , mm Hg
Silicone oil	0.95	55	28	5
Tap water	1	1	73	20
Acetone	0.79	0.33	24	175

test, but this was not found to be a critical factor. No precise measurements of film thickness were made.

In general, each fluid was tested at specific frequencies ranging from 20 to 300 Hz and at ambient pressure ranging from one atmosphere down to the vapor pressure of the fluid.

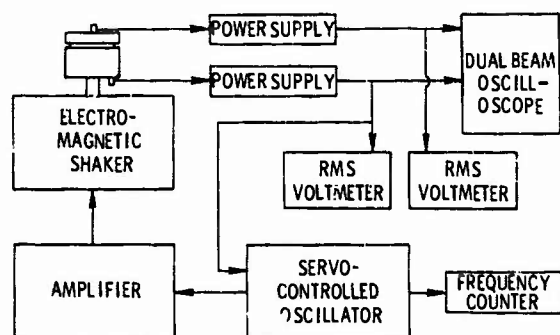


Figure 5.- Block diagram of test instrumentation and shaker controls.

## RESULTS AND DISCUSSION

The test program consisted of an examination of the magnitude of an oscillating load required to break a liquid squeeze-film bond as a function of the variables: load per unit contact area, ambient pressure, fluid vapor pressure, and frequency of the oscillating load. The primary objectives were to demonstrate the feasibility of using squeeze-films for supporting vibratory loads and to study the application of the modified Reynolds theory for predicting the load support capacity.

### Effect of Ambient and Vapor Pressure

The variation of the fluid film bond strength with ambient pressure is shown in figures 6 through 8. The detachment acceleration of the mass in earth gravity units is presented as a function of the ambient pressure in atmosphere for several combinations of fluids, frequencies of vibration, and weight-per-unit-contact-area ratios. Also presented in each figure is a plot of equation (13), that is, the modified Reynolds equation with no liquid tension effects. (Note that 1.0g is added to compensate for earth gravity.) The data of figures 6(a) and 6(b) were obtained using a 55 cp silicone oil squeeze-film at frequencies of 100 and 40 Hz for a weight per unit area of  $1365 \text{ N/m}^2$ . Figures 7(a) and 7(b) show data for the same conditions except that the weight per unit area is  $8020 \text{ N/m}^2$ . In each case the variation of the data with ambient pressure is predicted by the equation, and this variation is independent of frequency. An effective liquid

tension exists which is equal to the difference in the data points and the curve for the equation. This tension is independent of pressure and exists even when the ambient pressure equals the vapor pressure of the oil. The effective liquid tension does vary with

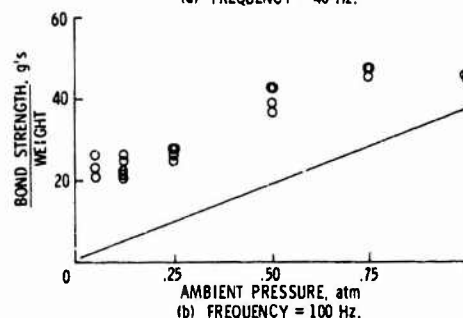
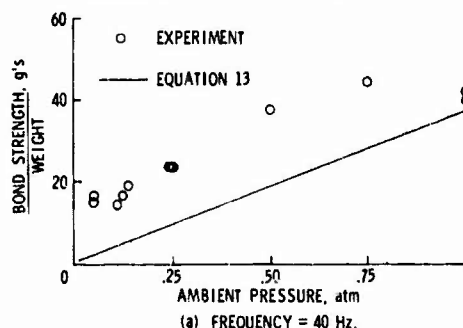


Figure 6.- Detachment acceleration as a function of ambient pressure for two frequencies using 55 cp silicone oil.  $mg/A = 1365 \text{ N/m}^2$ .

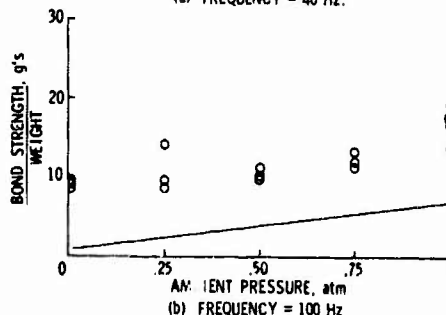
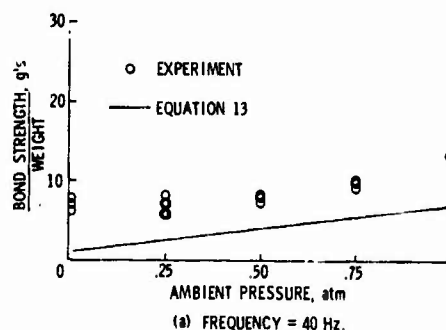
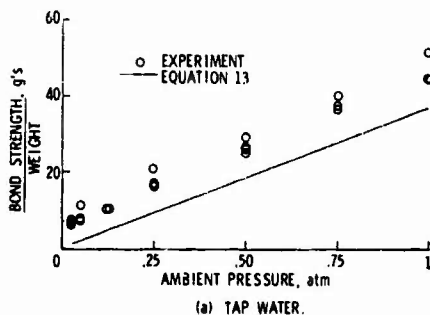
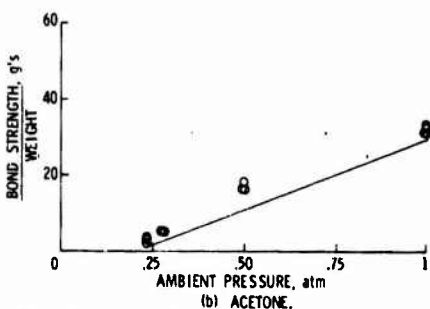


Figure 7.- Detachment acceleration as a function of ambient pressure for two frequencies using 55 cp oil.  $mg/A = 8020 \text{ N/m}^2$ .



(a) TAP WATER.



(b) ACETONE.

Figure 8.- Detachment acceleration as a function of ambient pressure at 100 Hz using two fluids.  $mg/A = 1365 \text{ N/m}^2$ .

frequency as will be discussed later. Figures 8(a) and 8(b) show a similar variation of the load with ambient pressure using tap water and acetone, respectively, for tests at 100 Hz with a weight/area of  $1365 \text{ N/m}^2$ . The water exhibited a load capacity and tension considerably higher than that of the acetone and near that of the silicone oil. Since the viscosity of the water was more nearly equal to that of the acetone than that of the oil, a viscous flow bond failure appears unlikely. A cavitation failure such as assumed in equation (12) more correctly explains the data.

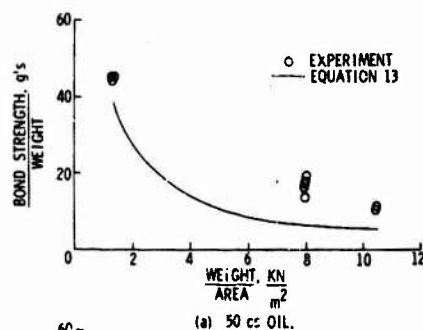
#### Effect of Mass and Area

The effect of mass and area on the detachment load is shown in figures 9(a) and 9(b). Acceleration at detachment is presented as a function of weight per unit area for oil and water at one atmosphere ambient pressure. A plot of equation (13), which varies as the inverse of the weight per unit area, is also presented. The correct trend is predicted by the modified Reynolds equation regardless of whether mass, area, or both are changed.

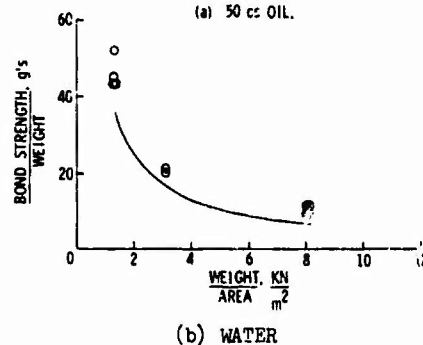
#### Effect of Film Thickness

As stated in the section on apparatus, no accurate measurements were obtained of the fluid film thickness in any of the experiments

conducted. However, a brief study was made of the time allowed for the mass to settle before beginning oscillation. This time is related to film thickness (ref. 3). Similar detachment accelerations were obtained for identical test conditions regardless of the settle time allowed even though this time was varied from a few seconds to as much as 2 days. Evidently, the thickness of the squeeze-film did not significantly affect its bond strength. This conclusion agrees with the prediction of equation (12) and, hence, depends on the occurrence of a cavitation type failure.



(a) 50 cc OIL.



(b) WATER

Figure 9.- Variation of detachment acceleration with weight per unit area for two fluids  $p_a = 1 \text{ atm}$ ,  $f = 100 \text{ Hz}$ .

#### Effect of Frequency

The variation of the detachment acceleration with vibratory load frequency is shown in figure 10 for frequencies ranging from 20 to 300 Hz. Data are presented for tests at one

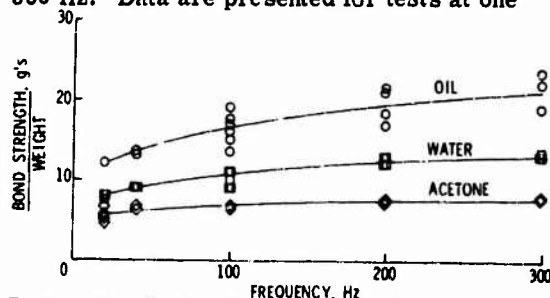


Figure 10.- Variation of detachment acceleration with oscillatory frequency.  $mg/A = 8020 \text{ N/m}^2$ ,  $p_a = 1 \text{ atm}$ .

atmosphere ambient pressure with the 7.62 cm diameter, 4020 kg mass using oil, water, and acetone squeeze-films. The bond strength is seen to increase with increasing frequency, and the rate of increase becomes small as the frequency becomes high. The frequency trend of the detachment data does not depend on the fluid although the magnitude of the detachment acceleration does. Similar trends were noted in all tests regardless of ambient pressure or weight per unit area.

### Liquid Tension

The effective tensile load for each fluid is shown as a function of frequency in figure 11. These curves were obtained by subtracting the computed detachment acceleration [equation (13)] from the faired data curves of figure 10. The curves indicate a higher effective tension in water than in acetone and the highest tension of all in the silicone oil. The frequency dependence of the tension can result from either time dependent cavitation pressure of fluids, as noted in reference 8, or from the time required for cavitation bubble growth as discussed earlier.

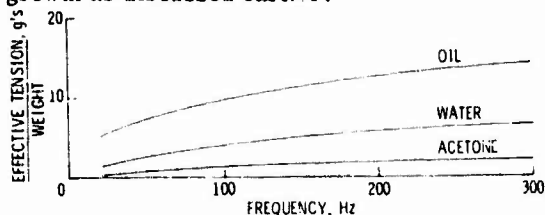


Figure 11.- Variation of effective tension with loading frequency.  $m_g/A = 8020 \text{ N/m}^2$ ,  $p_a = 1 \text{ atm}$ .

### Bubble Growth

A few experiments were conducted to give some information about the bubble growth phenomena. Figure 12 shows photographs of acceleration signals obtained in one 100 Hz, 1 atm. test using the  $8020 \text{ N/m}^2$  mass and water as the squeeze-film. The upper trace in each photograph is the acceleration of the mass, and the lower trace is the acceleration of the base. (The trace for the base acceleration is inverted because of the upside down mounting of the accelerometer.) When the peaks on the traces are farthest apart, the mass is moving toward

the base; and when they are close together, the mass is moving away from the base. The test is shown at two different acceleration levels and the transmissibility is one in each case. Cavitation occurrence is noted by the appearance of noise on the signal as the level increases. This noise is believed to be caused by collapse of the bubble as the mass moves toward the plate. Cavitation noise always appeared in the tests with water at between  $8g$ 's and  $9g$ 's with a slight dependence on frequency as compared to the calculated value of  $6.7g$ 's. Detachment occurred at the same levels shown in figure 12 (i.e.,  $8g$ 's to  $14g$ 's), depending on frequency. In similar experiments using oil as the squeeze-film, the cavitation noise appearance was decidedly dependent on frequency and occurred very near the detachment acceleration.

### CONCLUSIONS

An analytical and experimental investigation of the bond strength of liquid squeeze-films subjected to oscillating loads normal to the plane of the film was conducted. The effects of contact area; load magnitude and frequency; ambient pressure; and fluid vapor pressure, surface tension, and viscosity were considered. The following conclusions were reached:

1. A squeeze-film can be used to support a vibratory load of considerable magnitude even, in certain cases, under a near vacuum environment.
2. For very thin films a cavitation bubble forms near the center of the contact area and grows outward ultimately resulting in breaking of the squeeze-film bond. The time required for this growth enables additional load capacity which increases with the frequency of loading.
3. The minimum force required to produce a cavitation-type bond failure can be conservatively predicted using hydrostatic lubrication theory. The primary factor affecting the accuracy of this prediction will be the establishment of the fluid cavitation pressure.

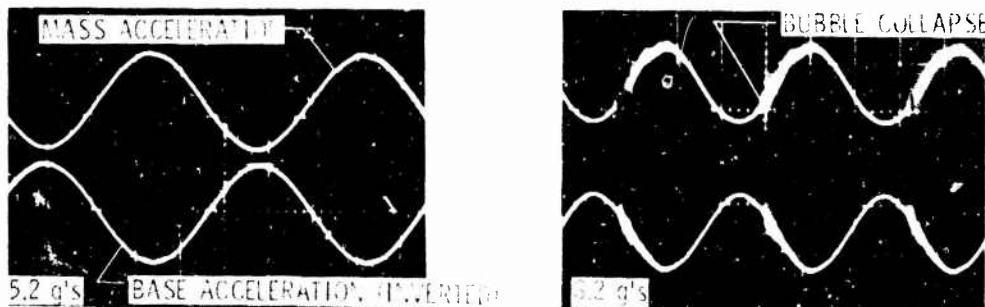


Figure 12.- Photographs showing acceleration before and after cavitation bubble formation in water.  $f = 100 \text{ Hz}$ ,  $m_g/A = 8020 \text{ N/m}^2$ ,  $p_a = 1 \text{ atm}$ .

4. A squeeze-film can support a tensile load in a vacuum environment only if the cavitation pressure is negative as is often encountered in liquid flow studies ( $p_c < 0$  can occur because of intermolecular forces in the fluid provided the fluid is clean).

5. There is no appreciable effect of film thickness on the capacity of a squeeze-film to hold a mass to a vibrating base providing the film is thin with respect to the contact area dimensions.

#### REFERENCES

1. Reynolds, O.: On the Theory of Lubrication and Its Application to Mr. Beauchamp Tower's Experiments, Including an Experimental Determination of the Viscosity of Olive Oil. Royal Society of London, Part I. Vol. 177, 1886, pp. 157-234.
2. Pinkus, O.; and Sternlich, B.: Theory of Hydrodynamic Lubrication. McGraw-Hill Book Company, 1961.
3. Fuller, D. D.: Theory and Practice of Lubrication for Engineers. John Wiley and Sons, Inc., 1956.
4. Sommer, Eugene A.: Squeeze-Film Damping. Machine Design, Vol. 38, May 1966.
5. Omelka, L. V.: Design and Use of Oil Film Vibration Systems. Proceedings of the Institute of Environmental Sciences, 1962, pp. 241-245.
6. Cottrell, A. H.: The Mechanical Properties of Matter. John Wiley and Sons, Inc., 1964, pp. 223-226.
7. Brown, Samuel J., Jr.: The Behavior of Tap Water Under Dynamic Tensile Stressing in a Non-Flow System. M.S. Thesis, Pennsylvania State University, June 1967.
8. Ruggeri, Robert S.; and Geider, Thomas F.: Effects of Air Content and Water Purity on Liquid Tension at Incipient Cavitation in Venturi Flow. NASA TN D-1429, March 1963.
9. Strasberg, M.: The Influence of Air-Filled Nuclei on Cavitation Inception. David Taylor Model Basin Report No. 1078, May 1957.
10. Sirotyuk, M. G.: Cavitation Strength of Water and Its Distribution of Cavitation Nuclei. Soviet Physics-Acoustics, Vol. 11, No. 3, January-March 1966.
11. Knapp, Robert T.: Investigation of the Mechanics of Cavitation and Cavitation Damage. (Final Report, Department of the Navy Contract Nonr-220(08)) California Institute of Technology, Pasadena, California, June 1957.
12. Hanks, Brantley R.: Investigation of the Tensile Strength of Liquid Squeeze-Films Subjected to Oscillating Normal Loads. M.S. Thesis, Virginia Polytechnic Institute, May 1968.

#### DISCUSSION

Mr. Beecher (Lear Siegler): What was the estimated thickness of the squeeze film in these experiments?

Mr. Hanks: We did not find the film thickness to be very important, as was shown in the equation for the cavitation. I would estimate the squeeze film to be of the order of 5 thousandths of an inch. However, we did run several tests in which we varied the time between putting the mass on the film and the start of the test from a matter of some 30 seconds to two days. There was no appreciable difference in the bond strength. This is discussed in the written version of this paper. As long as cavitation is the breakaway mechanism there should be no thickness effect except at very low frequencies.

Mr. Foster (University of Missouri): Did you run any tests or think about the cavitation

problem being related to surface roughness of the mass? A bubble formation sometimes comes off of a roughened piece of surface.

Mr. Hanks: Yes, this is generally in a flow tunnel type of experiment that surface roughness becomes very critical in the initiation of cavitation. In our particular tests, we are assuming the cavitation occurs at the very center of the disk. This may not be true, but since the velocity of flow there is very small, we think that this is not a very critical problem. Our test mass was not particularly smooth. It was just a normal machine turn down so it should not be a particular problem. The cleanliness of the fluid appears to be the most important thing. This is a real unsophisticated test program. We took tap water out of the city water supply. If we had used real clean fluid and tried to make sure that it had no gases or dust particles in it, we might have

gotten much higher values. Also if the surfaces had been smooth we could have gotten higher bond strength values.

Mr. Verga (Hazeltine Corp.): You had the breakaway plotted in terms of g's or force versus frequency. Was there a relationship with respect to the area over which the force was applied. Could we think in terms of g's per square inch?

Mr. Hanks: I showed you the effect of mass and area in one plot in the next to the last slide whereas the bond strength was plotted as a function of the weight per unit area. In these cases we had changed both the

area and the mass. We did not just add mass to the same area, and there did not appear to be any effect.

Mr. Berg: Would this liquid squeeze effect be the same in a high speed journal bearing? Is it necessary for the speed of the plate or the mirror relative to the fixture or the foundation to be zero in order for this behavior to occur as you've observed it?

Mr. Hanks: It may be. I am not prepared to say because I have not looked at the equations that apply in the case of tangential motion. That will change the pressure distribution considerably and I am not sure what type of upward pressure resistance we would get in that case.

POINT-TO-POINT CORRELATION OF SOUND PRESSURES  
IN REVERBERATION CHAMBERS

Charles T. Morrow  
LTV Research Center, Western Division  
Anaheim, California

The response of a structure to a noise field depends in part on the point-to-point correlation of the field. A diffuse sound field with correlation distances comparable to the separation between structural antinodes tends to excite all modes of vibration. A highly correlated field, such as that of low-frequency rocket noise, tends to produce relatively selective modal responses and somewhat reduced overall rms level. At the other extreme, very short correlation distances tend to decrease the response without making it selective.

High-intensity noise tests are generally intended to simulate rocket noise and/or aerodynamic turbulence about a space vehicle, both of which excite vibration modes somewhat selectively according to the portion of the trajectory considered. The best test policy may well be to use the reverberant field to simulate a composite flight condition and apply correction factors judiciously to the sound pressure level. In any event, the point-to-point narrow-band correlation of the reverberant field should follow closely some simple formula. The analysis given in this paper shows that the correlation of the field of a rectangular reverberation chamber can asymptotically approach a formula previously derived by Cook and provides some insight into circumstances that may lead to statistical or even systematic deviations.

INTRODUCTION

Since the time of Sabine's <sup>1</sup> first experiments in architectural acoustics, the reverberation chamber has become an important acoustical tool. It is used in measuring the sound absorption coefficients of surface materials, the total output of loudspeakers and high-intensity noise generators, and the sound transmission of building structures. Most recently large reverberation chambers have come to be used for a high-intensity noise test--environmental systems test of a complete space payload or major section of one. The reverberant field is in-

tended to simulate the noise fields and aerodynamic turbulence encountered in flight.

All of the applications imply diffuseness in the reverberant field. This in turn implies a microphone response independent of position and orientation and a standard behavior of the narrow-band point-to-point correlation of the sound pressures as two microphones are moved away from each other. Narrow-band correlation is essentially a matter of phase relationships. In an ideal reverberant field, phase relationships should approach randomness in a standard way, independent of direction,

<sup>1</sup> Wallace Clement Sabine, Collected Papers on Acoustics, Harvard University Press, 1927.

as the separation of two points becomes comparable to and increases beyond a wavelength.

For high-intensity noise testing, the point-to-point correlation of the reverberant noise field and that of the fields to be simulated are considerations of fundamental importance.

Consider a space vehicle that is completely symmetrical about its axis and exposed to a noise field propagating parallel to the axis. Imagine the vehicle sliced normal to the axis so as to define at the intersection with the skin a circle passing through some antinodal regions for a particular mode of vibration. If the rocket noise field should be completely correlated about this circle, structural excitation will occur only for modes that involve a variation of area during the cycle. For example, the mode shape shown in A in Fig. 1 will be excited efficiently, but the other mode shapes shown in Fig. 1 will not be excited. On the other hand, if the relative correlation of the pressures at adjacent antinodes should be low, as is possible at high frequencies, the excitation of the mode of A in Fig. 1 will be decreased, but all modes will be excited. At the other extreme, if the correlation should become small for point-to-point separations smaller than an antinodal region, as in the case of aerodynamic turbulence in a thin boundary layer, there will be a partial cancellation of the excitation within each antinode. All modes will be excited, but at a reduced level.

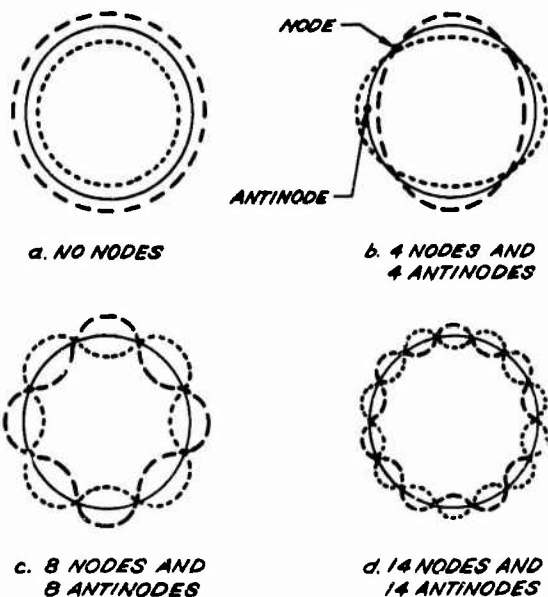


Fig. 1 MODE SHAPES IN A CROSS SECTION OF A UNIFORM CYLINDER

The structural response is dependent on an integration of the excitation not only around the circle, but along the length of the space vehicle as well. Here, the rocket noise exhibits a high degree of correlation with a time delay dependent on the difference between sonic velocity and the vehicle air speed. For modes such that coincidence occurs -- the propagation velocity is the same in the vehicle skin as in the air -- extremely efficient excitation will occur. For other modes, the phase change of the sound in passing from antinode to antinode will differ from  $180^\circ$ , and the excitation will be reduced. Aerodynamic turbulence will exhibit a similar selectivity of excitation, except that the time delay is of opposite sign and dependent on the convection velocity which is slightly less than the airspeed, and the eddies tend to die away as they propagate.

To summarize, the two environments to be simulated tend to exhibit a high degree of correlation parallel to the axis, with coincidence frequencies that vary in different ways along the trajectory. The modal responses are selective, variable with time, and at a somewhat reduced overall rms level by comparison with those in a reverberant field. Aerodynamic turbulence exhibits very short correlation distances, of the order of the boundary layer thickness, around the circle, which does not contribute to selectivity but does decrease the overall response.

A progressive-wave tube, which propagates sound parallel to the axis of a test item can provide a highly realistic simulation of rocket noise at launch or a rather crude simulation of aerodynamic turbulence for airspeeds in the neighborhood of Mach 1, but no way has been suggested of improving the simulation for other airspeeds.

The best test policy at present appears to be to carry out a composite simulation of excitation along the trajectory with the reverberant field and apply sound pressure level corrections as appropriate. A possible refinement may be to provide a background low-level broadband reverberant excitation and supplement it simultaneously with a narrow-band swept reverberant excitation tailored to simulate the effects of a coincidence frequency varying with position along the trajectory.



This implies that the point-to-point correlations of the reverberant field should be made to conform closely to a standard formula, and any statistical deviations from the formula should be understood.

#### COOK'S THEORY OF CORRELATION

Cook and others<sup>2</sup>, with a simple elegance reminiscent of Sabine's theory of architectural acoustics, have derived formulas for the narrow-band point-to-point correlation coefficients of a diffuse reverberant sound field and suggested the use of correlation measurements as a measure of diffuseness. Although their results are clearly correct, the physical model from which they started is liable to misinterpretation and gives limited insight into the conditions necessary for a diffuse field in a chamber of given wall geometry.

Cook obtains a formula for the correlation coefficient of the pressures at two points for a plane wave at a given angle of incidence. Remarking, "Our definition of such a (diffuse) field assigns equal weights to all directions of the incident sound," he averages the coefficient over all angles to obtain correlation formulas for two and three-dimensional fields. Then, he indicates that there will be a deterioration in the accuracy of the results if the sound covers a finite bandwidth.

Unless the reader meditates carefully on the wording of the actual definition given earlier in the paper, he is likely to jump to the interpretation that the formulas hold for a single frequency but deteriorate uniformly as the number of normal modes involved in the averaging process is increased. The actual situation is more nearly the reverse. A single frequency, exciting a single undamped normal mode, yields by itself a point-to-point correlation coefficient of  $\pm 1$ . As the bandwidth is increased to admit more modes, the average correlation may initially, under certain circumstances including high acoustic modal density, approach the formulas. Then, as the bandwidth continues to increase, a bandwidth dependent discrepancy will develop. The theory to be given in the present paper will be primarily in terms of averaging of normal modes in frequency space rather than in terms of averaging over vari-

ous physical directions. The intent is to show, not that Cook's formulas follow from a definition of diffusion, but that under certain conditions the correlation of the field in a rectangular reverberation chamber will asymptotically approach Cook's formulas. If the conditions are not satisfied, there may be statistical fluctuations away from the formulas, depending on the microphone locations and frequency bands considered, or even large systematic deviations.

#### DEFINITIONS

The notation and phraseology of random noise theory are by no means standardized, and we will not presume to impose such standardization by the present paper. However, we should examine our terms and symbols carefully enough to ensure that they will cause no misunderstanding of the present paper. It is important to distinguish between broadband variables, zero-bandwidth variables, and small but finite-bandwidth variables.

Let  $p_A$  and  $p_B$  represent the instantaneous broadband pressure variations at points A and B respectively. Let  $P_{AM}$  and  $P_{BM}$  represent the instantaneous pressure variations corresponding to a single reverberant mode, and  $p_{A\Delta f}$  and  $p_{B\Delta f}$  represent the instantaneous pressure variations in a square bandwidth  $\Delta f$ . The latter do not need to be corrected for phase shift of any filters used in measuring them, provided that the shift is identical for both pressures.

The cross-correlation function of the broadband pressures is the time-average

$$R_{AB}(p_A, p_B) = \overline{p_A(t)p_B(t+\tau)} \quad (1)$$

where  $\tau$  is a relative time delay. This may also be referred to as the covariance function, since  $p_A$  and  $p_B$  have zero mean. Equation (1) reduces to the correlation function if we set  $\tau = 0$

$$R_{ABO}(p_A, p_B) = \overline{p_A(t)p_B(t)} \quad (2)$$

<sup>2</sup> R. K. Cook, R. V. Waterhouse, R. D. Berendt, S. Edelman and M. C. Thompson, "Measurement of Correlation Coefficients in Reverberant Sound Fields," JASA Vol. 27 No. 6, November 1955, pp 1072-1077.

The broadband cross-correlation coefficient and correlation coefficient are given respectively by

$$c_{AB}(p_A, p_B) = \frac{P_A(t)P_B(t+\tau)}{[P_A^*(t)P_B^*(t)]^{1/2}} \quad (3)$$

and

$$c_{ABO}(p_A, p_B) = \frac{P_A(t)P_B(t)}{[P_A^*(t)P_B^*(t)]^{1/2}} \quad (4)$$

For stationary aerodynamic turbulence and free-field acoustic noise propagating from regions of such turbulence, a number of zero-bandwidth spectral density functions may be defined.

The power spectral density function or power spectrum is given by

$$w_A(f) = \lim_{\Delta f \rightarrow 0} \frac{1}{\Delta f} \overline{P_{A\Delta f}^*(f)} \quad (5)$$

and

$$w_B(f) = \lim_{\Delta f \rightarrow 0} \frac{1}{\Delta f} \overline{P_{B\Delta f}^*(f)} \quad (6)$$

If the broadband pressures extend from  $f_1$  to  $f_2$ , their mean squares are

$$\overline{P_A^2} = \int_{f_1}^{f_2} w_A(f) df \quad (7)$$

and

$$\overline{P_B^2} = \int_{f_1}^{f_2} w_B(f) df \quad (8)$$

For narrow bands, the time delay  $\tau$  in the cross-correlation function becomes equivalent to a phase lag. The cross-power spectrum is therefore given by a complex quantity

$$w_{AB} = w_{ABr} + jw_{ABi} \quad (9)$$

where the real part

$$w_{ABr}(f) = \lim_{\Delta f \rightarrow 0} \frac{1}{\Delta f} \overline{P_{A\Delta f}(f) P_{B\Delta f}(f)} \quad (10)$$

has been referred to as the correlation density [3], and the imaginary part,

$$w_{ABi}(f) = \lim_{\Delta f \rightarrow 0} \frac{1}{\Delta f} \overline{P_{A\Delta f}(f) P_{B\Delta f}^*(f)} \quad (11)$$

which is obtained by shifting  $P_{B\Delta f}$  by  $90^\circ$  before averaging, we will call the quadrature density.

These, like the broadband functions may be normalized. We will call

$$c_{ABr}(f) = \frac{w_{ABr}(f)}{[w_A(f)w_B(f)]^{1/2}} \quad (12)$$

the correlation density coefficient and

$$c_{ABi}(f) = \frac{w_{ABi}(f)}{[w_A(f)w_B(f)]^{1/2}} \quad (13)$$

the quadrature density coefficient.

The power spectral density for the sum of  $P_A$  and  $P_B$  is given by

$$\begin{aligned} w_{A+B} &= w_A + w_B + 2w_{ABr} \\ &= w_A + w_B + 2(w_A w_B)^{1/2} c_{ABr} \end{aligned} \quad (14)$$

Equation (14) is the fundamental reason for the importance of correlation in relation to the excitation of structure by acoustic noise. However, for an undamped reverberant field, which must be expressed in terms of sinusoids at discrete frequencies, the expressions of Equations (5) to (13) do not exist. Furthermore, as the correlation will not assume any simple behavior unless many modes are considered, the quantity of eventual interest will be defined for a chosen non-zero bandwidth  $\Delta f$ , and with a correction for difference in shapes of selectivity curve [4], may be regarded as approximately indicative of the response of a mechanical resonator of a given  $Q$ :

$$Q = \frac{2f}{\pi \Delta f} \quad (15)$$

where  $f$  is the center frequency.

For a single undamped reverberant mode, we define instantaneous modal pressures to be  $p_{mM}(t)$  and  $p_{mM}(t)$  or similar symbols with the subscript  $m$  replaced by the specific mode numbers (e.g.  $k_x, k_y, k_z$ ) considered. We define mean square

[3] Morrow, Shock and Vibration Engineering, Volume 1, John Wiley and Sons, 1963, p. 335.

[4] Morrow, Shock and Vibration Engineering, Volume 1, John Wiley and Sons, 1963, p. 86.

modal pressures to be

$$\overline{p_{AM}^2(t)} \text{ and } \overline{p_{BM}^2(t)},$$

the modal correlation function to be

$$\overline{p_{AM}(t) p_{BM}(t)}$$

and the modal correlation coefficient to be

$$c_{ABM} = \frac{\overline{p_{AM}(t) p_{BM}(t)}}{[\overline{p_{AM}^2(t)} \overline{p_{BM}^2(t)}]^{1/2}} \quad (16)$$

We define the narrow-bandwidth spectral densities to be

$$w_{A\Delta f} = \frac{1}{\Delta f} \sum \overline{p_{AM}^2(t)} \quad (17)$$

and

$$w_{B\Delta f} = \frac{1}{\Delta f} \sum \overline{p_{BM}^2(t)}, \quad (18)$$

where  $f$  is the center frequency of  $\Delta f$ , the narrow-bandwidth correlation density to be

$$w_{AB\Delta f}(f) = \frac{1}{\Delta f} \sum \overline{p_{AM}(t) p_{BM}(t)} \quad (19)$$

and the narrow-bandwidth correlation coefficient to be

$$c_{AB\Delta f} = \frac{w_{AB\Delta f}(f)}{[w_{A\Delta f}(f) w_{B\Delta f}(f)]^{1/2}} \quad (20)$$

The last expression is the subject of this paper and is equivalent to the coefficient discussed by Cook.

The time dependence of an undamped reverberant mode is expressed by a simple sinusoidal factor. Except for phase reversals at nodes, no phase shifts are associated with different points in the sound field. It follows from this and Equation (16) that  $c_{ABM} = +1$  and also that any quadrature density or coefficient must be zero.

## SIMPLIFIED MODAL THEORY

Before proceeding to the rectangular chamber, we will carry out a simple derivation that bears some resemblance to Cook's.

Assume for simplicity that all reverberant modes are undamped and excited to equal steady-state responses and that each mode shape is essentially a one-dimensional standing wave pattern. Let the  $x$  axis be aligned with the directions of propagation of the plane waves comprising one of these modes, as in Fig. 2.

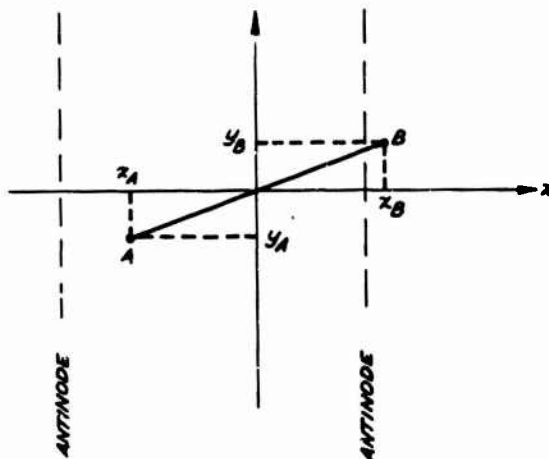


Fig. 2 POINTS IN A STANDING WAVE

For convenience, let the origin be chosen equidistant from two points A and B at which the relative correlation of sound pressures is to be examined. Let the pressure at A for a single mode be

$$p_{AM} = P \cos 2\pi f t \cos(kx_A - \theta) \quad (21)$$

and that at B be

$$p_{BM} = P \cos 2\pi f t \cos(kx_B - \theta) \quad (22)$$

where

$$k = 2\pi/\lambda. \quad (23)$$

If  $r$  is the distance between A and B,

$$x_A = -\frac{r}{2} \cos \theta \quad (24)$$

$$x_B = + \frac{r}{2} \cos \theta \quad (25)$$

$$P_{AM} = P \cos 2\pi f t \cos \left( \frac{kr}{2} \cos(\theta + \phi) \right) \quad (26)$$

$$P_{BM} = P \cos 2\pi f t \cos \left( \frac{kr}{2} \cos(\theta - \phi) \right) \quad (27)$$

$$\begin{aligned} \overline{P_{AM} P_{BM}} &= \frac{P^2 \cos \left( \frac{kr}{2} \cos(\theta + \phi) \right) \cos \left( \frac{kr}{2} \cos(\theta - \phi) \right)}{T} \\ &\times \int_0^T \cos^2 2\pi f t dt \\ &= \frac{P^2}{2} \cos \left( \frac{kr}{2} \cos(\theta + \phi) \right) \cos \left( \frac{kr}{2} \cos(\theta - \phi) \right) \\ &= \frac{P^2}{4} \left[ \cos 2\phi + \cos(kr \cos \theta) \right] \quad (28) \end{aligned}$$

For comparison

$$\overline{P_{AM}^2} = \frac{P^2}{2} \cos^2 \left( \frac{kr}{2} \cos \theta + \phi \right) \quad (29)$$

and

$$\overline{P_{BM}^2} = \frac{P^2}{2} \cos^2 \left( \frac{kr}{2} \cos \theta - \phi \right) \quad (30)$$

so that the correlation coefficient for the two pressures is  $\pm 1$ .

As a definition of a completely diffuse reverberant field within a small bandwidth  $\Delta f$ , we will take all values of  $\phi$  to be equally likely, and (for 2 and 3 dimensional spaces) all values of  $\theta$  to be equally likely. This implies an extremely high modal density and hence high frequency. First sum (or integrate) with respect to  $\phi$ .

$$\sum_{\phi} \overline{P_{1M} P_{2M}} \sim \frac{P^2}{4} \cos(kr \cos \theta), \quad (31)$$

$$\sum_{\phi} \overline{P_{1M}^2} \sim P^2/4 \quad (32)$$

$$\sum_{\phi} \overline{P_{2M}^2} \sim P^2/4 \quad (33)$$

This leads to a narrow-band correlation coefficient

$$c_{AB\Delta f\theta}(r, \theta, f) = \cos(kr \cos \theta), \quad (34)$$

or, if  $\theta=0$  as in the case of a 1-dimensional reverberant chamber (i.e. a long organ pipe),

$$c_{AB\Delta f1} = \cos kr \quad (35)$$

Now proceed to averaging with respect to  $\theta$ . Examination of Eqs. (11) to (13) shows that the same result will be obtained by averaging the correlation coefficient as by summing the correlation functions and mean square values and performing a division. For a 2-dimensional chamber, such as a room of height small compared to the wave lengths, or a harbor with surface waves in its interior,

$$\begin{aligned} c_{AB\Delta f2} &= \frac{1}{2\pi} \int_0^{2\pi} \cos(kr \cos \theta) d\theta \\ &= J_0(kr) \quad (36) \end{aligned}$$

as in Cook's paper. Likewise, for a three-dimensional chamber,

$$\begin{aligned} c_{AB\Delta f3} &= \frac{1}{4\pi} \int_0^\pi \int_0^{2\pi} \cos(kr \cos \theta) \sin \theta d\phi d\theta \\ &= \sin(kr)/kr \quad (37) \end{aligned}$$

Eqs. (35), (36) and (37) are compared in Fig. 3.

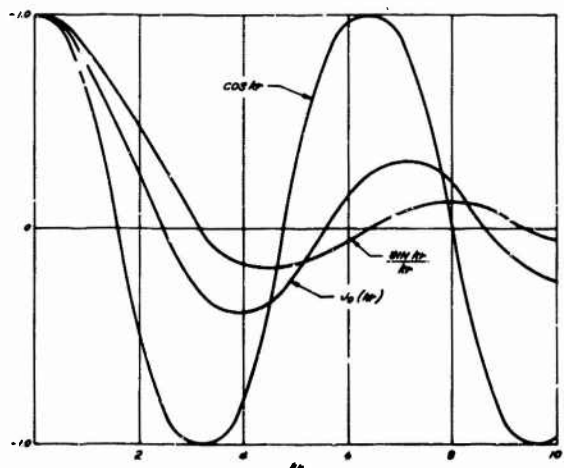
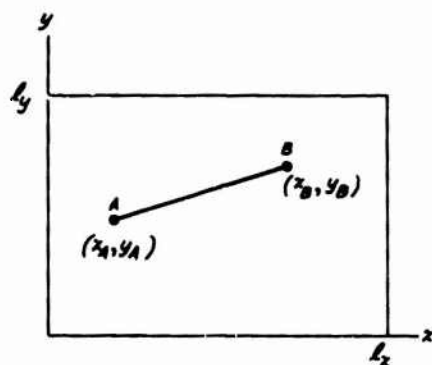


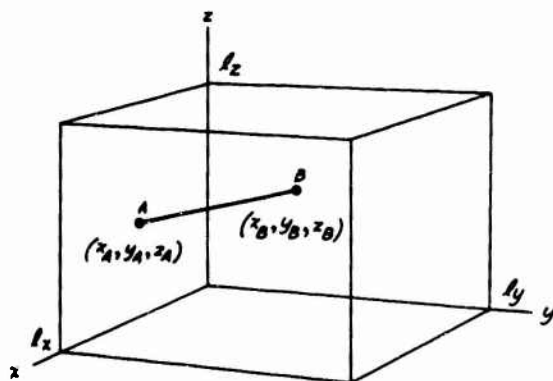
Fig. 3 COMPARATIVE NARROW-BAND CORRELATION COEFFICIENTS

## RECTANGULAR CHAMBERS

The physical model on which the previous calculation was based is more realistic than Cook's in that it recognizes the existence of resonant modes in the reverberation chamber and the need to consider many modes in a given bandwidth in order to define a diffuse field. However, the mode shape assumed is quite artificial as it was chosen for convenience in calculation rather than for physical realizability in practical chamber configurations. As the rectangular chamber is the most desirable configuration for which the wave equation is separable, it is of interest to carry out a similar calculation for actual mode shapes characteristic of rectangular 2-dimensional and 3-dimensional enclosures. To avoid considering both sine and cosine solutions to the wave equation and to establish a definite point for the excitation of the chamber, the origin will be taken at one corner as shown in Fig. 4.



(a) TWO-DIMENSIONAL



(b) THREE-DIMENSIONAL

Fig. 4 RECTANGULAR CHAMBERS

## TWO-DIMENSIONAL CHAMBER

Consider the 2-dimensional enclosure first. The frequency of any given mode is given by

$$f = (f_x^2 + f_y^2)^{1/2} \quad (38)$$

where

$$f_x = n_x c / 2l_x \quad (39)$$

and

$$f_y = n_y c / 2l_y \quad (40)$$

Averaging or summing with respect to phase and angle of arrival is replaced by summing with respect to  $f_x$  and  $f_y$  in frequency space. The pressures at points A and B, for a particular mode are

$$p_{AM} = P \cos(k_x x_A) \cos(k_y y_A) \cos 2\pi f t \quad (41)$$

and

$$p_{BM} = P \cos(k_x x_B) \cos(k_y y_B) \cos 2\pi f t \quad (42)$$

where

$$k_x = \pi n_x / l_x = 2\pi f_x / c \quad (43)$$

and

$$k_y = \pi n_y / l_y = 2\pi f_y / c \quad (44)$$

It follows that

$$\begin{aligned} \overline{p_{AM} p_{BM}} &= \frac{P^2}{2} \cos(k_x x_B) \cos(k_x x_A) \\ &\quad \times \cos(k_y y_B) \cos(k_y y_A) \\ &= \frac{P^2}{8} [\cos k_x (x_B + x_A) + \cos k_x (x_B - x_A)] \\ &\quad \times [\cos k_y (y_B + y_A) + \cos k_y (y_B - y_A)] \\ &= \frac{P^2}{8} [\cos k_x (x_B - x_A) \cos k_y (y_B - y_A)] + \zeta_2 \\ &= \frac{P^2}{16} [\cos r(k_x \cos \theta + k_y \sin \theta) \\ &\quad + \cos r(k_x \cos \theta - k_y \sin \theta)] + \zeta_2 \quad (45) \end{aligned}$$

where  $\zeta_2$  contains products that will yield negligible sums. Terms of forms such as  $\cos k_x (x_B + x_A) \cos k_y (y_B - y_A)$  or  $\cos k_x (x_B + x_A) \cos k_y (y_B + y_A)$  pass through maxima and minima more rapidly than  $\cos k_x (x_B - x_A) \cos k_y (y_B - y_A)$  as  $k_x$  and  $k_y$  are varied to permit summing over the strip shown shaded in Fig. 5. We assume that the contributions of the maxima tend to cancel those of the minima to the sum so that any net residual is negligible.

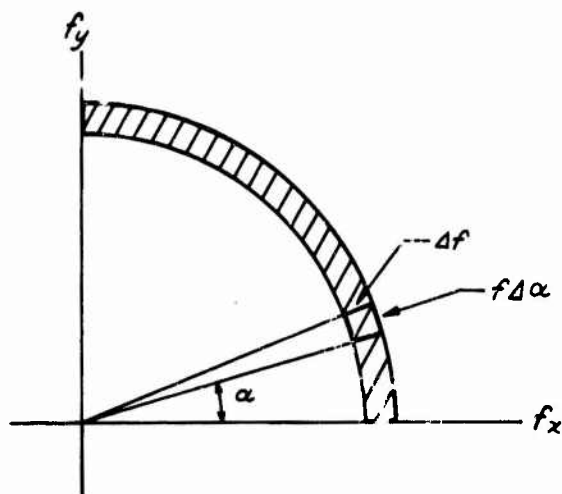


Fig. 5 REGION FOR INTEGRATION IN TWO-DIMENSIONAL FREQUENCY SPACE

We assume further that all modes have the same amplitude at the origin, that no two modes have identical frequencies and that the modal density  $m$  is large.

The narrow-bandwidth correlation density is given by the product of the modal density and the average value of the modal correlation function.

$$\begin{aligned}
 w_{AB\Delta f} &= \\
 m \frac{2P^2}{16\pi} \int_0^{\pi/2} \cos kr (\cos\theta \cos\alpha + \sin\theta \sin\alpha) d\alpha & \\
 + m \frac{2P^2}{16\pi} \int_0^{\pi/2} \cos kr (\cos\theta \cos\alpha - \sin\theta \sin\alpha) d\alpha & \\
 = \frac{mP^2}{8\pi} \int_0^{\pi/2+\theta} \cos kr (\cos(\alpha+\theta)) d(\alpha+\theta) & \\
 + \frac{mP^2}{8\pi} \int_0^{\pi/2-\theta} \cos kr (\cos(\alpha-\theta)) d(\alpha-\theta) & \quad (46)
 \end{aligned}$$

where the modal density  $m$  increases with frequency. But

$$\begin{aligned}
 \cos(kr \cos u) &= J_0(kr) - 2J_2(kr) \cos 2u \\
 &+ 2J_4(kr) \cos 4u - \dots \quad (47)
 \end{aligned}$$

Replace  $\alpha+\theta$  in one integral and  $\alpha-\theta$  in the other by  $u$ . Examination of the intervals of integration and noting that  $\cos 2nu$ , where  $n$  is an integer, is symmetrical about both 0 and  $\pi/2$ , yields

$$w_{AB\Delta f} = \frac{mP^2}{8} J_0(kr) \quad (48)$$

For comparison, the narrow-band spectral densities are obtained by averaging over the mode shape and over time and multiplying by  $m$  are:

$$w_{A\Delta f} = w_{B\Delta f} = \frac{mP^2}{8} \quad (49)$$

Consequently, the narrow-band correlation coefficient is

$$c_{12\Delta f} = J_0(kr) \quad (50)$$

for a two-dimensional reverberant field.

### THREE-DIMENSIONAL CHAMBER

For a three-dimensional rectangular chamber,

$$f = \left( f_x^2 + f_y^2 + f_z^2 \right)^{1/2} \quad (51)$$

where

$$f_z = n_z c / 2l_z \quad (52)$$

For a single mode

$$\begin{aligned}
 P_{AM} &= \\
 P \cos(k_x x_1) \cos(k_y y_1) \cos(k_z z_1) \cos 2\pi f t & \quad (53)
 \end{aligned}$$

$$\begin{aligned}
 P_{BM} &= \\
 P \cos(k_x x_2) \cos(k_y y_2) \cos(k_z z_2) \cos 2\pi f t & \quad (54)
 \end{aligned}$$

$$\begin{aligned}
 \overline{P_{AM} P_{BM}} &= \\
 \frac{P^2}{16} \cos k_x (x_2 - x_1) \cos k_y (y_2 - y_1) & \\
 \times \cos k_z (z_2 - z_1) + \zeta_3 & \\
 = \frac{P^2}{16} \cos(kr \sin\beta \sin\theta \cos\alpha \cos\theta) & \\
 \times \cos(kr \sin\beta \sin\theta \sin\alpha \sin\theta) & \\
 \times \cos(kr \cos\beta \cos\theta) + \zeta_3 & \quad (55)
 \end{aligned}$$

in accordance with Figs. 6 and 7 this is to be summed over a 1-octant shell of radius  $f$  and thickness  $\Delta f$ .

$$w_{12\Delta f} = \frac{m}{4\pi} \int_0^{\pi/2} \int_0^{\pi/2} \frac{1}{P_1 f P_2 f} \sin\beta d\alpha \quad (56)$$

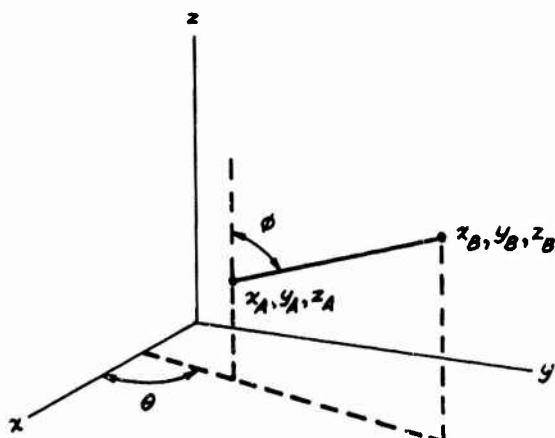


Fig. 6 POINTS IN THREE-DIMENSIONAL CHAMBER

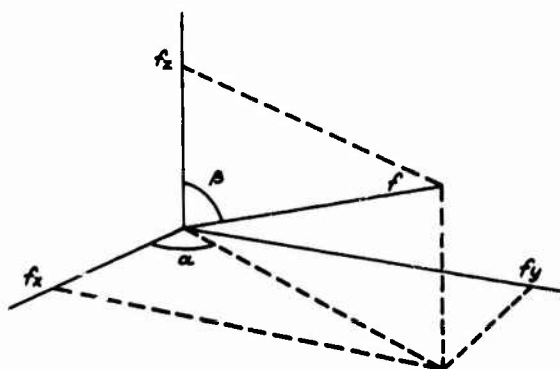


Fig. 7 FREQUENCY SPACE FOR THREE-DIMENSIONAL CHAMBER

For the reasons given in the 2-dimension derivation, terms in  $\zeta_i$  will not be considered in calculating the sum.

$$\begin{aligned}
 w_{12\Delta f} &= \frac{mP^2}{8\pi} \int_0^{\pi/2} d\beta \int_0^{\pi/2} \\
 &\quad \times \cos(kr \sin\beta \sin\theta \cos\alpha \cos\theta) \\
 &\quad \times \cos(kr \sin\beta \sin\theta \sin\alpha \sin\theta) \\
 &\quad \times \cos(kr \cos\beta \cos\theta) \sin\beta d\alpha \\
 &= \frac{mP^2}{16} \int_0^{\pi/2} \cos(kr \cos\beta \cos\theta) \\
 &\quad \times \int_0^{\pi/2} (kr \sin\beta \sin\theta) \sin\beta d\beta \quad (57)
 \end{aligned}$$

which is independent of  $\theta$ .

This amounts to proving that the integral is independent of direction in any plane parallel to a wall. Now consider two directions not parallel to a wall. Merely by varying  $\theta$ , they can be rotated into the  $yz$  or  $xz$  plane, where the integrals must be equal. Since their value is independent of  $\theta$ , the integrals for the original directions must be equal. Therefore Eq. (57) is independent of both  $\theta$  and  $\phi$ , and it is sufficient to integrate for  $\phi = 0$ . The narrow-band correlation density is therefore

$$\begin{aligned}
 w_{AB\Delta f} &= \frac{mP^2}{16} \int_0^{\pi/2} \cos(kr \cos\beta) \sin\beta d\beta \\
 &= -\frac{mP^2}{16} \int_{kr}^0 \frac{\cos(kr \cos\beta)}{kr} d(kr \cos\beta) \\
 &= +\frac{mP^2}{16} \cdot \frac{\sin kr}{kr} \quad (58)
 \end{aligned}$$

For comparison,

$$w_{A\Delta f} = w_{B\Delta f} = \frac{mP^2}{16} \quad (59)$$

so that the narrow-band correlation coefficient is

$$c_{AB\Delta f} = \frac{\sin kr}{kr} \quad (60)$$

An alternate method of evaluating of Eq. (57) is given in Appendix I.

## CONCLUSIONS

To obtain correlation formulas in agreement with Cook's, the following assumptions were found to be sufficient:

1. The reverberant field is undamped.
2. The modal density is high so that the bandwidth  $\Delta f$  contains many modes.
3. No two modes have the same frequency.
4. All modes are excited to equal amplitude at one corner.
5. Terms containing a factor such as  $\cos k_x(x_A + x_B)$  may be neglected in the summations or integrations.

We did not prove that all these conditions are necessary. However, it is obvious that if Assumption No. 2 is not satisfied, the integrations in frequency space are no longer accurate and large variations from the formulas may be expected. For example, if the frequency is low and  $\Delta f$  contains only one mode,  $\rho_{AB\Delta f} = \pm 1$ , for an undamped reverberant field.

Moreover, it is readily shown that extreme symmetry in the chamber, method of excitation, and placement of any test article for high-intensity noise testing can completely invalidate the formulas for certain measurement points. For example, in Fig. 8, the correlation coefficient for the points A and B must be  $\pm 1$ , even though they are a large distance apart. One effect of exciting the chamber at the center of a wall is to suppress many modes, especially those that would contribute to asymmetry in the reverberant field. Each excited mode yields a modal correlation coefficient of  $\pm 1$  for points symmetrically located, so that the average over a shell must also be  $\pm 1$ , regardless of the frequency band considered. Points not symmetrically located and not too close together may have as many  $-1$  as  $+1$  modal correlation coefficients and hence a zero narrow-band correlation coefficient. Since the planes of symmetry in the chamber of Fig. 8 must be velocity nodal planes, it is sufficient to imagine them as rigid walls, solve for the characteristics of the field of a sub-chamber of half the length and half the width, and obtain the remainder of the field as mirror images.

For any excitation point not at a corner, or for two excitation points excited with a definite phase relationship, some sorting and suppression of modes may be expected, so that the integrations in frequency space are no longer accurate. If there are redundant modes because of the particular ratios of dimensions of the chamber, there are additional complications in the integrations or summations.

In any event, it is reasonable to use Eqs. (35) and (37) as standards for determining the degree of diffuseness in a reverberant field. Furthermore, the formulation of the problem as given in the present paper lends itself to computer studies of statistical variations in the correlation when the modal density is low and narrow-bandwidths are of interest.

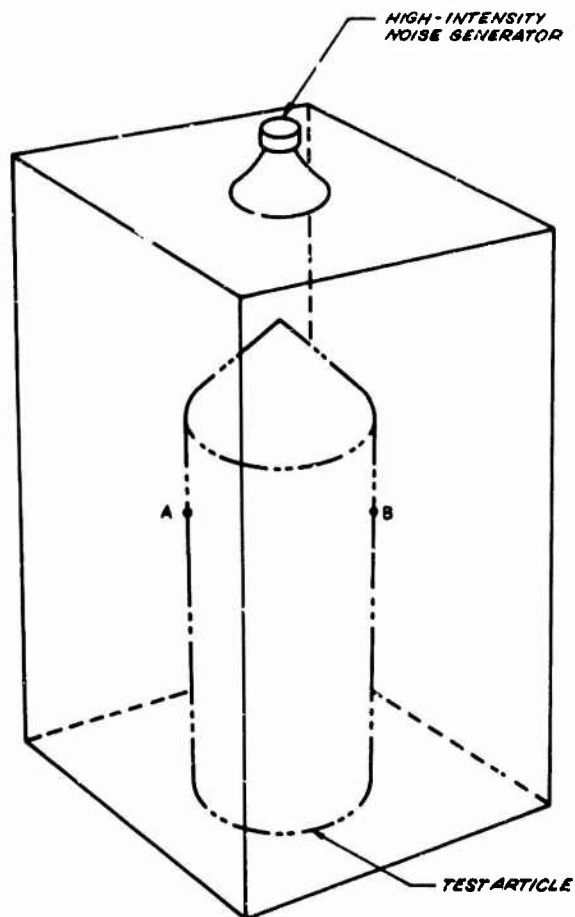


Fig. 8 A SYMMETRICAL CHAMBER

#### ACKNOWLEDGEMENT

I am indebted to the LTV Research Center, Western Division for support of this investigation and, in particular, to Peter K. Kasper for supplying the derivation in Appendix I.



# APPENDIX I

Alternate Evaluation of the Integral in Eq. (57). Let

$$I = \int_0^{\pi/2} \cos(kr \cos \theta \cos \beta) J_0(kr \sin \theta \sin \beta) \sin \beta d\beta,$$

$$J_0(kr \sin \theta \sin \beta) \sin \beta d\beta, \quad kr \cos \theta = a,$$

$$\text{and } kr \sin \theta = b.$$

$$I = \int_0^{\pi/2} \cos(a \cos \beta) J_0(b \sin \beta) \sin \beta d\beta$$

$$\cos(a \cos \beta) = \sum_{n=0}^{\infty} \frac{(-1)^n (a \cos \beta)^{2n}}{(2n)!}$$

$$J_0(b \sin \beta) = \sum_{m=0}^{\infty} \frac{(-1)^m (b/2)^{2m} (\sin \beta)^{2m}}{(m!)^2}$$

$$I = \sum_{m=0}^{\infty} \sum_{n=0}^{\infty} \frac{(-1)^{m+n} a^{2n} b^{2m}}{(2n)! (m!)^2 (2)^{2m}} \int_0^{\pi/2} \cos^{2n} \beta \sin^{2m+1} \beta d\beta$$

$$= \sum_{m=0}^{\infty} \sum_{n=0}^{\infty} \frac{(-1)^{m+n} a^{2n} b^{2m}}{(2n)! (m!)^2 (2)^{2m}} B(m+1, n+\frac{1}{2})$$

where

$$B(w, v) = \frac{\Gamma(w) \Gamma(v)}{\Gamma(w+v)}$$

is the Beta function. With some cancellation of factors,

$$I = \sum_{m=0}^{\infty} \sum_{n=0}^{\infty} \frac{(-1)^{n+m} a^{2n} b^{2m} (m+n)!}{n! m! (2m+2n+1) (2m+2n)!}$$

Let  $m = q \geq 0$  and  $n = p-q \geq 0$  with  $q \leq p$  so that

$$\sum_{m=0}^{\infty} \sum_{n=0}^{\infty} a_{mn} = \sum_{p=0}^{\infty} \sum_{n=0}^p a_{q, p-q}$$

$$I = \sum_{p=0}^{\infty} \sum_{q=0}^p \frac{(-1)^p (kr)^{2p} \cos^{2(p-q)} \theta \sin^{2q} \theta (p!)}{(q!) (p-q)! (2p)! (2p+1)!}$$

$$= \sum_{p=0}^{\infty} \frac{(-1)^p (kr)^{2p}}{(2p+1)!} \times \sum_{q=0}^p \frac{\cos^{2(p-q)} \theta \sin^{2q} \theta (p!)}{(q)! (p-q)!}$$

But, the second summation is the binomial expansion for

$$(\cos^2 \theta + \sin^2 \theta)^p = 1$$

for all  $p$ .

$$I = \sum_{p=0}^{\infty} \frac{(-1)^p (kr)^{2p}}{(2p+1)!} = \frac{\sin kr}{kr}$$

ENVIRONMENTAL LABORATORY MISSILE FAILURE RATE  
TEST WITH AERODYNAMIC FUNCTION SIMULATION

Raymond C. Binder and Gerald E. Berge  
Naval Missile Center  
Point Mugu, California

This paper gives the results of an investigation to improve the present laboratory missile failure rate test. The missile is installed in an environment chamber and exercised with an aerodynamic functional simulator and an oscillating target. A test arrangement is described in which the guidance and control system effective navigation ratio and time constant are measured. This ratio and the time constant are clear, definite and significant parameters for testing and evaluating the missile. While exercised by the simulator, the missile can undergo failure rate tests under various conditions, such as vibration, shock, humidity, temperature and altitude. During a test a malfunction or failure can be detected, and the exact time of failure identified.

Specific tests were made with a missile. A target was oscillated over a range of frequencies. A two-dimensional aerodynamic simulation was set up on an analog computer, with numerical values for Mach number, altitude and missile. With no malfunction the effective steady state navigation ratio  $N_s$  was an acceptable value; introduction of a malfunction gave a definitely unacceptable  $N_s$ . The malfunction was an open filament in a type 5703 tube. Using the Fourier integral method, a transient response was determined from a measured transfer function; this response agreed closely with other independent studies. The present study showed that the proposed test plan could provide an improved type of environmental laboratory failure rate test.

#### INTRODUCTION

The environmental laboratory missile failure rate test has merit because it involves the important feature of reliability as a function of time. This paper gives the results of an investigation to improve the present laboratory failure rate test.

A laboratory missile test involves a number of objectives and aspects. There are aspects of cost, significance of test, length of test time involved and the number of missiles. With the development of more complicated missiles, the number of missiles available for test may be limited. The laboratory test should not damage the missile permanently.

The significance of a laboratory simulation depends on the accuracy and completeness of the simulation. In the case of an electronic package to be tested, the simulation should include representative electrical loading in addition to the natural environment. Simulation of the electrical loading

of a missile can be accomplished by providing a representative input signal to the missile detector and completing any external feedback control loops.

There are important questions as to what data should be taken, and what reduced parameters might be useful in evaluating a missile system. Consideration might be given to the measurement of various individual features; example are limiter grid voltage, video signal-to-noise ratio, rate-gyro voltage, accelerometer voltage and head position voltage. Each of these measurements may involve an important individual factor. Each individual factor alone, however, may not give much of a useful, definite final conclusion in evaluating the entire missile. What is needed is some one or more compact parameters which would involve the entire missile performance including overall guidance, control, aerodynamic features and

navigation. During the test there should be an indication of either acceptable performance or a malfunction as a function of time.

The performance of any automatic control system can be completely determined by the frequency response of the system. Frequently a system is designed, built and tested on a frequency basis. It is helpful to have some significant time constant or some measure of the transient response of the system. Thus, the present laboratory failure rate test could be improved by giving attention to the guidance and control system frequency response and time constant of the missile to be tested.

The following presents a scheme for measuring the frequency response and time constant in terms of a significant navigation parameter. This navigation parameter is measured as a function of time, thus the exact time of a malfunction can be determined. An analytical framework will be blocked out first. After describing a test arrangement, an example will be given of a specific test with a two-dimensional aerodynamic simulation.

#### NAVIGATION PARAMETERS

Most air defense systems in use and under development use homing guidance to effect intercept of the target. Many homing systems employ some form of proportional navigation as the guidance law. A proportional navigation course is one in which the time rate of change of missile heading is directly proportional to the time rate of rotation of the line-of-sight from the missile to the target.

In order to illustrate basic features with a minimum of complication, two-dimensional missile motion in the horizontal plane will be considered. Let  $R$  represent missile yaw rate,  $\dot{\theta}$  missile side-slip angle time rate and  $V_M$  missile linear velocity. The missile lateral acceleration  $A_y$  is given by the expression

$$A_y = V_M [\dot{\theta} + R] \quad (1)$$

Let  $V_c$  represent closing velocity,  $\omega$  angular frequency,  $\lambda$  line-of-sight angle and  $\dot{\lambda}$  line-of-sight angle time rate. Various investigations have shown that a significant parameter is the

effective navigation ratio  $N(\omega)$ , a function of frequency, defined as the dimensionless ratio

$$N(\omega) = \frac{V_M}{V_c} \frac{[\dot{\theta} + R]}{\dot{\lambda}} = \frac{A_y}{\dot{\lambda} V_c} \quad (2)$$

Let  $1 = \sqrt{-1}$ . In general,  $N(\omega)$  is a complex number and can be expressed in the general form

$$N(\omega) = N_s \frac{[1 + B_1(\omega) + B_2(\omega)^2 \dots]}{[1 + C_1(\omega) + C_2(\omega)^2 \dots]} \quad (3)$$

where  $N_s$  is a dimensionless real number called the steady state effective navigation ratio, and the successive  $B$  and  $C$  coefficients have values depending on the system.

As an example, we will assume that the missile design objective is a value of  $N_s$  between 3 and 4; this range involves a reasonable level of lateral acceleration. A value of  $N_s$  of 2 may require a theoretically infinite missile acceleration at intercept, whereas a value of  $N_s$  greater than 4 may involve problems of noise.

In a laboratory test arrangement the target can be moved with simple harmonic motion over a range of frequencies. For a line-of-sight amplitude  $\lambda_0$ , the following relations hold

$$\lambda = \lambda_0 \sin \omega t \quad (4)$$

$$\dot{\lambda} = \lambda_0 \omega \cos \omega t \quad (5)$$

In a missile design, significant deviations from a linear analysis result in a greatly increased miss distance. Thus a major design task may be to insure that significant nonlinearities do not occur. Also, a linear analysis reduces the complexity of analysis and helps in predicting performance characteristics. For linear systems the Fourier integral or transform relations apply. Once the

frequency response is established, then the transient response to some simple representative input can be determined by the Fourier integral method.

#### GENERAL LABORATORY TEST ARRANGEMENT

There is a question as to how a laboratory failure rate test can be arranged to exercise a missile, in an environment, and measure the important parameters, as the effective navigation ratio as a function of frequency along with a guidance and control system time constant.

Figure 1 shows a schematic of a laboratory arrangement.

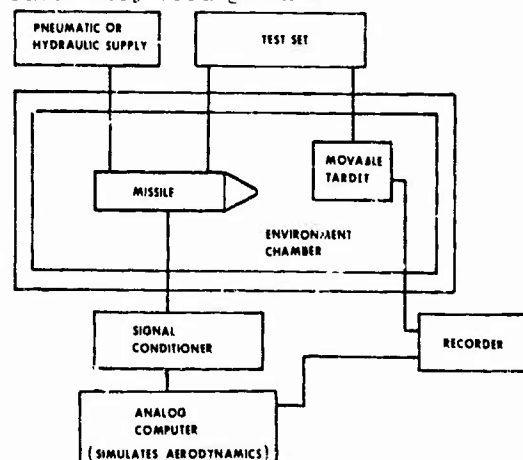


Fig. 1. Schematic arrangement of test apparatus.

The missile to be tested is installed in an environment chamber where it can undergo failure rate tests under various conditions, such as shock, vibration, humidity, temperature and altitude. During a test a malfunction or failure can be detected, and the time of failure identified. A pneumatic or hydraulic supply and a test set is connected to the missile. The analog computer is used as a simulator, in providing a functional simulation of the airframe or flight aerodynamics. An interface or signal conditioner is placed between the missile and aerodynamic simulator. The movable target serves to simulate some flight target movement.

Signals from the target, the missile and the simulator can be fed to a plotter or some other recording instrument to give various measurements as a function of time. For frequency response measurements the target can be moved with simple harmonic motion over a range of frequencies. The signal for missile lateral acceleration from the

aerodynamic simulator can be combined with the line-of-sight rate signal developed by the oscillating target to give the effective navigation ratio. The transient response, and thus a guidance and control system constant, is determined from the effective navigation ratio as a function of frequency.

#### SPECIFIC TESTS

Specific tests were made in order to check the new features of the proposed test arrangement. An oscillating target was arranged; this consisted of a variable-speed motor driving a scotch-yoke mechanism. A radar horn was fastened to the yoke. Referring to Fig. 1, the horn moved at right angles to the missile axis with simple harmonic motion. A potentiometer fixed to the yoke was used to record the actual displacement-time motion of the moving target. For a certain distance between the missile head and the moving radar horn, the displacement-amplitude of the horn can be used to determine the line-of-sight turning rate over a range of frequencies.

Figure 2 illustrates the test arrangement for a certain set of aerodynamic conditions.

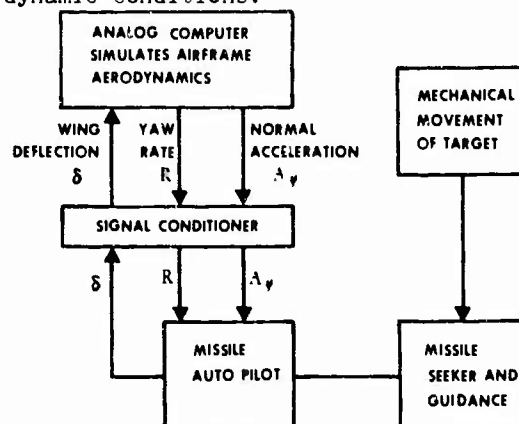


Fig. 2. Block diagram of functional simulation

The moving target develops a signal which results in a signal into the autopilot. The autopilot sends a wing deflection signal to the aerodynamic functional simulator. A calculation made in the aerodynamic simulator results in a yaw rate signal and a normal or lateral acceleration signal which is sent to the autopilot.

Considering the airframe aerodynamics, in the most general case there are six degrees of freedom, involving three force differential equations. In

the present study a particular representative case was taken, for a certain Mach number, altitude and missile. In this case it was assumed that the missile moves only in a horizontal plane with no roll. The missile can rotate about its vertical body axis with a yaw velocity and can have a lateral linear acceleration.

Let  $m$  represent mass of missile,  $q$  dynamic pressure of approach flow,  $\beta$  side-slip angle,  $\delta$  wing deflection angle,  $C_{L\beta}$  lift coefficient curve slope for  $\beta$ ,  $C_{L\delta}$  lift coefficient curve slope for  $\delta$ ,  $S$  reference area,  $I$  missile moment of inertia,  $c$  reference length,  $C_{m\beta}$  moment coefficient curve slope for  $\beta$ ,  $C_{m\delta}$  moment coefficient curve slope for  $\delta$ ,  $C_{mR}$  moment coefficient curve slope for yaw rate  $R$ , and  $\ddot{R}$  yaw acceleration. The differential equations of motion are

$$mV_M[\dot{\beta} + R] = mA_y = [-C_{L\beta}\beta + C_{L\delta}\delta]q \quad (6)$$

$$\dot{R}I = [-C_{m\beta}\beta + C_{m\delta}\delta]qsc + [C_{mR}\frac{sc^2}{2V_M}q]R \quad (7)$$

An aerodynamic simulation for Eqs. (6) and (7) was set up on an analog computer.

#### TEST RESULTS FOR TWO DIMENSIONAL AERODYNAMIC SIMULATION

A variety of laboratory missile tests were made using the simulation described in the previous section. Tests were made for different distances between missile head and the oscillating target. Thus, a range of line-of-sight rates were used. For each test the steady state effective navigation ratio  $N_s$  was measured as a function of time.

Figure 3 shows a plot of  $N_s$  versus frequency. The  $N_s$  values range between 3 and 4. For each of these tests a value of  $N_s$  between 3 and 4 showed that the missile was operating in an acceptable manner.

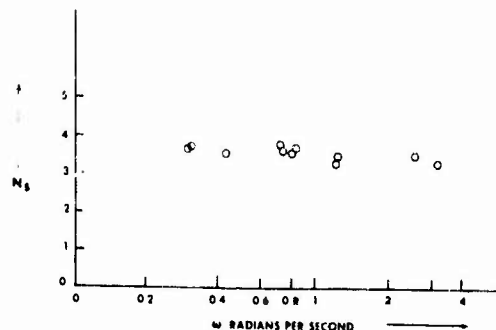


Fig. 3. Plot of test results.

By means of a switch arrangement the filament of a type 57<sup>12</sup> tube was opened as required to induce a malfunction. This particular malfunction had often occurred during some previous laboratory tests on this missile. Table 1 illustrates typical results. At one frequency with no malfunction, the steady state effective navigation ratio  $N_s$  was 3.9; this indicates acceptable performance. With a malfunction  $N_s$  was 16.1; this definitely was an unacceptable performance value.

Tests over a range of frequencies were used to obtain a system transfer function with line-of-sight rate as the input and the missile lateral acceleration unit step input was determined. Figure 4 illustrates a plot of response to a unit step input; this type of plot can be used to determine a time constant. The response obtained with the present test arrangement agreed closely with results obtained by other independent investigations.

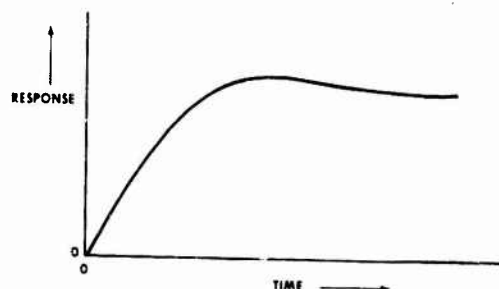


Fig. 4. Transient response to unit step input.

TABLE I  
TESTS WITH AND WITHOUT MALFUNCTION

	Frequency Radians Sec.	Line-Of-Sight Rate Radians Sec.	Acceleration FT Sec. <sup>2</sup>	Steady State Navigation Ratio
No Malfunction	0.358	0.0144	90	3.9
With Malfunction	0.358	0.0144	372	16.1

#### CONCLUDING REMARKS

Specific tests were made with a missile. The present study shows that the proposed test plan could provide an improved type of environmental laboratory missile failure rate test. The function simulation technique provides a diagnostic tool for indicating the exact time of a malfunction. The

proposed test plan will help in conducting better and more meaningful missile evaluations. The present study was made with a two-dimensional aerodynamic functional simulation. This functional simulation could be extended to higher degrees of freedom; this means more differential equations on the analog computer or simulator.

#### DISCUSSION

Mr. Jackman (General Dynamics, Pomona): Have you tried any environments on top of your failures with and without malfunctions? Have you tried any environments such as temperatures?

month or two. We are not trying to measure the performance of this missile. Our goal is to measure the failure rate and we will be interested in degradation under environmental conditions, however, our main goal is to measure failure rate.

Mr. Berge: No, but we probably will in a

## APOLLO CSM DYNAMIC TEST PROGRAM

A. E. Chirby, R. A. Stevens, W. R. Wood, Jr.  
North American Rockwell Corporation  
Downey, California

The dynamic tests performed on the Block II (lunar flight vehicle configuration) Apollo Command-Service Module Assembly (CSM 105/AV) at NASA's Manned Spacecraft Center Spacecraft Vibration and Spacecraft Acoustic (SVL and SAL) Laboratories were the culmination of a long series of Apollo CSM vibration, acoustic and vibro-acoustic ground tests. Prior to initiation of CSM 105/AV testing, random vibration criteria had been established for Block II CSM vehicles by extrapolation of response data obtained from Block I (earth orbit configuration) CSM flights and ground acoustic tests. In addition, Block II Service Module (SM) criteria were verified by vibro-acoustic tests of a 180° segment of a Block II SM.

Four vibro-acoustic tests were performed in the SAL on CSM 105/AV to determine, in addition to other objectives, the validity of the Block II CSM random vibration criteria. Part of the CSM 105/AV Vibro-acoustic Test Program consisted of several calibration tests of a Block I CSM which were run in the SAL. The calibration tests established the SAL acoustic environments which would produce Block I CSM random vibration levels (those vibration levels associated with atmospheric flight). Since the Block I and Block II flight environments were the same, the SAL acoustic environments established by the calibration tests were accurate acoustic forcing functions for CSM 105/AV.

In addition to a detailed explanation of the vibro-acoustic tests discussed above, the paper will describe the vibration portion of the CSM 105/AV test program. Prior to vibration of CSM 105/AV, a Block I vehicle was excited by electrodynamic shakers to establish techniques and procedures to be used. CSM 105/AV vibration tests were to demonstrate the CSM structural integrity and measure CSM vibratory responses in the 4 to 30 Hz frequency range. One of the vibration tests was a manned run. In the manned run, an astronaut, in addition to one anthropomorphic dummy, was secured in the crew couch while the CSM was excited in the frequency range which corresponded to that measured on the flight of AS 501.

### INTRODUCTION/BACKGROUND

#### Spacecraft Description

The principal components of the Apollo spacecraft are the Launch Escape System (LES),\* the Command Module (CM),\* the Service Module (SM)\* and the Spacecraft Lunar Adapter (SLA),\* with the Lunar Module (LM). Figure 1 depicts the major elements of the Saturn V stack.

The LES mounts on the top of the CM. Its purpose is to separate the CM from the stack during an atmospheric abort.

The control center of the spacecraft is the CM. The flight crew, the equipment to control and monitor the spacecraft systems and the equipment necessary for the comfort and safety of the crew are located in the CM.

\* Designed and built by North American Rockwell Corporation's Space Division, Downey, California, under contract to NASA's Manned Spacecraft Center, Houston

The SM houses the propulsion systems required for spaceflight operations. Cryogenic storage provisions, the fuel cells, the support surface for the space radiators for electrical power and environmental control systems and various other components supporting the CM and SM systems are also located in the SM.

The SLA provides structural connection between the SM and the Launch Vehicle. Its primary purpose is to house the Lunar Module.

#### Dynamic Environments

At lift-off, noise is generated in the turbulent boundary between the rocket engine exhaust and the surrounding atmosphere and is radiated to the surface of the spacecraft. The noise level decreases rapidly as the vehicle leaves the reflective surface of the launch pad. The aft section of the SLA is the only portion of the spacecraft (CM, SM and SLA) that is affected more by the booster engine-induced noise than the aerodynamic noise that exists later in flight. As the spacecraft velocity

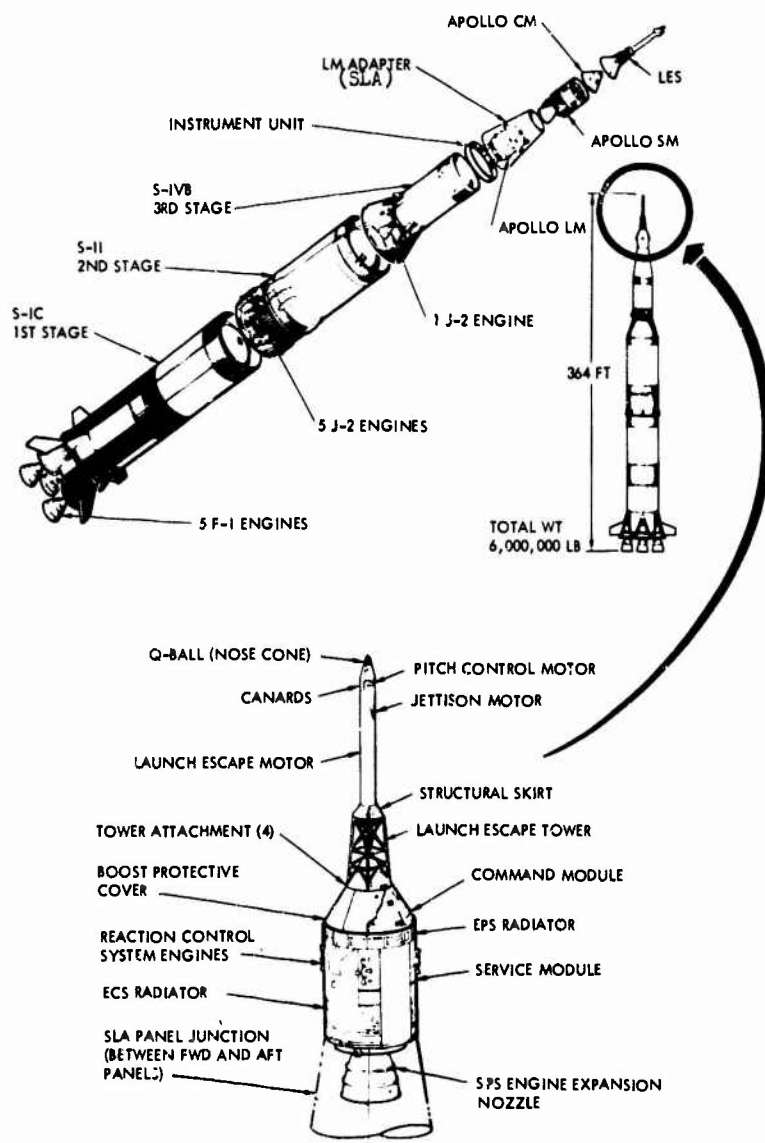


Figure 1. Apollo Spacecraft and Saturn S-V Booster



increases, the aerodynamic excitation resulting from turbulent air flow over the spacecraft surface increases. Near sonic velocity, air-flow separations occur on the SM, causing a transient peak in level (maximum SM excitation). Beyond sonic speed, steady flow conditions are re-established with a resulting reduction in the fluctuating pressure level. However, as the dynamic pressure increases, the fluctuating pressure levels again increase until another peak value (maximum CM excitation) is obtained near Mach 1.6 (Max Q). The noise levels diminish as the spacecraft moves out of the atmosphere.

An abort condition requiring LES engine operation is the other major source of acoustic excitation the spacecraft (CM only) may experience during atmospheric flight. LES engine operation (six seconds total duration) does not produce a CM acoustic environment greater than the CM Max Q environment, except at frequencies above 400 Hz. Figure 2 compares the CM Max Q flight acoustic environment and the CM Max Q abort flight acoustic environment.

Apollo Mission AS 501 revealed that significant low frequency vibratory loads, in

addition to random acoustic excitation, could be imposed on the spacecraft. These low frequency (4 to 7 Hz) oscillatory loads were produced by Saturn S-IC booster engines.

#### CSM Criteria Development

The principal prediction method used to establish the initial Command and Service Module random vibration criteria was that developed by Mahaffey and Smith (1) on the B-58 aircraft. Scale model wind tunnel test acoustic data was also used in support of the initial prediction.

Data acquired from fluctuating pressure transducers on early Apollo boilerplate\*vehicles were used to refine the flight acoustic environments previously established by the scale model wind tunnel testing. A series of static LES engine firings were used to establish the acoustic field around the CM during LES engine operation.

\* Basic shape, volume and weight only of CSM

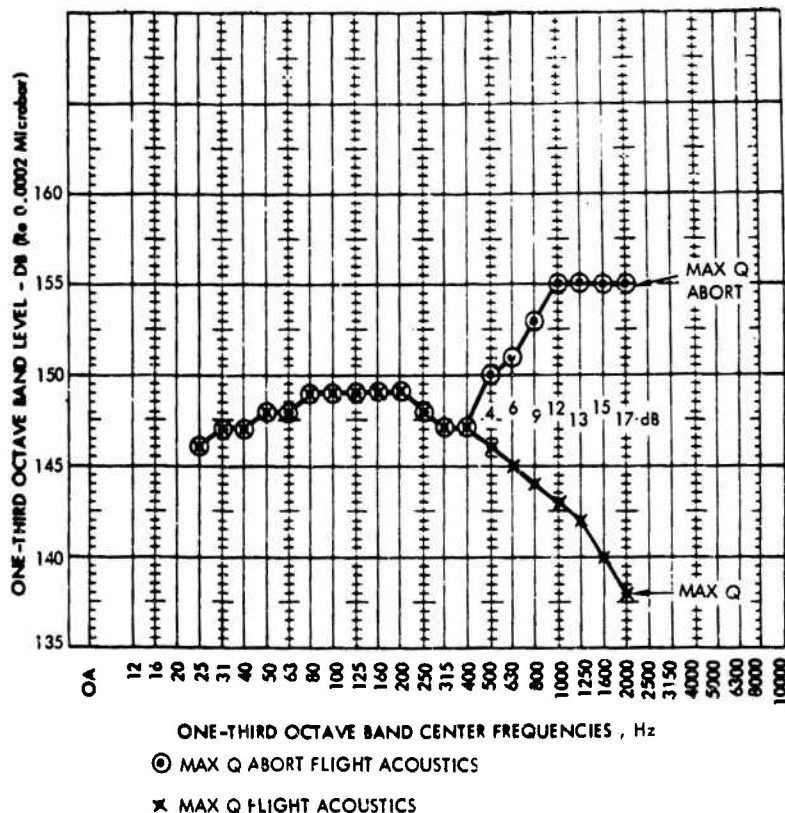


Figure 2. Comparison of Maximum Q and Maximum Q Abort Flight Acoustics

The first major ground acoustic tests were conducted at the North American Los Angeles Division acoustic facility using production Block I Command and Service Modules. The results of the Command and Service Module acoustic tests produced the following: 1) zonal areas of the Command and Service Modules were redefined in much more detail, 2) vibration criteria was updated for each of the redefined zones, and 3) major retest programs were conducted to delta qualify components and subsystems that were previously tested to the lower predicted vibration levels.

The "vibro-acoustic test" method (2) was applied to requalify the SM components. The basic concept of vibro-acoustic component (or subsystem) qualification testing is to develop an acoustic spectrum which will induce flight level vibration responses at specific locations on primary structure. The component or subsystem is then attached to the primary structure in its normal mounted configuration and the previously developed acoustic spectrum is used to excite the assembly.

In requalifying the SM components and subsystems a 180° segment of the SM was used. This segment, with test articles attached, was acoustically excited to the vibration levels previously established by the SM acoustic test and supplemented by flight test data. The SM component and subsystem requalification retest program was highly successful with few anomalies occurring. Minor redesign of components or subsystems corrected the anomalies which did occur.

Vibration response data obtained from the acoustic and vibro-acoustic tests of the command and service modules and from the SM 180° segment and Block I CSM flights were used to establish the vibration criteria for Block II vehicles. The development of Apollo CSM vibration test requirements is treated in greater detail in reference (3).

The dynamic tests conducted at MSC were the last in a series of major ground tests used for criteria development and demonstrating structural and functional integrity of the CSM for the atmospheric portion of flight. The paper describes the testing accomplished using CSM 105/AV as the test specimen.

#### CSM 105/AV TEST PROGRAM

##### Test Objectives

The dynamic test performed on the Block II Apollo Command Service Module assembly, CSM 105/AV, at the Manned Spacecraft Center (MSC), Spacecraft and Vibration and Acoustic Laboratories (SAL and SVL) had the following six objectives:

- (1) To determine the structural integrity of the Block II CSM when it is subjected to the dynamic loads resulting from spacecraft

exposure to the aerodynamic noise environment present during atmospheric flight.

- (2) To verify existing vibration criteria for Block II Command and Service modules.
- (3) To establish the vibration transmissibility characteristics of the Block II Command-Service Module (CSM) Assembly.
- (4) To qualify the side Command Module hatch mechanism.
- (5) Verify Block II CSM structural integrity in the low frequency vibration environment produced during atmospheric flight.
- (6) To obtain subjective interpretation of a crewman's ability to distinguish display panel annunciations and to successfully operate the abort controller while the CSM is subjected to axial oscillations which may occur during the first stage of the Saturn V flight. Also to obtain physiological data for correlation so that deviations from the normal could be identified and evaluated.

The first manned Apollo flight was constrained by the attainment of objectives 1, 2, 4, 5 and 6. Objective 3 was aimed at acquiring valuable, but not flight critical, engineering information.

##### Test Procedures

Table I chronologically lists the tests which were required to accomplish the test objectives. In general, both the vibration and acoustic test series utilized the concept of establishing test procedures and/or test environments on calibration vehicles prior to testing of CSM 105/AV. The specific procedures for each of the major tests were as follows:

##### DITMCO - CSM wiring harness check

DITMCO is an acronym for an automated, circuit continuity and wiring insulation checkout system. The CSM wiring harness baseline condition prior to test was established by DITMCO-1. DITMCO-2 established the condition of the wire harness following exposure to the vibration and acoustic environments.

##### CHECKS - pressure and functional

Critical CSM pressure systems were pressurized to operating pressures (except where facility safety requirements prohibited) and monitored at all times when excitation was applied to the vehicle. The redesigned CM side crew hatch was functioned before and after the VA-1 test series as part of its qualification requirements. Both the pressurization and hatch functioning procedures were performed at their appropriate times on tests VM-1, VA-2, and VA-3.

TABLE I - Test Matrix

TEST DESIGNATION	TEST CONDITION	TEST PURPOSE	TEST CONFIGURATION
DITMCO-1	CSM Wiring Harness Check	Verify CSM Wiring Harness O.K. prior to test	CSM 105/AV
VA-C1	CSM Low Frequency Vibration Calibration	Establish Test Procedures for VA-1 and VM-1	BP 27 LES and CM. SM 010 and SLA-6
VA-1	CSM Low Frequency Vibration	Primary Test Objectives 3 and 5	BP 27 LES, CSM 105/AV, SLA-6, and support fixtures
VM-1	CSM Manned Low Frequency Vibration	Primary Test Objective 6	BP 27 LES, CSM 105/AV, SLA-6, and support fixtures
VA-C2	CSM Maximum Q Calibration	Establish Maximum Q Acoustic Environment for VA-3	CM 011, SM 007, SLA-2, IU and S-IVB Forward Skirt
VA-C2	CM Maximum Q Abort Calibration	Establish Maximum Q Abort Acoustic Environments for VA-2	CM 011, SM 007, SLA-2, IU and S-IVB Forward Skirt
VA-2	CM Maximum Q Abort	Primary Test Objectives 1, 2, 3 and 4	CSM 105/AV
VA-3	CSM Maximum Q	Primary Test Objectives 1, 2, 3 and 4	CSM 105/AV, SLA-2, IU and S-IVB Forward Skirt
DITMCO-2	CSM Wiring Harness Check	Verify CSM Wiring Harness O.K. after VA-1, VM-1, VA-2 and VA-3 Testing	CSM 105/AV

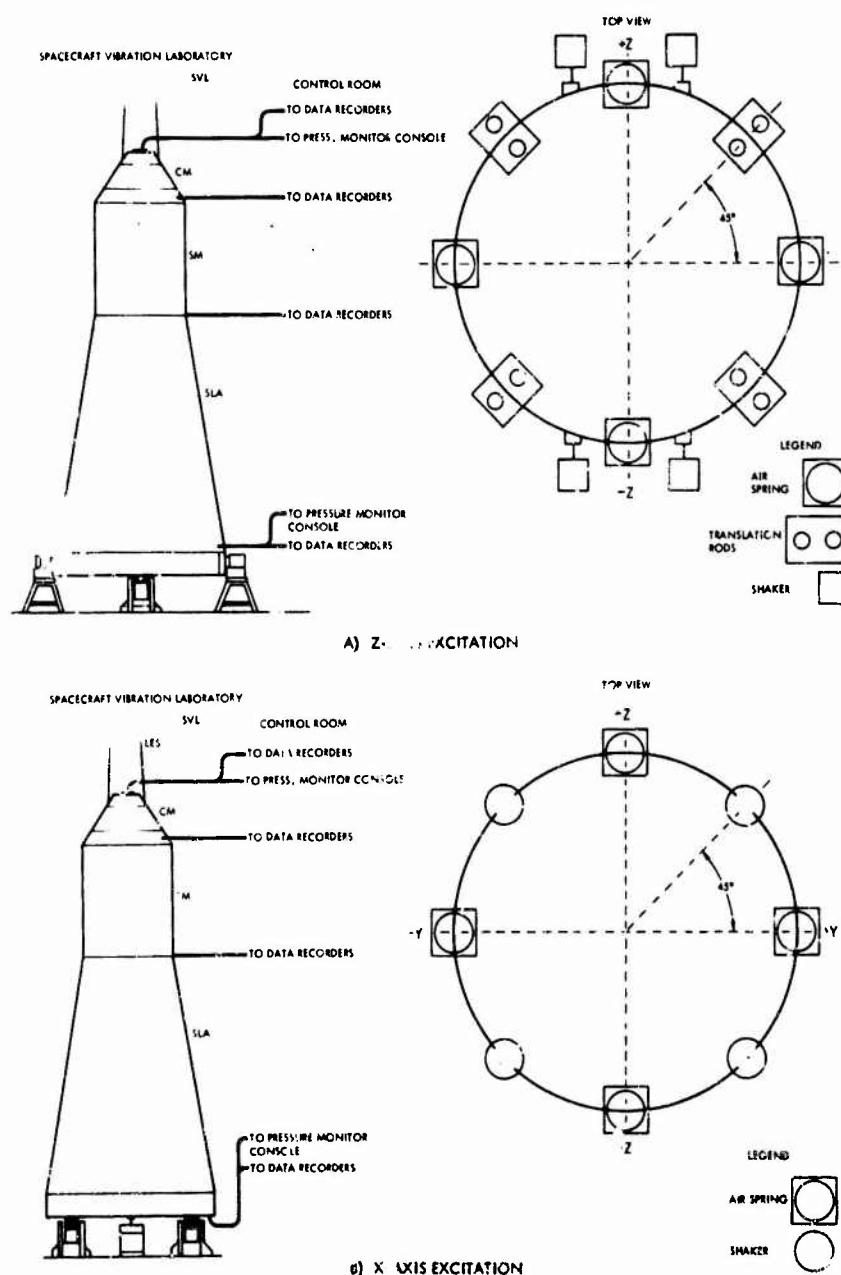
NOTE: Primary Test Objective 1: Verify Block II CSM structural integrity  
 2: Verify Block II CSM vibration criteria  
 3: Establish vibration transmissibility of CSM  
 4: Qualify Block II CSM side hatch mechanism  
 5: Verify Block II CSM structural integrity in the low frequency vibration environment  
 6: Evaluate crewman's performance when subjected to low frequency vibration

**VA-C1 - JSM low frequency vibration calibration**

The vibration calibration test was performed to demonstrate vibration test facility capability and to develop test procedures that would satisfy the test requirement without subjecting the test specimen to unrealistic loads. The test configurations illustrated in Figure 3 for the VA-1 tests are representative of those used for VA-C1 except

that Block I Command and Service Modules were used (see Table I).

The test fixture was a boxed construction ring which was rigid in the frequency range of interest. The SLA was secured to the top of the ring fixture with the vibration thrusters, and suspension system attached to the bottom. The suspension system for longitudinal testing consisted of four air springs located at 90 degree intervals around the test fixture.



**Figure 3 Low-Frequency Vibration Test Setup**

The air springs were pressurized to support the entire weight of the test specimen and fixture. The fundamental axial resonant frequency of the suspended test configuration was approximately 1 Hz. Four pairs of translation rods located at 45 degrees from the air springs were attached to the test fixture to react overturning moments generated during lateral testing.

The vibration excitation system consisted of four Ling Model 310, 10,000 pound force thrusters attached to the test fixtures as shown in Figure 3.

The vibration testing consisted of sinusoidal sweeps from 4 to 30 Hz followed by sinusoidal dwells at the predominant resonant frequencies. These tests were performed in the spacecraft "Z" and "X" axes (longitudinal and lateral).

The vibration responses during the sweep tests were controlled to 0.075 inch D.A. for the 4 to 8 Hz frequency range and 0.1 g peak for the 7 to 30 Hz frequency range with a response limit of 0.15 inch D.A. or 0.15 g peak except for those measurements at the end of the LES which were limited to 0.5 g peak. Response amplitude control was accomplished by connecting the thirteen most critical measurements for the specific run to a multilevel selector (SML) which in turn selected the highest amplitude signal and transmitted it to the servo-controlled thruster system. Following each sinusoidal sweep, all data were transferred from the tape recorders to oscillograph records for on the spot analysis.

A data evaluation team consisting of NR, NASA, GE and Boeing engineers immediately reviewed the vibration response data to determine the predominant resonant frequencies. Sinusoidal vibration dwell tests were then performed at each of the resonant frequencies. The intended technique for tuning each dwell frequency was to connect each control transducer to the vertical axis of an oscilloscope with the Constant Output Level Adapter (COLA) signal driving the horizontal axis and then vary the excitation frequency until the maximum number of closed lissajous were attained. The initial tuning amplitude was that used during the sweep and then it was increased to 0.15 inch P.A. or 0.25 g peak for final tuning and subsequent 20 second dwell. This technique for tuning resonances, although accurate, proved to be entirely too time consuming. The tuning method ultimately arrived at consisted of setting the excitation frequency to that determined from the sweep data and adjusting

the response amplitude on the selected control transducer to the sweep amplitude. With the thruster force maintained at a constant level, the frequency was varied until the maximum control transducer response was achieved. The excitation amplitude was then increased to 0.15 inch D.A. or 0.25 g peak, whichever was applicable, and the frequency was retuned to compensate for any resonance shift due to amplitude change.

#### VA-1 - CSM low frequency vibration

The CSM 105/AV vibration test requirements were derived from NASA analytical efforts supplemented by SC 009 (AS-201) and SC 011 (AS-202) flight tests and also from axial oscillations observed during the period of first stage boost on SC 017 (AS-501). The test configurations are illustrated in Figure 3. The test fixture, suspension system, and excitation systems were the same as those used in VA-C1.

Sinusoidal sweeps from 4 to 30 Hz were conducted in both the spacecraft "X" and "Z" axes, at a sweep rate of one octave per minute. The vibration response amplitude was maintained at 0.1 g peak at the transducer selected by the SML as the highest of the thirteen control transducers.

Additional sweep tests were required in the spacecraft "X" axis to account for axial oscillations observed on the Command Module forward bulkhead during the AS-501 mission. A linear sinusoidal frequency sweep test was performed from 4 to 6 Hz over a period of 130 seconds. The vibration response amplitude controlled at the Command Module forward bulkhead was varied linearly from 0.15 g peak at 4 Hz to 0.4 g peak at 6 Hz. Following the 4 to 6 Hz sweep test, an 18 second linear sinusoidal sweep from 6 to 7 Hz was conducted. The Command Module forward bulkhead vibration response was varied from 0.2 g peak at 6 Hz to 0.7 g peak at 7 Hz.

Predominant resonant frequencies were selected from the sweep data for the sinusoidal dwell tests. The selected frequencies were tuned utilizing the method developed in VA-C1 and 20 second sinusoidal dwells were performed at each frequency.

#### VM-1 - CSM manned low frequency vibration

Since the AS-501 axial oscillations were higher than had been expected for the Saturn V mission, it was advisable to determine the effects of this increased vibration level on crew members' ability to perform necessary operations during first stage boost. Therefore, the VM-1 test was conducted with Astronaut Colonel Gordon Cooper occupying the commander's station on the crew couch. An anthropomorphic dummy was secured to the right hand couch and the center couch was used for instrumentation.

Special instrumentation was used in addition to that required for VA-1. Several video recording cameras were installed to record Astronaut Cooper's reactions and communication equipment was installed to maintain voice communication with the test control room.

Test VM-1 consisted of two sinusoidal frequency sweeps. A 138 second linear frequency sweep was conducted from 4 to 6 Hz while the response amplitude at the Command Module forward bulkhead was varied linearly from 0.15 g peak at 4 Hz to 0.4 g peak at 6 Hz.

The second sweep was a 29 second linear sweep from 6 Hz to 7 Hz with the response amplitude varied from 0.2 g peak at 6 Hz to 0.7 g peak at 7 Hz. Astronaut Cooper performed manual operations typical of those that might be required during boost and provided a verbal commentary of his impression during the test.

#### VA-C2 - CSM maximum Q calibration

The VA-C2 calibration test established the SAL acoustic environment which would produce Block I CSM random vibration levels (those associated with atmospheric flight). Since Block I and II flight environments are the same, the acoustic environments established by VA-C2 were accurate forcing functions for CSM 105/AV (a Block II vehicle).

The SAL acoustic shroud assembly was positioned around the Block I acoustic calibration vehicle as shown in Figure 4.

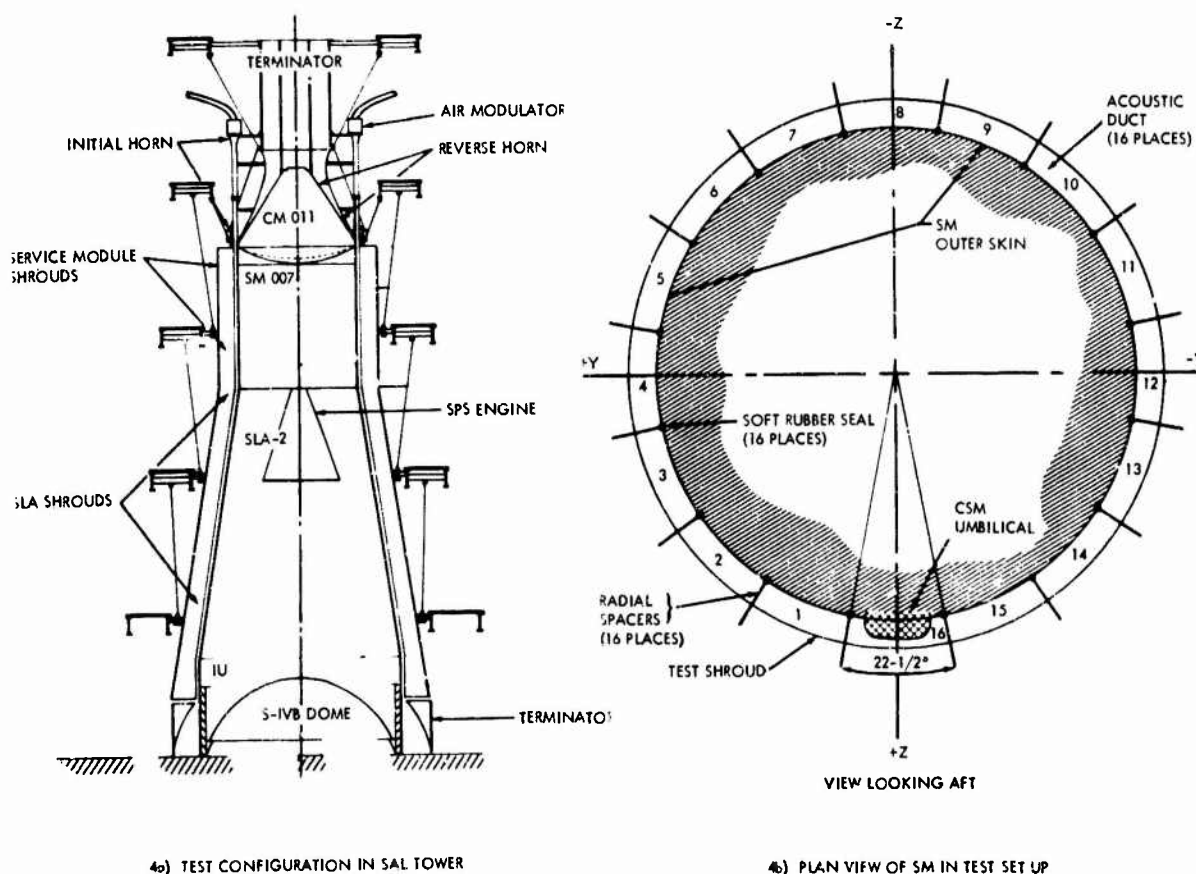


Figure 4 Maximum Q Calibration Test Configuration

The acoustic spectrum in each of the 16 ducts was adjusted until Block I responses (1/3 octave band analyses) were established on the SM outer shell and CM crew compartment heat shield. The 1/3 octave band spectrum equalizer settings for each of the 16 air modulators were then recorded. This was accomplished by tape recording the equalizer current applied to simulated load resistors and subsequently performing 1/3 octave band analyses on the signals. These 1/3 octave band current spectra (and consequently acoustic spectra) could then be reproduced prior to the CSM 105/AV test run by adjustment of the equalizers.

#### VA-C2 CSM maximum Q abort calibration

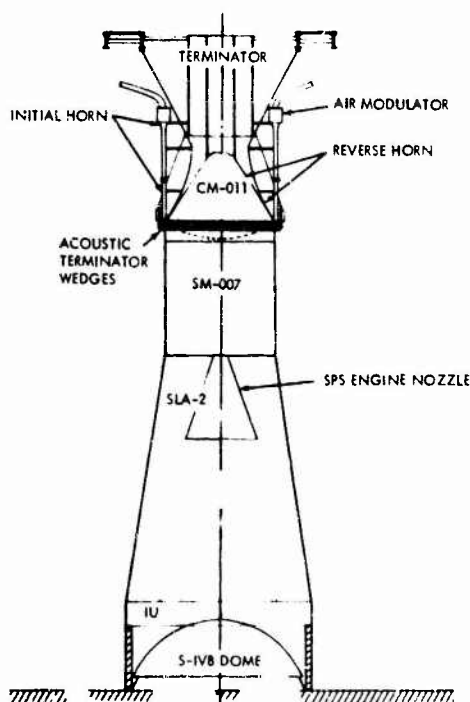
Figure 5 illustrates the acoustic shroud arrangement for the maximum Q abort calibration.

The acoustic spectrum was adjusted (in each duct) until Block I CM crew compartment heat shield responses (1/3 octave band analyzer), in the 20 to 400 Hz frequency range, were obtained on the calibration CM. The Block I CM heat shield response, produced by LES engine operation, had not been defined in previous testing. Since the LES engine produces predominantly high frequency fluctuating pressure (see Figure 2), an attempt was made to duplicate the measured (at sea

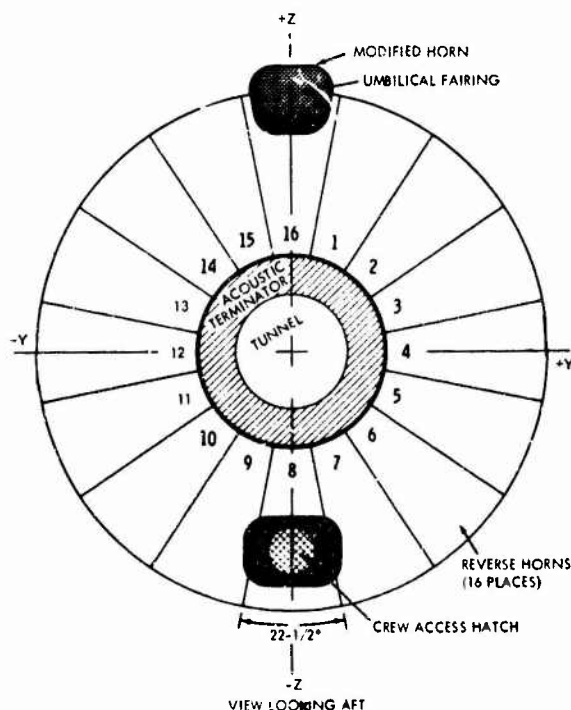
level) LES engine acoustic spectrum above 400 CPS and accept the resulting vibration. It was determined that the SAL was not capable of producing sufficient energy, above 400 Hz, to duplicate the LES engine spectrum without incurring an overtest condition in the lower portion of the frequency spectrum. Consequently, the maximum facility output above 400 Hz was accepted. Recording of the 1/3 octave band spectrum equalizer settings, for the 16 air modulators, was accomplished in the same manner as the maximum Q calibration run.

#### VA-2 CSM maximum Q abort

The vibro-acoustic test set-ups used for tests VA-2 and VA-3 were the same as those used during the calibration tests (VA-C2) except the calibration vehicle was replaced by CSM 105/AV. Since the CM vibration levels during VA-2 were expected to be quite severe, preliminary verification of the acoustic spectrum at a lower level was required. Therefore, short duration acoustic tests were conducted at levels significantly lower than that established by VA-C2. The verification test duration was held to the minimum necessary to stabilize the system and obtain a data sample. One third octave band analyses were performed on the control microphone data and compared to the VA-C2 spectrum for shape.



5a) TEST CONFIGURATION IN SAL TOWER



5b) PLAN VIEW OF CM TEST SETUP

Figure 5. Maximum Q Abort Calibration Test Configuration

Adjustments were made to individual ducts as necessary and a verification test was performed. When a low level run was completed that verified the VA-C2 spectrum shape, the full level maximum Q abort test was conducted for 10 seconds.

#### VA-3 - CSM Maximum Q

CSM 105/AV was subjected to three levels of acoustic excitation, each of which exhibited the same spectrum shape as that derived during VA-C2 for the maximum Q boost condition.

The lower level test was conducted at an overall sound pressure level (SPL) of 140 dB for a minimum of 130 seconds to account for the acoustic environment which exists in the test facility at KSC during pre-flight SPS firing tests. Short duration tests were conducted at the 140 dB level until the desired spectrum was reached and then the remainder of the required 130 second exposure was completed.

Short duration testing to verify the maximum Q acoustic excitation spectrum was performed until the desired spectrum was achieved and then the remainder of the 80 second minimum duration maximum Q test was conducted. At the end of the maximum Q test the overall SPL in all ducts was increased by 4 dB for an additional 10 seconds to provide the boost transonic exposure.

#### Instrumentation

The dynamic instrumentation employed during this test program was of standard laboratory quality. Signal transducers consisted of strain gages, piezoelectric accelerometers, velocity pickups, and piezoelectric microphones. A measurement list was devised, assigning a coded measurement number to each transducer installed on the test structure. For example, CA014 was an accelerometer on the Command Module, CS003 was a strain gage on the Command Module; SA-021 - accelerometer on the Service Module, etc. Information such as the exact location of the transducer, its sensitivity axis and direction, type, model number, serial number, sensitivity, test effectivity, and a photograph of its installation was cross referenced with the measurement number.

All output signals for the acoustic, vibration, and strain measuring systems were recorded on magnetic tape. Voice notations and time correlation in the IRIG B format were recorded on all tape recorders simultaneously. Each reel of tape contained at least one full scale calibration and an ambient instrumentation noise floor recording.

The vibration measurement systems for both the vibration and acoustic tests consisted of piezoelectric accelerometers and charge amplifiers. A maximum of 98 accelerometers were utilized in the vibration portion of the test and a maximum of 186 were monitored during the acoustic testing. The overall system frequency response of the vibration measurement systems was from 5 Hz to 2500 Hz. The transducers were secured to phenolic mounting blocks bonded (providing electrical isolation) to CSM test structure using proven epoxys and dental cement.

Calibration and end-to-end check-out of the vibration measurement systems were accomplished by the voltage "T" insertion method. This procedure was performed between the end of extension cable runs and the test facility patch panels. The capacitance of each system was calculated as well as measured so that the proper "T" insertion voltage could be calculated.

Because of their superior low frequency performance, up to 32 velocity pickups were used for controlling the vibration tests.

The strain measuring systems (a maximum of 40) consisted of strain gages and associated signal conditioners, with an overall system frequency response of 5 to 2500 Hz. The strain gages were installed in accordance with the procedures specified by the manufacturer(s) of the gages. Calibration was accomplished by the conventional shunt resistor technique.

The acoustic environment was monitored and controlled using piezoelectric type microphones and associated amplifiers. These data acquisition systems had a flat frequency response from 20 Hz to 2500 Hz. The microphone systems were calibrated and end-to-end checked prior to and preceding each test run by means of single-frequency voltage insertion method.



## Test Results

### VA-C1 - CSM low frequency vibration calibration

VA-C1 served adequately to develop test techniques, establish or confirm test amplitudes and to develop teamwork among the several agencies involved in the test operations. The suspension system, vibration fixture, and thruster system demonstrated their capability for supplying the forces to the vehicle necessary to meet operational requirements.

### VA-1 - CSM low frequency vibration

A total of 7 sinusoidal sweeps and 10 sinusoidal dwells, at resonant frequencies, were performed during VA-1 (see Table II). Thruster force and test specimen response data from the sinusoidal sweeps were reduced as x-y plots of acceleration, velocity or force versus frequency, force divided by velocity versus frequency, and phase of velocity versus frequency. Modal diagrams for the significant resonant frequencies were hand plotted from the velocity and phase versus frequency x-y plots.

No difficulties were encountered in the VA-1 testing, except during the 4 to 6 Hz and 6 to 7 Hz X vehicle axis sinusoidal sweeps. Distortion of the velocity control signal in these tests resulted in lower than specified CM forward bulkhead acceleration levels (Figure 6).

No structural failures were discovered during the VA-1 testing. No fluid leakage was detected nor was any pressure loss observed.

The response data obtained from the sinusoidal sweeps and dwells were considered sufficient to establish the vibration transmissibility characteristics of the CSM (primary test objective 3).

### VM-1 - CSM manned low frequency vibration

Sinusoidal vibration sweeps from 4 to 6 Hz and 6 to 7 Hz were conducted with Astronaut Colonel Gordon Cooper occupying the commander's crew station (Table II). Thruster force and test specimen response data were reduced as X-Y plots of acceleration, velocity or force versus frequency, and phase versus frequency.

Table II Summary of SC-105/AV Testing in Spacecraft Vibration Laboratory (SVL) VATF, MSC (VA-1)

#### VA-1 UNMANNED LOW-FREQUENCY SINUSOIDAL VIBRATION TEST

Test Run No.	Type of Excitation	Axis	Specified Frequency (Hz)	Frequency (Hz)	Control (G's - PK)	Duration (sec)	Date	Time of Day	Remarks
V01	Sweep	X	4 to 30	4 to 30	0.10	-	2/5/68	1334	Aborted at 5 Hz
V02	Sweep	X	4 to 30	4 to 30	0.10	180	2/5/68	1344	Completed
V03	Sweep	X	4 to 6	4 to 6	0.15 to 0.40	-	2/6/68	0108	Aborted
V04	Sweep	X	4 to 6	4 to 6	0.15 to 0.40	130	2/6/68	0908	Completed
V05	Sweep	X	6 to 7	6 to 7	0.2 to 0.7	18	2/6/68	1446	Completed
V06	Dwell - 1	X	8.7 ± 0.4	8.4	0.24	20	2/6/68	2055	Completed
V07	Dwell - 2	X	13.9 ± 0.4	13.6	0.26	20	2/6/68	2248	Completed
V08	Dwell - 3	X	16.3 ± 0.4	16.3	-	-	2/6/68	2306	Aborted
V09	Dwell - 3	X	15.3 ± 0.4	16.7	0.24	20	2/6/68	2325	Completed
V10	Dwell - 4	X	18.9 ± 0.4	19.2	0.22	20	2/6/68	2341	Completed
V11	Dwell - 5	X	22.3 ± 0.4	22.6	0.26	20	2/7/68	0125	Completed
V12	Sweep	Z	4 to 30	4 to 30	0.10	-	2/7/68	2347	Aborted
V13	Sweep	Z	4 to 30	4 to 30	0.10	180	2/8/68	0035	Completed
V14	Dwell - 1	Z	5.5 <sup>+0</sup> <sub>-0.8</sub>	-	-	-	2/8/68	1840	Aborted
V15	Dwell - 1	Z	5.5 <sup>+0</sup> <sub>-0.8</sub>	5.2	0.26	20	2/8/68	2112	Completed
V16	Dwell - 2	Z	9.1 <sup>+0</sup> <sub>-0.8</sub>	-	-	-	2/8/68	2139	Aborted
V17	Dwell - 2	Z	9.1 <sup>+0</sup> <sub>-0.8</sub>	8.5	0.25	20	2/8/68	2307	Completed
V18	Dwell - 3	Z	12.4 <sup>+0</sup> <sub>-0.8</sub>	11.7	0.20	20	2/8/68	2330	Completed
V19	Dwell - 4	Z	16.6 <sup>+0</sup> <sub>-0.8</sub>	16.2	0.25	20	2/8/68	2354	Completed
V20	Dwell - 5	Z	27.2 <sup>+0.8</sup> <sub>-0</sub>	27.7	0.25	20	2/9/68	0220	Completed

#### VM-1 MANNED LOW-FREQUENCY SINUSOIDAL VIBRATION TEST

V21	Noise floor						2/10/68	1810	
V22	Sweep	X	4 to 6	4 to 6	0.15 to 0.40	18	2/10/68	2337	Completed
V23	Sweep	X	6 to 7	6 to 7	0.20 to 0.70	29	2/11/68	0047	Completed

An undertest condition existed during both sweep tests due to the input signal distortion previously mentioned. Although the specified test levels were not reached during testing, the 6 to 7 Hz sweep did reach the vibration levels observed on the AS-501 mission (Figure 6)

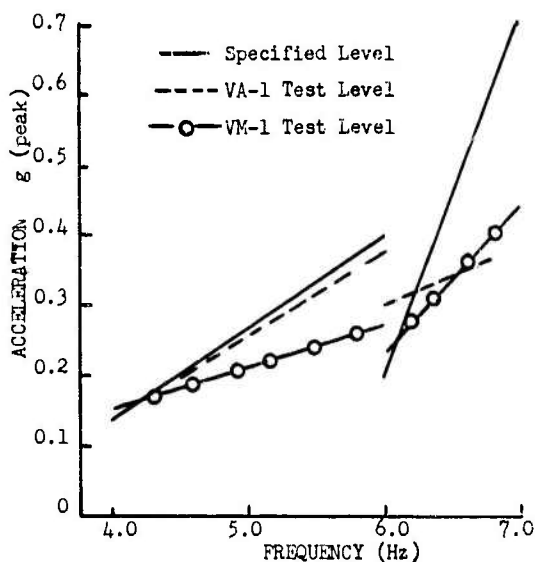


FIGURE 6. Acceleration Levels Attained During Low Frequency Vibration Tests VA-1 and VM-1 (4 to 7 Hz Sweeps)

No structural failures, fluid leakage or pressure losses were detected during testing but a crew compartment mirror was broken during an astronaut ingress maneuver. A polished aluminum mirror has been designed and installed to replace the glass mirror.

In view of the above, the Block II CSM structural integrity was verified for the Apollo mission AS-501 low frequency vibration environment (primary test objective 5).

A debriefing was conducted following the VM-1 tests and Colonel Cooper indicated that he experienced no difficulty in reading instruments or defining printing or scribed lines. He had been able to perform all manual operations satisfactorily and he did not consider the vibration environment seriously uncomfortable either with his head on the head rest or raised above it. Observation of the video replay of the test revealed a noticeable voice modulation which was not serious enough to influence understanding Colonel Cooper's comments. Consequently, the mission AS-501 low frequency vibration environment was not considered to have adversely effected a crewman's ability to perform his assigned duties (primary test objective 6).

#### VA-C2 - CSM maximum Q calibration

Examination of Figure 7 shows that VA-C2 met its objective of developing an acoustic environment capable of exciting Block I maximum Q flight level responses on the Command Module crew compartment heat shield and Service Module outer shell panels.

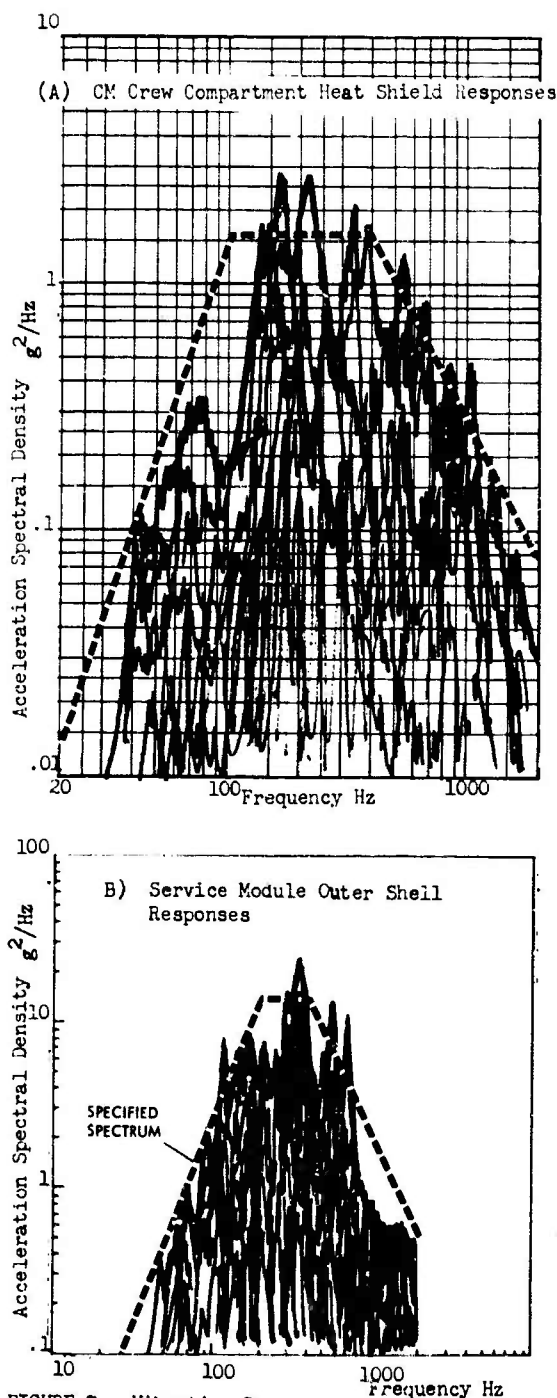


FIGURE 7. Vibration Responses, Maximum Q Calibration

It should be noted that the specified CM crew compartment heat shield and SM outer shell vibration response spectrums were developed by enveloping vibration responses measured on ground test vehicles, which were subjected to reverberant acoustic environments, in addition to flight test measurements. It must also be pointed out that the environmental vibration criteria development efforts were directed toward vibration shaker testing, so the spectrum envelopes often encompassed voids rather than imposing unreasonably difficult spectrum shaping requirements for subsequent vibration testing.

VA-C2 - CM maximum Q abort calibration

Figure 8 compares the Block I CM crew compartment heat shield responses obtained in VA-C2 with the Block I heat shield criteria. The overtest condition resulted from the attempt to overcome the limited high frequency

capability of the reverse horn shroud section of the SAL. It was decided to accept the overtest condition and to develop a set of scaling factors to be applied to the CSM 105/AV maximum Q abort responses (VA-2). The development of these scaling factors will be discussed in the following section.

VA-2 - CM maximum Q abort

The acoustic spectrum established in VA-C2 was almost exactly reproduced during VA-2 (Figure 9 (A)). Therefore, the overtest condition also occurred in VA-2. Consequently, the resulting vibration responses must be modified to reflect what would have existed had the SAL been capable of generating the desired maximum Q abort spectrum.

The maximum Q abort acoustic spectrum specified in the environmental design criteria was composed by adding the 1/3 octave band sound pressure level measured during launch escape engine ground firing tests to the 1/3 octave

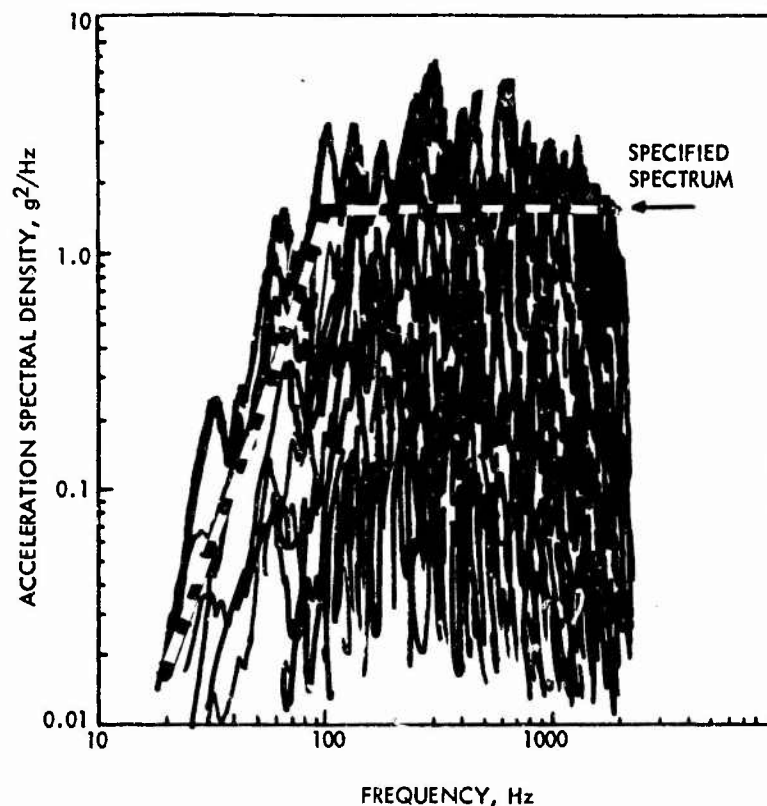


Figure 8. Crew Compartment Heat Shield Vibration Responses, Maximum Q Abort Calibration

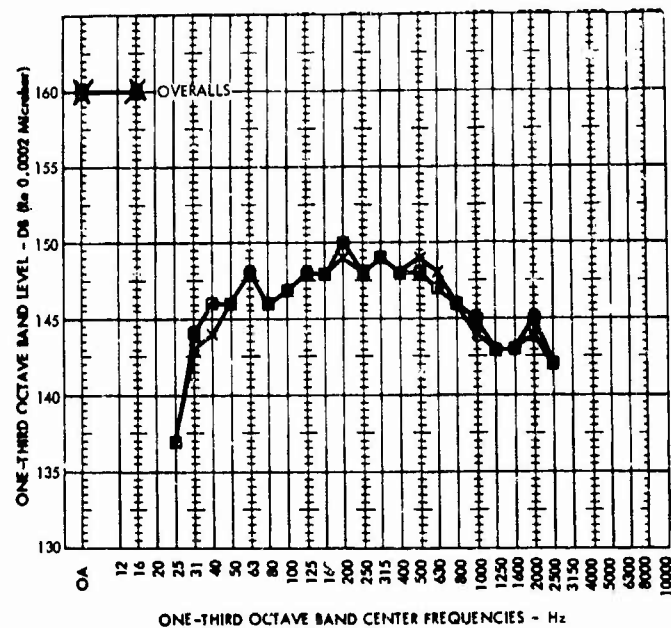


Figure 9(A). Comparison of VA-2 Acoustic Spectrum With Calibration Test Spectrum

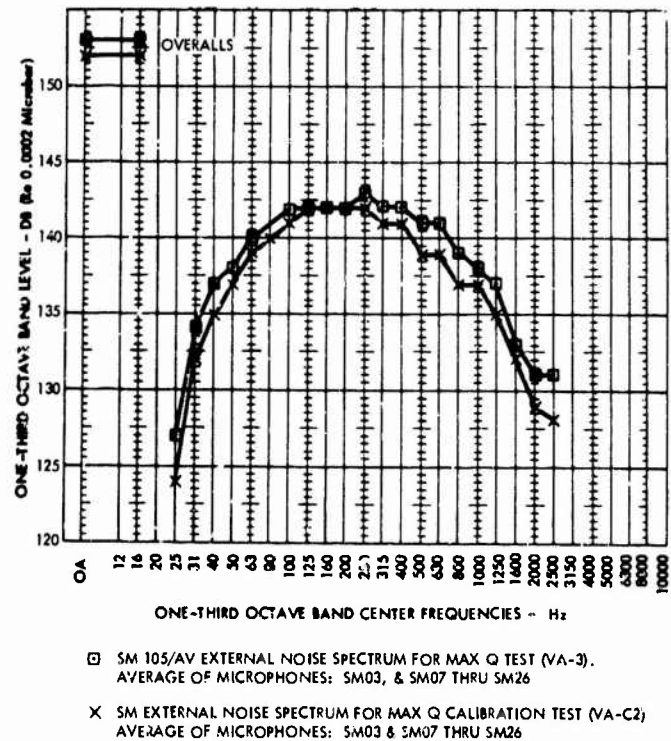


Figure 9 (B). Comparison of VA-3 Acoustic Spectrum With Calibration Test Spectrum

band sound pressure level measured at the Command Module during maximum Q flight. The difference in sound pressure level between the maximum Q acoustic spectrum and the derived maximum Q abort acoustic spectrum was measured for each 1/3 octave band. The maximum Q abort vibration criteria were then created by raising the maximum Q vibration criteria by a corresponding amount in the applicable frequency bands. Figure 2 shows the Command Module flight acoustic spectra specified for maximum Q and maximum Q abort.

Utilizing the above, the appropriate VA-2 acoustic spectrum can be derived as follows:

1. Determine the Command Module control microphone acoustic spectrum that would have been necessary to reduce the VA-2 vibration responses to those commensurate with the criteria specified for maximum Q. Figure 10 compares the envelope of crew compartment heat shield responses measured during VA-2 with the maximum Q vibration criteria. The VA-C2 maximum Q abort acoustic spectrum was then lowered by the difference between the response and criteria envelopes of Figure 10.

2. Raise the acoustic spectrum developed in Step 1 by the amount indicated in Figure 2 for each 1/3 octave band. The resulting acoustic spectrum is one that would have achieved the desired maximum Q abort vibration responses.

Figure 11 compares the CM maximum abort acoustic spectrum measured during the VA-2 test with that derived by Steps 1 and 2 above.

The correction factors shown in Figure 11 have been applied in the VA-2 vibration responses in order to relate them to the Block II vibration criteria. Comparisons of the scaled VA-2 vibration response envelopes with their corresponding vibration criteria spectra for each CM vibration criteria zone were made. (Figure 12). Inspection of these comparisons yielded the conclusion that the existing maximum Q abort vibration criteria were satisfactory and no revisions were necessary.

No indications of structural or system failures were observed during or upon conclusion of VA-2.

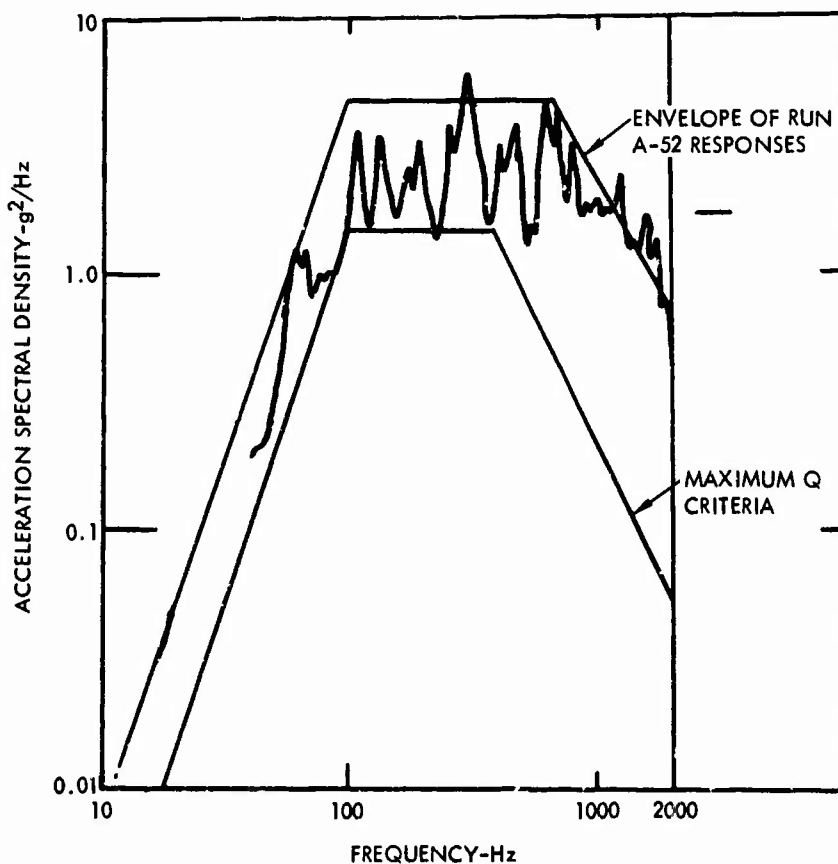


Figure 10. Comparison of Maximum Q Abort Calibration With Maximum Q Specification Criteria

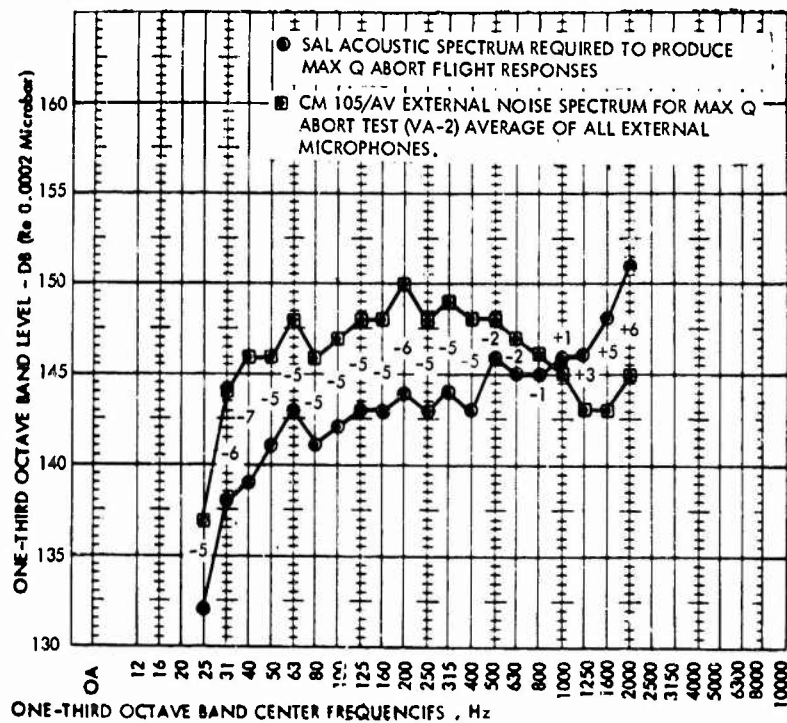


FIGURE 11. Comparison of Maximum Q Abort Test (VA-2) Acoustic Spectrum and SAL Acoustic Spectrum That Would Have Produced Maximum Q Abort Flight Responses

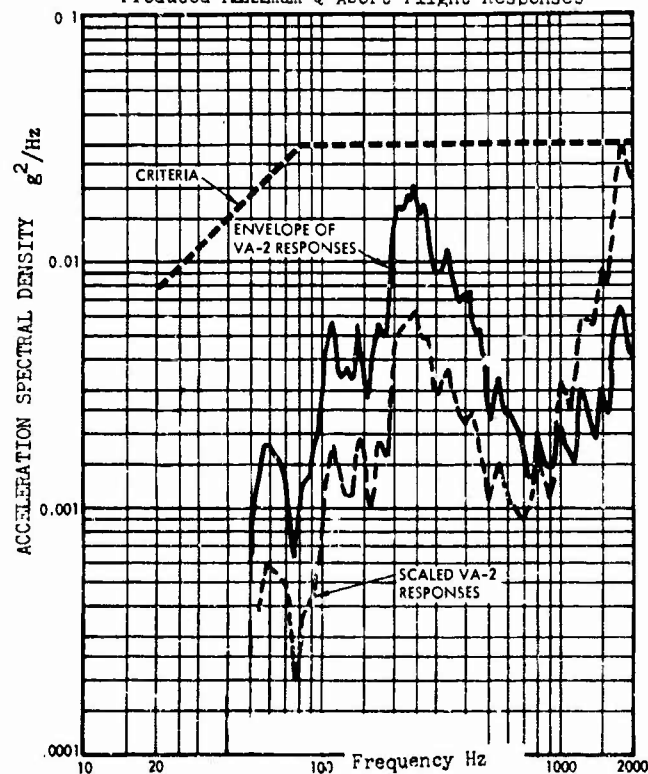


FIGURE 12. Example of Corrected Maximum Q Abort Test Responses (Command Module Right Hand Equipment Bay)

#### VA-3 CSM Maximum Q

Figure 9 (B) shows that the maximum Q spectrum established in VA-C2 was satisfactorily reproduced in VA-3. Comparison of the resulting vibration with existing Block II zonal vibration criteria on the SM revealed only three areas where revision of the existing criteria were indicated.

No structural or systems failures, attributable to VA-3 were observed. Successful functioning of the CM side crew hatch subsequent to VA-3 completed qualification of the hatch (primary test objective 4). Conclusion of VA-3 represented achievement of all of the primary test objectives.

#### CONCLUDING REMARKS

The CSM 105/AV test program represented a significant advancement in the concept of subjecting entire flight configuration vehicles to their flight environments. The added level of confidence gained in the vehicle's structural and operational performance, from these tests, resulted in reduced flight test requirements. The CSM 105/AV test program also established added confidence in the crewman's ability to perform critical tasks while experiencing flight level vibration in the 4 to 7 Hz range.

#### DISCUSSION

Mr. Mustain (McDonnell Douglas Corp.): How effective were your air springs and what were their frequencies in both the lateral and longitudinal directions?

Mr. Chirby: In the longitudinal direction the natural frequency of the air springs for this assembly was approximately 1 Hz. As I remember it was approximately the same for the lateral direction.

Question: Did they work effectively? Did you check to see if there was any coupling between that system and the structure and also the external structure?

Mr. Chirby: There was some concern about this, and partially as a result of this test, further testing of essentially the same stack configuration was conducted to give better modal type vibration response data for this portion of the stack.

Mr. Mustain: Would you still select air springs as the suspension system if you were doing it over again?

#### ACKNOWLEDGEMENTS

The authors express their gratitude to H. K. Pratt of North American Rockwell Corporation for his assistance in preparation of this paper and to the NASA, MSC staff, particularly Mr. R. A. Colonna and Mr. W. D. Dorland, who were responsible for performing the tests at the Houston facility.

#### REFERENCES

1. P.T. Mahaffey and K.W. Smith, "Method for Predicting Environmental Vibration Levels in Jet Powered Vehicles," presented at the 28th Shock and Vibration Symposium, February 9-11, 1960, Washington, D.C.
2. R. A. Stevens, H. C. Allen, H. K. Pratt, "Vibration Qualification of Fly-Away Umbilical by Acoustic Test Method," Presented at the 13th Annual Technical Meeting of the Institute of Environmental Sciences, April 10, 1967, Washington, D. C.
3. D. E. Newbrough, R. A. Colonna, J. R. West, Jr., "Development and Verification of the Apollo Command and Service Module Vibration Test Requirements," presented at the 37th Shock and Vibration Symposium, October 24-26, 1968, Orlando, Florida

Mr. Chirby: Yes.

Mr. Mustain: On acoustics - did you make any correlation studies, and if so what kind of correlation lengths did you have?

Mr. Chirby: By correlation, do you mean a comparison with the flight acoustic environment?

Mr. Mustain: No - the correlation length of the acoustics itself on the structure? Was it correlated over a 12-inch distance, or 24-inch distance?

Mr. Chirby: No studies of that sort were made. It was simply a matter of generating flight level responses on the outside of the vehicle and essentially accepting that acoustic environment.

Mr. Mustain: Will there be any correlation studies made of that in your data?

Mr. Chirby: No, none is presently planned.

## MODAL SURVEY RESULTS FROM THE MARINER MARS 1969 SPACECRAFT\*

R. E. Freeland  
Jet Propulsion Laboratory  
California Institute of Technology  
Pasadena, California

and

W. J. Gaugh  
Northrop Systems Laboratories  
Northrop Corporation  
Hawthorne, California

Complementary programs of analysis and test have provided the basis for determining the response of the Mariner 1969 spacecraft to dynamic loading conditions. This paper describes the objectives and techniques of a test program to determine the spacecraft modal characteristics. The modal survey results of the Mariner 1969 Developmental Test Model are presented. Generalized mass matrix calculations are shown to evaluate the validity of the test data and the mass distribution. Typical test mode shapes and frequencies are correlated with values obtained from analysis.

### INTRODUCTION

Normal modes represent a fundamental form of the dynamic characteristics inherent in any linear structural system. The accuracy of analytical predictions depends on the validity of many assumptions regarding the structural and inertial property idealization. Modal survey testing provides valuable correlative results so that dynamic response predictions may be made with greater confidence.

The prediction and comprehension of modal characteristics are facilitated by an analysis procedure [1, 2] that allows each system to be analyzed as separate subsystems. The calculated modal characteristics [3] for these subsystems are subsequently recombined progressively until the modal characteristics of the whole structural system are obtained. These results, together with estimates of modal damping, are used to predict the overall structural response to excitation forces. That the modal characteristics can be established separately for each subsystem is a great advantage in investigation of the system as a whole.

The objectives of this paper are to describe the coordinated test and analysis approach, to indicate how correlated modal survey results were used to evaluate analytic modes, and to describe the modal survey equipment and techniques. An earlier companion paper [4] is primarily concerned with the modal combination aspects of the analysis procedure. The analysis and test results and two mode shapes are presented as examples. This paper emphasizes some experimental techniques used to investigate and evaluate modal characteristics and the correlation of analytical and test results.

### INTEGRATED ANALYSIS AND TEST PROGRAM

The primary objective of the structures and dynamics support effort of the Mariner Mars 1969 (MM 69) program was to insure confidence in the structural integrity of the Mariner 1969 spacecraft for all specified static and dynamic loading conditions. To accomplish this objective, a correlative approach was used, which capitalized on the synergistic effect of combined analysis and

\*This paper presents the results of one phase of research carried out at the Jet Propulsion Laboratory, California Institute of Technology, under Contract No. NAS 7-100, sponsored by the National Aeronautics and Space Administration.



test. This required that certain analyses and test objectives be established and satisfied. The analysis objective was to develop an adequate mathematical model that could be used with confidence to predict the forced response characteristics at any point of the structure. The test objective was to obtain the normal mode shapes and frequencies of the structural assemblies in the 5- to 200-Hz frequency range.

Analyses and tests were undertaken only if they supported some design decision or contributed to the insurance of satisfactory structural qualifications. Early in the program a crude spacecraft, the Structural Analysis Model (SAM), was subjected to static, modal, and forced-vibration tests. Test data were correlated with corresponding data obtained from an early mathematical model that was continually updated as the design progressed. Later in the program, the more representative Developmental Test Model (DTM) spacecraft was subjected to a more extensive structural test program. The calculated modes correlated with modal survey results were used in analysis of the loads and deflections to be expected during the qualification test. Correlation of analytical data with forced-vibration test results provided increased confidence in spacecraft structural integrity.

For structural dynamic investigation purposes, the Mariner 1969 spacecraft was divided into "secondary" and "primary" subsystems. The secondary structures consisted of relatively light appendages, the high- and low-gain antennas and four solar panels which are tip-latched together during launch. The primary structure consisted of two adapters together with the supported octagonal bus (bus/adapters), a propulsion subsystem (PROPS), and a planetary scan platform (PSP). A previous paper [4] presented the modal results for the secondary structures. The present paper is devoted to three configurations of the DTM primary structure.

The DTM structural assemblies were flight-type hardware wherever possible. Mockups possessed inertial properties, weights, centers of gravity, and moments of inertia similar to the components being replaced. Stiffness characteristics of mocked-up components were simulated for those components having structural resonances below 200 Hz.

#### DESCRIPTION OF DTM TEST CONFIGURATIONS

Figure 1 shows the forced-vibration configuration of the DTM which weighed 911 lb, including the weight of the 21-lb Centaur adapter. Figure 2 depicts modal test configuration 3, which consisted of the bus with adapters and which weighed 780 lb. Before installation of the 47-lb PROPS and the

156-lb PSP, the bus weighed 491 lb. This bus weight is composed of 30 lb of distributed structure, 119 lb of "bracketry," and 342 lb of electronic packages mounted inside the octagonal shaped bus structure.

Configuration 2 consists of the bus/adapter plus the PROPS.

Configuration 1 concerns only the bus/adapter from an analysis view point.

The SAMIS [3] computer program was used to calculate the normal modes of each structural mathematical model using six degrees of freedom (d. o. f.) at each structural joint. The program permits 10,000 d. o. f., of which 130 unrestrained d. o. f. may include inertia. Assuming three degrees of translational freedom at each mass loading point, the total number of such points must be less than 44.

Figure 3 indicates the various points on the DTM configuration at which lumped weights were distributed for analysis purposes. The bus/adapter, configuration 1, mathematical model had lumped masses at eight equally spaced points around the interface between the two adapters, at four equally spaced rings of eight points each that intersect the bus longeron corners, at one point at the center of the top ring and at one point at the center of the bottom ring of the bus structure.

For simplicity, the center of gravity of each electronic package was assumed at the centroid and in the plane of the outer shear plate for the particular octagon bus bay in which that electronic package was located. The mass of each electronic package was evenly distributed to four points on each adjacent bus ring longeron intersections. The distributed mass of a structural member or the localized mass of a "bracket" was ratioed geometrically between adjacent lumped mass points. The lumped mass approach used for the primary structure is believed to be reasonable because the mass of the load-carrying structure is a small percentage of the total spacecraft mass.

Figure 3 also indicates the center-of-gravity locations of the six PSP instruments: the infrared radiometer (IRR), the wide angle television (WATV), the ultraviolet spectrometer (UVS), the narrow angle television (NATV), the infrared spectrometer (IRS), and the gas bottles (GAS).

#### MODAL TEST EQUIPMENT AND TECHNIQUE

Modal- or resonance-testing of a linear lightly damped mechanical system is accomplished by harmonically exciting one or more points so that every point in the system responds at the same frequency, either in phase or exactly out of phase with any arbitrary reference point.

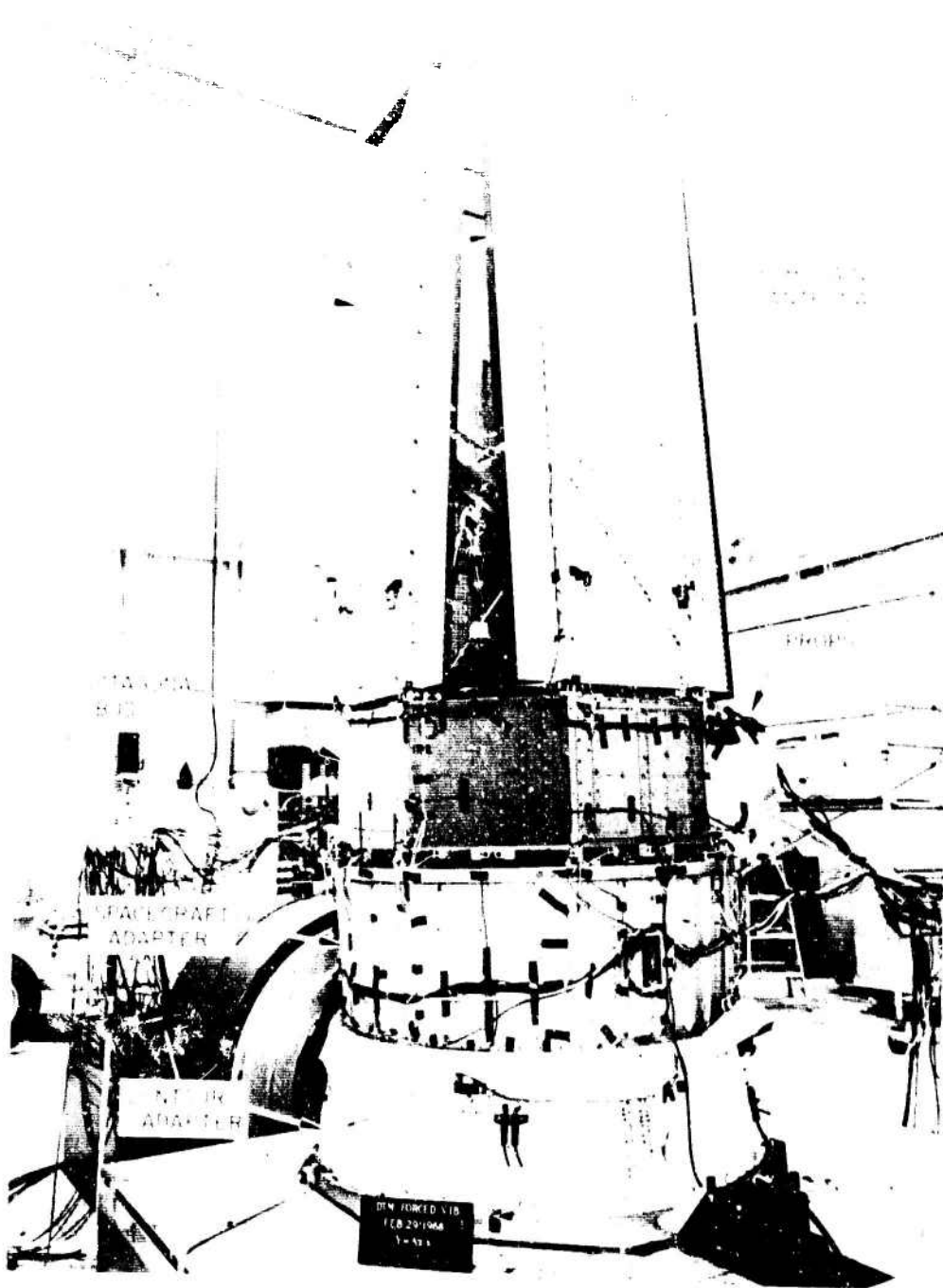


Fig. 1 - Developmental test model forced vibration test mounting

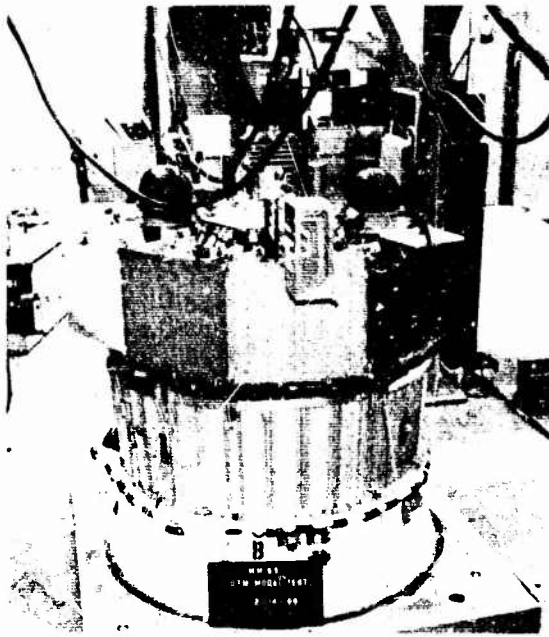


Fig. 2 - Configuration 3 with modal excitation shakers

The various amplitudes of the mode are at a maximum when the frequency of the excitation force is equal to the "natural frequency" of the mode. This process is usually accomplished with a multi-shaker system which includes instrumentation suitable for identifying and recording normal modes.

The existing JPL equipment for excitation of normal modes consists of 10 channels of excitation. This system permits simultaneous operation of one to ten electrodynamic vibration exciters, each rated at 25-lb maximum vector-force. All shaker channels have a common input from a sine-wave signal generator. Each shaker channel has its individual armature current gain control and a phase switch, which reverses the polarity of the driving signal, allowing any shaker to be driven either in phase or 180 degrees out of phase relative to a reference shaker. The shaker output velocity is obtained directly from a velocity sensor attached to the armature shaft which operates in the flux of a permanent magnet located in the shaker case, and is displayed on the x-axis of a cathode-ray oscilloscope (CRO). Shaker performance is evaluated by the magnitude of armature current, which is proportional to the shaker force and is displayed on the y-axis of the CRO. A shaker force versus specimen velocity Lissajous figure is generated on the CRO, which collapses into a reasonable simulation of a straight line at resonance. The slope of the Lissajous ellipse major diameter is a direct measure of the force to velocity ratio and the width of the ellipse minor diameter is a measure of the force to velocity phase difference.

The current JPL accelerometer system consists of eight accelerometers. Usually only two accelerometers are used for a modal test. For any given mode, a large oscillation point on the structure is selected as the location for the "reference" accelerometer for that mode only. The "roving" accelerometer is moved about to obtain data at the other structural points.

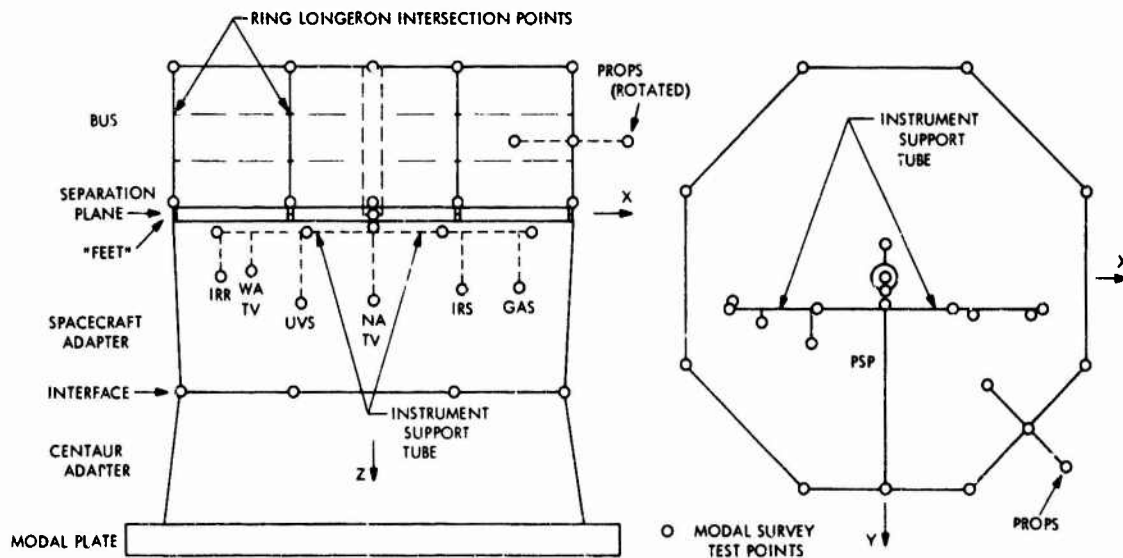


Fig. 3 - Location of lumped mass and modal survey points on the DTM modal configurations

The accelerometer electronics is compatible with transducers of dc capability, either variable resistance or variable reluctance usable in the frequency range from zero to 250 Hz. The carrier amplifier system operates at 2 kHz and provides integral demodulation. The demodulated amplifier output may be used directly for acceleration measurements or may be integrated as required to provide velocity or displacement measurements. Any two of the transducer channels may be displayed on dual vacuum tube voltmeters for magnitude measurements, and simultaneously displayed versus time on a dual beam CRO to provide phase and waveform information.

An eight-channel direct write oscillograph record is analyzed for the logarithmic decrements of the structural motion after abrupt termination of the shaker armature current. These motion decay curves provide an excellent indication as to the purity of the normal mode oscillation which should be smooth and without beats. From good quality decay curves, a value for the modal structural damping coefficient can be determined.

Problems were encountered with the implementation of standard state-of-the-art modal test techniques when applied to light, fragile structural subsystems, such as solar panels and high-gain antennas. It was observed that the mass of standard 3-gram accelerometers de-tuned the isolated normal modes when the accelerometers were attached at points of relatively high structural amplitude. The accelerometers increase local generalized mass, reducing the natural frequency and distort the natural mode shape. The mass loading of the shaker armature and attachment linkage also produce this effect on lightweight structures. The problem of transducer mass loading was solved by mass-loading each grid point equal in magnitude to the weight of the accelerometer. Mapping was then accomplished by replacing each mock weight by the transducer without affecting normal mode oscillation.

Higher mode excitation of the parabolic honeycomb high-gain antenna was done acoustically to reduce the number of shakers required by standard techniques. Nodal lines for plate modes of the dish were defined by the geometry of powder placed on the face of the dish during excitation by acoustic speakers. After several minutes of steady-state excitation, the nodal lines of each mode still contained powder and a photograph recorded the node line location on the dish grid.

#### SOLAR PANEL QUALIFICATION MODAL TEST

Modal test techniques were utilized for flight acceptance dynamic testing of single solar panels for the Mariner II and Mariner Mars 1969 programs. This test was a quality assurance verification rather than the

conventional simulation of a three-sigma-high dynamic environment. The test consisted of exciting the significant normal mode with a large vibration exciter. To assure excitation of the proper mode only, a modal survey was performed with small shakers prior to full level excitation. The panel response at the point of maximum amplitude was controlled to a preset acceleration that corresponded to the desired stress level. The frequency range of excitation was band-limited to avoid stimulation of undesired modes. The test mode selected was the first plate mode of the solar panel corrugation. The mode shape, dynamic gain, and frequency of this mode were dependent on the quality of the bond joint between the corrugation and its supporting spar, acceptance being based on uniformity from panel to panel. Initial comparisons were made between the four DTM prototype solar panels, after which tests were conducted on ten flight panels. The maximum variance of modal frequency was less than 1 Hz for ten panels, while the point of maximum amplitude varied less than one-half an inch along the 84-in. longitudinal axis of the panel, and the transmissibility at resonance varied less than 15%.

#### TEST QUALITY AND GENERALIZED MASS MATRIX

A number of test techniques were used to obtain quality test data. The structural excitation frequency and the shakers' output amplitudes were carefully adjusted until maximum response amplitudes were obtained at all structural survey points. A sufficient number of shakers were used so that all points of the excited structure vibrated in- or out-of-phase with each other. The overall excitation level was increased until the signal-to-noise ratio was satisfactorily high. The final recorded accelerometer decay traces, obtained at many points on the structure, were smooth exponential decays without evidence of "beats." Despite the utilization of these test data quality indices, the best means of establishing the quality of the measured normal mode shapes and mass distributions was to calculate the generalized mass matrix.

A common method of using the generalized mass matrix as an indicator of test and mass distribution quality is to normalize the principal diagonal terms to unity and consider the values of the larger off-diagonal terms. If all off-diagonal terms have values less than 0.1, it is the authors' opinion that satisfactory test mode shapes have been obtained and an adequate mass distribution has been used for this spacecraft. Intuition suggests that this criterion may be unnecessarily severe where the vast majority of off-diagonal terms are small but a few terms exceed 0.1 (especially where a large number of modes are included).

Table 1 presents a generalized mass matrix derived from configuration 3 mode shape measurements, with the matrix normalized to give unit generalized mass in each

TABLE 1.  
Normalized Generalized Mass Matrix  
(Based on 49 point modal survey of the DTM modal configuration)

Mode No.	Frequency, Hz					
	35	37	43	54	56	90
	1	2	3	4	5	6
1	1.0	-0.031	0.011	0.069	-0.014	-0.024
2		1.0	0.036	-0.018	0.005	0.011
3			1.0	0.013	-0.051	-0.006
4				1.0	-0.013	0.009
5		Symmetric			1.0	0.035
6						1.0

normal mode. Ideally, the off-diagonal elements should be zero, because, by definition, there is neither elastic nor inertial coupling among normal modes. Table 1 results tend to indicate that a more than adequate number of mass points have been used and that the modal survey errors are small, since the maximum off-diagonal term is 0.069 (less than 0.1). Errors may result from the instrumentation, recording techniques or calculation procedure, inexact "tuning" of the normal mode, or inadequate accounting of the physically distributed mass. If too few, or incorrectly located or sized, mass points are used, it is impossible to obtain the appropriate modal amplitudes associated with a given kinetic energy.

For comparison purposes only, and without implying any statistical significance, a "shorthand" method of summarizing the off-diagonal values has been used. For example, in Table 1, the arithmetic mean value of the off-diagonal absolute values is 0.023 with a standard deviation of each off-diagonal absolute value of 0.018.

The six PSP instruments are relatively inaccessible because they are "buried" inside the spacecraft adapter. It is difficult to obtain the modal amplitudes of their respective center-of-gravity locations unless many "fixed" accelerometers are used instead of the "rover." Conversely, it is comparatively easy to obtain amplitude data on the tube that supports these instruments. A study was made to determine the relative importance of obtaining the instrument amplitude data during a modal survey test.

Table 2 summarizes the results obtained by using calculated modes from an isolated, mathematical model. Columns 1,

2, 3, 4, 5, 6, and 7 list the case numbers, the number of mass points, the number of degrees of freedom with inertia, the absolute value of the maximum off-diagonal error ( $|x_{max}|$ ), the mean value of the absolute errors  $|x|$ , the standard deviation of the absolute errors  $|s|$ , and "Remarks," respectively.

The investigation used the first six calculated modes for a 28-mass point PSP mathematical model with the instrument moments of inertia included (cases 1, 2, and 3) and omitted (case 4). The case 1 results indicate the effect of reducing the number of modal survey mass points from 28 to 15. The case 2 results provide an indication of the effect of neglecting the angular rotational inertia of the six instruments about their center of location during a modal survey test. Cases 3 and 4 results show the degradation that results by assuming the six instrument translational amplitudes correspond to modal test survey points taken along the instrument's common support tube.

Whereas the Table 2 summaries give an indication of typical off-diagonal values for an isolated subsystem, Table 3 considers the overall spacecraft primary structure, configurations 2 and 3.

Case 5 of Table 3 summarizes the results obtained by using the first seven modes obtained from a mathematical model of configuration 3 where the six PSP instrument center-of-gravity locations were taken to lie along the instrument support tube. Case 6 involves the same assumptions but low excitation level modal survey test data were used. Case 7 is similar but high excitation level test data were used.

The normalized, generalized mass for Case 8 was presented in Table 1 and indicates the results obtained by including the six PSP

TABLE 2.  
Off-Diagonal Summary From Six Calculated PSP Modes

(1)	(2)	(3)	(4)	(5)	(6)	(7)
Case No.	No. of Mass Points	No. of Inertia Degrees of Freedom	$ x_{\max} $	$ \bar{x} $	$ s $	Remarks
Effect of PSP Instrument Inertia Values and Location						
1	15	63	0.05	0.02	0.01	With Rotary Inertia
2	15	45	0.19	0.04	0.05	Without Rotary Inertia
3	9	27	0.42	0.15	0.11	CG on Support Tube
4*	9	27	0.31	0.15	0.08	CG on Support Tube
*Case where instrument rotary inertia values were not included in the mathematical model.						

center-of-gravity translation amplitudes. Case 9 indicates the effect of adding the seventh mode.

Case 10 gives the results obtained from configuration 2 using low level excitation.

It is concluded that to obtain a satisfactory representation of the kinetic energy present in the various modes of configuration 3 that the PSP instrument center-of-gravity amplitudes must be measured in the modal survey test, but their corresponding angular amplitudes need not be obtained.

#### CORRELATION OF ANALYSIS AND TEST

In a previous (DTM) test using configuration 3, good agreement [4] was achieved for the first two modes, corresponding to "shear-bending" of the bus/adapters. The fourth mode was analytically predicted at 70 Hz as a torsional mode, but the test results indicated it to be the sixth mode, at 92 Hz. This discrepancy in analysis was attributed to the omission of the electronic package stiffnesses and to the omission of the PSP rotary inertia terms from the mathematical model.

TABLE 3.  
Off-Diagonal Summary for Two DTM Configurations

Case No.	Configuration	$ x_{\max} $	$ \bar{x} $	$ s $	Remarks
PSP Instrument Weights on Support Tube, 7 Modes, 35 Survey Points					
5	3	0.26	0.08	0.07	Calculated
6	3	0.59	0.10	0.14	Low Level Test
7	3	0.54	0.11	0.13	Hi Level Retest
PSP Instrument Weights at CG, High Level Retest, 41 Survey Points					
8	3	0.07	0.02	0.02	Six Modes
9	3	0.18	0.03	0.04	Seven Modes
DTM Less PSP, Six Modes, 29 Survey Points					
10	2	0.16	0.08	0.04	Low Level Test

A new analysis has subsequently been completed for configuration 1, the bus/adapters, which includes a crude approximation of the stiffness of the structure internal to the electronic packages. Column 2 of Table 4 lists the first seven calculated modal frequencies. The third mode is again torsional but its frequency is only 63 Hz. Based on the known test results for configuration 2 (listed in column 6), the calculated bus/adapters third modal frequency of 63 Hz was increased to 93 Hz. This change anticipated the frequency reduction which results from the PROPS installation. At present the torsional discrepancy is believed to be caused by the inconsistency in the computer program structural element available at this time for modeling the adapter skin sections and the inadequate modeling of the electronic package stiffnesses and their center of gravity locations.

The Modal Combination program [2] was used to combine the calculated PROPS modes with the first eleven bus/adapters modes to obtain configuration 2. Only six PROPS modes were used because their corresponding frequencies, listed in column 4 of Table 4, are high relative to those of configuration 1. The results, listed in column 5, compare favorably with the test results, column 6.

Figure 4 presents a comparison of analysis and test results for the first mode of configuration 2. Circled points are used to denote the displacements of the three effective mass points on the PROPS, the eight corners of the bus top ring and the top center point of the bus. The eight lower corners of the bus and the lower center point displacements are denoted

by squares. The test results indicate a consistent translation of the PROPS and bus corners along the spacecraft x-axis but the center tube appears to twist and translate. The analysis indicates a translation direction of the PROPS and bus points which is skewed with respect to the x-axis. A similar comparison of the second mode shapes (not shown) indicates displacements normal to those of the first mode; e.g., along the y-axis for the test results.

This translation discrepancy may result from either the adapter plate mathematical model formulation which ignored access cut-outs, differences in the stiffness of the electronic packages, or the lumped mass distribution. Another possibility is the method used to attach the PROPS at three points to the bus. For simplicity, it was assumed that the PROPS and bus/adapters modes cannot influence each other locally. This assumption can be removed by including the three attachment modes which correspond to the static deflection flexibility influence coefficients.

Two modal survey tests were conducted on configuration 3. The first test results are summarized in Ref. [4]. More recent retest results are presented in this paper.

Table 5 indicates the effect of adding the PSP to the above configuration 2 to obtain configuration 3. The calculated modal frequencies of configuration 2, listed as column 5 of Table 4, are listed again as column 2 of Table 5. The calculated modal frequencies obtained by analysis of an isolated PSP mathematical model, including the rotary inertias of the six instruments, are listed in column 3

TABLE 4.  
Modal Characteristics of the DTM Modal Configuration Components

Mode No.	Configuration					
	1	1	---	2	2	2
	Bus/adapters Analysis $\omega$ , Hz	Bus/adapters Corrected $\omega$ , Hz	PROPS Predicted $\omega$ , Hz	DTM Less PSP Calculated $\omega$ , Hz	DTM Less PSP Test $\omega$ , Hz	Dominant Type of Test Mode Shape
1	42	42	110	39	40	"Shear-Bending"
2	43	43	137	41	41	"Shear-Bending"
3	63	93	152	88	89	"Torsion"
4	102	102	158	98	103	"Bus Breathing"
5	111	111	222	119	126	"Bus Breathing"
6	113	113	228	127	144	"Bus Breathing"
7	119	119	---	140	151	"Bus Breathing"

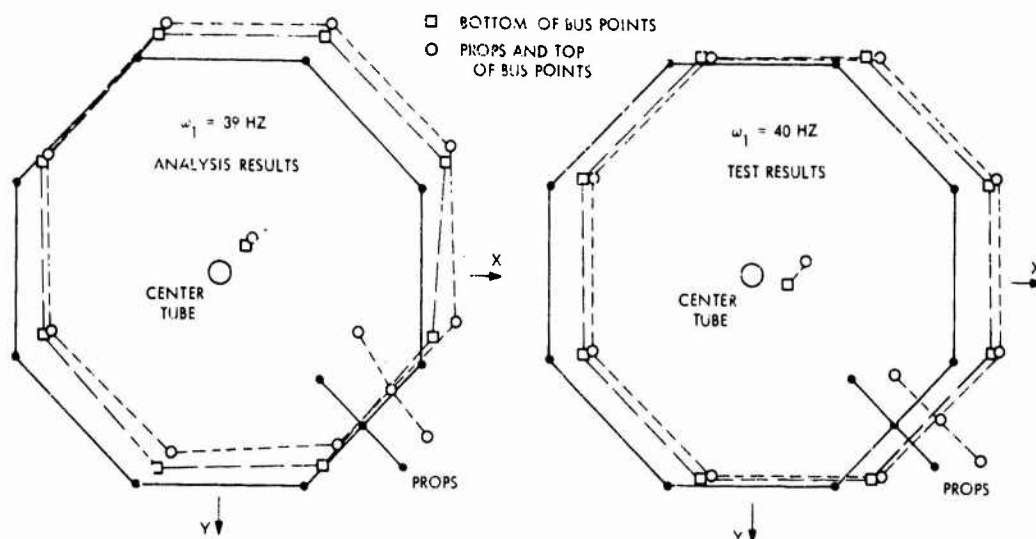


Fig. 4 - Mode shape comparison for the first frequency of configuration 2

of Table 5. The Modal Combination program was used to combine the modal characteristics of these two structures to obtain configuration 3. The results are given in column 4. Column 5 lists the modal frequencies obtained from the retest of configuration 3, which used higher force levels. Again, the calculated values are in good agreement with test results for the first two modes.

The sixth column of Table 5 presents a brief description of the dominant test mode shapes where the third through fifth mode shapes are best characterized by various PSP

motions. The sixth and seventh test modes appear as "torsion" and "bus breathing," respectively.

The calculated frequencies for the analytical configuration 3 model are listed in column 4 of Table 5. The first torsional mode appears as the seventh calculated mode. As discussed previously, the isolated bus/adapters, configuration 1, third mode was torsional and its frequency was increased from 63 to 93 Hz. This arbitrary frequency increase is justified because it makes the calculated first torsion (configuration 3) mode frequency agree with the

TABLE 5  
Modal Characteristics of the DTM Modal Configuration

Mode No.	Configuration				
	2	---	3	3	3
	DTM Less PSP Calculated $\omega$ , Hz	FSP Predicted $\omega$ , Hz	DTM Calculated $\omega$ , Hz	DTM Retest $\omega$ , Hz	Dominant Type of Retest Mode Shape
1	39	60	34	35	"Shear-Bending"
2	41	79	36	37	"Shear-Bending"
3	88	97	50	43	"PSP Rocking"
4	98	111	68	54	"PSP Plunging"
5	119	155	72	56	"PSP Rotating"
6	127	160	78	90	"Torsion"
7	140	---	90	102	"Bus Breathing"



90-Hz retest value. Because the calculated configuration 3 third, fourth, and fifth modes are characterized by various PSP motions, which occur at frequencies higher than the test values, it can be concluded that the PSP mathematical model is too stiff.

Figure 5 presents plotted analysis and retest results for the first mode configuration 3. Circled points are used to denote the amplitudes of three points on the PROPS, the eight corners and center point of the bus top ring, and various points along the PSP support structure. As might be expected at this relatively low frequency, the PSP was translating laterally. The observation that the analytically predicted PSP amplitudes are less than half the test values is consistent with the conclusion that the PSP mathematical model is too stiff. Relative to the previous discussion of Fig. 4, installation of the PSP has reduced the first mode frequency but has not appreciably influenced the direction discrepancy that occurs between the analytical and test results for the lateral translation of the bus top ring.

The Modal Combination computer program (used to predict the spacecraft structural response) requires as input a complete set of spacecraft low-frequency orthogonal modes. At present, the Modal Combination results are based only on calculated mode shapes, but one modal frequency value is based on test results.

Although the proper analytic prediction of the configuration 1 torsional characteristic remains an unsolved problem, it is not considered critical to the Mariner Mars 1969 program since the primary objective of the

analysis has been achieved. Early in the program, analysis indicated that the maximum load and dynamic clearance conditions involved primarily the first two low frequency modes. Early static and modal test data verified that the initial analysis results were sufficiently accurate for design purposes. Later, static and modal test data correlated well enough with analytical calculations to establish great confidence in the predicted forced-vibration response levels. Fortunately, no difficulty was encountered during the ultimate load level forced-vibration test. However, an adequate mathematical model was available for problem investigation had difficulties arisen.

It is suggested that future mathematical models incorporate several changes. The improved skin section elements, currently being installed into the SAMIS program should be used as this might provide the proper reduction in PSP stiffness and increase in bus/adapters torsional stiffness. The bus mathematical model must include a more realistic way of accounting for the electronic package stiffnesses and inertia properties. Modes associated with the attachment reaction forces should be included when the PROPS and PSP modes are combined with those of the bus/adapters.

## CONCLUSIONS

A correlative approach has been presented which uses the synergistic effect of analysis and test to evaluate the modal characteristics of the Mariner Mars 1969 spacecraft. From past experience, an adequate modal test procedure has evolved and was used to investigate

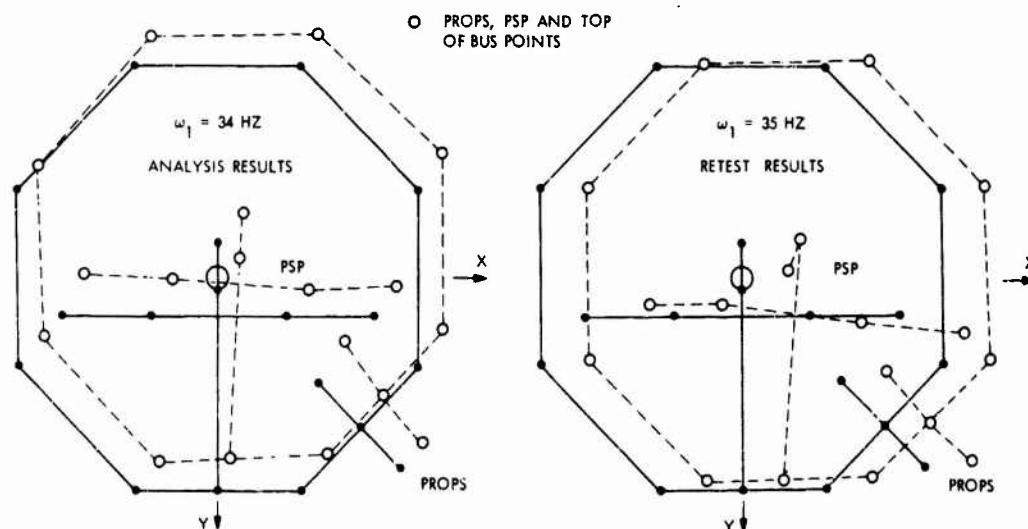


Fig. 5 - Mode shape comparison for the first frequency of configuration 3

the individual and composite structural systems. Satisfactory test techniques, developed previously, were used to obtain the modal characteristics of lightweight, fragile structures as typified by the solar panels and high-gain antenna reflector and for flight acceptance quality assurance verifications. A mathematical model has been developed that provides a means for investigating the complex relationships which exist between the various structural subsystems.

#### ACKNOWLEDGEMENT

The authors wish to express appreciation to Mr. H. J. Holbeck, Group Supervisor, Mariner Structures and Dynamics Group of the Jet Propulsion Laboratory for his helpful criticism and discussion during the course of this effort.

#### REFERENCES

1. Hurty, W. C., "Dynamic Analysis of Structural Systems Using Component Modes," AIAA Journal, Vol. 3, pp. 678-685, 1965.
2. Bamford, R. M., "A Modal Combination Program for Dynamic Analysis of Structures," JPL TM 33-290, August 1966.
3. Melosh, R. J., Diether, P. A., and Brennan, M., "Structural Analysis and Matrix Interpretive System (SAMIS) Program Report," JPL TM 33-307, December 1966.
4. Holbeck, H. J., Arthurs, T. D., and Gaugh, W. J., "Structural Dynamic Analysis of the Mariner Mars '69 Spacecraft," 38th Shock and Vibration Bulletin, Part 2, 1968.

## UPRATED SATURN I FULL SCALE DYNAMIC TEST CORRELATION

Charles R. Wells, and John F. Hord  
Chrysler Corporation Space Division  
New Orleans, Louisiana

A full scale vibration test was conducted for the Uprated Saturn I vehicle to determine its bending and torsion frequencies and mode shapes. The test was performed in the Uprated Saturn I dynamic test tower located at the Marshall Space Flight Center, Huntsville, Alabama. This paper presents a brief description and the correlation of these tests with theoretical results of a multibeam dynamic model currently being used to generate bending and torsion modes of the clustered tank Uprated Saturn I configuration. Good correlation is shown in most cases.

### INTRODUCTION

The dynamic test vehicle, SA-200-D, a full scale prototype of the Uprated Saturn I vehicle, was tested in four total vehicle configurations to simulate the AS-202, AS-203, AS-204, and AS-207 flight vehicles. The test was performed in the Uprated Saturn I dynamic test tower located at Marshall Space Flight Center, Huntsville, Alabama. The theoretical dynamic models briefly described and correlated in this paper are currently being used to generate bending and torsion modes for flexible body wind response studies and control system design during first stage flight.

### DESCRIPTION OF UPRATED SATURN I VEHICLE

The booster stage of the Uprated Saturn I vehicle consists of a cluster of eight outer 70" LOX and RP-1 fuel tanks alternately positioned around a 105" center LOX tank. Outer tanks are attached on top to the "spider beam" and on bottom to the "thrust structure" at two points on each end of the tanks. Fig. 1 shows an exploded view of the S-IB stage. This clustered arrangement of the booster necessitates the simulation of the vehicle by a multibeam mathematical model rather than a single beam analogy as is customary for a missile. The upper stages normally consist of an S-IB/S-IVB interstage, an S-IVB second stage, an Instrument Unit stage (I.U.) and an Apollo spacecraft.

Four flight configurations were simulated during the dynamic test. The AS-202 vehicle was a heat shield re-entry test and was tested and launched with the Apollo spacecraft minus the Lunar Module (LM).

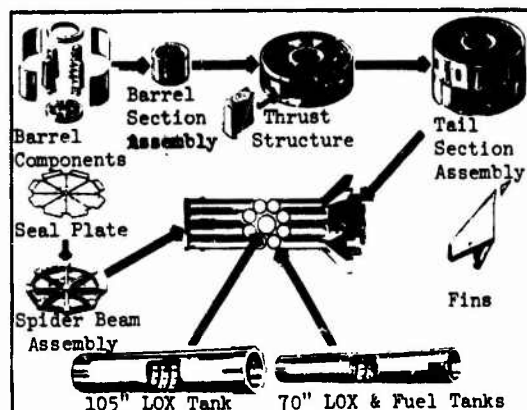


Fig. 1. Saturn IB Stage "Exploded" View

The AS-203 vehicle was a liquid hydrogen experiment with the Apollo spacecraft removed and a nose cone fitted to the Instrument Unit. The nose cone was simulated in the dynamic test by leaving the empty LM adapter on top of the I.U.

The AS-204 vehicle has a "LM Only" mission. At the time the test was conducted it was scheduled to carry the fully loaded LM and a stripped down boiler plate Apollo spacecraft and was tested in this configuration. The flight configuration, however, was recently flown with a nose cone on top of the LM adapter.

At the time of the test the AS-207 was a rendezvous mission with a partially loaded LM and an Apollo spacecraft. This mission has also been changed to exclude the LM.

#### DESCRIPTION OF TEST SETUP

The ground vibration tests (1) were accomplished by supporting the test vehicle vertically in the Up-rated Saturn I dynamic test tower with a system of cables and springs as depicted in Fig. 2. The vehicle was then excited electro-dynamically in the lateral and torsional planes, while suspended in a simulated free-free condition. The suspension system was composed of a series of bridge-strand steel cables running upward from the cable adapter plates, which were sandwiched between the fins and the booster at all eight fin locations, to the spring assemblies, which consisted of twelve springs per assembly. Immediately above the spring assembly, hydraulic cylinders were used at each suspension point to lift the vehicle approximately one inch clear of its hold-down structure. Spring assembly constants were such that the rigid vehicle rocking modes were below 0.5 cps.

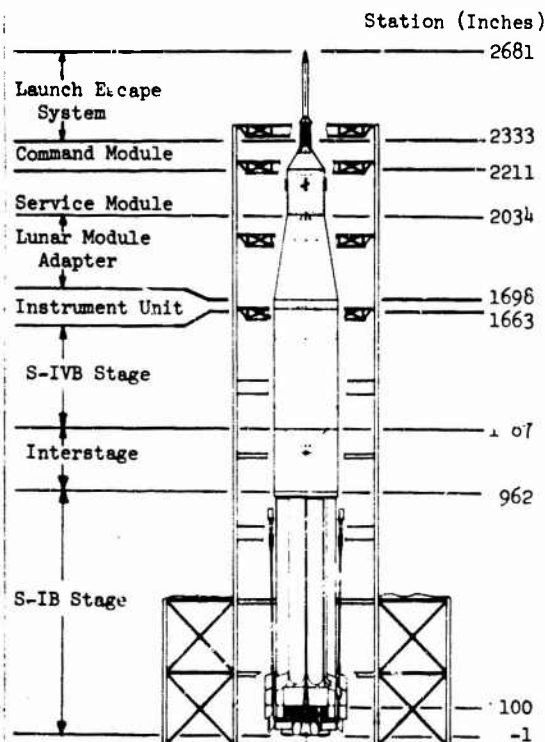


Fig. 2. Sketch of Up-rated Saturn I Dynamic Test Tower

Vehicle excitation was performed by applying a sinusoidal force near the engine gimbal plane with an electrodynamic shaker through a push-rod that had a double-bridge load cell to measure the shaker force. The shaker force was introduced through the stub fins near Station 118. The shakers were of two capacities, 500 pounds for torsional excitation and 1500 pounds for lateral excitation. During torsional testing, two exciters were operated in opposite directions directly across from one another.

In order to agree with documented weight distribution and center of gravity locations of the flight vehicle, it was necessary to use a propellant simulant. Since de-ionized water is slightly lighter than LOX and slightly heavier than RP-1, it was used to simulate both LOX and RP-1 in the S-IB booster, the S-IVB LOX tank and the Service Module. The correct amount of water required in the LOX and fuel tanks was maintained by observing sight gages installed alongside the tanks. Lead and steel ballast were also used to further adjust the mass distribution.

Solid ballast was used to simulate propellant and hardware in the Launch Escape System (LES) rocket, the Command Module, (CM), and the Lunar Module Test Article (LTA-2).

Two types of ground transducers, strain-gage-viscous-damped accelerometers with a range of  $\pm 1.0g$ , and inertial-spring-mass-viscous-damped accelerometers with a range of 0.5 to 5.0g, and two types of airborne systems transducers, inertial-spring-mass-viscous-damped accelerometers with a range of 10 m/sec<sup>2</sup> and 25 m/sec<sup>2</sup>, and rate gyros having full scale range of 10 degrees per second, were used to measure response of the test vehicle. It was necessary to locate the transducers at points inside the test vehicle structure as well as on its outer surface. The outputs from approximately 175 accelerometers, 30 rate gyros and a small number of strain gages were recorded to determine the dynamic response of the vehicle. These sensors were subdivided into three groups for specific use of the dynamics, control, and structures disciplines. Fig. 3 shows the Up-rated Saturn I dynamic test tower with the test vehicle enclosed. In the background is the Saturn V dynamic test tower.

#### THEORETICAL MODEL IDEALIZATION

The theoretical models were developed using the "recoupling of element modes" approach rather than a complete "direct stiffness" method. Using this approach, the total motion of the individual elemental structures is idealized as the sum of contribution from uncoupled modes which satisfy the boundary conditions and are weighted by the generalized coordinates. Equations of motion were derived by applying Lagrange's equations to the kinetic and potential energy expressions of the system and are documented in Ref. (1).

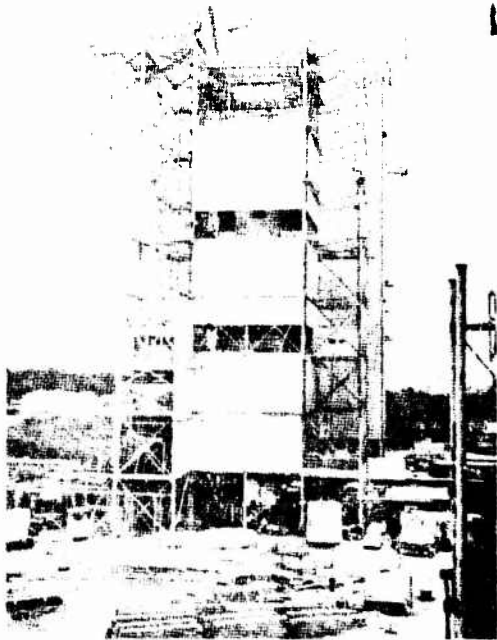


Fig. 3. Uprated Saturn I  
Dynamic Test Tower

Fig. 4 shows a cross section of the booster stage in the "spider beam" area. Because of the two support point arrangement, the principal planes of motion of the outer tanks are in the radial and tangential directions. Earlier tests of Block II Saturn I vehicles had shown that lateral translation of the spider beam and thrust structure attachment points was small enough to consider the tanks as "pinned-pinned" beams with rotational end springs in both the radial and tangential directions.

In the radial direction the LOX tanks have only small rotational restraints given by the compression studs at the forward end and the tied-down sockets at the aft end. In the tangential direction the LOX tanks are highly restrained at both ends.

The fuel tanks have only a small angular spring rate at the spider beam due to the sliding pin joints and essentially no restraint in the radial direction from the ball-socket joints at the thrust structure. In the tangential direction at the thrust structure, the fuel tanks have a spring constant of about half the value of the LOX tanks, since the ball-socket supports cannot carry tension, one side lifting out if a moment is applied to the tank. In addition, certain cross-coupling spring constants are necessary to account for elastic coupling of the spider beam and thrust structure.

The modal approach allows each of the basic directions of motion to be represented by a summation of as many uncoupled modes as required to describe a given frequency range. In the bending model, six "center barrel" free-free modes are calculated after removing four outer fuel and two outer LOX tanks. This leaves the center LOX tank with one outer LOX tank on each side as the basic bending structure. This idealization was used because of the high tangential restraint on the ends of the LOX tanks. The tank modes were coupled to the "center barrel" through radial and tangential springs on the ends of the tanks. Consideration was given to the method (explained previously) of attachment of the individual tanks to determine the springs which were needed to simulate potential energy in the spider beam and thrust structure. Only the longitudinal compression and tension of the two LOX tanks previously removed was included in the model as effective springs, since the fuel tanks with the sliding pins forward cannot carry tension or compression. Three pinned-pinned modes were used in simulating additional radial and tangential motion of the outer tanks and two pinned-pinned modes were used for the 105" center LOX tank. Rigid body modes of vehicle translation and rotation were included which forced the summation of forces and moments of the coupled system to equal zero, satisfying free-free conditions. This gives a total of twenty-two degrees of freedom for the bending model. Only about two-thirds of these modes are valid however, since more than six "center barrel" modes must be included to sufficiently cover the frequency range of three-pinned-pinned tank modes. The higher modes are included only to refine the mode shapes and frequencies of the lower modes.

In the torsion model, four "center barrel" torsion modes were included. These modes were calculated by using the total moment of inertia per unit length of the clustered booster, but only the stiffness of the eight outer tanks about their own centerlines. This idealization was used since a static analysis of the S-IB stage using a detailed stress model showed that for a torque loading at the spider beam, 60.2% of the torque load was carried by twisting of the outer tanks, 24.4% by center LOX tank twisting and 15.4% by bending in the outer tanks. Three pinned-pinned modes for each type outer tank were used for tangential motion. For the 105" center LOX tank, a rigid rotation and the first free-free torsion mode were used and coupled through the "spoke wheel" rotation springs of the spider beam and thrust structure. To ensure a free-free coupled model, one rigid vehicle rotation mode was also included. This resulted in a total of thirteen degrees of freedom for the torsion dynamic model. Again, the higher modes were included only to refine the lower modes.

Some clarification is needed to explain why separate bending and torsion models can be used, as well as possible simplifications in the degrees of freedom considered. When the complete

coupled equations of motion for the pitch, yaw and roll planes are written, it becomes apparent that because of the inherent symmetry of the cluster (four fuel and/or four LOX tanks each  $90^\circ$  apart) the pitch, yaw and roll planes are essentially uncoupled dynamically. Furthermore, since diagonally opposite tanks are alike, the system contains four radial tank modes and two tangential tank modes where tanks diagonally across move in the opposite direction. These modes produce no resultant forces or torques on the rest of the vehicle and therefore are completely uncoupled from themselves and the rest of the system. The directions of these six "pulsating" modes are depicted in Fig. 4. They have no effect on control system design because the upper stages which contain the control system sensors have no motion. They were also not excited in the test, since shakers were not put on the tanks. These modes would only be of interest if total motions of the tanks, excited by such things as aerodynamic turbulence during flight, were desired. They also require no extensive analysis since they are just the pinned-pinned modes of the tanks with rotational springs simulating the spider beam and thrust structure stiffnesses. Elimination of these modes from the system is accomplished by lumping together tanks diagonally across from one another in the bending model and by lumping all similar tanks together in the torsion model. The fact that pitch and yaw modes are uncoupled can be physically interpreted by requiring that in a pitch (or yaw) bending mode, the LOX and/or fuel tanks have a net zero force motion in the yaw (or pitch) plane. This interpretation is the heart of the mathematical transformation which rigidly uncouples the pitch, yaw and roll planes and is a direct result of similar tanks being  $90^\circ$  apart.

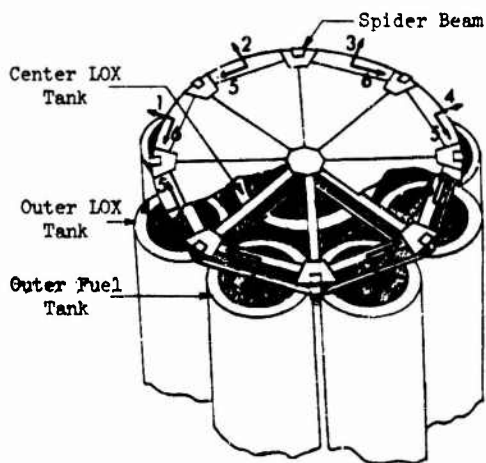


Fig. 4. Uprated Saturn I "Spider Beam" Details Depicting Directions of the Six Outer Tank "Pulsating" Modes

To reiterate then, the degrees of freedom of the clustered arrangement can be greatly reduced by recognizing the fact that, except for possible upper stage asymmetries, the pitch, yaw and roll planes are dynamically uncoupled and the "pulsating" modes of the tanks are uncoupled from control system feedback problems. These two conditions allow the outer tank motion to be reduced from sixteen directions (two planes of motion for eight tanks) to six; four in the pitch/yaw bending model (LOX radial, LOX tangential, fuel radial, fuel tangential), and two in a torsion model (LOX and fuel tangential). From the original sixteen directions, four are eliminated by disregarding radial "pulsating" modes, two by disregarding tangential "pulsating" modes and four by the fact that the pitch and yaw planes have identical modes. Twisting degrees of freedom of the outer tanks were not considered since their frequencies are very high ( $> 40$  cps) because the propellant does not contribute to the tank roll moments of inertia.

Final spring constant values in the model were determined by changing calculated values to obtain better test correlation. Differences between calculated and correlated values averaged about 10%.

#### EFFECTIVE STIFFNESS VALUES FOR APT PORTION OF S-IB/S-IVB INTERSTAGE

During the course of correlating the multibeam theoretical model with the full scale dynamic test results, it was noted that the numerical value of the geometric EI for the aft portion of the interstage was too large. It was assumed that this was caused by the shell properties of the interstage and the 20 inch offset in the load path as loads are transmitted from the interstage into the outer LOX tanks. In order to verify this assumption, a detailed shell model of the spider beam - aft interstage combination, developed for stress calculations, was used to determine an effective stiffness of the aft portion of the interstage from Station 962 to 1104. This portion of the interstage was cantilevered at Station 1104 and various loading conditions simulating pure shear and bending moment applied at the outer LOX tank attachment points. It was determined that the structure could not be strictly idealized as a beam and that its effective EI depended on the loading condition. Evidence of this was also noted during the test, as recorded by one test engineer during first bending resonance of AS-202-D, "Very pronounced panel mode in S-IVB/S-IB interstage". However, for purposes of the multibeam dynamic model, an effective EI distribution to produce good correlation on the lower modes was determined and was used in all theoretical modes presented in this paper.

# EFFECTIVE STIFFNESS VALUES FOR SERVICE MODULE/ COMMAND MODULE INTERFACE

The test results also showed that the service module-command module torsion restraint was much lower than design data for this area. The low restraint is due to the lack of any side struts on the triangular supports at the top of the service module which "cradle" the command module. First bending mode shapes and low values of second bending frequency also indicated a bending weak spot in the service module-command module area. By correlating test results, effective torsional and bending stiffnesses were determined for this area. Bending stiffnesses were later verified by the results of static tests performed on a service module-command module configuration and are discussed later in the paper.

# TEST CORRELATION OF FREQUENCIES AND MODE SHAPES

Using theoretical multibeam models previously discussed, the results of the full scale dynamic tests were compared to calculated modes. Table 1 presents a comparison of frequencies from the test and the model. The first and second columns for each configuration give the test and model frequencies. The third column gives the percentage increase required in the model frequencies due to coupling with sloshing, since the multibeam model does not contain sloshing modes. The resultant percent error is given in the fourth column. The last column of the table gives the average percent error for each mode over the four vehicle configurations. The average percent errors are given not as tolerance factors on the modes, but as an indication of how effective one model was in simulating a variety of configurations.

TABLE I  
COMPARISON OF TEST AND THEORETICAL BENDING  
AND TORSION FREQUENCIES FOR S-IB STAGE FLIGHT

BENDING MODE DESCRIPTION	AS202-D				AS203-D				AS204-D				AS207-D				AVG. % ERROR
	f(CPS)		% ERROR		f(CPS)		% ERROR		f(CPS)		% ERROR		f(CPS)		% ERROR		
	TEST	MODEL	SLOSH	TOTAL	TEST	MODEL	SLOSH	TOTAL	TEST	MODEL	SLOSH	TOTAL	TEST	MODEL	SLOSH	TOTAL	
-LIFTOFF-																	
1ST BENDING	1.35	1.20	2.7	-9.0	2.30	2.17	1.8	-4.0	1.34	1.27	1.6	-3.6	1.32	1.24	1.9	-4.6	-5.3
1ST FUEL RAD.	1.65	1.61	0.3	-2.8	1.61	1.60	0.3	-0.1	1.65	1.61	0.2	-2.2	1.65	1.61	0.4	-1.5	-1.8
1ST LOX RAD.	2.10	2.06	0.3	-1.9	2.05	2.05	0.4	0.6	2.02	2.06	0.4	2.4	2.10	2.06	0.3	-1.4	-0.1
2ND BENDING	2.27	2.12	0.4	-6.1	6.30	5.89	3.8	-3.0	2.15	2.15	0.5	0.3	2.26	2.18	0.4	-3.1	-3.1
1ST FUEL TANG.	2.45	2.45	0.7	1.0	-	2.55	0.8	-	-	2.49	0.1	-	2.40	2.48	0.4	3.9	2.5
1ST LOX TANG.	3.57	3.51	0.9	-0.8	3.65	3.64	0.6	0.5	3.42	3.63	0.6	6.8	3.40	3.58	0.4	5.7	3.1
3RD BENDING	4.14	3.89	2.1	-4.0	8.06	7.59	0.5	-5.3	3.85	4.28	1.7	13.1	3.79	3.98	1.2	6.3	2.5
2ND FUEL RAD.	5.90	5.60	0.5	-4.6	5.72	5.50	0.8	-3.0	-	5.66	0.6	-	6.00	5.66	0.6	-5.1	-4.2
4TH BENDING	6.67	6.36	1.2	-3.4	-	10.47	-	-	5.82	6.31	0.9	9.5	5.78	6.32	1.0	5	5.5
-110 SECONDS-																	
1ST BENDING	1.64	1.31	3.8	-17.1	3.84	4.00	7.0	11.5	1.41	1.37	1.5	-1.1	1.44	1.34	2.2	-4.9	-2.9
2ND BENDING	2.57	2.36	1.1	-7.1	6.74	8.96	2.6	36.5	2.65	2.65	1.2	1.3	2.61	2.57	0.9	-0.6	7.5
1ST FUEL RAD.	6.04	5.66	3.1	-3.4	-	4.70	2.8	-	5.10	4.66	2.3	-6.5	5.10	4.66	2.5	-6.4	-5.4
1ST LOX RAD.	4.80	4.91	2.5	4.8	5.00	5.26	3.4	8.8	5.46	5.92	2.7	11.4	5.44	5.89	2.7	11.2	9.0
3RD BENDING	7.70	6.78	1.0	-11.1	-	13.74	-	-	5.80	6.42	0.9	12.1	6.09	6.54	1.2	8.7	3.2
1ST FUEL TANG.	9.39	8.87	1.5	-4.2	7.80	7.88	4.5	5.6	-	8.24	1.8	-	-	8.27	2.5	-	0.7
1ST LOX TANG.	-	8.35	2.2	-	-	8.34	-	-	-	10.33	-	-	9.70	10.33	-	6.6	6.6
4TH BENDING	9.69	9.89	-	2.1	-	-	-	-	-	8.88	-	-	-	9.16	-	-	2.1
-BURNOUT-																	
1ST BENDING	1.64	1.39	2.6	-13.1	3.88	4.05	7.0	11.7	1.45	1.43	1.4	0.2	1.48	1.41	1.7	-3.3	-1.1
2ND BENDING	2.60	2.37	1.2	-7.5	-	-	-	-	2.65	2.67	1.7	2.4	2.59	2.58	0.8	0.6	-1.5
3RD BENDING	6.88	7.12	1.5	5.0	-	-	-	-	5.83	6.39	0.7	10.3	6.28	6.51	1.0	4.7	6.7
4TH BENDING	8.95	10.46	-	16.9	-	-	-	-	-	10.21	-	-	7.58	10.59	-	39.7	28.3
EMPTY CANTILEVERED	-	-	-	-	-	-	-	-	(AS-204 PULL TEST)	-	-	-	-	-	-	-	-
1ST BENDING	-	-	-	-	-	-	-	-	.95	.99	-	4.2	-	-	-	-	-
2ND BENDING	-	-	-	-	-	-	-	-	3.80	3.73	-	-1.9	-	-	-	-	-
TORSION MODE DESCRIPTION																	
-LIFTOFF-																	
1ST FUEL TANG.	2.41	2.42	0	0.4	2.39	2.42	0	1.4	2.40	2.42	0.1	0.9	2.38	2.42	0.1	1.9	1.2
1ST TORSION	3.51	3.50	0.1	-0.2	3.52	3.56	0.1	1.1	3.53	3.46	0.1	-1.7	3.54	3.49	0.1	-1.1	-0.5
COMMAND MODULE	4.74	4.41	0	-6.8	-	-	-	-	6.42	6.45	0	0.6	4.40	4.42	0	0.5	-1.9
1ST LOX TANG.	5.60	4.94	0.1	-11.6	5.36	4.81	0	-10.2	5.05	4.66	0	-7.6	5.40	4.93	0	-8.7	-9.5
2ND FUEL TANG.	6.79	6.91	0.1	1.9	6.68	6.94	0.1	4.0	6.85	6.89	0	0.7	6.86	6.84	0	-0.3	1.6
2ND LOX TANG.	9.67	9.70	0.1	0.3	9.81	9.71	0	-1.1	9.10	9.53	0	4.8	9.68	9.68	0.1	0.1	1.0
-110 SECONDS-																	
1ST TORSION	4.25	4.17	0	-1.7	-	-	-	-	-	-	-	-	4.20	4.13	0	-1.7	-1.7
COMMAND MODULE	5.10	5.12	0	0.4	-	-	-	-	-	-	-	-	5.00	4.98	0	-0.4	0
1ST FUEL TANG.	7.66	9.19	0.2	20.3	-	-	-	-	-	-	-	-	7.60	8.12	0.2	7.1	13.7
1ST LOX TANG.	-	9.71	-	-	-	-	-	-	-	-	-	-	-	10.86	-	-	-
-BURNOUT-																	
1ST TORSION	4.55	4.36	-	-4.0	-	-	-	-	4.83	4.77	-	-1.2	-	-	-	-	-2.6
COMMAND MODULE	5.36	5.43	-	1.3	-	-	-	-	6.53	6.70	-	2.6	-	-	-	-	2.0



Several areas of large discrepancy are noted. The 203-D vehicle analyses at 110 seconds and burnout conditions show large differences. Frequency responses of the test for these two configurations were very poorly defined above the first bending mode. Good resonance peaks did not exist, especially for the second bending mode, with the accelerometer amplitudes gradually rising and falling as though the modes were very heavily damped or obscured by some non-linear phenomenon. To further complicate matters, the 203-D bending is heavily influenced by the S-IVB LOX sloshing mode because of its large sloshing mass (78,000#). This sloshing mass was much larger than those of the other configurations since the S-IVB LOX tank was only half full. It was also located near the first bending mode shape node making the coupling extremely sensitive to sloshing mass location. Considerable time was spent trying to accurately evaluate the effects of sloshing on the 203-D vehicle. This effort resulted in the conclusion that much more detailed study would be necessary to determine if a spring-mass sloshing analogy is accurate enough to account for coupling with bending in the case of a very large sloshing mass near a node.

AS-202-D test frequencies are very hard to explain based on 204-D and 207-D results. Examination of the mass distribution documented during the test would indicate that without a change in stiffness properties of the vehicle, the first and second bending modes would be lowest for the 202-D configuration. The test results show the opposite effect to a large degree. This inconsistency was not resolved during the test evaluation. In view of the facts that lower frequencies are normally more critical from a control system design standpoint and that producing better test correlating for the 202-D configuration would seriously affect correlation for configurations without the LES tower such as AS-203, it was decided that the best compromise was to produce good correlation by a single model over all four configurations.

It should also be realized that such things as engine modes, LM modes, shell modes, etc. will affect higher modes and have not been accounted for in this correlation. It has recently been determined that LM modes greatly affect the 204-D results around 6 cps and that the mode at 5.8 cps is probably a LM mode.

In general good torsional frequency agreement was obtained for the limited test data available. The most significant differences are noted in the fuel tangential modes. Mode shapes for these modes also indicated that the coupling of the fuel tangential tank to the center barrel motion is not correctly simulated in the dynamic model. The actual non-linear spring attachment of the fuel tank at both ends is reasoned to cause this discrepancy, since the same idealization was used on both the fuel

and LOX tanks, the LOX tanks producing good results. This area was not considered detrimental to control system design since the first fuel tangential mode from the model has relatively good frequency correlation, with the deflection at the gimbal point being larger than the test data. Sloshing coupling proved to be insignificant for the torsion modes.

Fig. 5 shows a comparison of bending and torsion mode shapes for AS-207-D at liftoff. Mode shape comparison is good except for some of the higher modes in the area near the middle of the S-IVB stage. Effects of discrepancies in the mode shapes will be discussed in the next section. These mode shape correlations are typical of other configurations and other flight times.

#### EVALUATION OF ERRORS RELATED TO ATTITUDE CONTROL SYSTEM DESIGN

The data presented in the previous sections represents a good overall correlation of the experimental and theoretical results. Attitude control system design, however, is greatly affected by errors in local deflections and slopes at control sensor locations and by overall effects such as frequency and generalized mass. In order to completely define the difference in the experimental and theoretical results, as related to control system design, a complete stability analysis would have to be made with the experimental data. A less sophisticated comparison can be made, however, by utilizing the method given in Ref. (3). The departure modulus of the root locus from an open loop pole (a pole situated in the complex plane at the coupled natural frequency and damping ratio) is given by

$$R = \frac{T Y'(IU) Y(GP)}{2 M_b \omega_b} K(i\omega_b) \quad (1)$$

where

- $T \sim$  gimballed thrust
- $M_b \sim$  generalized mass of bending mode
- $\omega_b \sim$  frequency of bending mode
- $Y'(IU) \sim$  bending mode slope at Instrument Unit
- $Y(GP) \sim$  bending mode deflection at gimbal point
- $K(i\omega_b) \sim$  gain thru the control system per unit slope at the Instrument Unit

The form given in Eq. 1 is applicable to the Saturn IB (neglecting the load relief control accelerometer which is heavily filtered) since the position and rate gyros are both located in the Instrument Unit. In making a fair comparison with experiment two things must be considered, the magnitude of  $R$  and the difference in  $R$  between the test and calculated modes. For purposes of this comparison, only modes with  $R > .005 \omega_b$  were considered important. Theoretically then, a comparison can be made by



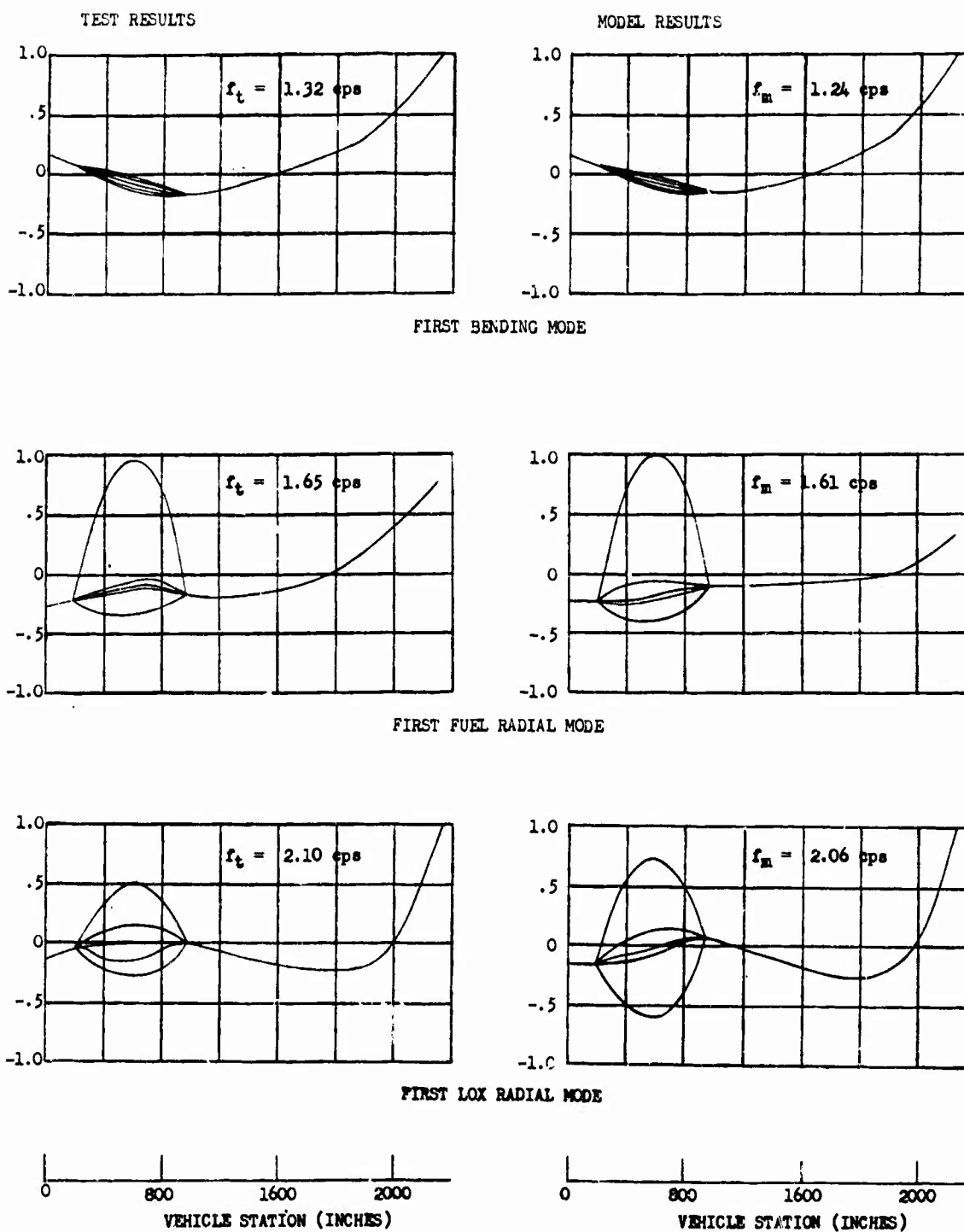


Fig. 5. Comparison of Test and Theoretical Mode Shapes for the SA-207-D Configuration at Liftoff

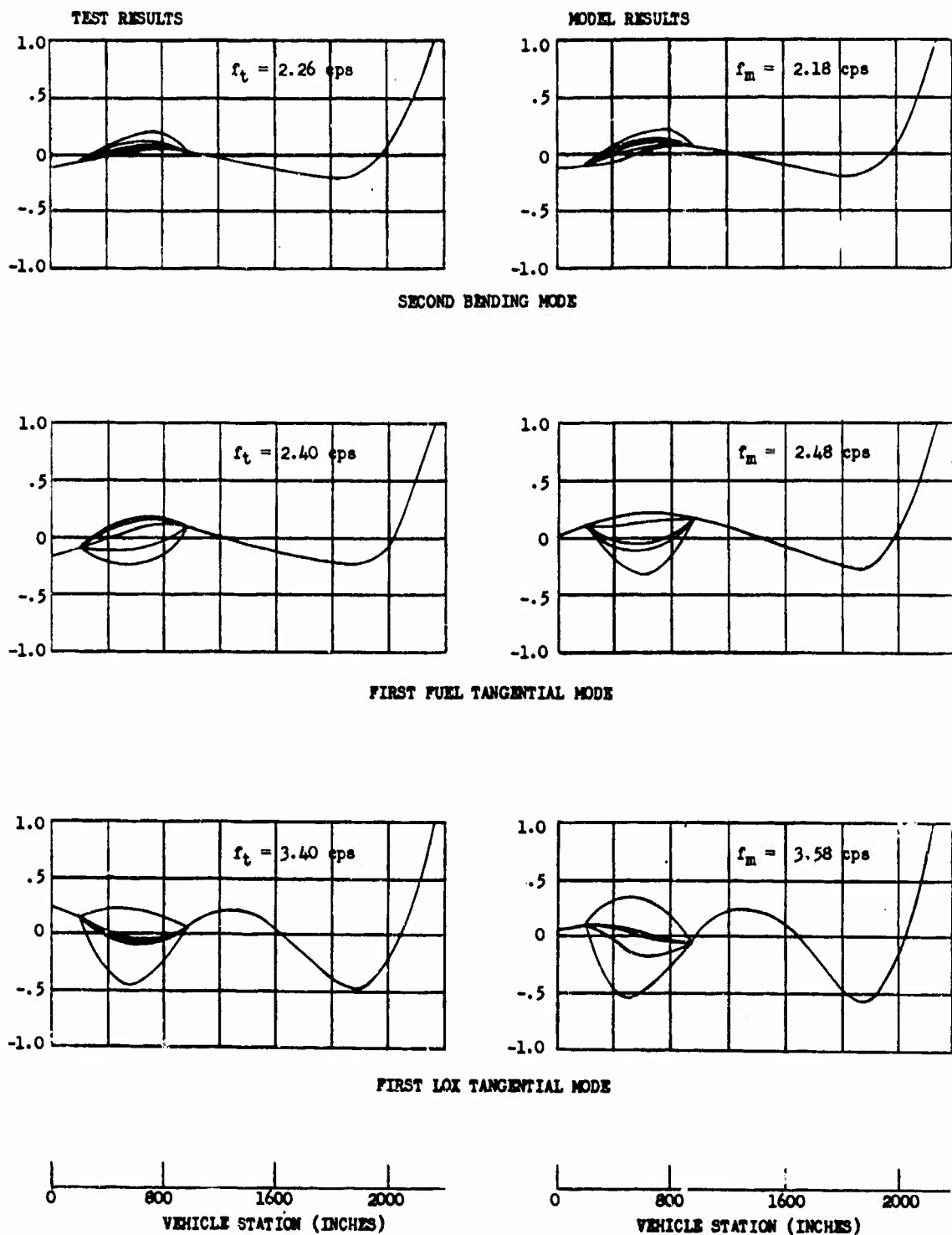


Fig. 5, Comparison of Test and Theoretical Mode Shapes for the SA-207 configuration at Liftoff

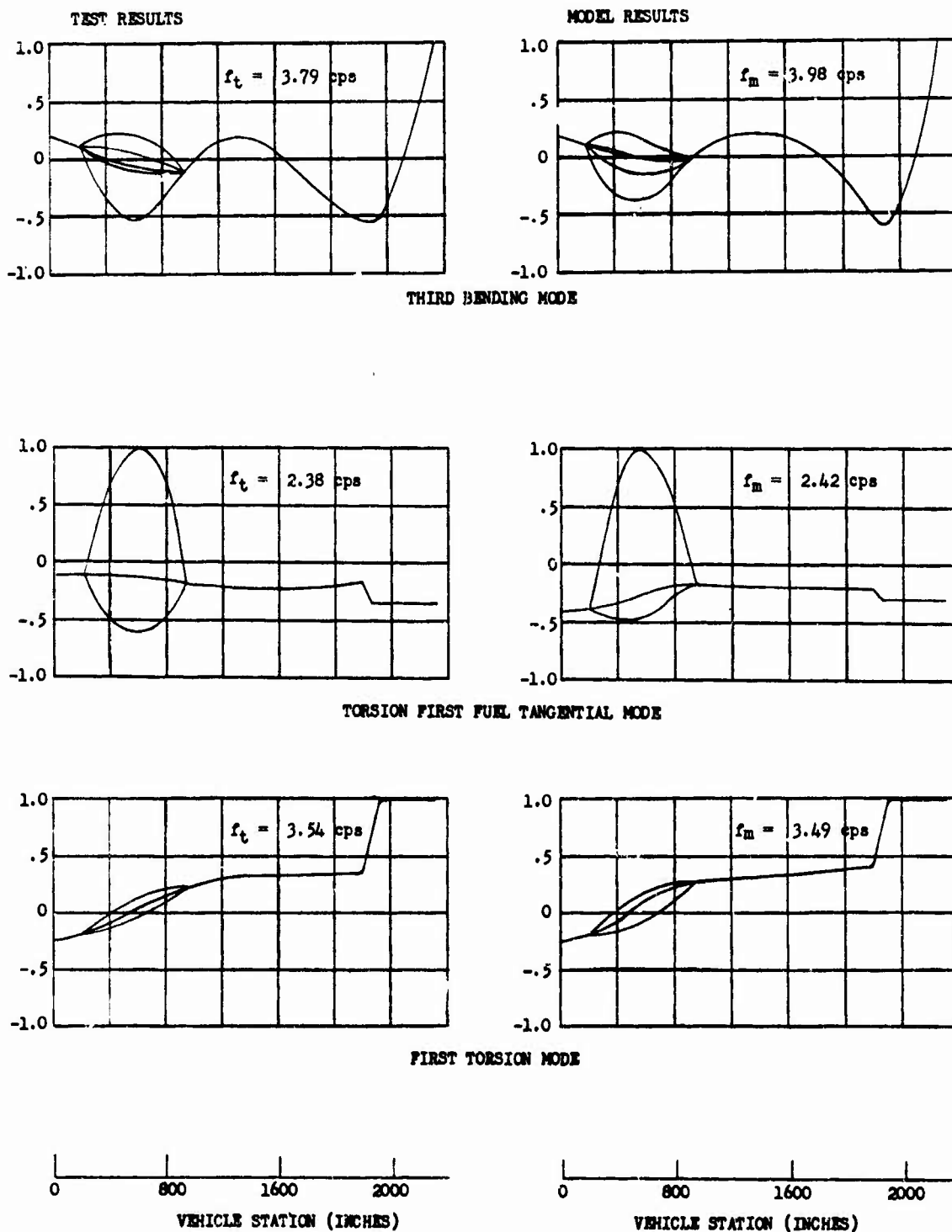


Fig. 5. Comparison of Test and Theoretical Mode Shapes for the SA-207-D Configuration at Liftoff

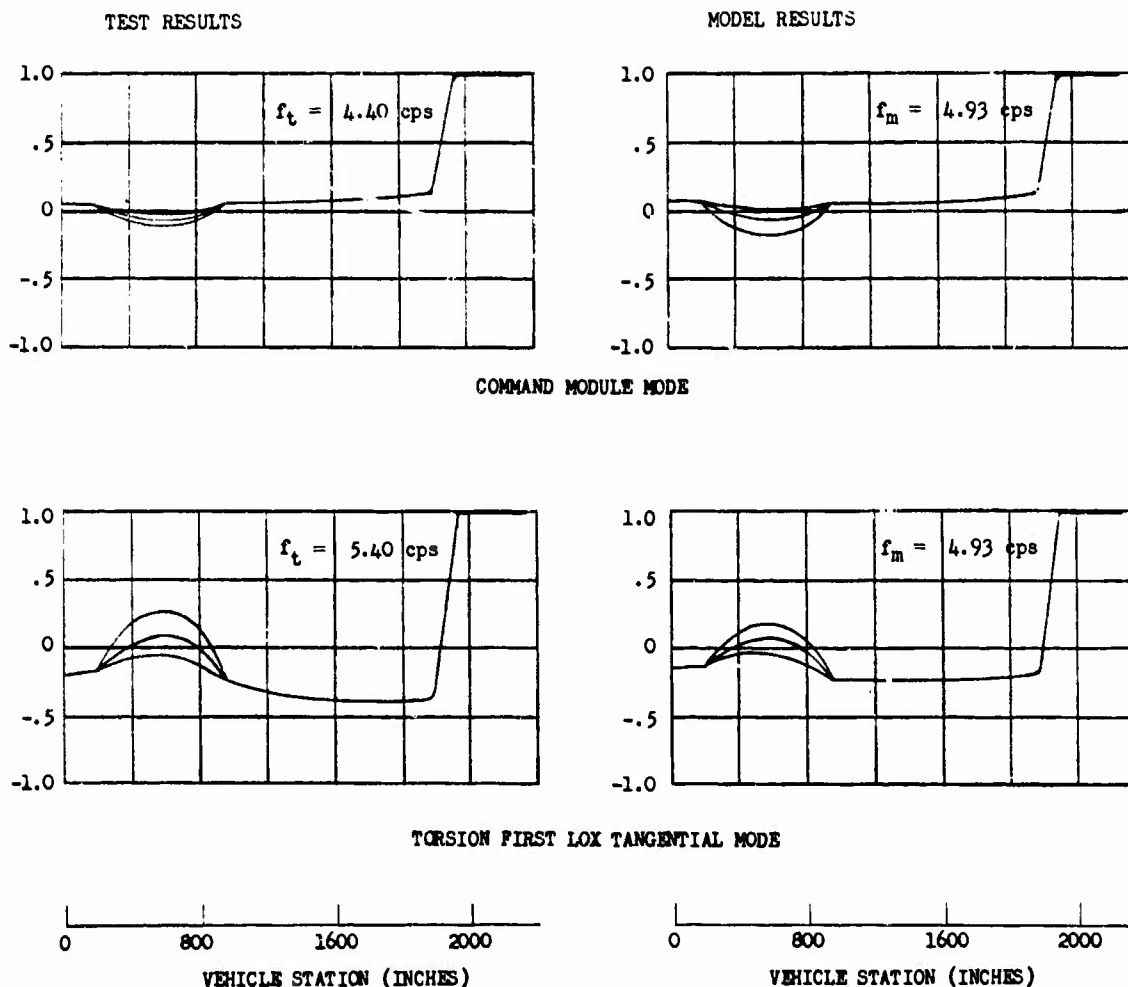


Fig. 5. Comparison of Test and Theoretical Mode Shapes for the SA-207-D Configuration at Liftoff

$$\frac{R_t}{R_m} = \frac{Y_t'(IU)}{Y_m'(IU)} \frac{Y_t(GP)}{Y_m(GP)} \frac{\omega_{bm}}{\omega_{bt}} \frac{M_{bm}}{M_{bt}} \quad (2)$$

where

$F_t \sim$  shaker force  
 $\gamma_t \sim$  test damping ratio  
 $\ddot{z}_t(X_n) \sim$  test deflection acceleration at the point on the vehicle where the theoretical mode is normalized

Several drawbacks however are inherent in Eq. 2. First, the gimbal point deflection is usually small and ill-defined in the test results. Second, the generalized mass cannot be read directly from test results and attempts to calculate it based on test modes and mass distributions are rather poor. In order to circumvent these difficulties, the following reasoning was used. Assuming a second order equation at resonance for each mode, the generalized mass is given to a good approximation by

$$M_{bt} \approx \frac{F_t Y_t(GP)}{2 \gamma_t \ddot{z}_t(X_n)} \quad (3)$$

The ratio  $M_{bt}/Y_t(GP)$  can then be determined by well known parameters, the least well known being the damping ratio. Eq. 2 then becomes

$$\frac{R_t}{R_m} = \frac{Y_t'(IU)}{Y_m'(IU)} \frac{\omega_{bm}}{\omega_{bt}} \frac{M_{bm} 2 \gamma_t \ddot{z}_t(X_n)}{F_t Y_m(GP)} \quad (4)$$

Table 2 gives values from Eq. 4 for the bending test results. The same reasoning can be applied to the torsion modes and data is also presented in Table 2. It is desirable to keep this ratio below 2.0 since the control system is designed on a spread of twice the nominal gain. Several modes show potential problems, the first fuel radial mode, the first LOX tangential mode, and the third bending mode. The discrepancies in all of these, as shown in Fig. 5, center around the incorrect slopes of the Instrument Unit location. These particular modes were re-checked using test results and found to be adequately stabilized by the filters in the control system. The data given in Table 2 is subject to criticism as to its absolute accuracy. Mode shape slopes and damping ratios were rather hard to obtain from the test results. Damping ratios varied from 0.7% to 2.0% for different modes, an average value being 1.4%. Local effects at the sensor locations should also be considered in comparing test and theoretical results. The authors believe that part of the problem of accurately defining the test mode shapes and damping ratios lies in the fact that only one shaker was used in the full scale test. This is partly verified by the fact that the test results from configuration to configuration seemed to change much more than corresponding changes with mass distribution in the theoretical model. A system of shakers, possibly only an additional one at the spider beam, would

probably have produced much better mode shape definition of the low response tank modes. Complete tank definition also was not possible in most cases due to the limited number of accelerometers on the tanks, only two in the center portion. From 5 to 6 accelerometers are needed to accurately define higher modes.

#### ADDITIONAL USEFUL TESTS

After the results given in previous sections were determined several other tests were conducted for various other reasons from which other information concerning the bending dynamic model could be extracted. Static and dynamic pull tests (4) were conducted on the AS-204/LM-1 (Apollo 5) vehicle on Launch Complex 37 at Cape Kennedy, Florida. These tests were conducted primarily to determine the vehicle cantilevered bending characteristics while constrained on the launch pad for application to ground wind load studies. For the static pull test, a pull ring was attached to the top of the spacecraft LM adapter at Station 2033. Lateral loads of 600, 1500, 3000, 4500, and 6000 lbs. were applied to the pull ring and deflections measured at Station 1994, 1662, 1540, 1212, 1187, and 962. In the dynamic pull test, the vehicle was oscillated until a displacement of 4 inches was reached at the pull ring and then released to oscillate freely. Accelerometers were mounted at Station 2033, 1540, 1270, and 962. Table 1 gives the results of the frequency correlation, while Fig. 6 shows a least squares curve fit of the static pull test deflection data normalized to a unit Kip load. Comparison of the theoretical static deflection indicates differences of approximately 0% at Station 962 to 8.5% at Station 2033. The theoretical curve was

TABLE 2  
CONTROL SYSTEM GAIN RATIOS  
(Liftoff Configuration)

Vehicle	Bending Mode	$\frac{\omega_{bm}}{\omega_{bt}}$	$\frac{Y_t'(IU)}{Y_m'(IU)}$	$\frac{M_{bm}(2Y_t'Z_t)}{F_t Y_m(GP)}$	$\frac{R_t}{R_m}$
AS-202	1st Bending	.91	1.15	.98	1.02
	2nd Bending	.94	.46	.62	.27
	1st LOX Tang.	.99	1.84	.53	.96
	3rd Bending	.96	2.80	1.01	2.73
AS-203	1st Bending	.96	.89	1.14	.97
	1st Fuel Rad.	1.00	3.18	2.12	6.74
	1st LOX Rad.	1.01	1.27	1.85	2.35
	2nd Bending	.97	.87	.69	.58
	1st LOX Tang.	1.01	1.86	.92	1.72
AS-207	3rd Bending	.95	.97	7.52	6.90
	1st Bending	.95	1.20	1.06	1.22
	2nd Bending	.97	1.12	.70	.76
	1st LOX Tang.	1.06	1.89	3.20	6.41
	3rd Bending	1.06	1.81	.48	.92
Vehicle	Torsion Mode	$\frac{\omega_{tm}}{\omega_{tt}}$	$\frac{\theta_t(IU)}{\theta_m(IU)}$	$\frac{I_t(2Y_t'\theta_t)}{T_t \theta_m(GP)}$	$\frac{R_t}{R_m}$
AS-202	1st Fuel Tang.	1.00	1.20	.30	.37
	1st Torsion	1.00	1.01	1.39	1.40
	1st LOX Tang.	.88	1.27	.93	1.04
AS-203	1st Fuel Tang.	1.0	1.50	.26	.39
	1st Torsion	1.01	.92	1.22	1.13
	1st LOX Tang.	.90	1.18	1.15	1.22
AS-207	1st Fuel Tang.	1.02	1.18	.25	.30
	1st Torsion	.99	.78	1.66	1.28
	1st LOX Tang.	.91	2.13	.62	1.20

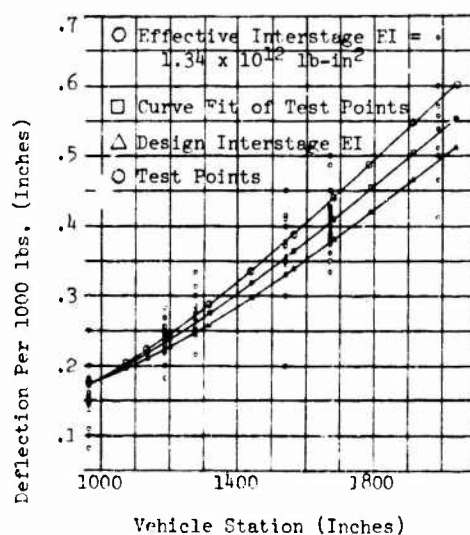


Fig. 6. Pull Test Reflection Data, AS-204

calculated from the static solution for a 1000 lb. lateral load applied at Station 2033, using the first 12 cantilevered bending modes from the dynamic model as degrees of freedom. Since both the deflection curves and the first cantilevered frequencies were high, it was felt that only a complete review of the idealizations used in the dynamic model could produce more accurate results. Acceptable correlation accuracies were  $\pm 5\%$  in frequency and  $\pm 10\%$  in deflection and since these were achieved, any revision to the dynamic model was deemed unnecessary.

The combined Apollo command module-service module configuration was also tested (5) for

static loads conditions. Although these tests were made primarily for loads verification, deflections were measured and used to verify stiffness data used in the Saturn IB bending analysis. Fig. 7 shows a summary of the resultant loads applied to the CM/SM configuration. These loads were applied to a beam having the stiffness properties used in the dynamic model. Fig. 7 also compares the actual versus theoretical deflection. The theoretical results show slightly more deflection outboard of the CM/SM interface. A slight change in the CM/SM interface stiffness resulted in the dashed curve. These changes when applied to the dynamic model produced slight local mode shape changes resulting in only 3 to 4% change in the gain of the mode thru the attitude control system.

#### CONCLUSIONS

Full scale vibration tests conducted for the Up-rated Saturn I vehicle were adequately correlated by theoretical results. The value of performing vibration tests was demonstrated by pointing out weak areas and anomalies such as the Command Module-Service Module interface and the S-IVB interstage. The experimental results also allowed adjustments in the idealizations and input data of the theoretical models to produce more accurate results for different flight vehicle configurations.

In testing, consideration should always be given to multiple shaker inputs to better define mode shapes. Better methods of determining generalized masses and damping ratios are also needed. In addition, local differences in mode shapes must be examined closely in areas of control sensor location to ensure adequate system stability.

The authors believe that the use of the modal approach to this type of dynamic problem, rather than a complete direct stiffness approach, greatly simplifies the understanding and computer implementation of large dynamic system models.

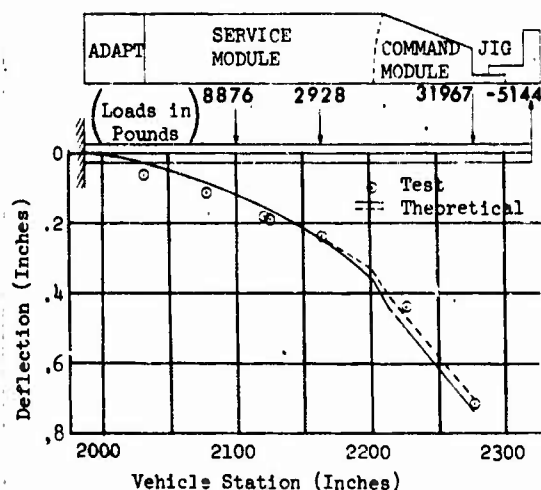


Fig. 7. Command Module/Service Module Test Versus Theoretical Deflection - Static Loads Test

#### REFERENCES

1. "Final Report of Total Vehicle Testing of Saturn IB" Chrysler Corp. Space Division, HSM-R856, January 31, 1966.
2. "Dynamic Test Correlation, S-IB Stage Flight Bending and Torsion" Chrysler Corp. Space Division, TN-AP-66-148, November 15, 1966.
3. "Simplified Approximations of Bending and Sloshing Mode Root Loci of Gimbaled Engine Attitude Controlled Missiles" by Charles R. Wells, Chrysler Corp. Space Division TN-AE-64-63, June 10, 1964.
4. "AS-204/LM-1, Static and Dynamic Pull Test Correlation", Chrysler Corp. Space Division, TN-AP-67-294, January 16, 1968.
5. "AS-205/CSM-101 Correlation of Spacecraft Static Test Deflection Data", Chrysler Corp. Space Division, TN-AP-68-360, Aug. 19, 1968.

## AN APPROACH FOR DUPLICATING SPACECRAFT FLIGHT-INDUCED BODY FORCES IN A LABORATORY

S. M. Kaplan and A. J. Soroka  
General Electric Company  
Philadelphia, Pennsylvania

This paper describes a test approach capable of imparting both internal and external body forces to a test article that effectively duplicate loadings expected in flight. This encompasses not only internal loads on primary structure, but also load factors for major mass items, equipment, and secondary structure. This sinusoidal vibration test approach, evolved from existing test methods, employs existing test equipment. The test levels, established at the inception of a program, will remain invariant, barring major redesigns. This approach represents a deviation from present practice, in that it advocates the tailoring of the test environments to the specific spacecraft.

### INTRODUCTION

The most perplexing of spacecraft laboratory test simulation problems to date has been the reproduction of the stresses, or loading fields, produced during liftoff and powered flight. This problem has existed primarily because of the inability of laboratory simulations to duplicate the launch vehicle's impedance and boundary conditions. To partially compensate for this, the force-notched sinusoidal vibration test was developed<sup>(1)</sup>. In this currently employed technique, the spacecraft is subjected to specified acceleration levels at its launch vehicle interface. Simultaneously, shaker inputs are restricted from inducing bending moments or shear forces in excess of those anticipated in flight. When stresses induced by flight loads are exceeded, shaker-provided excitations are commensurately reduced, placing a "notch" in the specified test spectrum.

The sinusoidal test approach subjects the test article to body (acceleration) forces, enabling adequate testing of systems with inaccessible mass items. The utilization of the "force-notch," however, has been restricted exclusively for the benefit of primary structure at a few discrete frequencies. Test levels outside of these bandwidths remain unaffected--they may, but probably will not, induce those loads anticipated in flight.

This paper is intended to show how this test approach can be greatly enhanced with regard to establishing test levels outside of these notched regions. It is specifically addressed toward the

transformation of both vehicle primary structure and equipment internal loads/load factors induced by critical flight-loading conditions into a test program that yields nearly identical results in the laboratory.

Such approaches have been explored in the past. Clevenston *et al.*<sup>(2)</sup> for example, derived means for establishing test levels based on flight-measured sinusoidal transients. However, their approach, like the force-notched concept, was based upon the spacecraft idealized as a one-degree-of-freedom oscillator. Extensions of such approaches are desirable which reflect the effects of stimuli at higher structural system resonances (where major mass items and equipment/secondary structure peak responses occur). Spacecraft systems are complex, multidegree-of-freedom structures. Their unique vibration characteristics must be reflected in the synthesis of test environments.

### TEST PROGRAM REQUIREMENTS

The basic objective of any test program must be to verify the structural integrity of the system. This essentially means that the test must:

- a. Induce within the primary vehicular structure, those peak (quasi-steady) internal loads (shear forces, bending moments and axial loads) expected in flight, multiplied by the appropriate factor of safety.

- b. Subject primary mass items (e. g., propulsion subsystem) to those peak quasi-steady acceleration load factors expected in flight, multiplied by the appropriate factor of safety.
- c. Impose upon spacecraft equipment ("black boxes") those peak expected acceleration load factors expected in flight, multiplied by the appropriate factor of safety.
- d. Simultaneously, exert the minimum possible influence upon spacecraft design.

Of these, the loads data cited in items (a) and (b) is obtainable from combined spacecraft-launch vehicle loads analyses (or, in the design synthesis stage, from sources such as Reference 1). Equipment design load factors can be synthesized from (vibro-acoustic) flight measurements data involving instrumentation located in the vicinity of spacecraft equipment on previous flights. Thus, the necessary data is available to synthesize sets of equivalent static design loads.

The critical item then (and the motivation behind this investigation) is the minimization of the test's influence upon spacecraft design. Past practices have generally resulted in the test levels providing the critical loading conditions and consequently, significantly influencing design<sup>(3), (4)</sup>.

In essence, what is required then is a complete marriage between the three cornerstones involved in the design-test triangle (Figure 1): (a) the flight-expected loads (multiplied by the appropriate factor of safety); (b) the spacecraft's unique vibration characteristics (mode shapes, frequencies and resulting vibration transmissibility spectra); and (c) the environmental test levels. These flight environments (or load factors), which in turn can be quite readily transformed into internal loads, are readily known quantities.

The spacecraft vibration characteristics indeed represent a given vehicular configuration's "structural fingerprints." Each given generic design or vehicle family, contains similar modes of vibration, within each of which, unique and different phenomena occur. Certain modes, for example, reflect total structural system resonances, e. g., "body bending" modes, while in others, the response of primary major mass items or equipment (on its brackets) predominates. Phenomena involving such "structural fingerprints" have been demonstrated both analytically and experimentally on the ATS spacecraft<sup>(3)</sup>, and on Nimbus for example. This merely represents vestiges of the law of dynamic similitude, namely, that dynamically similar systems respond in similar manners under dynamic excitation. Additional substantiation and comments regarding this

are provided in subsequent sections.

With the critical flight loads dictated by launch vehicle selection, and vibration characteristics being unique characteristics of a given design, it then remains the function of the environmental test levels to form the basis from which the design-test triangle (Figure 1) is formulated.

#### TEST APPROACH

Spacecraft sinusoidal vibration test levels in the proposed test approach are established from: (a) spacecraft primary structure loadings established from combined spacecraft-launch vehicle flight loads analyses, (b) equipment/secondary structure load factors expected in flight, and (c) a set of spacecraft mode shapes and frequencies for a specific spacecraft supported at its launch vehicle interface station. Test inputs to the spacecraft are adjusted at various frequency bands to enable the achievement of flight-anticipated load factors and internal loads. Such an approach overcomes the previously cited limitations of both the current force-notched test approach<sup>(1)</sup> and the method of Clevenston et al<sup>(2)</sup> (and is a direct and major evolution from both approaches). This test approach advocates one major change in spacecraft environmental test stipulations--that test levels be tailored to the vibration characteristics of one specific spacecraft. Current practice specifies one test level for all spacecraft employing a specific booster<sup>(1)</sup>. The concepts presented herein are based on the actual behavior of spacecraft systems as complex, multidegree-of-freedom structures. As such, these concepts permit a more realistic and representative simulation of flight-anticipated loads than do current techniques.

The conventional sinusoidal vibration test at low sweep rates (e. g., 4 octaves/minute) has been employed as the test technique for several reasons. This traditional method, employed on virtually all programs, uses existing test equipment; as such, it is readily implemented. This would allow for amenable transitions to the test approach advocated herein on existing and future spacecraft programs.

In developing this approach, attention was concentrated on providing satisfactory answers for questions regarding:

- a. How vibration test levels are explicitly derived for a new vehicular configuration early in the program.
- b. How sensitive these vibration levels are to subsequent design changes and variations in subsystems stiffness and mass content (and also, possible errors in dynamic analyses).



- c. How damping variations can be taken into account, and what procedures should be employed for their inclusion into specifications.

Answers are best provided through illustrative analyses involving a typical proposed spacecraft.

#### ILLUSTRATIVE EXAMPLE

##### Spacecraft System

To illustrate the validity and applicability of this approach, a proposed interplanetary spacecraft design (Figure 2) has been subjected to dynamic test simulation analyses. This proposed 20,000-pound spacecraft system features a 5000-pound capsule/lander (for planetary entry), 11,500 pounds of liquid propulsion tankage, the LEMDE engine, an electronics module, a 10-foot diameter antenna and a planet scan platform. Proposed to be launched by a Saturn V, its "over-the-nose" separation requirements dictate the placement of its separation plane in close proximity to the system center of gravity.

This proposed spacecraft will be subjected to a lateral sinusoidal vibration test, the levels of which we will first seek to establish. At one time or another during this test, the system, its subsystems and equipments must be exposed to the following flight limit loads: (a) 2g for major mass items (e.g., capsule, tanks) and primary structure; (b) 10g for equipment and secondary structure (e.g., LEMDE electronics) and (c) a peak bending moment of 778,000 inch-pounds at its separation plane. In addition to these flight-expected loads, a minimum allowable spacecraft frequency criterion of 7 Hz is imposed.

In conjunction with these Saturn V flight-expected loads, an adequately detailed set of spacecraft vibration characteristics were used to establish lateral test requirements. This data was determined by analytical procedures already demonstrated to be capable of highly accurate predictions<sup>(3)</sup>. Full particulars are given in the Appendix, with regard to the synthesis of these vibration characteristics. Vibration transmissibility spectra were obtained from these mode shapes for this vehicle, clamped to the test fixture at its spacecraft separation plane, and subjected to lateral stimuli at that locus. A modal damping ratio of 5 percent of the critical value was assumed.

With both the response requirements and transmissibilities known, the test inputs at each frequency were established on the basis of a "best data fit." The following lateral test spectrum was obtained;

Frequency Band (cps)	Test Level (g; 0 to peak)
1 - 10	+0.18
10 - 25	+0.50
25 - 100	+0.75

The analytical results summarized in Table 1 show how well this test spectrum enables the test objectives to be met. It also indicates the frequencies where each maximum test-induced loading was achieved. It is noted that the peak separation plane bending moment, and maximum tank assembly load factor, occur at the principal vehicle resonance (8.5 Hz). The peak LEMDE engine loadings are experienced at 10.5 Hz, and the maximum capsule/lander load factors occurs at 20 Hz. The electronics and the planet scan platform peak loads take place at still another resonance (31.5 Hz). Response-frequency spectra for these items are also given herein for the separation plane bending moment (Figure 3), capsule/lander (Figure 4), tank assembly capsule/lander (Figure 4), tank assembly (Figure 5), electronics (Figure 6) and LEMDE motor case (Figure 7).

Table 1 and Figures 3 to 7 are felt to clearly demonstrate how well test objectives can be attained by employing test levels tailored to the requirements of a specific spacecraft.

The upper test limit has been established conservatively at 100 Hz. This is based on the presence of a significant range of low transmissibilities extending above 60 Hz. Similar low transmissibility ranges separating principal structural resonances from higher frequency phenomena have been likewise observed (both analytically and experimentally) in other spacecraft configurations<sup>(3)</sup>.

##### Parametric Analyses

Parametric dynamic test analyses were performed on this spacecraft to assess the sensitivity of the previously derived test levels, to possible or anticipated changes in spacecraft design. Stiffness/frequency characteristics were parametrically varied on three items considered most susceptible to such variations (capsule/lander, tank support structure, and LEMDE attachment plane support structure). Full particulars regarding these variations are given in the Appendix.

The peak test-induced responses experienced by various items on the spacecraft are given in Figure 8, as functions of the lander lateral frequency. Similar data is given in Figures 9 and 10, reflecting

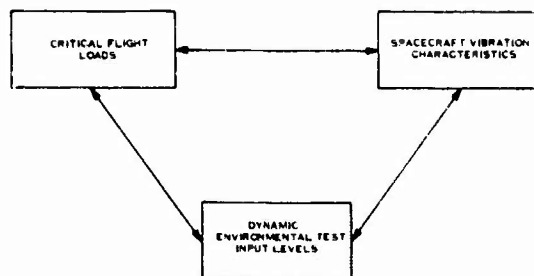


Fig. 1 - Design-test triangle

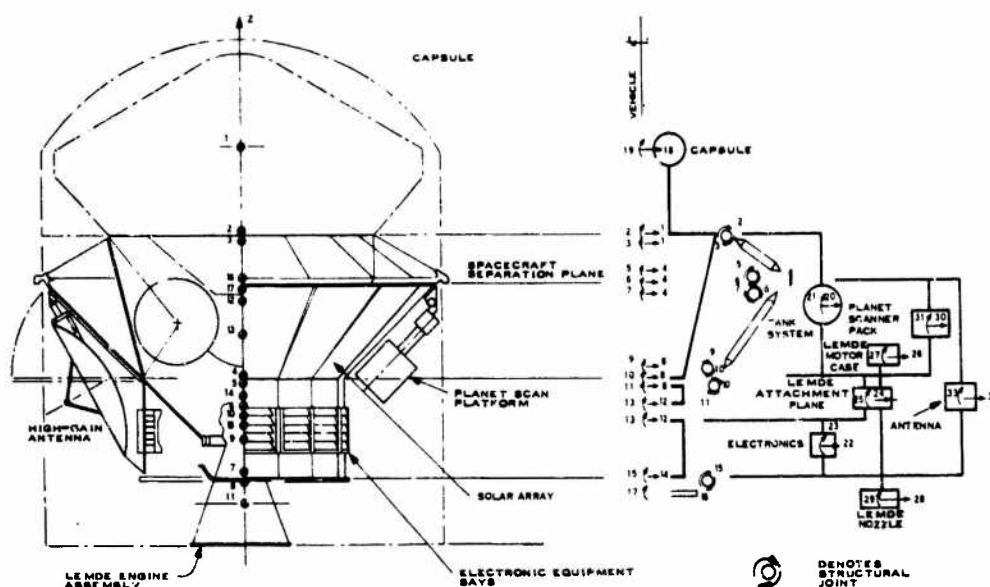


Fig. 2 - Analytical model of proposed interplanetary spacecraft

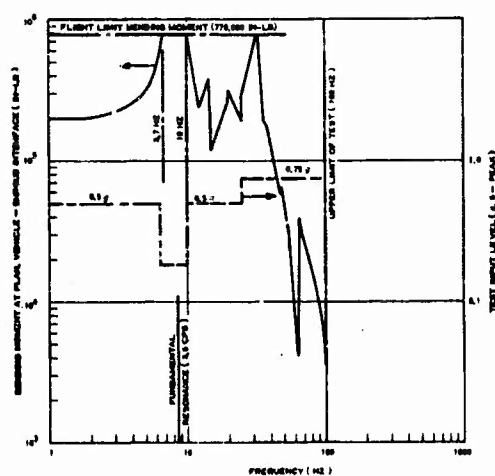


Fig. 3 - Bending moment at spacecraft separation plane during lateral test of baseline design

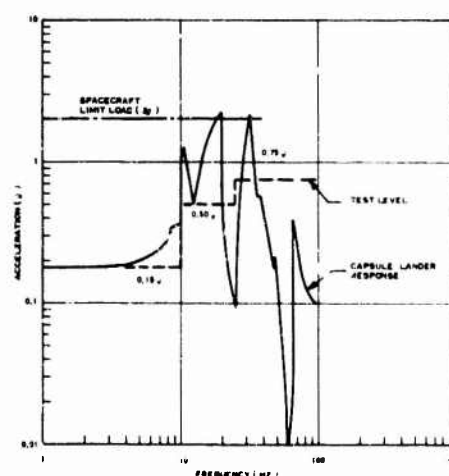


Fig. 4 - Capsule/lander response during lateral test of baseline design

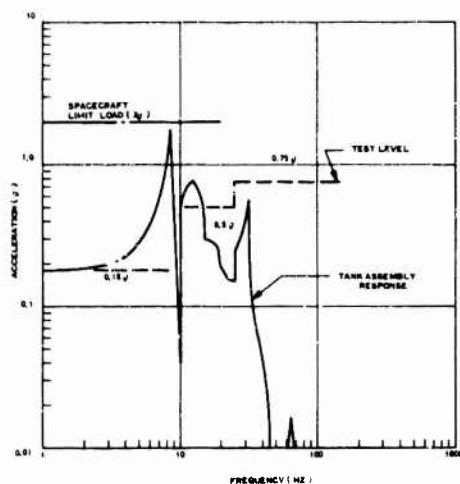


Fig. 5 - Tank assembly response during lateral test of baseline design

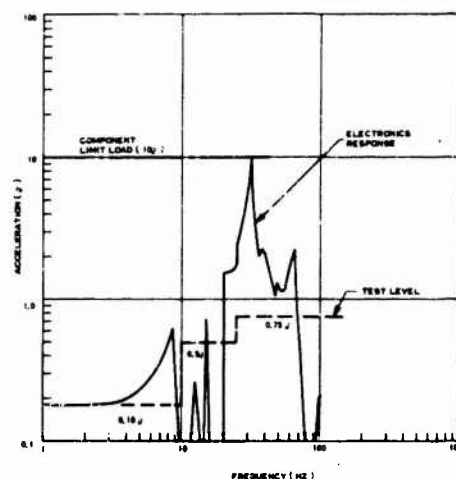


Fig. 6 - Electronics response during lateral test of baseline design

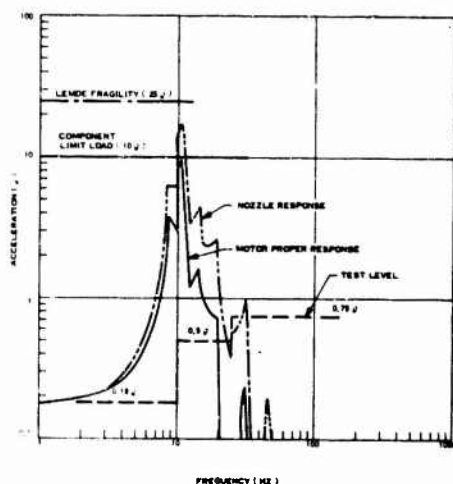


Fig. 7 - LEMDE motor response during lateral test of baseline design

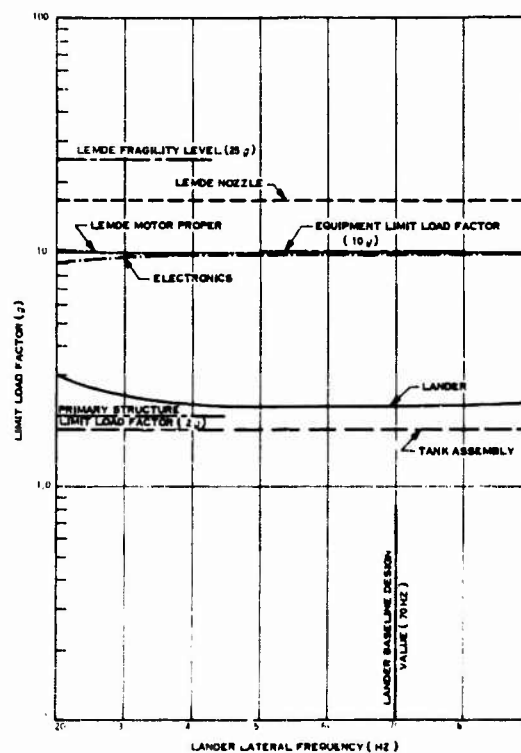


Fig. 8 - Variation of test-induced maximum lateral load factors with lander lateral frequency

TABLE 1  
Results of Analytical Simulation of Lateral Vibration Test

Location	Flight Limit Load	Test Simulation Results	
		Maximum Test Load	Frequency Where Achieved During Test
Capsule/Lander	2 g	2.2 g	20.0 Hz
Tank Assembly	2 g	1.8 g	8.5 Hz**
Electronics	10 g	9.8 g	31.5 Hz
LEMDE Engine Case*	10 g	10.0 g	10.5 Hz
LEMDE Engine Nozzle*	10 g	17.0 g	10.5 Hz
Planet Scan Platform	10 g	11.4 g	31.5 Hz
Bending Moment at Spacecraft Separation Plane	778,000 in.-lb.	778,000 in.-lb	8.5 Hz**

\*LEMDE engine fragility level is 25g (as per data furnished by its manufacturer)

\*\*Principal lateral resonance

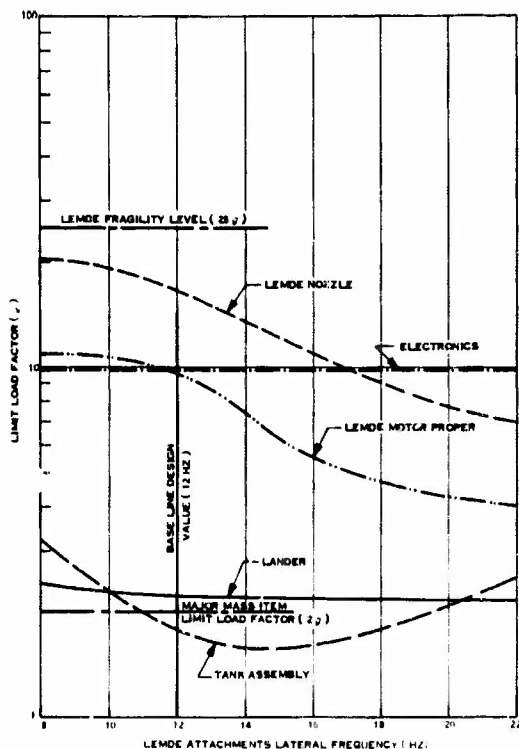


Fig. 9 - Variation of test-induced maximum lateral load factors with LEMDE attachments lateral frequency

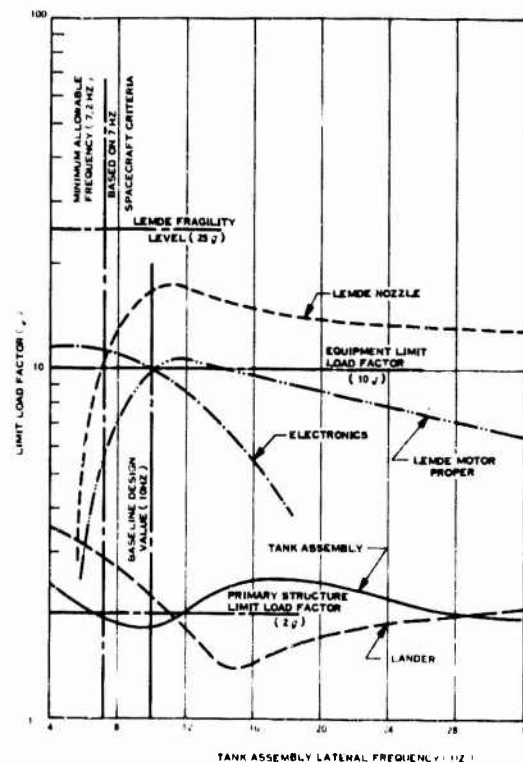


Fig. 10 - Variation of test-induced maximum lateral load factors with tank assembly lateral frequency

variations in the frequencies of the LEMDE attachments (support structure) and tank assembly support structure, respectively.

As evidenced by Figure 8, extreme variations in capsule/lander frequency produce no appreciable loading variations. In contrast (Figure 9), variations in LEMDE engine attachment frequencies produce significant reductions in LEMDE loadings (above 12 Hz) and increases in tank assembly loads at LEMDE frequencies less than 11 Hz. (Above 11 Hz, changes in the LEMDE attachment frequencies cause no appreciable variations in tank loads, until an 18 Hz frequency is attained. The probability of attaining 18 cps with this spacecraft configuration is remote, however, by virtue of the associated weight penalty.) Hence, adequate simulation of the flight-induced stresses can indeed be maintained by LEMDE attachments at or slightly above the recommended minimum frequency of 12 Hz.

Varia tions in tank assembly lateral frequency create significant variations in loadings throughout the vehicle (Figure 10). This might well be expected, since this assembly contains more than half of the planetary vehicle weight. Relatively stabilized peak loadings (within +25%) are attained for tank assembly frequencies at or in excess of 10 cps. (A slightly lower tank assembly frequency value, 7.2 Hz, would create a lateral frequency below the minimum allowable planetary vehicle value. The weight penalties associated with tank assemblies having frequencies much above the recommended 10 Hz minimum value would preclude the emergence of such an occurrence in practice. Thus, significant variations in the peak responses induced by the previously established test levels take place only when the design exhibits excessive and inefficient expenditures of structural weight within its subsystems. It may therefore be taken that the test environments postulated at the inception of a program will remain invariant, provided: (a) the basic vehicle configuration remains unchanged, and (b) the design does not become unwieldy (i. e., significant over-design of subsystems). In cases where the latter condition is manifest, the design of the subsystem in question and possibly the total vehicle, would become subject to extensive review. In such an event, the need to revise test levels would manifest itself as one possible symptom of the existence of an unwieldy design.

#### DAMPING CONSIDERATIONS

The validity of the damping ratios involved in establishing test levels are questionable, when confronted with a completely new and different vehicular configuration, i. e., one with no generic predecessors. Still, this should not prove to be an insurmountable problem.

To circumvent this problem, the damping factor ( $\zeta$ ) originally employed to establish these test levels should be identified. The test specifications would likewise state that these levels (A) would be scaled up or down, according to the relationship:

$$\frac{[A(f)] \text{ Test Actuals}}{[A(f)] \text{ Predicted Levels}} = \frac{(\zeta) \text{ Used in Predictions}}{(\zeta) \text{ Measured in Test}}$$

This scaling would, of course, be done subject to controlling agency review and approval.

The test values of damping input levels would be established on the basis of low-level sweeps involving spacecraft test models employing a flight-quality structure subsystem. In conjunction with this, a peak selection network would be employed for these low-level sweeps to preclude over-testing. (Selected spacecraft-mounted strain gages and accelerometers with preset peak settings are used within this peak selection network to accomplish this.)

#### CONCLUSIONS

A test approach has been derived that is capable of imparting body forces to a test article that effectively duplicate loadings expected in flight. This encompasses not only internal loads on primary structure, but also load factors for major mass items, equipment, and secondary structure. This procedure, evolved from existing test methods, employs existing test equipment. The test levels, established at the inception of a program, will remain invariant, barring major redesigns. This approach represents a deviation from present practice, in that it advocates the tailoring of the test environments to the specific spacecraft.

#### APPENDIX ANALYSES INVOLVING ILLUSTRATIVE EXAMPLE

##### IDEALIZED MASS STATIONS

The proposed interplanetary spacecraft has been idealized by a 17 (lumped) mass station physical model. These mass stations are defined in Figure 2 and in Table 2 together with the inertial and geometrical descriptions of these mass stations. Eight (stations 2 to 7, 16, 17) represent structural stations, and three (stations 9 to 11) represent the LEMDE engine. The other six stations each represent the lander center of gravity (station 1), tank module (station 12), bay electronics (station 15), high-gain antenna (station 14), planet scan platform (station 13) and aft-solar panel (station 8).

To facilitate analyses, the mass properties of non-primary structural components were idealized as being constituents of (i. e., lumped into) equivalent toroidal masses. This was accomplished by defining

individual units in terms of their location on the spacecraft proper, i.e., the component mass properties were allocated to various mass stations such as the lander, tank assembly, bay electronics, high-gain antenna or planet scan platform.

This analyses assumed that there was no lateral-longitudinal-torsional vibration coupling, i.e., that the axis of shear centers coincided with the vehicular centerline throughout, and that likewise, the mass of the vehicle at any planetary vehicle station had its center of gravity on the vehicular centerline. Consequently, separate analytical models were established for the lateral and longitudinal vibration cases; only the former will be discussed herein.

#### GENERALIZED COORDINATES

Thirty-three (33) lateral coordinates of motion (degrees of freedom) were selected. These include both translational and rotational motions, and incorporate the effects of rotational discontinuities across the structural joints. These are described in Table 3 and illustrated in Figure 2.

#### STRUCTURAL STIFFNESS

The elasticity of the primary vehicular structure was taken into account in a gross sense. This structural idealization is illustrated schematically together with appropriate coordinates of motion in Figure 2 for the lateral case. In synthesizing these stiffness distributions, the analytical modeling techniques employed are those described in References 3 and 5 for systems without inherent dynamical interactions between principal structural resonances (i.e., "body bending" modes) and other structural resonances (i.e., breathing modes or truss element modes). This idealization, in assuming effective rigid rings at the extremities of the individual structural elements, is consistent with the centerline coordinate system described in Figure 2.

Essentially, the basic structure can be described as consisting of a truss/adaptor module connected in series to the electronics module (thrust tube) at mass station 5. The adaptor module consists of a conical "w" space truss assembly and semimonocoque shell inter-connected in series (at their largest radii) at mass station 17, the separation plane. The other extremities of this assembly are connected in parallel to an inverted semimonocoque conical shell, at mass stations 2 and 4. The thrust tube is a semimonocoque shell onto the aft-end of which, a shell (a circular honeycomb plate mounting additional solar cells) is attached. The other extremity of this shell is described by mass station 7. Stiffness distributions for each structural element in this module were described implicitly, i.e., in terms of their physical and geometrical properties.

The effects of the structural joints at mass stations 3, 4, 5, 7, 16 and 17 have been taken into account using techniques described by Alley and Ledbetter (Reference 6).

The LEMDE engine nozzle and thrust chamber were idealized as equivalent toroidal masses each cantilevered off the LEMDE attachment plane, also a toroidal mass. Stiffness coefficients for these idealized springs were established from the propulsion manufacturer-furnished motor mass properties and motor-proper vibration characteristics. The frequencies of the motor nozzle, thrust chamber, and attachments are 70 Hz, 70 Hz and 12 Hz, respectively.

The LEMDE engine toroidal mass idealization is cantilevered from the tank support module (mass station 12) by the engine support structure. This tank module was also treated as an equivalent toroidal mass attached to the primary structure at mass stations 3 and 4. The 10 Hz translational and 15 Hz rotational frequencies representing the tank support module vibration characteristics were based on separate dynamic analyses of the tank support structure (attached to a "rigidized" vehicle)<sup>(7)</sup>.

Similar representations were employed for the (70 Hz) capsule/lander, the electronics (60 Hz), high-gain antenna (20 Hz), and planet scan platform (35 Hz). While the capsule/lander frequency was assumed, the other values cited herein were based on separate dynamic analyses of the individual items<sup>(7)</sup>.

#### DYNAMIC ANALYSIS

The analytical model was used to establish spacecraft dynamic characteristics and test simulations with the aid of standard GE digital computer routines. For these investigations, the analytical model was taken as clamped at its launch vehicle (shroud) attachment plane, i.e., spacecraft separation plane in Figure 2.

The nominal  $\pm 1g$  lateral sinusoidal excitation was provided to the system throughout the 0 to 100 Hz frequency spectrum. A nominal value of 5 percent (of critical) modal damping was assumed.

#### PARAMETRIC ANALYSES

Employing the spacecraft system described above as the base line, parametric dynamic test simulation analyses were undertaken. These computer-aided investigations involved altering the stiffness/frequency characteristics of individual items in the spacecraft, to assess the effects of these changes on system test results. The matrix of cases (computer runs) involved in this parametric analysis is summarized by Table 4.

TABLE 2  
Analytical Model Mass Station Description

Mass Station	Description	Weight (lb.)	Location (in.)
1	Capsule/lander cg	5000	-50.00
2	Capsule-bus separation plane	165	0
3	Conical shell-forward support truss interface	165	0
4	Conical shell-aft support truss interface	389	75.00
5	Conical shell-thrust tube interface	389	75.00
6	Thrust tube	85	84.00
7	Thrust tube-shell interface	136	87.50
8	Aft solar panel	136	87.50
9	Motor attachment plane	207	79.50
10	Motor case cg	207	66.00
11	Motor nozzle cg	104	122.50
12	Tank module	11500	37.50
13	Planetary scanner	162	47.50
14	High gain antenna	81	68.75
15	Electronics module	790	100.75
16	Forward support truss-separation plane interface	172	20.00
17	Aft support truss-separation plane interface	172	20.00

TABLE 3  
Lateral Analytic Model Coordinate Description

Mass Station	Coordinate Numbers (Degrees of Freedom)			
	Lateral Translation (x, y)	At Mass Station	Lateral Rotation (x, y)	Forward of Station
1	18	19		
2	1	2		
3	1		2	1
4	8		9	10
5	8		10	11
6	12	13		
7	14		15	16
8	14	17		
9	24	25		
10	26	27		
11	28	29		
12	20	21		
13	30	31		
14	32	33		
15	22	23		
16	1		5	6
17	4		6	7

TABLE 4  
Scope of Parametric Dynamic Analysis

Item	Case/Computer Run Designation			
	Frequency (Hz) of Item in Baseline Design	Frequency Variations in Parametric Study		
		Lander Frequency Variations (Hz)	Tank System Frequency Variations (Hz)	LEMDE Attachments Plane Frequency Variations (Hz)
Lander	70	20; 40; 60; 80	70	70
Tank System	10/15*	10/15	6/10; 10/15; 14/19; 18/23; 20/25; 25/30; 30/35; 35/40	10/15
LEMDE Attach Plane	12	12	12	9, 15, 20
LEMDE Motor Case	70	70	70	70
LEMDE Nozzle	70	70	70	70
Electronics	60/75	60/75	60/75	60/75
Planet Scanner	35/40	35/40	35/40	35/40
High Gain Antenna	20/25	20/25	20/25	20/25

\*X/Y Designates: X Hz Translational Resonance, Y Hz Rotational Resonance

# REFERENCES

1. NASA/GSFC Document S-320-D-2, "General Environmental Test Specification for Spacecraft and Components Using Launch Environments Dictated by Improved Delta Launch Vehicle (DSV-3E, 3F, 3G and 3H), " 1 June 1965.
2. Clevenson, S.A., Martin, D.J., and Pearson, J., "Representation of Transient Sinusoids in the Environmental Vibration Test for Spacecraft," presented at 11th Annual Technical Meeting of the Institute of Environmental Sciences, Chicago, Illinois, April 21-23, 1965.
3. Kaplan, S.M., and Terkun, V., "Dynamic Analysis of the ATS-B Spacecraft," Shock and Vibration Bulletin, No. 36, Part 7, pp. 41-62, 1967.
4. Baruch, M.J., and Davis, S., "Implications of Spacecraft Vibration Qualification Testing Requirements on Structural Design," Shock and Vibration Bulletin, No. 35, Part 2, pp. 203-220, 1966.
5. Kaplan, S.M., "Analytical Modeling Techniques for Spacecraft Structural Dynamic Analysis," General Electric Technical Information Series, Document 67SD202, 1967.
6. Alley, V.L., Jr. and Ledbetter, S.A., "Prediction and Measurement of Natural Vibrations of Multistage Launch Vehicles," AIAA Journal, Vol. 1, No. 2, pp. 374-379, February 1963.
7. GE-MSD DIN Report 67SD4373, "Voyager Dynamic Analysis Report," September 1967.



## FLEXURE GLIDES FOR VIBRATION TESTING

Alexander Yorgiadis, Stanley Barrett  
North American Rockwell Corporation  
Downey, California

Vibration testing often involves components and fixtures which are relatively large and heavy compared with the moving assembly of the vibration exciter. In such cases the fixture should have external guides, both for reducing cross-axis vibrations and for protection of the exciter mechanism from damage.

Many types of guides are used for this purpose; namely, slip tables, hydrostatic bearings, roller guides, and various flexure devices. This paper is limited to the study of the flexure system known as the "parallel movement."

Flexure guides are described and their mechanical characteristics are expressed in terms of the significant dimensions and the material properties. Mathematical relationships are derived for the six natural frequencies of the vibration system consisting of a series of parallel flat-plate flexures, and a fixture-specimen assembly.

The paper develops the basic theory of flexure design and discusses the parameters which the designer must consider. Typical situations in which such flexure systems have been used are described. Formulas are presented for bending stresses, arc depth, and natural frequencies in terms of flexure plate dimensions, and properties of the fixture-specimen assembly. Design charts are provided to facilitate rapid selection of flexure dimensions for practical applications.

### INTRODUCTION

Commercial vibration exciters are built with internal guides which are designed to produce linear vibration of the moving coil assembly. The most common such guides are flexures of various types and designs, but linear bearings, rollers, and other guiding devices are also used. Small and light test items can usually be supported and guided by attaching these directly to the vibration table of the exciter.

With larger test items and associated vibration fixtures, the guiding capacity within the exciter becomes inadequate, particularly for tests covering typical wide frequency spectra from 5 Hz to 2000 Hz. The situation is aggravated when the specimen or the fixture are unsymmetrical relative to the axis of vibration. In such cases, it becomes necessary to provide external guides to keep the test item vibrating in the desired axis with a minimum of cross motion.

Several types of guides are available for this purpose, including slip tables, hydrostatic bearings with one or two degrees of freedom, roller guides, and various flexure devices. Each guide system has advantages, disadvantages and limitations, and the most suitable guide for a given situation depends upon the specific test requirements and test conditions. This study is limited to one type of flexure system, sometimes known as "parallel movement."

### FLEXURE DEVICES

The idea of supporting moving parts on thin strips of metal or other elastic material is by no means new. Flexures were used in commercial testing machines built as far back as 1897[1,2], possibly earlier. It was significant to the users that those elastic components were essentially free of hysteresis friction wear and lost motion which occur in other devices, hence had distinct advantages.

Analyses and design charts for flexure devices for various purposes have been published by Eastman[2] and Thorp[3], among others. Geary[4] prepared a comprehensive biographical survey on the subject, and discussed numerous flexure configurations, including the "parallel movement" flexure system which is of particular importance for vibration tests.

In principle, the ideal function of such flexure guides is to permit motion in one linear direction, while preventing all other linear and rotary motions. The actual system is constructed by attaching a set of parallel, thin flexures between a moving element, and a stable, stationary base. The flexures are oriented in a plane normal to the desired direction of motion. Displacement in the test direction is lightly restrained since such motion subjects the flexures to bending of the thin material. Design of the flexures requires that the bending strains be within the limits permissible for the selected flexure material to avoid fatigue failure during service. Displacements in any other direction or mode are severely restrained since such motions induce axial or shear strains in the flexure itself, which require considerably larger forces and moments than needed for the bending strains.

Application of flexures to vibration testing requires consideration of both usual flexure design problems as well as some new problems. The vibrating assembly together with the flexure guides constitute a spring-mass system which has many resonant frequencies in various modes. Some of these frequencies are likely to be within the test spectrum. Even though most of these resonant modes do not have components in the direction of excitation, the resulting responses can be quite severe because of the resonance amplification factor "Q" of the elastic flexures. The two commonly used approaches are: (1) to raise the natural frequencies of the flexure-fixture system by increasing flexure stiffnesses and/or reducing the mass of the fixture, since the damage-causing tendency of such extraneous resonances tends to diminish with increasing frequency; (2) to introduce additional damping in the flexure system, thus reducing the amplification "Q" and the cross-motion response.

Development of suitable flexure guide systems for vibration tests requires both analytical and experimental effort. In instances where frequencies of test are up to 2000 Hz, neither the vibration fixture nor the stable base can be considered as ideal masses, and it is difficult to define and analyze the mathematical model representing the total assembly. At frequencies below the "resonant" or "natural" frequencies of the system, the flexures will usually perform very effectively and when properly designed will give long trouble-free service without the need for maintenance. In some critical vibration test applications, flexures offer the best, if not the only practical, economical solution to fixture guiding.

## FLEXURES FOR PARALLEL MOVEMENT

A typical arrangement of parallel movement flexures in a vibration system is shown in Figure 1. The fixture-stamen assembly, represented as a rectangular lid, is driven horizontally by a vibratory exciter. A number of simple flat-plate flexures (six in this case) are attached between the fixture and a heavy reaction base below. The flexures are oriented normal to the direction of excitation and their width is comparable to that of the fixture. The intended action of the flexures is to absorb lateral forces and moments which are transmitted to the stable reaction mass through the flexures. The flexures restrict the freedom of motion of the fixture in all directions except the direction of excitation.

There are variations to this simple "parallel movement" flexure system. Instead of having flexibility for the entire length of the plate, flexing may be limited to the extremities by stiffening the intermediate part of the flexure. This design has advantages for high amplitude low frequency testing. Still another variation, useful in guiding assemblies of appreciable width, is to use flexure rods at the four corners or sides of the fixture, instead of full-width flat flexures. Further variations include flexures which are machined from heavy plate or forgings, leaving the thin plate with two heavy ends. These ends provide means for rigid mechanical connection, and minimize the clamping stresses, fretting, and problems associated with attachment of the flexures.

## ANALYSIS OF FLEXURE ELEMENT

During vibration tests, the action of each flexure element of Figure 1 is approximately as shown in Figure 2. The relationship between bending stress amplitude in the flexure and the displacement amplitude is as follows:

$$s_b = \frac{3Ehx_o}{L^2} \quad (1)$$

where  $s_b$  = Maximum bending stress (psi) of flexure at the section near the clamped end. (Should not cause fatigue failure.)

$E$  = Modulus of elasticity of the flexure material in direct stress, psi

$h$  = Uniform thickness of the flexure, inches

$L$  = Unsupported length, inches, and

$x_o$  = Amplitude of vibration, inches.

Equation (1) assumes that the material is stressed only in the elastic range, that the amplitude  $x_o$  is small relative to the length  $L$ , and that the fixture vibrates in a straight

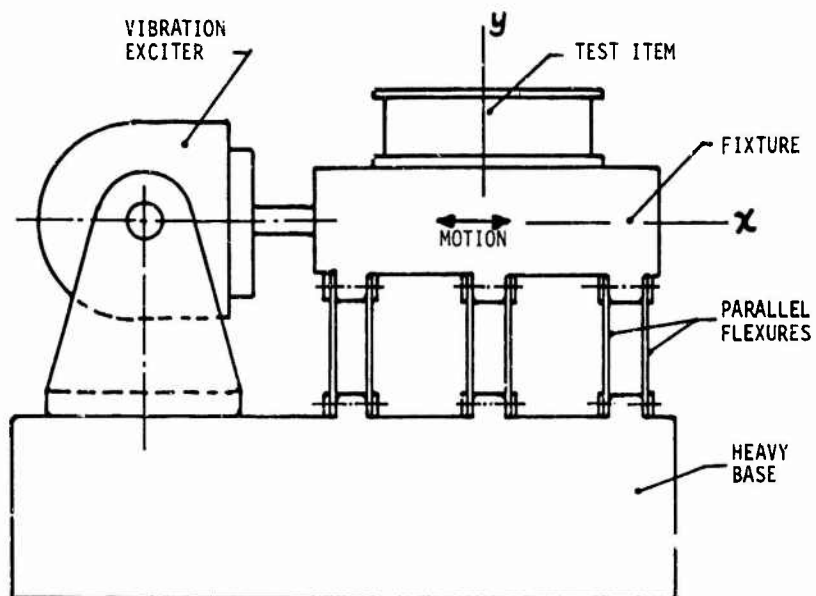


Fig. 1 - Flexure guided vibration test system

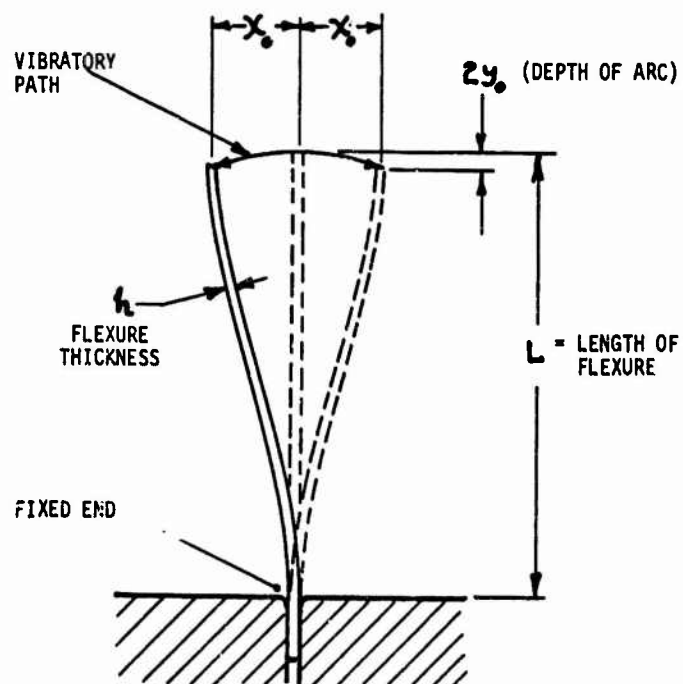


Fig. 2 - Actual motion of flexure element

line without rotation, so that the slopes of the two ends of the flexure remain parallel. A further assumption is that the inertia effects of the vibrating flexures contribute negligibly to the maximum bending stress. This is valid insofar as the large displacements and stresses are only applied at the lower frequencies.

An ideal flexure guide should:

- (1) Permit motion in only one direction (x axis), with minimum of resistance.
- (2) Offer infinite resistance to all other motions.

None of these idealized conditions is satisfied by practical designs, primarily because of the inherent material characteristics and the geometry of plate deformation.

One reason for deviation from idealized condition (1) above is that the actual vibratory path of the upper end of a flexure of finite length is along a shallow arc rather than a straight line, as shown in Figure 2. If the length of the flexures remains unchanged during the vibration cycle, then, when the x-motion is defined by

$$x = x_0 \cos \omega t \quad (2)$$

there is a y-component of motion, expressed by:

$$y \approx \frac{x_0^2}{3L} [1 + \cos 2\omega t] \quad (3)$$

and the ratio of these two amplitudes is:

$$\frac{y_0}{x_0} = \frac{x_0}{3L} \quad (4)$$

Given a required test amplitude  $x_0$ , the only means of reducing  $y_0$  is by increasing the length  $L$ . For practical reasons,  $L$  cannot be increased indefinitely. When cross-amplitude of motion  $y_0$  is limited to one percent of motion  $x_0$ , the ratio  $L/x_0$  becomes 33.3. Such cross-motion should be tolerated in most instances. It should be added, however, that the frequency of motion  $y$  is twice that of  $x$ , as can be seen from Equations (2) and (3). Thus, the acceleration ratio in the two directions becomes:

$$\frac{(\ddot{y})_0}{(\ddot{x})_0} = \frac{4 x_0}{3L} = \frac{4 y_0}{x_0} \quad (5)$$

and if the displacement ratio  $y_0/x_0$  is one percent, the acceleration ratio becomes four percent.

Cross-motion  $y_0$  is aggravated if the flexure is improperly aligned initially so that it deflects unequally relative to its unstressed

position. In cases where motion of the flexure is entirely in one direction, i.e.,  $x = x_0(1 - \cos \omega t)$ , then the excursion  $y_0$  is four times as high as that expressed in Equation (4). It should be added that the above y-axis excitation analysis was based on the assumption that the length of the flexure remains unchanged during a vibratory cycle. This, however, only applies when the fluctuating axial stresses in the flexure are negligible. Because of the acceleration component of the fixture in the y-direction, axial vibratory forces are indeed applied to the flexure, which will therefore be elongated. Without resonance amplification, such deformations are usually negligible.

#### SELF EXCITATION OF FLEXURES

Another reason for deviation from perfectly linear motion is that the supported flexure section may be excited into the various fixed beam modes, as shown in Figure 3. The frequencies for the first three of these modes are as follows:

$$\text{The fundamental mode } f_1 = 1.025 \frac{ah}{L^2} \quad (6)$$

$$\text{The second mode } f_2 = 3.03 f_1 \quad (7)$$

$$\text{The third mode } f_3 = 5.40 f_1 \quad (8)$$

where  $a = \sqrt{\frac{E}{\gamma}}$ , velocity of sound in material of flexure,

and  $\gamma$  = mass-density of material. For steels, aluminum, magnesium, "a" is very nearly 200,000 inches/second.

In order to minimize these extraneous motions, damped coatings have been applied over the thin part of the flexures.

#### MULTI-FLEXURE SYSTEMS - NATURAL FREQUENCIES

Consider a vibrating system such as shown in Figure 4. The fixture-specimen "moving assembly" is supported by a set of flat, parallel flexures, held in turn by a heavy base. The fixture is subjected to vibration in the x-direction by an exciter and a drive rod, as shown in Figure 1.

The mathematical model of this study is based on several simplifying assumptions, of which the following are most significant:

- (1)  $W$ , representing the weight of the fixture and the specimen, is a perfect mass, infinitely rigid.
- (2) The vibration exciter applies vibratory forces to the specimen along one direction only, namely, the x-axis, but otherwise exerts no restraints or forces on the fixture.

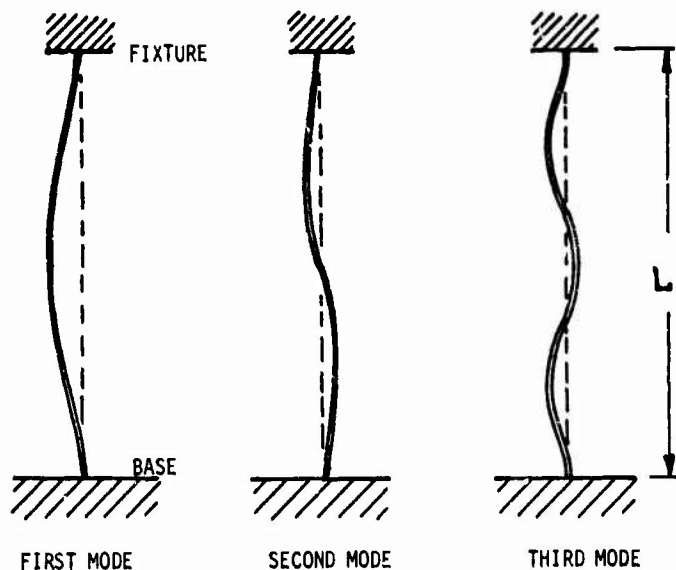


Fig. 3 - Self-excited bending modes of flexures

- (3) The fixed ends of the flexures are rigidly held to an infinitely heavy base, and therefore are totally motionless.

The following nomenclature has been used in the analysis:

- x - direction of vibratory excitation
- y - "cross-axis" direction, along axis of flexures
- z - "cross-axis" direction at right angles to flexure axis
- n - number of flexures (six in example of Figure 4)
- L - free length (span) of flexures
- b - width of flexures
- h - thickness of flexures, usually uniform
- E - modulus of elasticity of flexure material (axial)
- G - shear modulus of elasticity of flexure material

- $\mu$  - Poisson's ratio for flexure material
- $K_x, f_x$  - linear spring constant of flexure system in the x-direction, and natural frequency of vibration of fixture-flexure mechanical system in x-direction
- $K_y \text{ \& } f_y$  - similar symbols for the y-direction
- $K_z \text{ \& } f_z$  - similar symbols for the z-direction
- $I_{xx}, I_{yy}, I_{zz}$  - mass moment of inertia of fixture assembly about axes indicated by subscripts
- $\rho$  - distance between axes x and  $x_1$  (see Figure 5)
- $R_r, R_{xz} \text{ \& } R_{xy}$  - radii of gyration of fixture assembly
- $f_r, f_{xz} \text{ \& } f_{xy}$  - angular natural frequencies of vibration in "roll" mode, "yaw" mode and "pitch" mode, respectively

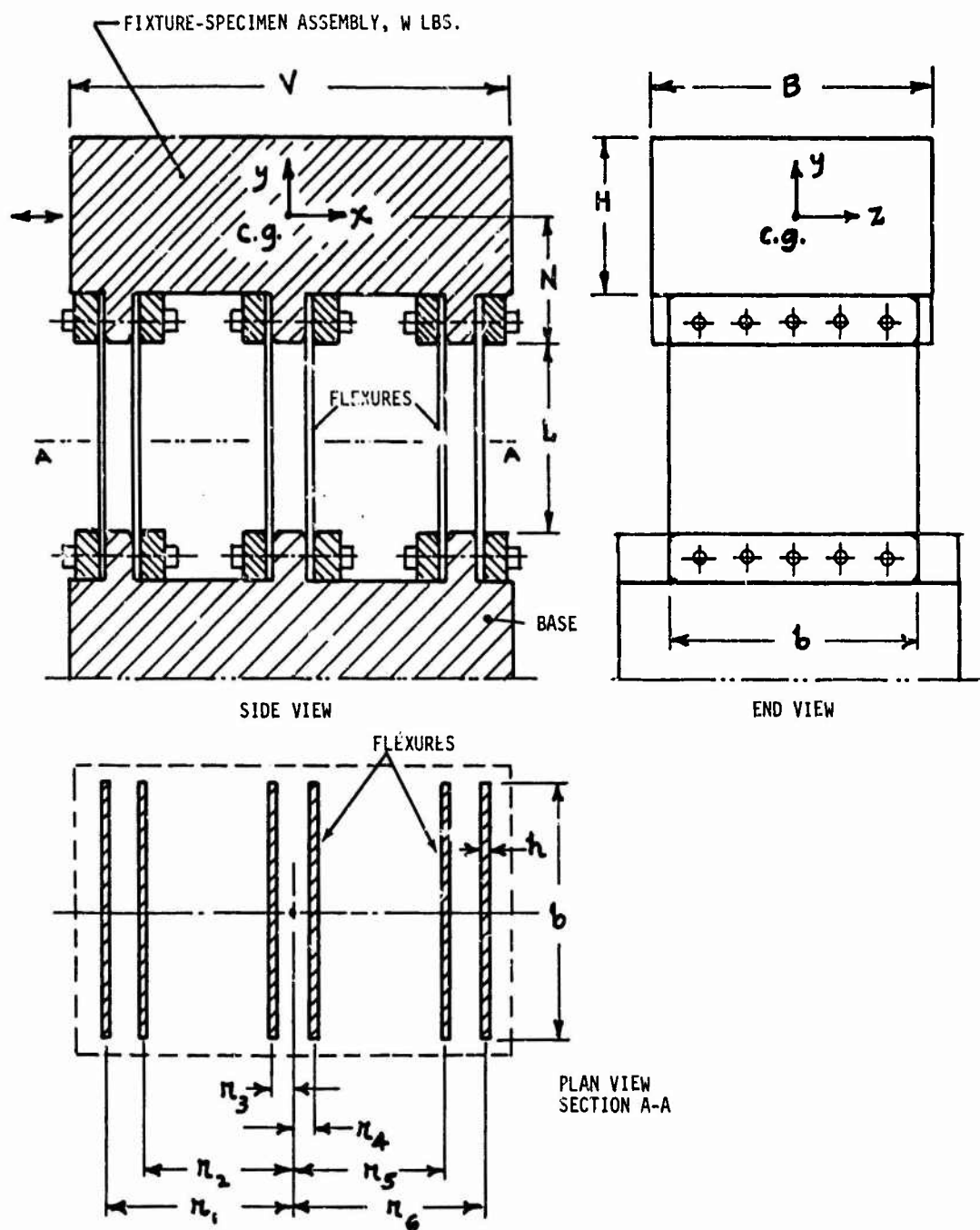


Fig. 4 - Configuration of a parallel motion flexure guide system

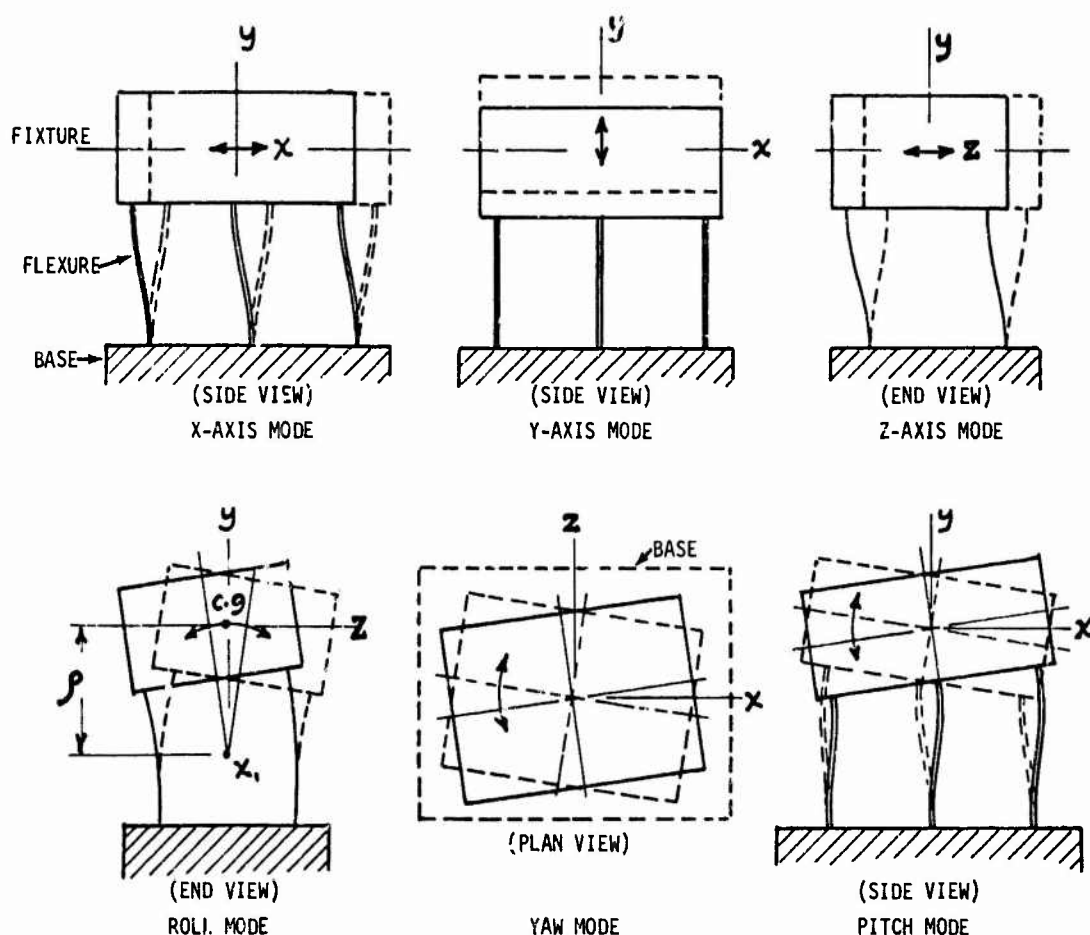


FIG. 5 - Modes of linear and angular motion

$r_1, r_2, \dots, r_n$  - distance between elastic center of flexure system and each individual flexure as indicated by subscripts 1, 2, to n.

$N$  - distance along the y-axis, between center of gravity of mass  $W$  and the upper end of the flexures

$$\beta = 1 + 3\left(\frac{N}{L}\right) + 3\left(\frac{N}{L}\right)^2 \quad (9)$$

$$\bar{r} = \sqrt{\frac{1}{n} (r_1^2 + r_2^2 + \dots + r_n^2)} \quad (10)$$

Elementary single-degree-of-freedom analyses

were conducted on the vibratory system and the results are presented in tabular form. Table I lists equations for calculating the linear spring constants and the linear natural frequencies of the system. Equations for determination of angular motion characteristics appear in Table II. The six modes of motion that were analyzed are illustrated in Figure 5.

The x-axis linear data refer to properties of the system in the direction of the excitation. The significant parameter in this case is the spring constant  $k_x$ , since this, with amplitude  $x_0$ , determine the elastic restraining force exerted by the flexures at low frequencies. This must be overcome by the exciter, and is an added force. As the frequency is raised, the natural frequency  $f_x$  is reached,

TABLE I  
Linear Motion Characteristics of Flexure-Guided Test Assembly

DIRECTION OF MOTION	FLEXURE SYSTEM SPRING CONSTANT, LB/IN	NATURAL FREQUENCY Hz
X-AXIS	$K_x = nE \left(\frac{h}{L}\right)^3 b$	$f_x = 3.13 \sqrt{\frac{K_x}{W}}$
Y-AXIS	$K_y = nE \left(\frac{h}{L}\right) b$	$f_y = 3.13 \sqrt{\frac{K_y}{W}}$
Z-AXIS	$K_z = \frac{nG \left(\frac{h}{L}\right) b}{1 + \frac{I}{2(1+\mu)} \left(\frac{L}{b}\right)^2}$	$f_z = 3.13 \sqrt{\frac{K_z}{W}}$

TABLE II  
Angular Motion Characteristics of Flexure-Guided Test Assembly

AXIS OF ANGULAR MOTION	MASS MOMENT OF INERTIA	RADIUS OF GYRATION OF MASS	NATURAL FREQUENCY Hz
X <sub>I</sub> -AXIS "ROLL MODE"	$I_{xr}$	$R_r = \sqrt{\frac{I_x + W\rho^2}{W}}$	$f_r = \frac{\rho}{R_r} \cdot f_y \cdot \frac{I}{\sqrt{2(1+\mu) + 48 \left(\frac{L}{b}\right)^2}}$
Y-AXIS "YAW MODE"	$I_y$	$R_{xz} = \sqrt{\frac{I_y}{W}}$	$f_{xz} = \frac{\bar{r}}{R_{xz}} \cdot f_z$
Z-AXIS "PITCH MODE"	$I_z$	$R_{xy} = \sqrt{\frac{I_z}{W}}$	$f_{xy} = \frac{\bar{r}}{R_{xy}} \cdot f_y$



the inertia forces  $W\ddot{x}$  cancel this elastic restraint. At still higher frequencies, x-axis linear properties are of no concern.

The other five modes in Tables I and II represent "cross-motion" and other parasitic modes, in directions other than needed or required for the typical vibration test, which specifies only one direction of motion. Even though the vibration exciter applies excitation forces along one direction only (the x-axis), significant amplitudes can be excited in these undesirable modes when the exciting frequency corresponds to these natural frequencies. This is because of the resonance amplification of the lightly damped metal flexures which constitute the elastic spring of the vibratory system.

The safest way of avoiding these problem areas is to design flexures that result in system natural frequencies that are higher than the frequency spectrum of the test. If this is not possible, it is still desirable to raise these frequencies as high as possible by design, since cross-motions induce less severe structural stresses at the higher frequencies than at lower frequencies.

A brief review of the equations in Tables I and II indicates that high natural frequency is obtained with short, wide and thick flexures. There are, however, other limiting considerations, in that the bending stresses of Equation (1) increase as  $h$  increases and  $L$  decreases. Also, cross-axis y-excitation is aggravated as  $L$  decreases, as shown in Equation (3). Thus, for any given situation, a compromise must be reached between these various requirements and characteristics so as to select the optimum flexure design.

Typical flexure guided assemblies are shown in photographs of Figures 6 and 7. These have performed well over a frequency range of 5 to 2000 Hz, under both sine and random excitation. Figure 6 shows a horizontally excited fixture, guided with six parallel flexures (three pairs), each pair being wrapped with adhesive rubber tape or damping tape so as to prevent build-up of the self-excited bending modes of the flexures as shown in Figure 3. The fixture of Figure 7 uses two pairs of similar flexures which guide the fixture vertically.

#### CONCLUDING REMARKS

The applications of parallel movement flexure guides to vibration testing have been reviewed, and the more important dynamic properties affecting their design discussed. It is not claimed that these provide the answers to all guidance problems, since the best type of guide system to be used in a test depends on the particular application. However, the inherent simplicity and economy of a flexure system makes it a logical candidate in many situations. Flexures are particularly

advantageous if a test must be conducted under conditions of temperature extremes, when lubricants needed for slip tables and hydrostatic bearings may encounter viscosity problems. Alignment difficulties which may be caused by thermal deformations under such conditions are also best solved by flexures.

#### REFERENCES

1. A. H. Emery, "Fulcrum for Scales," U. S. Patent 1,041,609 (1912)
2. Fred S. Eastman, "The Design of Flexure Pivots," Journal of the Aeronautical Sciences, Vol. 5, pp. 16-21, November 1937
3. Arthur G. Thorp, II, "Flexure Pivots-Design," Product Engineering Magazine, pp. 192-200, February 1953
4. P. J. Geary, "Flexure Devices," British Scientific Instrument Research Association, Research Report M.18, 44 pages, 1954

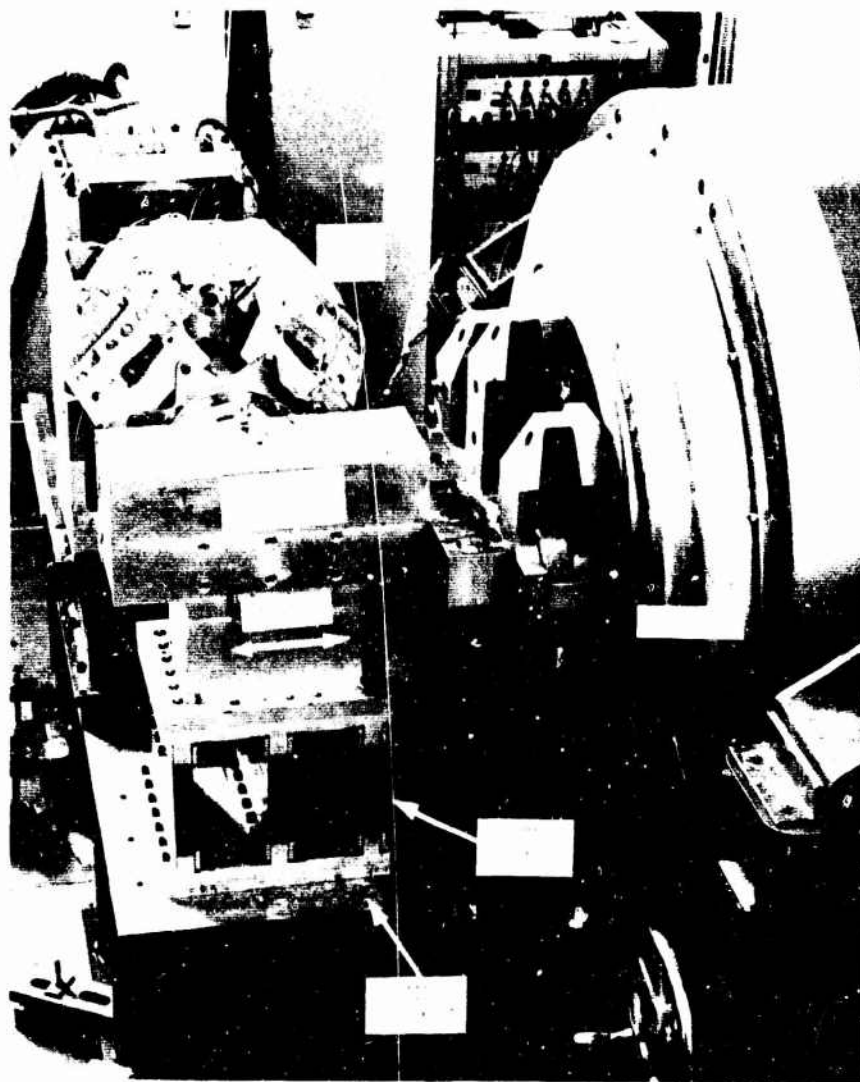


Fig. 6 - Fixture guided for horizontal vibration

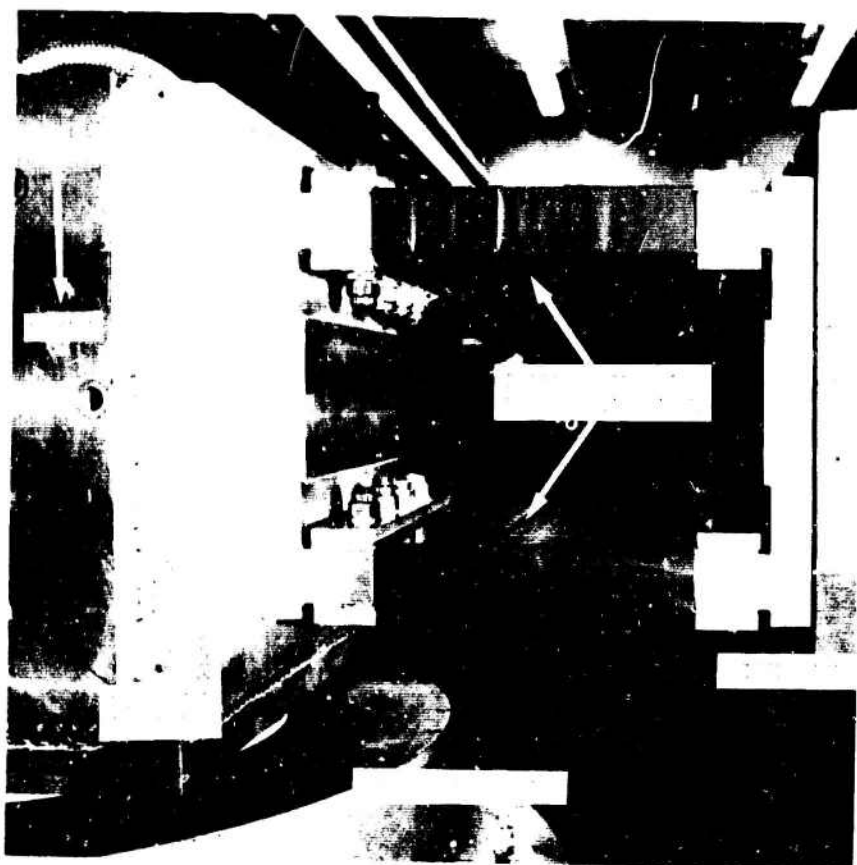


Fig. 7 - Vibration fixture guided to move vertically

## APPENDIX

### CHARTS FOR FLEXURE DESIGN

The various mathematical equations which have been compiled and tabulated will provide the necessary solutions to most flexure design problems. However, such work can be tedious in that several iterations may be necessary before arriving at an acceptable design. In order to facilitate selection of flexure parameters to suit particular requirements, five charts have been prepared and presented as Figures 8 through 12. These charts are based on the following properties of the flexure material:

- (1)  $E = 30 \times 10^6$  psi
- (2) Poisson's ratio = 0.3
- (3) Acoustic velocity  $a = 200,000$  inches/second
- (4) Allowable reversed bending stress = 20,000 psi. (This design stress takes into consideration the stress concentration at the clamped ends.)

Readily available plate materials which satisfy these requirements include:

- (1) Half-Hard stainless steel, Grade 302
- (2) Alloy Steel AISI 4140 or 4340 in heat-treated condition (140,000 psi minimum UTS)

The recommended procedure to use with the charts is given below:

1. The maximum vibration displacement amplitude,  $X_0$ , is given in the test specification. Using this value of  $X_0$ , Figure 8 can be used to tentatively define several combinations of  $h$  (flexure thickness) and  $L$  (length). Geometrical considerations may dictate  $L$ , and availability of material can restrict choice of  $h$ . Other limitations often exist, but Figure 8 can be used to select the most convenient values for  $h$  and  $L$ . Note that this figure includes a boundary corresponding to  $X_0/L = 0.03$ . Combinations of  $h$  and  $L$  falling to the left of this boundary are unsuitable, since they allow the vertical cross-talk motion of the supported specimen to exceed the recommended limit of 1% of  $X_0$  (see Figure 2).

2. Having selected  $h$  and  $L$ , the first three self-excited natural frequencies,  $f_1$ ,  $f_2$  and  $f_3$ , may be found from Figure 9. If these fall within the frequency range of the test, steps should be taken to increase the damping in the flexures, as discussed earlier in this paper.

3. The next step involves selection of the number of flexure elements,  $n$ , and their width,  $b$ . The product of  $n$  and  $b$ , namely the sum of the widths of all the flexures, is a measure of the strength and rigidity of the guide system. The number  $n$  often depends upon the beam stiffness of the fixture, and the number of places

the fixture must be supported to prevent severe fixture bending modes. For a system intended for higher test frequencies, the width,  $b$ , of the flexures should be roughly the same as that of the fixture, and if this is not the dominant consideration,  $b$  can be somewhat smaller.

4. Having selected  $h$ ,  $L$ ,  $n$  and  $b$ , Figure 10 can be used to determine system stiffness  $K_X$  by the intersection of abscissa value  $h/L$  with appropriate curve for the product  $nb$ . The maximum elastic force  $F_X = K_X X_0$  is now calculated. Since this force must be supplied by the shaker at low frequencies, it may be a limitation, and the value of  $nb$  may have to be reduced.

5. The chart of Figure 11 is helpful in obtaining natural frequencies  $f_X$  and  $f_Y$ . For this, the vibrating weight  $W$  of the fixture plus specimen must be known. The ratio  $K_X/W$  is used to enter the chart. The corresponding value of the system natural frequency in the input direction,  $f_X$ , is read from the horizontal axis. This value of  $f_X$  is then used to re-enter the chart to find the system frequency in the  $y$  direction,  $f_Y$ , for the appropriate value of the ratio  $h/L$ . The latter frequency is read from the right-hand vertical scale.

6. The system frequency in the  $z$  direction is found from the final chart, Figure 12, by entering with the value of  $f_Y$  and using the proper  $L/b$  line to determine  $f_Z$ .

### NUMERICAL EXAMPLE

The process just described is illustrated in the design charts for the following numerical example, representing the system shown in Figure 4.

Let  $X_0 = 0.11$  in. by specification, and select material thickness  $h = 0.050$  in. Then, from Figure 8,  $L \approx 5$  in. From Figure 9, for  $L = 5$  in. and  $h = 0.050$  in., we find  $f_1 = 400$  Hz.,  $f_2 = 1584$  Hz. and  $f_3 = 2108$  Hz. Now select  $n = 6$  flexures and  $b = 10$  in. Enter Figure 10 using  $h/L = 0.010$  and  $nb = 60$  to obtain  $K_X = 1800$  lb/in. Assume the combined fixture/specimen weight to be 20 lb.; then  $K_X/W = 90$  so that Figure 11 gives  $f_X = 30$  Hz. For  $h/L = 0.10$  we find that  $f_Y = 3000$  Hz. Finally, from Figure 12, entering this value of  $f_Y$  and using  $L/b = 0.5$  leads to  $f_Z = 1700$  Hz.

The natural frequencies of the system in the angular modes (roll, pitch and yaw) illustrated in Figure 5 should now be calculated. Since these depend on the inertia characteristics of the particular fixture and specimen tested, their calculation is not amenable to graphical solution. They can easily be calculated using the equations summarized in Table II. The roll mode often tends to be the one with the lowest natural frequency.

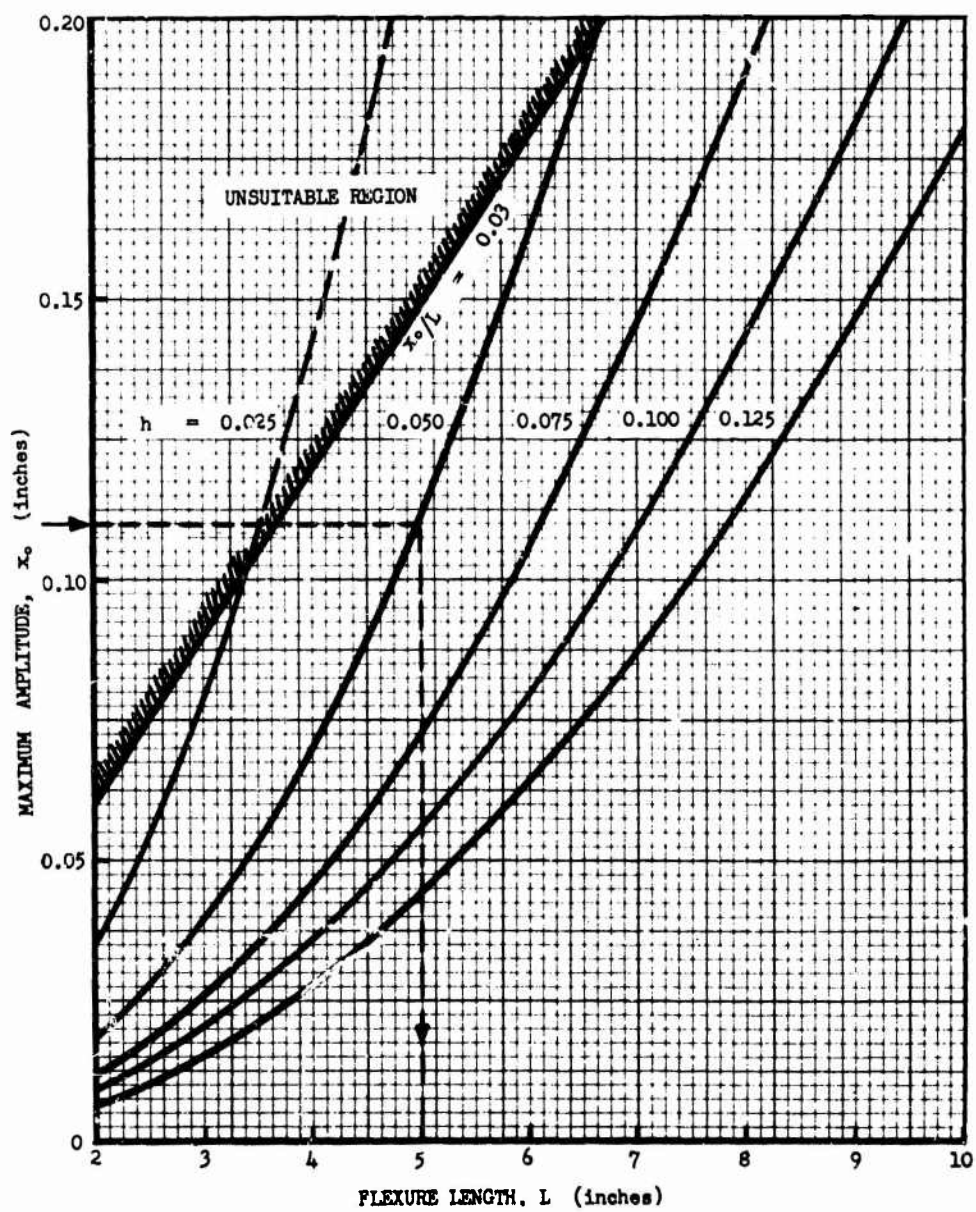


Fig. 8 - Chart for selecting flexure length and thickness

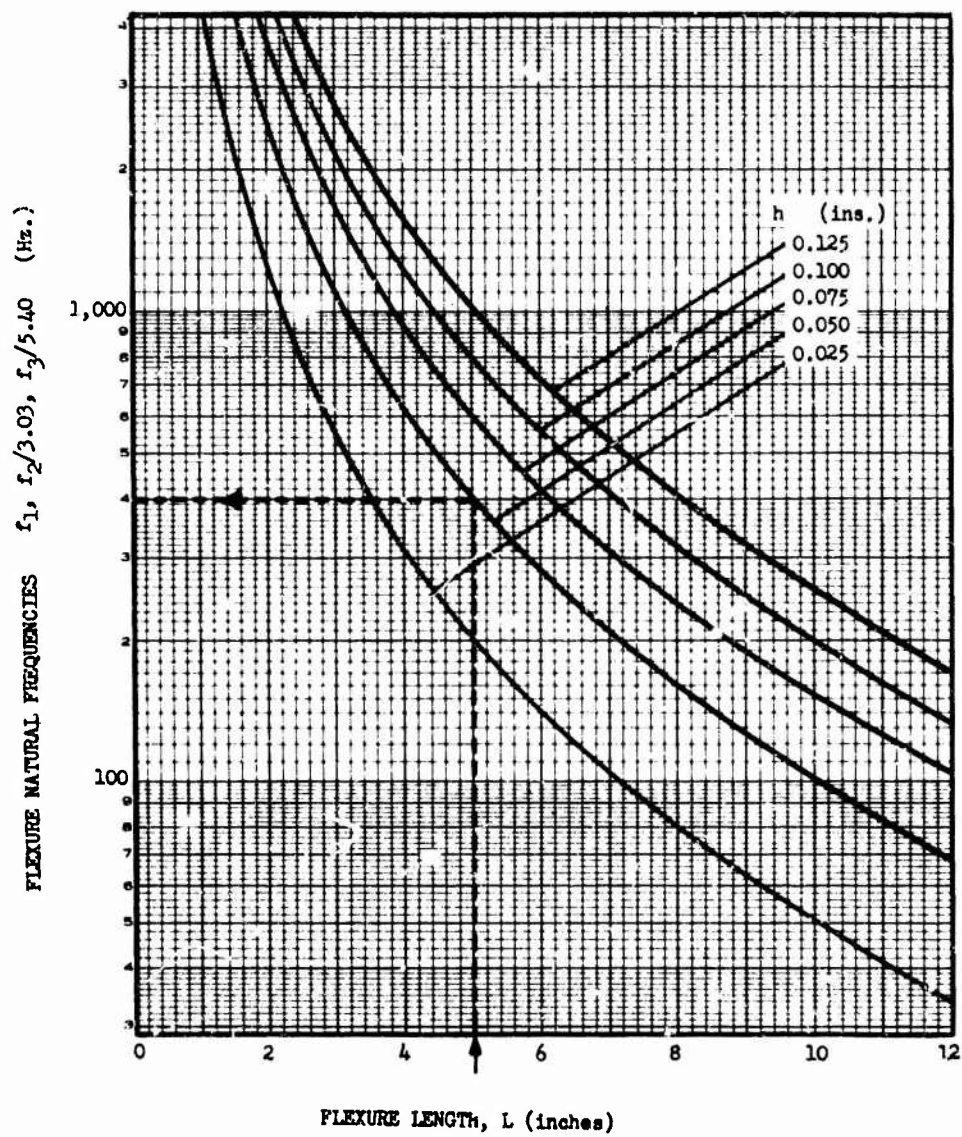


Fig. 9 - Chart for finding flexure natural frequencies

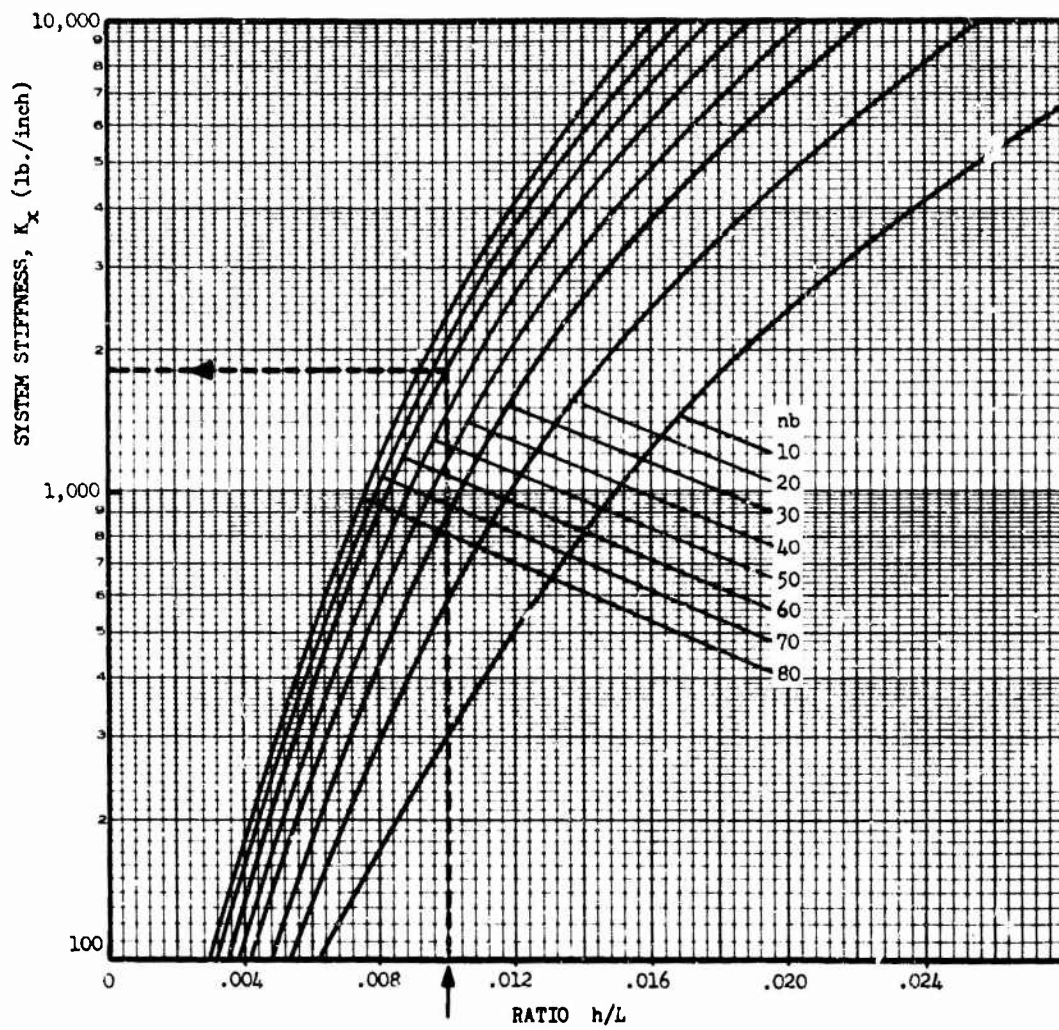


Fig. 10 - Chart for finding system stiffness along x axis



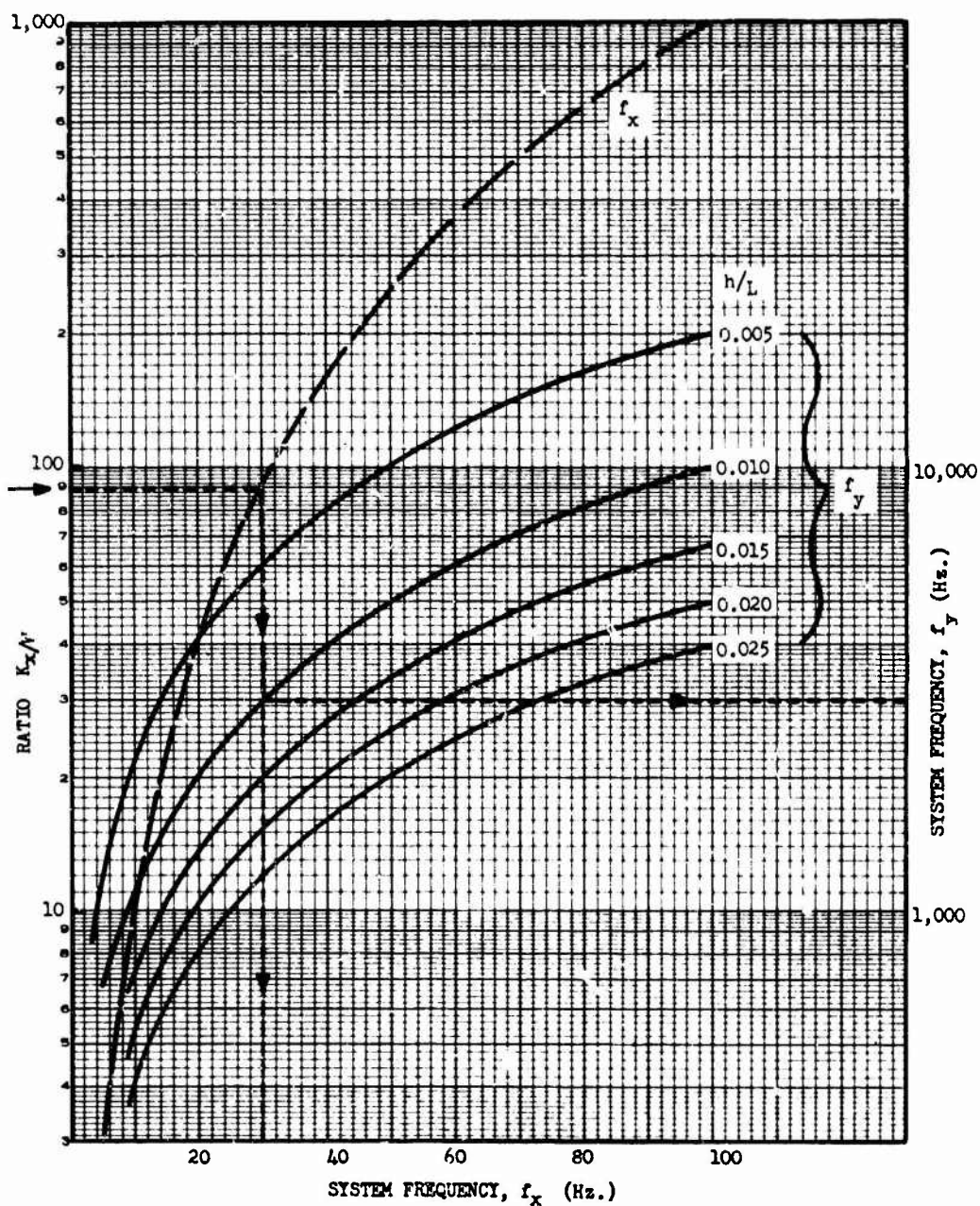


Fig. 11 - Chart for finding system frequencies along x and y axes



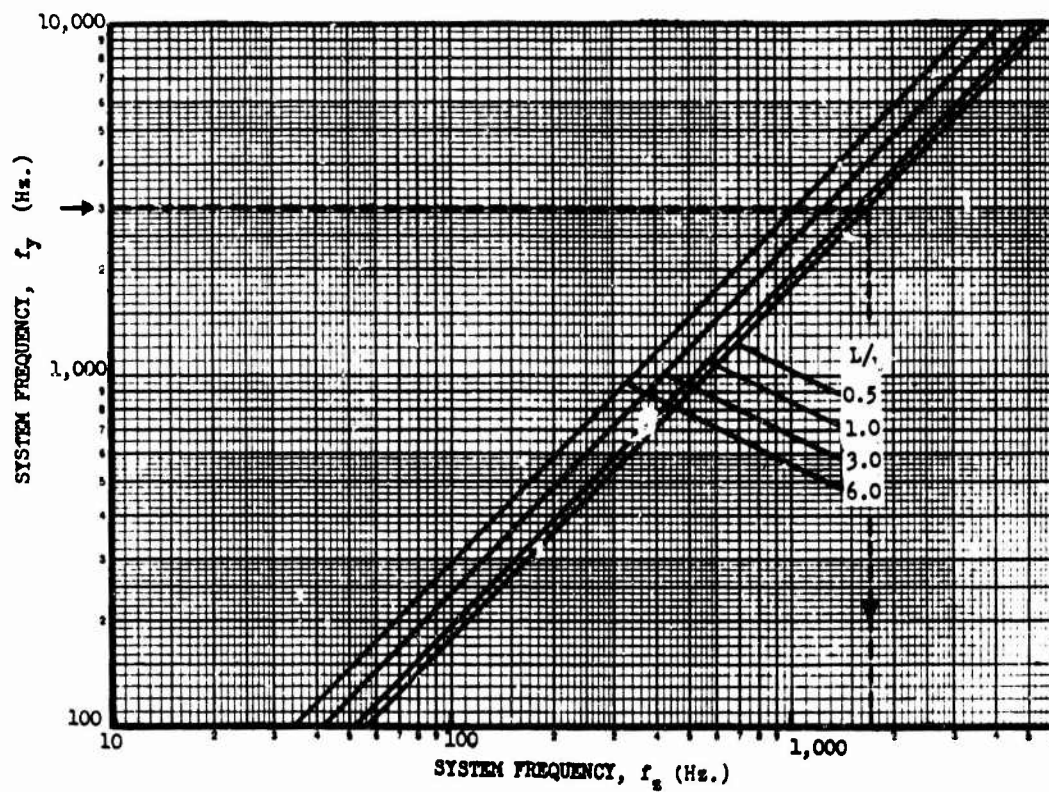


Fig. 12 - Chart for finding system frequency along z axis

## DISCUSSION

Mr. Cost (Naval Weapons Center): What are you trying to prove here? In 1958 at the Shock and Vibration Symposium it was quite dramatically pointed out that flexures are one of the sorriest ways to tie onto a shaker. White Sands Missile Range Technical Paper No. 32 published in 1963 also points this out. There is no physical way you can tie on using a flexure without inducing cross axis motion.

You say that this eliminates the problem of viscosity at low temperatures with slip tables. This is a matter of heat transfer and can be cured by keeping the bearings warm, if you're using a Team bearing, or keeping the oil warm or isolating the slip table from the cold temperature. Maybe I've missed the point but it looks to me as if we have gone back 10 years in history. What is your point?

Mr. Barrett: The point is very simply that in a number of large scale vibration tests conducted at North American, flexures were found to be the only solution after trying all of the other common methods.

Mr. Cost: It is physically impossible for a flexure to eliminate crosstalk - it induces it. Because the flexure is bent the arc length causes it to shorten and you induce crosstalk. I cannot see how you could possibly say crosstalk is eliminated by using a flexure. Maybe my thinking is wrong, but when you bow a straight piece of metal, the distance between the two ends shortens, and if it shortens cross motion is introduced.

Mr. Barrett: No, your observation is very true, and in fact this is discussed in the paper. The limitations which should be placed on the design of the flexures to minimize this effect is shown. We do not claim to get zero crosstalk. We claim to get less crosstalk than many of the other methods, and while you may know it is physically impossible, the specimens we tested and the accelerometers measuring the crosstalk apparently did not know, because they show that it was a very effective way of reducing the crosstalk.

Mr. Cost: Did you try hydrostatic bearings?

Mr. Barrett: Yes.

Mr. Cost: And you got less crosstalk with a flexure than you did with hydrostatic bearings?

Mr. Barrett: There were applications where the hydrostatic bearing should have been ideal but it turned out they were not satisfactory for the wide frequency range through which we were operating and for the heavy mass of fixture.

Mr. Shipway (Wyle Labs.): To rise to the defense of the speaker he did not claim that flexures were the ultimate. His paper I think, as I got it, endeavored to give some design parameters for those who wish to use flexures when the use of flexures is appropriate. And whether you know it or not there are lots of people in this world that still use flexures for many applications. Nobody is pretending that a flexure is the best restraint device - I think each restraint device has its appropriate place - hydrostatic bearings sometimes, something else some other time, an oil table next time, but the next time perhaps it is flexures. He is trying to tell you how to design when the time comes that you want to use flexures.

Mr. Cost: If I might answer Mr. Shipway, the question was: to eliminate crosstalk would you use flexures? And I state again, it is mechanically and physically impossible to eliminate crosstalk with flexures and I am shocked to hear that anyone from Wyle Labs would even suggest the use of flexures.

Mr. Shipway: It's a matter of degree as the speaker said. He does not claim zero crosstalk for flexures but if you have got 100 percent crosstalk without them and 10 percent with them, perhaps that is not bad. It is a matter of degree and the particular application and whether you can stand the amount of crosstalk that flexures give you.

## A COMPRESSION-FASTENED GENERAL-PURPOSE VIBRATION AND SHOCK FIXTURE

Warren C. Beecher  
Instrument Division  
Lear Siegler, Inc.  
Grand Rapids, Michigan

The fixture under discussion in this paper is the result of a program to achieve the economies of a universal fixture for vibrating and shocking different units with little or no compromise from the results that would have been obtained if an individual fixture had been specially fabricated for each one. In carrying out this objective, a method of wedge compression was developed to install individual adapter plates into a mother fixture. This method eliminates the spring constants of bolted connections, and the discontinuities of welded connections, resulting in a high frequency first resonance with low magnification and cross mode vibration.

Many attempts to construct a general-purpose vibration and shock fixture have resulted in serious compromises which would have made individualized fixtures for each test item desirable, if not mandatory. The essential problem in designing a universal fixture lies in the necessity for fastening adapter plates for different units into a mother fixture. Frequently, this has resulted in a multiplicity of bolted joints which create a corresponding multiplicity of resonances, many of which may fall within the frequency range of the test. This situation usually causes cross-mode vibration at one or more frequencies in excess of 100% of the desired mode, and thus invalidates the test.

A large number of items that pass through our test facility fall into two categories of black boxes.

- Type 1. This unit has a flat bottom mounting surface or mounting feet to attach upon a flat surface.
- Type 2. This unit attaches to a flat surface while its main body extends through a hole in this surface, as an instru-

ment mounted into an instrument panel, where it is held by a circumferentially constructed integral mounting ring, or by the front bezel.

At first glance, it does not seem probable that a satisfactory fixture can be designed to accommodate both types of units, especially when random equalization must be accomplished and verified to 2000 cps.

With many shaker systems it is undesirable to tip the shaker for directly supported or oil-film table operation where a high quality random or sine vibration with low cross-modes is required. In any event, when the through-panel type black box is to be tested, a properly braced vertical surface must be erected normal to the shaker tabletop. Since the fixture under consideration is to handle both type 1 and type 2 items, the design should be capable of permitting all vibration to be performed with the shaker axis vertical, if so desired. At the same time, the number of vibration surface interfaces should be minimized.

With type 1 units, and three planes of vibration, a bolted-together universal vi-

bration fixture usually requires at least seven bolted interfaces. This includes a horizontal adapter plate to bolt to the shaker head (1), a vertical plate erected there-upon to which the unit is fastened (2), and two triangular braces to stiffen the vertical plate (4). This set-up will accomplish vibration, but may require additional fixturing interfaces for shock.

With type 2 units, and provision to accomplish shock with both the face up and face down positions, a bolted together plate box with a central cavity results in fourteen or more bolted interfaces - twelve in the box, and the remaining two consisting of the unit-to-box, and box-to-shaker interfaces. The above bolted-together universal box can be considerably improved by welding all its internal interfaces except the end plates which usually have to be individualized to accept different units. This reduces the number of bolted interfaces to four. Unfortunately, the discontinuities across the welds also produce some deterioration in the vibration characteristics of the fixture.

The design objectives of the fixture discussed in this paper are met by constructing a hollow box in the following ways:

1. The main body of the fixture (which retains two individualized end plates) is machined from a single forging, usually of aluminum.
2. The outside surfaces of this body are rectangular to permit convenient mounting to place the unit in either a horizontal or vertical plane on the shaker adapter plate. Two of the outside surfaces have a uniform pattern of 1/4-20 bolt holes to permit a bolt-on-the-surface type unit to be held on one surface by an adapter plate and to permit counterbalancing on the opposite surface by another unit, or by a balancing weight if required. For a few critical applications, the unit mounting holes are also placed in one of these surfaces to eliminate the unit adapter plate. A third surface of the fixture is used to bolt it to the shaker adapter plate, and this arrangement permits two of the three planes without unbolting the main fixture. The remaining plane could be achieved by a hole pattern on the top of the fixture body, but is usually done directly on the shaker

adapter plate.

3. The inner surfaces are round to present a non-uniform cross-section of great rigidity and a capability of a high first resonant frequency with a low magnification factor. There are two larger round recesses, one in each end, to mount individualized circular adapter plates for each type of through-the-panel mounting unit. These can be rotated 90 degrees for two planes, and through other convenient angles for specialized tests. The main fixture usually does not have to be unbolted for two planes, and is unbolted and turned on end for the third plane. Bolt-holes counter-bored to within two bolt-diameters of the bottom pass through the outer shell wall of the circular cavity in the two orthogonal mounting directions without penetrating each other, or the space occupied by the unit. One of the recessed end plates has an individualized cut-out to match a particular through-the-panel mounting unit. The opposite end has a cut-out that permits cables or other appurtenances of the unit to be brought through.
4. In addition to the functional purposes mentioned above, and most importantly, the recessed end plates are used to rigidize the fixture and raise its resonant frequency. These end plates present a tapered edge to a matching tapered recess in the end of the hollow box fixture. The hold-down bolts for these plates are used to wedge the end plates into a rigid compression fit with the mother box. They are left installed as a safety feature in case the operator fails to torque the plate bolts properly, but a properly torqued-in plate is held into the fixture by the wedging action, and must be extracted with a pulling tool after the test. Since the contact between the plate and the mother fixture is an intimate one of two pieces of the same material, there is no discernible discontinuity across the joint, as there would be with a welded joint, and because of the wedge fit, the bolt spring-constants do not control the rigidity of the assembly, or its lowest resonant frequency. This results in a highly

rigid fixture with minimum weaving and cross-vibration, and with a low magnification factor, high frequency first resonance.

#### FIXTURE DESIGN DETAILS

Some of the mechanical features of the design are illustrated in two embodiments. Fig. 1 shows a 12" outside dimension cubical fixture known here as the LEM fixture, and in Fig. 2 a 10" x 10" x 12" long fixture known as the GEMINI fixture. Details of the wedge fit are illustrated in Fig. 3. Grid lines permit approximate scaling with 1/2" squares on Fig. 1 and Fig. 2, and 1/4" squares on Fig. 3.

Historically, the GEMINI fixture came first, and was used to hold the Incremental Velocity Indicator, The Attitude Director Indicator (The Eight-ball of TV fame) and many other components of this space vehicle during sine and random vibration, and during shock tests. The main body of the fixture without adapter plates weighs 67 lb.

The larger LEM fixture is now being used to vibrate and shock the Lunar Excursion Module Indicator which is a through-panel indicator and the Gimbal Angle Sequence Transducer Assembly which is a bolt-on-a-surface unit. The main body of this fixture weighs 89.4 lb. without adapter plates. An even larger fixture is being readied for another space program.

The GEMINI fixture was designed to have a lowest resonant frequency in the vicinity of 2000 Hz. The resonant frequency was just over 2000 Hz in two planes, and just under 2000 Hz in the remaining plane, as measured at the instrument attachment location on the instrument adapter plate. (Fig. 4a). Cross-axis vibration responses shown (Figs. 4b, c, d) include shaker cross-axis vibration which is substantial on a relatively small shaker carrying a heavy load. With a stiffer armature suspension, these curves could show considerable improvement. These curves were measured with 1.0g peak sine input.

The LEM fixture had an original design requirement of 1500 Hz minimum for the lowest resonant frequency, which was later dropped to 750 Hz because many vendors were having difficulty in meeting it. This fixture shows a lowest resonant frequency of 2000 Hz (Fig. 5a) vibration axial (along the direction

of bore of the main fixture body), and 2050 Hz with vibration radial (Fig. 5b), or transverse to the bore of the main fixture body. These curves were obtained by submitting the shaker-fixture combination to a flat unequalized random input producing a level of  $.02g^2/Hz$  over the flat portion of the fixture response. This flat spectrum input was terminated at the high end by a 3000 Hz low-pass filter and plots were carried out to this frequency.

The cross-axis response curves (Figs. 6a, b, c, d) were produced by equalizing in the primary direction of a tri-axial accelerometer mounted at the instrument attachment location on the instrument adapter plate (top trace at  $.02g^2/Hz$  equalized) and plotting the transverse motion response curves. This level was picked to insure that all fixture resonances would be adequately excited. The cross axis response curves also include shaker cross-axis motion.

In the event that some surprise arises from the claim to a higher resonant frequency with the shake in the axial direction for the larger fixture, it should be pointed out that the resonance in this direction is largely controlled by the stiffness of the unit adapter front plate that wedges into the fixture. The measurements shown were on the weakest adapter plate that was made for the Gemini fixture, and are an indication of minimal, rather than optimal performance conditions. Heavy enough weights could be hung on a front plate for the LEM fixture to bring this axial resonance below 2000 Hz, but this reduction is not apt to exceed 10%, with any unit that would fit the fixture. The curves are a good indication of this design as a holding fixture for fairly good-sized panel instruments.

Some niceties that should be observed in the design are contained in the following rules:

1. None of the bolt-holes in the fixture are allowed to intersect each other or the central cavity, except the holes that lie outside or beneath the front and back wedge plates. These have reach-through holes for a long-handled Allen wrench of some 12" to 18" of length with an extension handle, the length being dependent on the dimensions of the fixture.
2. All bolt hole dimensions are refer-

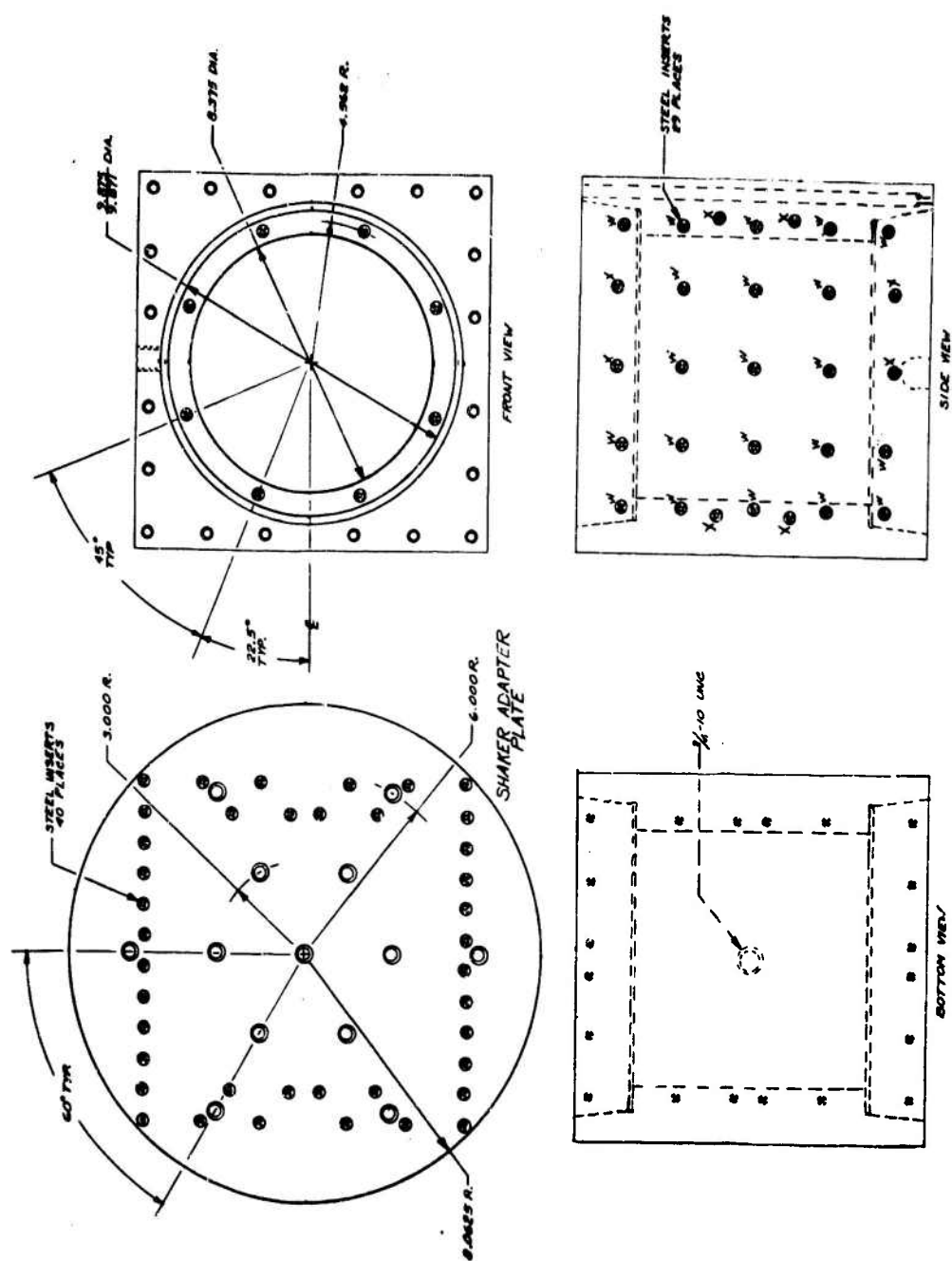


Fig. 1 - 12" Cubical Fixture

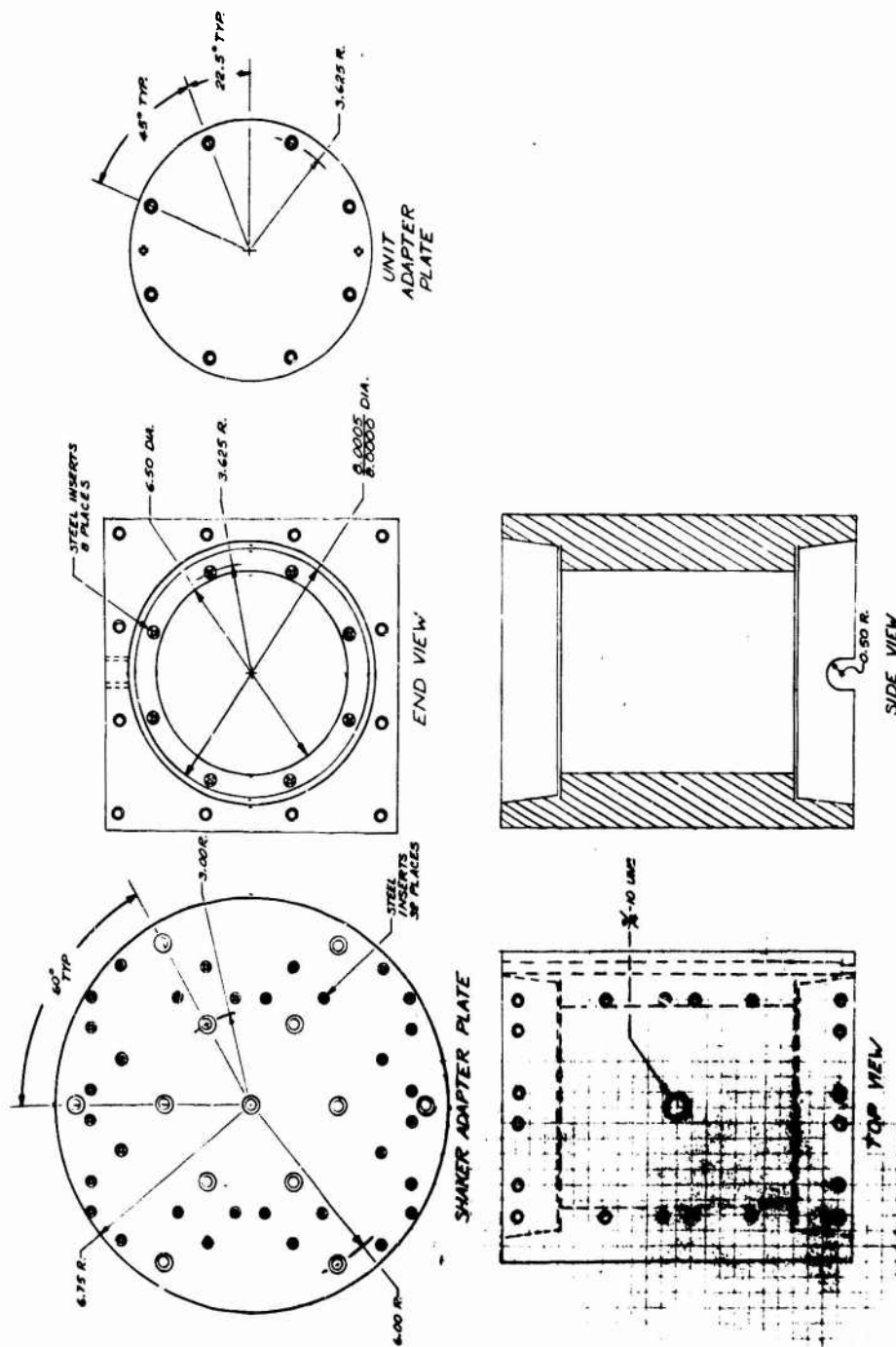
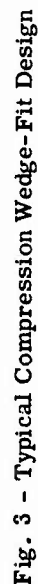


Fig. 2 - 10" x 10" x 12" Long Fixture

Diameter  $D$  = .021" as measured at gage diameter, as shown in circle V.  $U \times X$  = an exact multiple of one inch for the fixture mounting base surface  $U$ .  $U + X$  = the distance from the center of the fixture mounting base surface  $U$  to the hole in the fixture to be mated symmetrically spaced as per the hole spacing and circumference. This, together with the custom of double-bolting the thinnest part of the lip at the mounting base of the fixture, requires that each side of center on the mounting base has had to locate the first two "X" holes  $1\frac{1}{2}$ " above and below center, and  $1\frac{1}{2}$ " between the first two "X" holes. Since the fixture holding bolts in the fixture design to date are  $1/4$ -30 cap screws, we have held the maximum separation of bolts spaced around the mounting base to 10.5" or less, if possible.

1. Diameters A, B, E, F to be round within .0005" TIR, and concentric within .002" TIR.
2. Diameter A shall be normal to Surface C, and Diameter E shall be normal to Surface G.
3. Tolerance on Diameters D and E shall be .002" in each case.
4. Both hole patterns shall be held out on the surface .005 of wet and centers shall be located within .005 of true position. The opposite end of a hole shall be located as above shall be within .010 of the center-hole, regardless of length, and the concentricity error of the counter-bore shall be within .001".
5. Surface roughness shall not exceed RMS 32 on any mating surfaces, including flange to shaker adapter.
6. Surface G shall never contact Surface C when the wet has adapter plate is drawn into its mating cavity. The preceding design gives an initial separation of .105"  $\pm$  .005". Most of the wear will occur in the center of the hole, reducing the initial separation by .004"  $\pm$  .003" on the average.
7. The above considerations apply to all alloy 6061-T6 such have been heat-treated to T6 and then stress relieved and stabilized for both phases.
8. Dimension P = .951",  $\phi$  = .400",  $\phi$  = .3"  $\pm$  .000",  $\phi$  = .3"  $\pm$  .000",  $Z$  = .3"  $\pm$  .000".





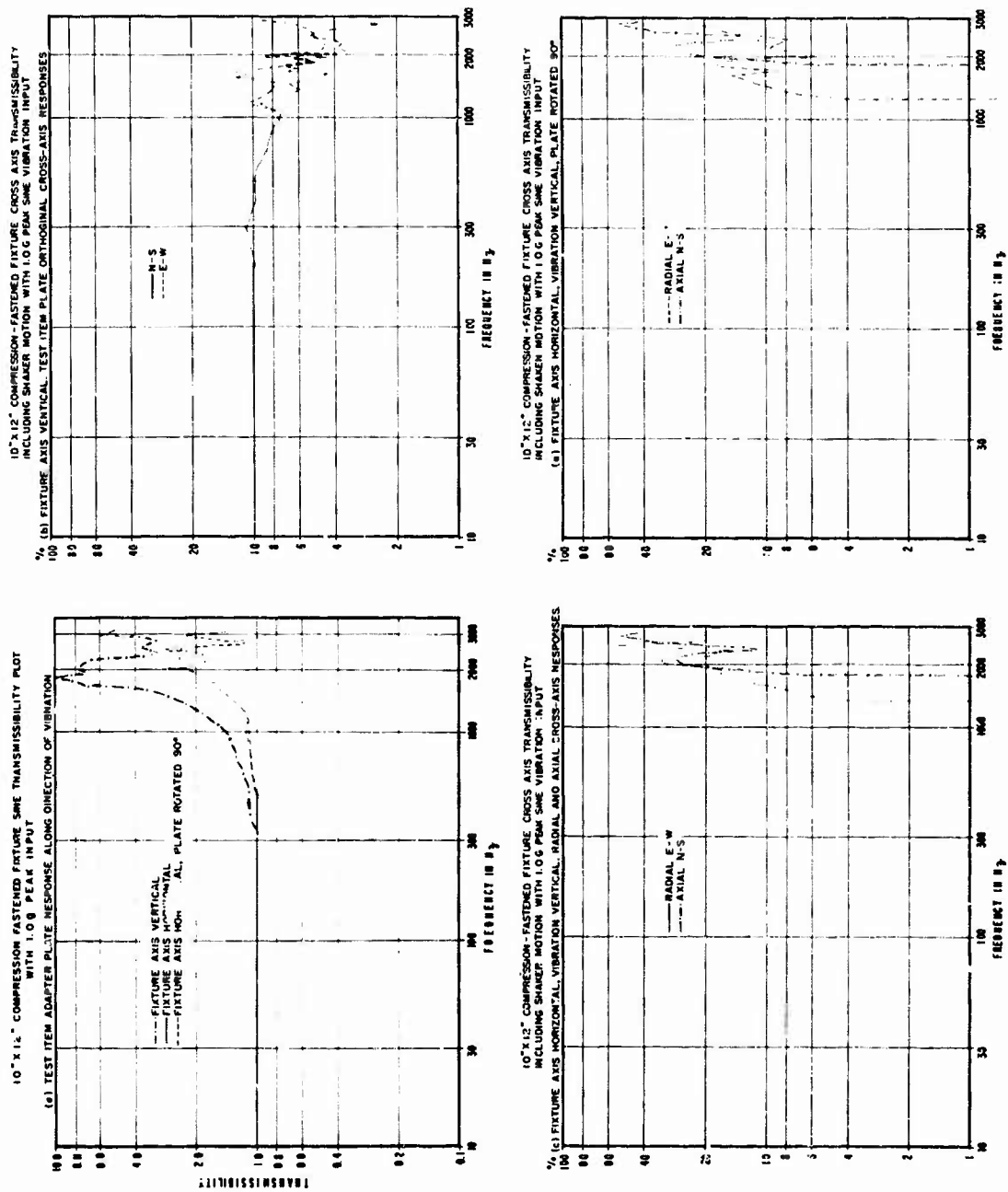


Fig. 4

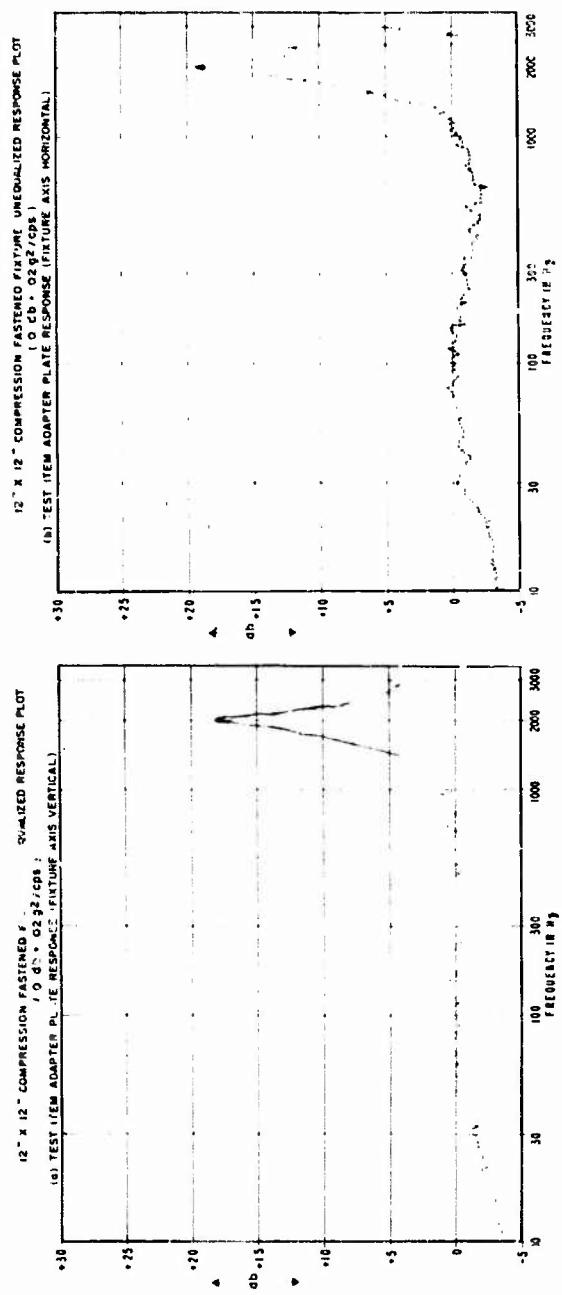


Fig. 5

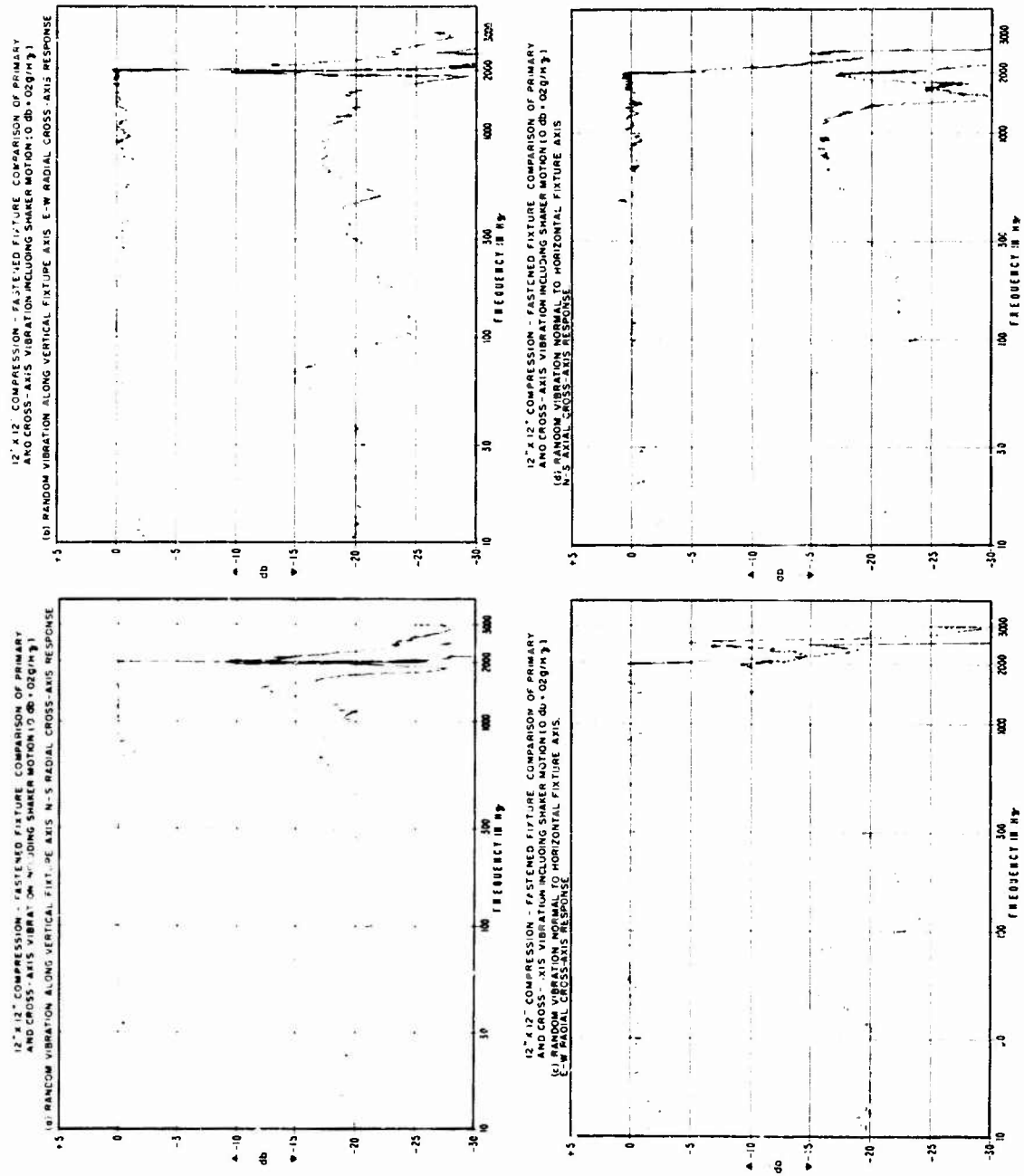


Fig. 6

enced to the bolted surfaces of two mating pieces and are located within .005" TIR. The opposite ends of these holes are located within .010" of true position including the maximum counter-bore concentricity error of .001". Where holes and counter-bores are 10" long or longer, this requires considerable accuracy in the boring operation.

3. Surface flatness and parallelism (or perpendicularity) shall be held within .005" TIR.
4. Surface smoothness of mating surfaces shall be held to RMS32 or better.
5. Accuracy of taper angle in the bore or in the mating plate should be held to +0', -1'. Other details are shown in Fig. 3.
6. All other angles shall be held within  $\pm .1^\circ$ .
7. Aluminum pieces should be purchased as pieces of the same forging by preference and subsequently heat treated to T6, stress-relieved and stabilized. Critical surfaces should be finished at 68° - 70°F after heat treat.

In other words, care in details of workmanship are necessary to realize the potential of the design. Some details, such as the angle of the taper, were selected because good working data were available for this particular angle, and are not necessarily sacred. The same remark applies to the materials that were used, although further experience should show the present ones as among the more desirable.

#### BOLTING PRACTICE

To insure the maximum rigidity of the fixture and shaker adapter plate interface, and proper wedging of the fixture and unit adapter plate interface, the 1/4-20 bolts normally used are torqued near maximum permissible values [1]. The same statement applies to the 3/8-24 bolts which tie the shaker adapter to the shaker in our installation. Where all the surfaces involved are steel the preferred practice is to torque to 75% of yield torque for an average screw

[2]. To permit large torques, steel inserts are used to replace the weaker threads which would result from bolting into the aluminum parts of the fixture. Self-tapping inserts are definitely preferred because of strength and wear considerations for this service. The inserts are set .015" below the surface and the full diameter of the untapped insert hole is extended approximately 1/2 the length of the insert beyond it. This insures that there is no danger of bottoming the screw if a standard length is used. For 1/4" cap screws a standard 1" long screw is used for all bolts in the fixture. If a 1/2" long insert is used, approximately 2 bolt diameters of length are left under the head in the unthreaded and counter-bored piece and approximately 2 bolt diameters are engaged in the thread in the mating piece. Since the material under the head is aluminum for the fixture and magnesium for the shaker adapter plate, the 75% of yield torque figure mentioned above is not entirely applicable. Steel inserts could be used at this point also, but are not entirely necessary, particularly in aluminum. The situation is more marginal in the case of magnesium. In any event, experience with these materials has indicated a reduced maximum figure of 60% of yield torque for T-6 aluminum under-head conditions and 50% of yield torque for magnesium. It should be noted that there is a definite fall-off in bolting efficiency below 40% of yield torque in any of these materials. Typical yield torque for 1/4-20 bolts is about 250 inch pounds [2]. The torque that is actually applied will ultimately depend on the user's judgment in each instance.

For convenience in lifting these fairly heavy fixtures, a 3/4-10 threaded hole bottom tapped to 3/4" deep is installed in the top center of the fixture to hold an eye-bolt. No other holes are ordinarily required in the top surface of the fixture aside from the tie-down bolt holes. A bolt hole pattern that meshes in between other existing patterns may be placed on the sides of the fixture. One side will hold a bolt-on-a-flat-surface unit and the opposite side a counter-balancing plate. The unit may be mounted with an adapter plate ("W" holes in side view in Fig. 1) or special unit mounting position holes may be installed ("X" holes in Fig. 1). Steel inserts protect these holes.

The various bolting provisions are more easily visualized by examining photographs of different fixtures in typical in-use conditions: (Fig. 7).

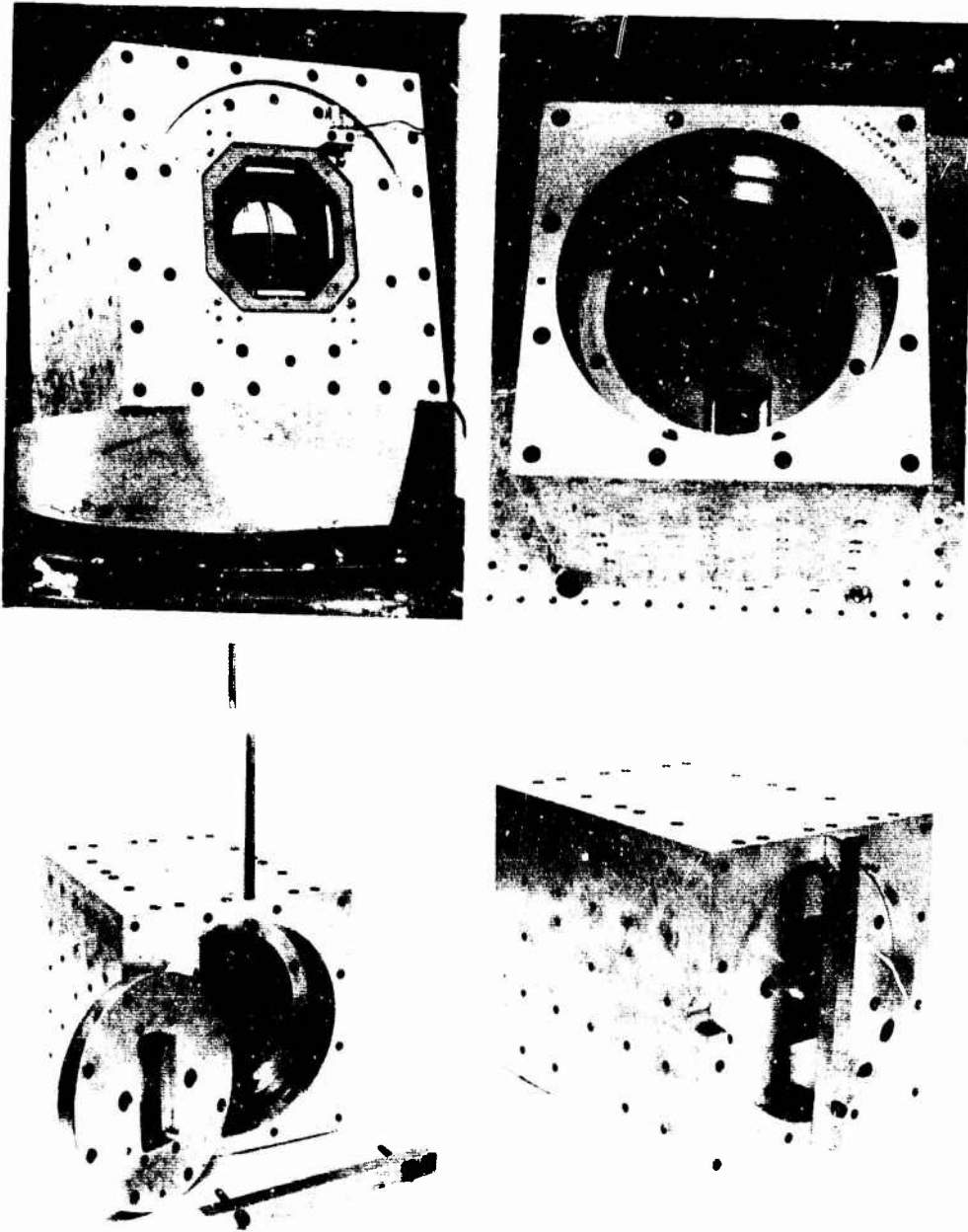


Fig. 7 - The Design In Use

The upper left view shows a view of the 12" cubical fixture mounted to a 5000 force-pound shaker with a special tilting adapter plate. A typical indicator is installed for a vibration test.

The upper right view shows the 10" x 10" x 12" fixture with a typical unit installed on the front plate. This plate has been mounted where the back plate would normally be in order to permit an upside down vertical drop as shown on the shock machine table. Various details of the interior cavity of the fixture are visible.

The lower left view shows a typical back plate with slot through which electrical connections from the unit exit to outside test equipment. When the unit is mounted face up on a shaker or shock machine the fixture

surface facing the viewer is bolted to the machine adapter plate. The electrical cable continues its exit from the fixture through the large slot seen in the view to the right. A typical reach-through Allen wrench is shown ready to bolt the fixture body to its machine adapter plate, and the extra bar is lying in front of the fixture.

The lower right view shows how the extractor bar is used to pull the compression wedged back-plate out of the fixture.

#### REFERENCES

1. O. John Zamparo, "Designing Tight Bolted Joints for Vibration Environment," The Shock and Vibration Bulletin No. 34 Part 5 PP 273 - 277 (Feb. 1965).
2. Holo-Krome Socket Screw Selector Number 1063. Holo-Krome Company, Hartford, Connecticut. (A slide-rule device).

#### DISCUSSION

Mr. Jackman (General Dynamics/Pomona): It would seem that with its bevel edges the expense of making this fixture would be quite an item. Could you tell us the advantage of this particular fixture over the more conventional type for a particular case? You undoubtedly have made such comparisons.

Mr. Beecher: We have made these comparisons and the advantage is that this one fix-

ture can be used for a multitude of instruments. If it were designed for a single instrument the cost could be prohibitive. In one case we have used the fixture for what may turn out to be only a single unit for the simple reason the instrument itself is critical on a manned space vehicle, and we had no other way to get the particular crosstalk levels. We felt the item was sufficiently critical that the cost was justified.

## VIBRATION EQUIVALENCE: FACT OR FICTION?

LaVerne Root  
Collins Radio Company  
Cedar Rapids, Iowa

The idea of vibration equivalence is as old as vibration testing. Any time we imply that a laboratory vibration test simulates the field vibration, we have implied that some form of equivalence exists. Therefore, vibration equivalence is fact.

Several of the equivalence theories are discussed in the paper and the controversial aspects of vibration equivalence are outlined. A monograph on "Vibration Equivalence" is being prepared by Collins Radio Company under the sponsorship of the Shock and Vibration Information Center. The contents of the monograph are outlined in the paper and it is shown how the monograph may be used to improve the equivalence between laboratory tests and field vibration.

Opinions expressed in this paper are those of the author and they are not necessarily the opinions of Collins Radio Company or the Shock and Vibration Information Center.

### INTRODUCTION

"The development of the ubiquitous accelerometer has enabled us to postulate a numerical equivalence (in units of g) between a laboratory shock test and a ride as cargo in the back of a truck, or between a vibration test and a ride in a guided missile. But again, the equivalence in each case relates to a single fact of the two realities: the acceleration of a single point in a single dimension. If we propose to disregard all the other features that contribute to a true equivalence - all those, in fact, to which we cannot ascribe simple numerical values - is not our preoccupation with accuracy a little intemperate?" [1].\*

The above quotation represents the opinion of one expert who would probably vote that proposed vibration equivalences are fiction. Other experts [2] would probably vote that many of the proposed equivalences are fact. All forms of vibration equivalence, including time scaling, are somewhat controversial; but it is

necessary to pursue the subject of equivalence since exact duplication of use vibration is not generally practical [3].

The purpose of this paper is to outline a few of the major equivalences suggested in the literature and to try to draw some conclusions on the validity of the equivalence concepts. A secondary purpose is to contact other persons interested in the equivalence problem. A monograph on "Vibration Equivalence" is being prepared under the sponsorship of the Shock and Vibration Information Center and I would like to consider all results either pro or con for inclusion in the monograph.

### TYPES OF EQUIVALENCES

Equivalences may be divided into two general types that will be designated type I and type II. The type I equivalences include those equivalences that depend only on the current value of some parameter and are independent of the past history of the given parameter.

\*Numbers in square brackets refer to references.

One of the simpler type I equivalences [4] consists of a sine input that gives an rms response at a single resonance that equals the overall rms response due to the random vibration spectrum. A variation of the approach [4] consists of a sine input that gives an rms response at a single resonance, which is a constant multiplicative factor times the rms response at the single resonance due to the random vibration spectrum. Correlation was checked using both simple mechanical specimens and electronic equipment. The primary conclusion from the paper is that substitute sine tests obtained using the two methods are probably unsuitable for complex electronic equipment.

Another type I equivalence consists of substituting a sweep random test for a wide-band random test by matching the distribution of response peaks above some arbitrary level [5]. An electrical analog of a single degree of freedom system was used to verify the distributions of peak responses.

A third type I equivalence consisted of an experimental study of the electrical noise caused by various levels of sweep sinusoidal vibration and random vibration [6]. The electrical noise at specific frequencies was cross plotted to determine the degree of correlation. In general correlation was found to be poor.

The type II equivalences include those equivalences that are dependent on both the current value of some parameter and the past history of the parameter. The type II equivalences are useful in accelerating vibration tests. Although type II equivalences could be based on any time dependent form of degradation, it appears that all type II equivalences are based on fatigue damage accumulation.

One of the earliest type II random-sine equivalences [7] used the Palmgren-Miner hypothesis of fatigue damage accumulation [8,9]. Although not dealing directly with random-sine vibration equivalence, the paper includes several fatigue damage formulas, which have been the basis for a number of papers on vibration equivalence.

A much later work [10] develops a complete set of equivalence equations based on Palmgren-Miner hypothesis and the Corten-Dolan hypothesis [11] for random, sine sweep, and sine dwell vibration. These equations are checked using single degree of freedom mechanical test speci-

mens. Equations based on the Palmgren-Miner hypothesis gave excellent correlation between the random, sine sweep, and sine dwell tests derived from the field vibration, but the correlation between any of the laboratory tests and the field vibration test (two different random spectrums) was poor.

Many more equivalences of both types have been suggested. The bibliography contains a list of recent papers on vibration equivalence. Although the list is far from complete, it is apparent that considerable interest in the problem of vibration equivalence exists.

#### AREAS OF CONTROVERSY

Three primary areas of controversy exist. These include random-sine equivalence, laboratory and field vibration equivalence, and accelerated vibration tests. Of these areas of controversy, the random-sine equivalences have generated the most heated discussion. Many papers [2, 10, 12] have obtained close correlation for random and sine tests using a single criteria such as fatigue damage. All of the fatigue damage accumulation hypotheses are simple models of a complex phenomena and as such, they fail to account for order of stress application, changes in damage mechanism as damage accumulates, and material changes. The simplified models plus large inherent scatter in fatigue tests may account for poor correlation obtained in some papers [13, 14] based on fatigue damage. In cases where the correlation has been based on complex parameters such as electrical noise generated [6], the correlation has been poor.

The opinions expressed by various researchers on the concept of random-sine equivalences range from strong support [10] to complete disagreement [15]. Random-sine equivalences do exist but a single equivalence will not account for all types of degradation or failure which a single equipment might experience.

The second area of controversy concerns the equivalence between field vibration and laboratory tests. Most laboratory tests are intended to determine the suitability of the test specimen for usage under field conditions. If this is to be done without requiring excessive oversize of the test item, the laboratory test must be equivalent to the field vibration. Experts are currently raising serious questions



about test levels and test methods being used. The practices of enveloping measured field data [1] and using infinite impedance mounting surfaces [6] are two items which are being seriously disputed. The equivalence may be so poor in some cases that the laboratory test becomes an overtest by an order of magnitude [7].

I believe that the availability of equivalence theory in a single document will allow translation of measured field vibration into more meaningful laboratory tests. The equivalence theory, plus a better control of mechanical impedance, should allow considerable improvement in the equivalence between laboratory tests and field usage.

The third major area of controversy is the accelerated test or change of time scale. Since many test items are exposed to vibration throughout their useful lives, it is not possible to maintain a unity time scale during laboratory vibration tests. This requires the vibration level to be increased in order to reduce the test time. In many cases, the time scale must be changed by a factor of over 1000, which requires a significant increase in the vibration level. The techniques used in accelerating vibration tests are based on simple models and they generally assume linear response of the test item. Equivalence theory will not solve the above but, at least, the limitations should be pointed out.

Accelerated tests, as currently used, have an additional controversial aspect. The present test philosophy is to develop an accelerated test to check the life of the test item and to also use the same test levels to check the operational characteristics of the test item. This requires that the test item be capable of satisfactory operational performance at vibration levels several times higher than it will ever see in service. To obtain operational tests, the type I equivalences should be used rather than the accelerated test levels.

#### CONTENTS OF THE MONOGRAPH

A number of shortcomings of the techniques used in developing laboratory vibration tests have been considered. The "Vibration Equivalence" monograph will provide documentation of the current state of the art in vibration equivalence theory. The monograph will not provide solutions for all problems associated with vibration testing, but it will allow a more rational approach to selecting test levels.

The monograph will include a discussion of current technique for developing vibration tests, and suggestions for substituting equivalence theory in place of current techniques. All known papers on equivalence theory will be included in the annotated bibliography and the major papers will be considered in detail in the body of the monograph. The bibliography attached to this paper gives a preliminary listing of recent equivalence papers.

#### CONCLUSIONS

Equivalence theories exist for many simple situations and the author believes this information should be readily available to the test engineer responsible for developing laboratory vibration tests. These equivalences will allow the test engineer to arrive at more meaningful tests if he will break with the current tradition of trying to develop a single test which is everything to everybody.

Vibration tests should be made up of two distinct tests. These two tests can be any type of vibration the test engineer desires, but one test should be obtained using type I equivalences in order to arrive at a meaningful operational test. The second test should use type II equivalences to arrive at an accelerated life test. This approach, that is, separate operational and life tests, differs from the present philosophy of developing an accelerated life test and using this same test for the operational test.

The equivalence theory is available in current literature plus unpublished reports. The purpose of the monograph is to make this theory available in a single document and to document all relevant research on the various equivalence theories proposed.

#### ACKNOWLEDGEMENT

The work on which this paper is based has been sponsored by the Shock and Vibration Information Center.

#### REFERENCES

- [1] J. Salter, "Advances in Numerology," Shock and Vibration Bulletin 37, Part 3, pp. 1-6, January 1968.
- [2] C. Crede and E. Lunney, "Establishment of Vibration and Shock Tests for Missile Electronics as Derived from the Measured

- Environment," WADC Technical Report 56-503, 1 December 1956.
- [3] M. Gertel, "Derivation of Shock and Vibration Tests Based on Measured Environments," Shock and Vibration Bulletin 31, Part 2, pp. 25-33.
  - [4] W. Trotter, "An Experimental Evaluation of Sinusoidal Substitutes for Random Vibrations," Shock and Vibration Bulletin 29, Part 4, pp. 1-14.
  - [5] G. Booth and J. Broch, "Analog Experiments Compare Improved Sweep Random Test with Wide Band Random and Sweep Sine Tests," Shock and Vibration Bulletin 34, Part 5, pp. 67-82, February 1965.
  - [6] J. Foster, "Random-Sinusoidal Vibration Correlation Study," WADD-TN-61-43, February 1961.
  - [7] J. Miles, "On Structural Fatigue Under Random Loading," Journal of the Aeronautical Sciences, pp. 753-762, November 1954.
  - [8] M. Miner, "Cumulative Damage in Fatigue," Journal of Applied Mechanics, pp. 159-164, September 1945.
  - [9] A. Palmgren, "Die Lebensdauer Von Kugellagern," Zeitschrift des Vereines Deutscher Ingenieure, 1924.
  - [10] I. Gerks, "Optimization of Vibration Testing Time," NASA CR-77338, June 1966.
  - [11] H. Corten and T. Dolan, "Cumulative Fatigue Damage," Proceedings of the International Conference on the Fatigue of Metals, 1956.
  - [12] L. Root, "Random-Sine Fatigue Data Correlation," Shock and Vibration Bulletin 33, Part 2, February 1964.
  - [13] A. Head and F. Hooke, "Random Noise Fatigue Testing," Proceedings of the International Conference on the Fatigue of Metals, pp. 301-303, 1956.
  - [14] P. Smith and C. Malme, "Fatigue Tests of a Resonant Structure with Random Excitation," The Journal of the Acoustical Society of America, pp. 44-46, January 1963.
  - [15] C. Morrow and R. Muchmore, "Shortcomings of Present Methods of Measuring and Simulating Vibration Environments," The Journal of Applied Mechanics, pp. 367-371, September 1955.
  - [16] J. Otts, "Force-Controlled Vibration Tests: A Step Toward Practical Application of Mechanical Impedance," Shock and Vibration Bulletin 34, Part 5, pp. 45-53, February 1965.
  - [17] I. Vigness, "Measurement of Equipment Vibrations in the Field as a Help for Determining Vibration Specifications," Shock and Vibration Bulletin 33, Part 3, pp. 179, March 1964.

#### BIBLIOGRAPHY

- [1] K. M. Eldred, "Vibroacoustic Environmental Simulation for Aerospace Vehicles," Shock and Vibration Bulletin 37, Part 5, pp. 1-11, January 1968.
- [2] G. Kachadourian, "Spacecraft Vibration: A Comparison of Flight Data and Ground Test Data," Shock and Vibration Bulletin 37, Part 7, pp 173-203, January 1968.
- [3] D. E. Newbrough, R. A. Colonna and J. R. West, "Development and Verification of the Vibration Test Requirements for the Apollo Command and Service Modules," Shock and Vibration Bulletin 37, Part 5, pp 89-103, January 1968.
- [4] D. E. Newbrough, M. Bernstein and E. F. Baird, "Development and Verification of the Apollo Lunar Module Vibration Test Requirements," Shock and Vibration Bulletin 37, Part 5, pp 105-115, January 1968.
- [5] Fogelson, "Digital Analysis of Fatigue Damage to a Multimodal System Subjected to Logarithmically Swept Sinusoidal Vibration Spectra," Shock and Vibration Bulletin 36, Part 5, pp 17-40, January 1967.
- [6] B. M. Hillberry, "Fatigue of 2024-T3 Aluminum Alloy Due to Broad-Band and Narrow-Band Random Loading," PhD Thesis, 1967, Iowa State University.
- [7] R. W. Peverley, "Acoustically Induced Vibration Testing of Spacecraft Compo-

- nents," Shock and Vibration Bulletin 36, Part 3, pp 39-46, January 1967.
- [8] J. A. Callahan, "Gemini Spacecraft Flight Vibration Data and Comparison with Predictions," Shock and Vibration Bulletin 35, Part 7, pp 67-76, April 1966.
  - [9] S. Clevenson and R. Steiner, "Fatigue Life under Various Random Loading Spectra," Shock and Vibration Bulletin 35, Part 2, pp 21-31, January 1966.
  - [10] A. Curtis, J. Herrera and R. Witters, "Combined Broadband and Stepped Narrow-Band Random Vibration," Shock and Vibration Bulletin 35, Part 2, pp 33-47, January 1966.
  - [11] J. A. Kasuba, "A Realistic Derivation of a Laboratory Vibration Test to Simulate the Overland Transportation Environment," Shock and Vibration Bulletin 35, Part 5, pp 37-48, February 1966.
  - [12] R. Morse, "The Relationship Between a Logarithmically Swept Excitation and the Build-up of Steady-State Resonant Response," Shock and Vibration Bulletin 35, Part 2, pp 231 - 262, January 1966.
  - [13] W. Beecher, "Pitfalls in Random Simulation," Shock and Vibration Bulletin 34, Part 5, pp 1-14, February 1965.
  - [14] W. R. Forlifer, "Problems in Translating Environmental Data into a Test Specification," 1965 Institute of Environmental Sciences Proceedings, Page 185, April 1965.
  - [15] H. Katz and G. Waymon, "Utilizing In-Flight Vibration Data to Specify Design and Test Criteria for Equipment Mounted in Jet Aircraft," Shock and Vibration Bulletin 34, Part 4, pp 137-146, February 1965.
  - [16] Panel Discussion. "The Specification Problem," Shock and Vibration Bulletin 34, Part 4, pp 153-163, February 1965.
  - [17] J. Putukian, "Simulating Missile-Firing Acoustical Environment by Equivalent Mechanical Vibration," Shock and Vibration Bulletin 34, Part 5, pp 83-91, February 1965.
  - [18] L. Root, "Selection of Vibration Test Levels Using Fatigue Criteria," Shock and Vibration Bulletin 34, Part 5, pp 55-65, February 1965.
  - [19] A. Silver, "Problems in Adding Realism to Standard Specifications," Shock and Vibration Bulletin 34, Part 4, pp 133-136, February 1965.
  - [20] J. Callahan, "The Use of Mercury Data to Predict the Gemini Vibration Environment and Applications to the Gemini Vibration Control Program," Shock and Vibration Bulletin 33, Part 1, pp 15-33, February 1964.
  - [21] A. Curtis, "A Statistical Approach to Prediction of the Aircraft Flight Vibration Environment," Shock and Vibration Bulletin 33, Part 1, pp 1-14, February 1964.
  - [22] J. McClymonds and J. Ganoung, "Combined Analytical and Experimental Approach for Designing and Evaluating Structural Systems for Vibration Environments," Shock and Vibration Bulletin 34, Part 2, pp 159-175, December 1964.
  - [23] A. Sinkinson, "Designing Electronic Equipment for the Combined Random and Sinusoidal Vibration Environment," Shock and Vibration Bulletin 34, Part 2, pp 137-144, December 1964.
  - [24] K. W. Smith, "A Procedure for Translating Measured Vibration Environment into Laboratory Tests," The Shock and Vibration Bulletin No. 33, Part 3, Page 159, March 1964.
  - [25] E. Soboleski and J. N. Tait, "Correlation of Damage Potential of Dwell and Cycling Sinusoidal Vibration," Shock and Vibration Bulletin No. 33, Part 3, Page 113, March 1964.
  - [26] G. B. Booth, "Relationships Between Random Vibration Tests and the Field Environment," Shock and Vibration Bulletin No. 31, Part 2, Page 164, March 1963.
  - [27] S. H. Crandall and W. D. Marks, Random Vibration in Mechanical Systems, Academic Press. New York, 1963.

- [28] Panel Discussion, "The Relationship of Specification Requirements to the Real Environment," Shock and Vibration Bulletin No. 31, Part 2, Page 287, March 1963.
- [29] M. Vet, "Dwell-Sweep Correlation," 1963 Institute of Environmental Sciences Proceedings, Page 433, April 1963.
- [30] L. Marin and R. C. Kroeger, "A Preliminary Investigation of the Equivalence of Acoustics and Mechanical Vibrations," Shock and Vibration Bulletin No. 30, Part 4, Page 103, April 1963.
- [31] G. S. Mustin and E. D. Hoyt, "Theoretical and Practical Bases for Specifying a Transportation Vibration Test," Shock and Vibration Bulletin No. 30, Part 3, Page 122, February 1962.
- [32] M. Vet, "Study Program to Modify the Vibration Requirements of MIL-T-5422E and MIL-E-5272C," Collins Engineering Report 1552, May 1962.
- [33] L. T. Waterman, "Random Versus Sinusoidal Vibration Damage Levels," Shock and Vibration Bulletin No. 30, Part 4, Page 128, April 1962.
- [34] A. J. Curtis and H. T. Abstein, "An Investigation of Functional Failure Due to Random and Sinusoidal Vibration," WADC Technical Note 61-24, September 1961.
- [35] J. R. Fuller, "Cumulative Fatigue Damage Due to Variable-Cycle Loading," Shock and Vibration Bulletin No. 29, Part 4, Page 253, June 1961.
- [36] B. M. Hall and L. T. Waterman, "Correlation of Sinusoidal and Random Vibrations," Shock and Vibration Bulletin No. 29, Part 4, Page 218, June 1961.
- [37] C. M. Harris and C. E. Crede, Shock and Vibration Handbook, McGraw-Hill Book Company, 1961.
- [38] R. M. Mains, "Simulation of Shock and Vibration Environments," 1961 Institute of Environmental Sciences Proceedings, Page 39, April 1961.
- [39] J. Monroe, "A Problem of Sinusoidal versus Random Vibration," 1961 Institute of Environmental Sciences Proceedings, Page 571, April 1961.
- [40] Panel Session, "The Establishment of Test Levels from Field Data," Shock and Vibration Bulletin No. 29, Part 4, Page 359, June 1961.
- [41] H. R. Spence and H. N. Luhrs, "Structural Fatigue under Combined Random and Sinusoidal Vibration," Space Technology Laboratories Report BSD-TDR-62-8, November 1961.
- [42] G. B. Booth, "Sweep Random Vibration," 1960 Institute of Environmental Sciences Proceedings, Page 491, April 1960.
- [43] A. E. Galef, "A Quasi-Sinusoidal Vibration Test as a Substitute for Random-Vibration Testing," Shock and Vibration Bulletin No. 28, Part 4, Page 114, August 1960.
- [44] H. R. Spence, "Random-Sine Vibration Equivalence Tests on Missile Electronic Equipment," 1960 Institute of Environmental Sciences Proceedings, Page 501, April 1960.
- [45] E. L. Lunney and C. D. Crede, "The Establishment of Vibration and Shock Tests for Airborne Electronics," WADC Technical Report 57-75, January 1958.

#### DISCUSSION

Mr. Swanson (MTS Systems Corp): I found the presentation rather interesting to see the holy grail of equivalence being flashed before our eyes once more. I have seen this over a number of years. I have studied random load fatigue for sometime, and I think that one of the main areas of lack of realism in vibration testing is in this quest for equivalence. I was not quite sure which area of equivalence he

was referring to but he seemed to draw mainly on the area of fatigue. In fatigue the initiation, the propagation, the location, the sites of cracks, etc., all show one pattern if you test under constant amplitude conditions on even program constant amplitude conditions, but a different result with random amplitude. In fact, I have just finished a series of tests which show that repeating the same random cycle

over and over again, where it is a random cycle of fair length, results in an increase in the life by a factor of 3 or 4 over that using an infinite span, such as you would have with a noise generator. So I am just a bit worried that we should go down this path again. I think it is a mistake, and I would like to take the opposite side, and paraphrasing Patrick Henry, I do not agree with you - I am not even sure that I would stake my life on defending you.

Mr. Root: Well put - I am aware of many of these things and perhaps I stressed fatigue because there do seem to be more papers in this area and some of the results are quite good. One of the gentlemen at Collins did a study here about 3 years ago that compared the random, the sine dwell and the sine sweep, using both Palmgren-Minor and Corten-Dolan hypotheses, and obtained what we thought was excellent correlation. But again this was on simple models - aluminum cantilever beams - so there is an extrapolation to electronic equipment or any other type of equipment.

Mr. Swanson: The more you test Corten-Dolan, Palmgren-Minor, etc., the more you find its a matter of coincidence rather than equivalence.

Mr. Mutter (Boeing Company): I think one must consider, that the vibration experts can't come up with an equivalence for sine-random, and some of these other parameters. Often the designers are in worse shape than we are, so I think we need to investigate any possibility of a sine-random equivalence or any other equivalence to assist the designer who has less background than we do. He is trying to come up with a meaningful design on his hardware to survive in the environment to which his equipment will be subjected. So I don't think we can blindly say let's not go down that path again. I think we need to do what we can to try to help the designer in his efforts.

Mr. Beecher (Lear Siegler): I agree with the last speaker. I had a case to investigate random noise on a multidegree of freedom system. I spoke very briefly on this topic four years ago. I found that even if we partition random noise - say, if it is a 2000 Hz spectrum and we have a shaker that we do not want to overload, and we apply only 500 Hz at a time, breaking the spectrum up into three or four groups, we do not get the same response in the test item if you measure it with an accelerometer. I refer to a relatively simple test item such as a rectangular plate fixed at the edges. You do not get the same responses that you do if you apply the entire 2000 Hz random spec-

trum at once, let alone the question as to whether you can simulate that adequately with sine test. Again, I agree with the last speaker - the most useful application of equivalence is to give a designer some handle on his problem, rather than as a testing device.

Mr. Swanson: The whole idea of seeking equivalence, I believe, is implicit with the assumption that we are not able to generalize on random processes, and this is just not true any longer. Ten years ago it was true, but now one can generalize with PSD and RMS simulations. I honestly think that by using generalized random processes and harmonic analysis it is not necessary to go back to these deterministic signals when you have a problem that is vitally important and you should really simulate the proper environment, because you can generalize that environment.

Mr. Root: I believe you missed one of the key points that the random sine equivalence is only part of it. Now the accelerated testing is another major problem.

Mr. Verga (Hazeltine Corp.): Perhaps one of the most popular problems of equivalence in vibration is estimating from the levels in the field, the levels to be used in the test room. For instance, one finds resonances of a system and dwells with the prescribed test levels at those resonances. What happens many times - and this causes many arguments - is that a system has different chassis which have different resonances. If two of these chassis have resonances at frequencies within one Hz, then the best technician would just dwell at one resonance, for 1/2 hour, say. If on the other hand, the resonances of these two separate systems in the major system differed by as much as 2 or 3 Hz, then the technician would proceed by dwelling at say x frequency for 1/2 hour, and x +  $\delta f$  frequency for another 1/2 hour. This could be looked upon as simulating almost twice as much damage in that system. The specifications do not say anything as to how to separate one natural frequency from another. This might be one consideration to study.

Mr. Root: This is probably not a point that we will answer in the monograph but we certainly can try to tell you how to pick these sine dwell levels, so that they are more reasonable. Rather than measuring a level in the field, which is probably changing frequency, and then applying it as a dwell level there should be again an equivalence, providing it is sinusoidal in the field and a sine dwell. But as to the question of one resonance dwell versus

the two dwells at closely spaced frequencies, we can not answer that.

Mr. Gettle (TRW): The two people who suggested that finding equivalence would be a great boon for the designer seem to be implying that the designer knows exactly how to design for sinusoidal input and that random input is a terrible mystery to them. I submit that this is nonsense. He does not know how to design for sinusoidal. And he knows how to design for random as well as he knows how to design for sinusoidal.

Mr. Root: Probably the only point here is that he may have a larger backlog of experience with sinusoidal, and certainly, given time, he will be able to design as well to random from this experience.

Mr. Mutter: I guess I need some of his designers on my team. I think what the designer normally can do is convert the sine levels into an equivalent static load, and he does not have quite the same finesse in trying to convert the random environment to an equivalent static load.

**"PROVIDING REALISTIC VIBRATION TEST ENVIRONMENTS  
TO TACTICAL GUIDED MISSILES."**

K. R. Jackman\* and H. L. Holt\*\*  
General Dynamics  
Pomona, California

Emphasis has been placed, during the last several years in more realistic laboratory simulation of flight and ground-imposed environments on complete missiles or airplanes, and also at the component level. This is emphasized by the more-rigorous evaluation of flight instruments, as units, and as finally assembled at missile level, to environments reflected from flight telemetry and as imposed during ground handling. The intermediate or "section" level of testing experimental and tactical guided missiles has not received its just emphasis, as a quality-assurance tool to guarantee missile adequacy for service, for better reliability.

This paper provides descriptive information on functional and test capabilities of the environmental equipment for quality-assurance testing a medium-sized missile "section" assemblies at Pomona, California, as developed by General Dynamics, Pomona Division.

**BACKGROUND**

The design of a good environmental test program must be based on firmly established design requirements. Likewise, good engineering practice requires that prior to design release of the missile, assurance of satisfactory performance in the intended environment be demonstrated by laboratory tests.

A quick review will be made of test philosophies adopted over the last few years by most missile and aircraft companies in the United States, at least to some degree in early design stages.

George E. Padgett, Structural Dynamics specialist at General Dynamics/Pomona, contributed a valuable review of environmental test criteria in a paper<sup>1</sup> before the I.E.S. last April 1968 in St. Louis, Missouri. He clearly, and with examples, pointed out that the development of sound environmental design criteria and test requirements requires a definition of both the life history profile for an item, as well as the specific environmental conditions associated with each portion of the history profile. The life history profile includes all events from production of an item to end use, and can be divided readily into phases. Five such typical phases for a tactical guided missile may be:

1. Production and Assembly
2. Logistics
3. Tactical Storage
4. Ready Service
  - a. Captive Flight
  - b. Field Transportation and Handling, or
  - c. Shipboard
5. Free-Flight to Target Intercept.

Each of the above portions of the life of a missile may be influenced by a wide variety of environmental conditions, appearing singly or in combination, and depending upon the type of missile, service use, launch method, geographical area of use, and many other factors. Realistic test environments may include shock, vibration, acoustic noise, steady acceleration, temperature, humidity, pressure, solar radiation, salt fog, rain, hail, dust, sand and others. Padgett clearly pointed out that the relative importance, or damage potential, of each of these environments is different for each phase of the life history profile.

**REALISTIC VIBRATION TEST ENVIRONMENTS**

Since one of several vibration environments is usually critical on missile structure and delicate electronic equipment, for simplicity this environment

\*K. R. Jackman - Chief Technical Specialist, Advanced Technology Branch

\*\*H. L. Holt - Senior Design Engineer, Automatic Support Systems,  
General Dynamics, Pomona, California

will be considered on a typical "medium-sized" missile throughout this paper. The levels and durations for the same environmental category, such as vibration, may vary widely with the different phases of the life history profile. For instance, using a hypothetical air-launched guided missile as an example, the vibration levels encountered during the long-duration captive flight phase are usually much lower than those imposed during the shorter-duration free-flight phase and the frequency spectrum may differ significantly for the two phases. Another factor which must be considered is whether the item must function, have warhead-up power applied, or be turned off during the particular test phase. Padgett emphasized the need of considering test equipment capability in defining realistic environmental requirements. To assure adequate test requirements, the profile phase duration, the item operational requirements, and the associated environmental conditions must be considered; requiring the environmental specialist to work closely with the designer, system engineer, operations analyst and the test engineer.

This paper is divided into two sections. In the first, problems confronting a manufacturer of a radically-new experimental missile will be discussed, from early engineering to small-scale production, in the light of test requirements to prove adequacy and reliability of the design. The "pros" and "cons" of testing missiles at "section-level" and at all-up "missile round" level will be reviewed. Since "section-level" testing of missiles offer many advantages, the second part of this paper will illustrate how one missile manufacturer, General Dynamics at Pomona, California, uses temperature and vibration testing of missile "sections," on the production line, to Quality Control production.

#### HOW SHOULD MISSILE PARTS BE TESTED?

Here is a policy point on which there is no common denominator, either between companies, or in fact is there uniformity of test opinion within a given company. So as to review this test policy of "section" versus "round-level" evaluation in an unbiased manner, the author has collected some facts based upon his long experience in testing aircraft and missiles, together with thoughts of engineers and production men actively engaged in missile manufacture and flight testing.

#### "BANG" MISSILE BUILT BY THE NEW "HITTLE COMPANY"

Basic assumptions of policy, activity, and operation of this "Hittle Company" must be reviewed prior to analyzing their test-level potential. These are as follows:

1. Engineering Department of "Hittle Company" has developed this new design for the "Bang" missile.
2. They have accumulated a minimum quantity of flight environmental data from a few flights of "Launch Test Vehicles" (LTV's), and "Control Test Vehicles" (CTV's), with adequate telemetry test data.
3. Both budgets and manpower are somewhat limited, but adequate for the "Hittle Company" to produce "Bang" through engineering evaluation, prototype flight tests, "pilot line" production and into limited production of the "Bang" missile at medium production rate.
4. "Bang" is a "medium-sized" missile, capable of subdivision into 5 or 6 distinct "sections," each complete in function within itself and therefore capable of independent "section-level" tests.
5. Test requirements for the "Bang" missile are realistic, and clearly defined by the "customer" to the "Hittle Company," and by the flight-test analysts to the test engineers.
6. Communications and technical decisions are rapid and decisive between representatives of the prime contractor, the Hittle Company, their subcontractors, and the "customer."
7. Unfortunately, some conventional schedule slippages have occurred in early design, factory release, and even in production schedules of this young company.
8. The usual priority-definition problems exist in the Hittle Company, as in their competitors, and demand for early sections cause the usual problems in experimental engineering, production groups, and contracted flight obligations, due to very tight delivery schedules of "pilot" and "tactical" missiles.
9. Conventional design and engineering evaluation program schedule "over-runs" exist, such that the "contracted" test time is seriously shortened, with dwindled budget availability.
10. Fortunately, there are minimal changes by the "customer" in the "contract obligations" during the first years of the experimental engineering phase, in so far as test programs effects are concerned.



11. Production sampling and quality assurance tests on the "Bang" missile are specifically for product manufacturing, material and functional shop test control, and are not designed for engineering evaluation of incorporated "late changes." All major engineering redesigns, due to incompatibility of "interfaces" of sections, flight failures and corrections, and changes in "check-out" procedures, are evaluated by the repetition of engineering evaluation tests (EET), and possibly by a new design evaluation test (DET) for "customer" approval, either at the affected "section-level," or the total missile "round."

With the above operational characteristics of the "Hittle Company" and its "Bang" missile, it should now be possible to analyze the advantages and disadvantages of performing tests for engineering evaluation and for production control.

A. Engineering-Evaluation Tests and Parameter Confirmation (based on five (5) experimental items and fifty (50) in "pilot-line").

1. Missile "Round-Level" Tests

a. Advantages

- (1) Tests of final configuration, all-up missiles give total functional effects, with "interface" compatibility.
- (2) Fewer parameters to be measured in closed-system, hence tests are cheaper per specimen.
- (3) Specifications dictated by the customer are for the total assembled missile, and are therefore easily applied to test programs.
- (4) Confidence level, at missile level, is raised by overtesting in environments known realistically to exist.
- (5) The missile system is working, within boundary parameter tolerances, as a total functioning system, during the application of environmental extremes.
- (6) Assurance is developed by the missile passing the assembled-"round" test in environments. This also demonstrates "fly-away" operational capability, within the best of ground test methods.
- (7) Test equipment and test station costs, for a "single" test station, using assembled missiles, will probably be less expensive than providing a test station for each of several "sections."

b. Disadvantages

- (1) Full parametric evaluation, at "all-up missile" level, is difficult due to few external test points.
  - (2) Costly schedule delays and "crash" failure corrections will be caused by major failures during "round-level" testing late in an experimental development program; this may delay retrofits into pilot-line missiles.
  - (3) Usual and unavoidable engineering changes in the first few flight missiles, as the program develops, make early formal missile tests in all critical environments subject to expensive retests.
  - (4) The time delay in obtaining one to three complete missiles, for initial tests, can prove critical. The sample size is too limited, and the expense per missile is great. At least three (3) missile rounds are desirable for statistical evaluation but seldom more than one "all-up" missile is available, with few spare parts.
  - (5) If later production demands "section-level" testing to meet production schedules, early plans must be made to include this type of testing.
  - (6) Difficulty exists in selecting ground tests to duplicate critical service conditions and environments in all areas of missile. Tests might represent only "overall" conditions, and not critical parameters for some systems.
2. Missile "Section Level" Tests - Engineering Evaluation Phase
- a. Advantages
- (1) Individual test specimens of "sections" are much cheaper, as hardware, than the assembled missiles.
  - (2) "Section-level" hardware is easier to handle, smaller, and therefore easier to put through accurate environmental tests.

- (3) Evaluation tests are desirable at the "lowest indenture" level practical. Under normal conditions, and in some missile designs, the "section-level," each involving complete functioning systems, are the lowest entity breakdown capable of withstanding realistic application of specified environmental test requirements.
- (4) Because of early availability of "sections," it is desirable that responsible designers use this functioning level both without and with critical environments, to screen and confirm their designs, as breadboards, prior to final assembly of missiles.
- (5) Earlier availability of "sections" also permit early detection of faults, with consequent more rapid correction, and prevention of later more expensive retests.
- (6) For given critical "sections," more hardware can be tested, in short scheduled test periods, with more test data points, and therefore with greater confidence with early test results and in the final mission reliability.

b. Disadvantages

- (1) Interface integrity at "section-level," and practical interchangeability problems, cannot be determined by individual section tests.
- (2) Difficulty and lack of accurate transfer functions exist in extrapolating from known missile parameter requirements to "section-level" test parameters. Hence real danger unknowingly exist in "overtesting" or undertesting hardware.
- (3) Adequate test facilities are seldom available for "section-level" hardware, early in experimental and pilot-lot production, to duplicate critical environments in ground testing.
- (4) Functional and environmental tests, on all the "sections" of a missile round, are considerably more costly than when integrated into the final "all-up" missile. This

greater expense extends to duplication of test facilities to meet specific "section" parameters, more environmental test facilities to accommodate tight and overlapping test schedules, and more personnel to run the simultaneous testing on a carefully scheduled basis. However, multiple tests, of more than one section soaked in environment at one time, can reduce costs.

- (5) Proper long-term planning, for primary testing on the "section-level" policy, is considerably more costly and requires greater lead-time in planning, procurement, set-up, check-out and compatibility testing with hardware, than can usually be tolerated in urgent experimental missiles. Consequently, rapidly-conceived "jury-rigs," for testing early section adequacy, many times prove inadequate to meet final missile parameters, with resulting test and redesign and retest problems occurring late in experimental, and even in pilot-line, missiles.
- (6) Present day greater use of solid-state electronic circuitry, with resulting low-voltage power supplies, is prone to produce unrealistic parameters at "section-level" evaluation, since "overall" functions with the section "looking-into" realistic impedances and full-length cable harnesses are seldom accurately duplicated. This aspect of "open-loop" section-level testing, as compared with "close-loop" testing of missile round, must be faced as a early test policy decision in the program-planning and contract-signing stage, years before expected "pilot-line" runs, in order to have sufficient funds and test hardware "lead-time," and to provide adequate impedance matching between early "section-level" and later formal "round-level" hardware and tests.
- (7) Difficulty exists in contriving evaluation tests, even at the "section-level" functional systems, to affect all vital elements of the system in a manner expected in flight and service life. For this reason, adequate and realistic evaluation of all

parts, components, modules, and sub-section assemblies is expected, and vitally necessary, prior to all "section-level" test programs.

B. Production-Quality Assurance and Assessment  
(anticipating a small tactical missile contract at 75 missiles/month).

1. Missile "Round-Level" Tests

a. Advantages

- (1) Periodic missile test programs including Quality Assurance Environmental Test (QAET) and/or Periodic Conformance Inspection (PCI), Production Proofing, or MET is desirable at "round-level" to check manufacturing assembly parts, components, and instruments, and to detect any changes in material, workmanship and in fabrication on production tooling that may result in adverse changes in missile characteristics or lacking capability to meet realistic service functional and environmental requirements.
- (2) Only a few "critical" environments, applied at "round-level" singly, or in combined-environment tests, as determined minimum by D.E.T. and previous engineering evaluation tests, can be applied for overall functioning system appraisal. Limited parameter determinations, on the final tactical product will give functional and contractual assurance of adequacy prior to delivery to customer.
- (3) Production missile-level tests confirming effects of critical parameters with and without critical environments, and permitting early failure-diagnosis, correction, and retest, can be compared directly with initial engineering evaluation tests and "D.E.T." if test facilities and test techniques between Engineering and Production Laboratories are similar and compatible.
- (4) Periodic tests of production missile "round-level" hardware after "sell-off" and ready for delivery to customer and passing a minimum-acceptability level for adequate service life will give added statistical reliability and confidence in the design to the "too-small" engineering evaluation sampling.
- (5) Production missile "round-level" tests are far less costly than the more-complex multiple "section-level" tests, and highly desirable if production schedules will permit "periodic" withdrawal and subsequent delayed delivery schedules on several Q.A.E.T. missiles.
- (6) Adequate "product-proofing" at missile "round-level" with firm and final hardware using production c/o methods is necessary for "tolerances" determination at ambient and under critical environments. This produces a final check to compare to D.E.T. results prior to production missile manufacture and assures overall system adequacy determined by QAET review and realistic screening (without and with critical environment) at part, component, instrument, module, plate, and section levels.
- (7) Sometimes more confidence and higher reliability factors can be obtained by testing missile "rounds" through periodic engineering evaluation tests (EET) using the basic "DET" test facilities and experienced test personnel, thus providing a systematic review of parameters under critical environments which would not fall within the scope of a missile level QAET. Such tests, on previously approved facilities, insures compatibility of setups and direct comparison of test results.
- (8) Production-level tests on missile rounds to evaluate "simulation," "stimulation," and "operation" of

all deliverable missile hardware may be adequately determined by any or all of a series of techniques known as "P. L. I." (Pilot-Line-Inspection), "M. E. T." (Manufacturing Evaluation Test), "Q. A. E. T." (Quality Assurance Evaluation Test), and others described hereafter.

b. Disadvantages

- (1) Serious manufacturing or material problems "flagged" by production missile "round"-level periodic testing result in failure diagnosis, repair, and retest at "section-level" either on experimental (EET) section-test equipment or, if available, on production-type QAET section-test equipment. Dual tests, if critical failures are possible or anticipated at missile or "section-levels," are costly and cause serious production schedule slippages.
- (2) Hardware problems at the missile "round-level" usually occur in "tight" contractual flight delivery schedules in that QAET missiles with final checkout papers are scarce and a high priority must be maintained by the Quality Control Department over flight deliveries if continuous and periodic evaluation of production is maintained.
- (3) If customer control on the missile contractor is maintained in the production phase, by "lot-bonding" of groups of finished missiles and delay of delivery until "lot-sampling" missiles have passed the QAET, any failure on a missile affecting adversely a required critical parameter will require correction and retest until satisfactory results have been obtained. The programming and scheduling of this type of task must include consideration of the short time constant corrective action implementation which can result in economic inefficiencies and consequent undesirable personnel loading factors. Such action prevents the "crash" test program (3 shifts, round-the-clock, 7 days a week) which proves so costly in costs and schedules.

- (4) Production test policies at missile and section levels should be crystallized and actuated early in the experimental engineering phase (preferably during missile contract pre-design and contract-negotiation phases).

2. Missile "Section-Level" Tests -- Production Quality Assurance

a. Advantages

- (1) Production of a vitally-needed tactical missile even on an initially "small-scale" basis (say 75 missiles per month), requires test facilities at "section-level" to determine rapidly the "go-no-go" characteristics. With adequate lead-time and test budgets anticipated and approved such automated "QAET" test equipment can be ready on time to meet production hardware availability schedules for section uniformity and interchangeability control.
- (2) Since "section-level" sampling can be made earlier in production (shortly after "pilot-line" sections have been evaluated and produced with necessary engineering changes incorporated) and each section specimen is cheaper than the total missile, greater numbers of "sections" passing through "section-level" tests (QAET or engineering evaluated problem areas) give greater confidence to designers and customer, and provides a higher anticipated reliability statistical record.
- (3) The failure of one specimen, in a "lot-bonded" production "section-level" program, is easier to rectify than at missile "round-level." easier to retest if automated QAET test equipment is available, and quicker to release "lot" for final assembly of missiles. This makes a more-rapid return, at "section-level" sampling, to normal production schedules, even with intermittent failures and "bonded-lot" retests, than is normally possible at "missile-level."

b. Disadvantages

- (1) Quality Control by testing all sections, on a periodic basis, especially

if section-level lot bonding has been negotiated by the customer, in multiples of five or ten tests per section, and with probable failures and retests, is an expensive operation. The "pros" and "cons" of the need for elaborate, automated "section-level" test facilities, times the number of different sections tested, should be evaluated carefully with the customer early in the contract phase of the engineering experimental contract — and balanced against the high expenditures necessary over a two-year lead time prior to the availability of the first QAET section hardware.

- (2) The implementation of an environmental assessment program such as QAET, involving "section level" tests requires that automatic section level test equipment, adapted for environmental testing, be planned, developed and delivered prior to program execution. Such test instrumentation must be designed to provide adequate correlation with that test equipment used in RDT and EET test phases, thus permitting the correlation of hardware failures in QAET with an in-depth data base established in the R&D and Pilot phases. Failure to adhere to this type of planning can only result in unnecessarily high production costs as the QAET program is initiated with its last minute "jury-rigged" or "borrowed" EET-type equipment. In many instances, several years of advance thought and planning is necessary to provide adequate automated test equipment.
- (3) Missile "section-level" tests, planned on automated "go-no-go" basis, requires relatively large factory floor areas, near the missile "check-out" production area, for the many pieces of test equipment required in functional and environmental evaluation tests on all sections. Such an area, in a vital production location, much exceeds such a QAET area at missile "round-level." The cost of this large test area, together with more "section-level" test equipment, more environmental test facilities, and more manpower

for QAET, makes this program costly but very desirable for control of production missiles.

#### DEFINITIONS OF TEST CONTROLLING MISSILE INTEGRITY AND FUNCTION

Several types of tests have been referred to above; i.e., "DET," "QAET," etc. These may have different meanings to various readers. To avoid confusion, simple (and possibly too limiting) definitions are given in the Appendixes I and II.

Fig. 1 shows the correlation of various tests required in the engineering and production phases of a weapon system. A distinction between the development and evaluation tests has been noted.

#### RESULTS OF ENGINEERING SURVEYS MADE BY THE "HITTLE COMPANY" ON THE "BANG" MISSILE

Fortunately, the engineering management of the "Hittle Company" in early contract negotiations and engineering pre-design phases, on their medium-sized "Bang" missile, had covered wisely the problem of how much testing to provide in engineering evaluation and in production quality control. Their Engineering Manager, Dr. Van Brown, when faced with this perplexing problem of missile "round-level" versus "section-level" test control, with all the possible "pros" and "cons" made a wise decision. In evaluating the budget situation faced by his "Bang" missile Project Office, at the time of contract negotiation budget talks with the customer, Dr. Brown recommended that an Engineering Consultant, with good missile test experience be located and interviewed for a four-month consulting contract, to recommend the best contract test policies for this particular missile program.

Fortunately, too, the Engineering Manager met Dr. Ken Smith, formerly with several aircraft and missile companies in responsible positions, and most recently affiliated as "Chief of Laboratories" at the "Belair Division" of the Bolling Company, on the "Killer" aerial torpedo and "terminal" missile programs for several U.S. Government services. Military security prohibits comment on these two uniquely successful weapon programs, except to say that the "Belair Division" management reflected to the "Hittle Company" President J. D. Jones and to its customer full confidence in Dr. K. Smith as a competent consultant in missile test policies and program analyses, and added, as a footnote, that both the "Killer" and "Terminal" weapon programs owed much of their success, to Dr. Smith's forward-looking policies, during each contract-negotiation phase, in his analyses in follow up contracts, and test programs successfully completed, both in engineering evaluation and QAET production control. They pointed to his active participation, two-years previous to his retirement, in the "Penetrator"

weapon program, of the Fort Worth Division of MacDonald Company, in the test programs of this vehicle, now gaining so much national publicity on several "War" fronts.

Dr. K. Smith joined the Hittle Company, in their prime Red River Division, Phoenix, Arizona, three years ago, as consultant, and, in his six month stay with them, laid the foundation of a test program in engineering and production, which has been followed closely by the Hittle Company management ever since. Mr. J. Doe Jones, President of the Red River Division, Hittle Company, in a recent interview given to this writer, relative to the phenomenal reliability and target acquisition/kill record, stacked up in the last year on our "Eastern Front" skirmishes, stated - "I can truthfully say, that had we not been fortunate in locating a consultant with Dr. Smith's missile design and test background in 1965, and had the Hittle Company not followed fully his experienced leadership in the "Bang" Missile policies, especially in his proposed evaluation and production control test programs from 1965 to date, I doubt seriously whether the "Bang" missile would today be enjoying such success and with such commendations from our U.S. contractor".

#### REVIEW OF DR. K. SMITH'S TEST PROGRAM ON THE HITTLE COMPANY "BANG" MISSILE

Your writer followed up President J. D. Jones' statement of several months ago, relative to the Hittle Company consultant's prime part in the "Bang" missile test program, by an interview with Dr. K. Smith in his Southern California home, following his recent return from a year of aircraft consulting in Japan.

Dr. K. Smith, in reviewing his recommended test policies of 1965 on the "Hittle Company" "Bang" missile program, indicated that the early budget problems, in the engineering and experimental phases of "Bang" made adequate testing plans appear questionable. However, he reviewed the desirability of running comprehensive test programs on the "Bang" missile, first at all lower indenture test levels, then exhaustively at the "section" and missile round-levels", both in engineering evaluation and later in production quality control, with the Hittle Company and with the U. S. Government contractor. He was provided the needed extra funds to promise completion. Before he left Hittle's Red River Division 2 1/2 years ago, President Jones and the contractor had settled on a budget of \$730,000 for all E.E.T. and D.E.T. programs, exclusive of the specimen costs, and over \$1,432,000 for all production type tests, both "section" and "missile round"-levels. Of this production figure, over \$67,000 was advanced on a two-year instrumentation program in which the Hittle Company's "Bang" test equipment section was to design and build two complete sets of factory "section"-

level test equipment. These "section" testers were developed in close coordination between the Hittle Company and General Dynamics, at Pomona, California. In fact, the General Dynamics Pomona Division QAET section-level tester, here after discussed, is very similar to testers used at Red River, Phoenix, Arizona on the "Bang" missile sections.

Dr. K. Smith proved very helpful to this writer with facts gathered in 1966 on missile level test policies. The advantages and disadvantages to "round" and "section" tests, previously listed, were from Dr. Smith's report to the Hittle Company. He had come to the conclusion that both "round" and "section" level testing was necessary in production on the "Bang" missile to maintain their production rate of 75 missiles per month. Other missile designs, differing widely in end-uses and parameters, might not need both systems. He added - "If a given system is designed so that the major sub-system interfaces are also functional interfaces; in particular if all guidance "RF" is contained in a single subsystem (section) then system level testing (round-level) is not nearly so important. If, in addition to the above, the design carefully considers sub-system (section) testing; i.e., low impedance outputs, etc. - then the system (round-level) test can theoretically be discarded. Recognizing, however, that such a design is rather "Utopian", I feel that a system (overall missile) test is necessary at least to demonstrate that plugs have been properly connected".

Dr. Smith then added - "There are two reasons why I use the word "Utopian" - first, it is virtually impossible to get hardware to exactly implement the desired equations, and second, it is often too expensive to completely define system requirements and interfaces".

#### REFLECTIONS ON DR. K. SMITH'S OBSERVATIONS

Obviously the "flight-of-fancy" by your authors into "never-never" land, with fictitious characters and places, can do two things for the engineer; - one, talk about a "dream-world" where experiences are received "afresh," pre-conceived notions and out-moded specifications do not exist, and where managements can make unlimited decisions - unlimited by budgets, schedules, etc., - and two, a positive, forward looking company, like the "Hittle Co.," of Phoenix, Arizona, under the able guidance of President J. D. Jones and Consultant Dr. K. Smith, can think "out-loud" some of each engineers' dreams.

Coming back to earth again, the reader has every right to ask "so what?" to the pages of "pros" and "cons" gathered from Dr. K. Smith on missile "round" versus "section-level" tests. "When?", the interested reader might add - "does Pomona Division of General Dynamics recommend - and why?" General Dynamics actually uses both tests at Pomona, to differing

degrees on different missiles - both in engineering and production. But this has been, primarily, a decision of the involved project office, and for many reasons not capable of review in this paper.

The point to be emphasized is that the reader, if faced with this decision on his program, must review all facts based on the characteristics of his specific missile, its flight objectives, method of launch, storage provisions prior to launch, operational area of use and its climatic environments and many other parameters. He can then select "pros" and "cons" similar to those above, and make his decision. Or he can employ a consultant, like Dr. K. Smith, to prepare facts for him.

The very fact that circumstances at the Hittle Company and at General Dynamics, Pomona Division appeared very similar on their respective missiles, and that each company, quite independently, had surveyed their test needs, and had come to similar conclusions - to perform production QAET control using automated "go" - "no-go" section-level test equipment with test results recorded on magnetic tape, made it desirable for the writer to review the "QAET" test program with Mr. Herb Holt, Senior Design Engineer at General Dynamics, at Pomona, California. He has been responsible for much of the "section level" test equipment and environmental facilities assembled along a 200 ft. stretch of production area in Building #2, Pomona. With Herb's help we will saunter along this unsecured QAET area, and look carefully at each tester, via photographs, of one of the first such automated test lines in the USA.

#### SECTION QAET AT GENERAL DYNAMICS, POMONA, CALIFORNIA

The basic missile "section-test" set will be briefly described in the adjacent photographs, counterparts of the color slides to be used in the short presentation in Anaheim.

This facility includes a specially-designed R. F. dark room accommodating an electro-magnetic shaker, provisions for temperature environments, and the necessary test fixtures for testing missile sections over the extended vibration range.

A second shaker system exists, external to the darkroom, which is time-shared with the darkroom shaker, for those missile sections that do not need the R.F. environment.

The station and equipment is completely automated and programmed for testing missile sections from magnetic tape, except that the temperature equipment is stabilized at the condition desired. All measured parametric values are composed and recorded with accepted tolerance limits for the specific action. "Accept" - "Reject" of specific parameters

are noted by means of "green" - "red" lights and printed-out for additional detailed analysis and reference.

The test results obtained from this realistic vibration environment, in the Pomona QA laboratories, when combined with a combined high/low temperature, air-conditioning servo unit and environmental chamber, will be discussed as permitted by Security and proprietary limitations.

Figure 1 takes the reader into the QAET area of Building #2. Here we will visit new environmental test facilities and various testers of several sections of a possible now in production. This general factory area, located alongside a wide access aisle, shows the "R.F." shielded "dark room" to the right rear, and in the foreground the high and low temperature chamber servicing the "RF" darkroom through elephant-trunk flexible ducting. Environments of -40°F to +250°F can be provided at inlet to the "RF" dark room. A 4000 force-pound vibration head is mounted at center of the dark room as will be seen later. Figure 3 shows some of the operational status wall-charts used in the "QAET" area. The TE 5700 charts shown, carry a daily status of each test station - whether it is "active," "in calibration" cycle, or "in repair." Sections for test are delivered to the "QAET" area on pallets, shown in the left of Figure 3. As much as practical, all wiring between testers and to plant electric-power sources are run overhead, as shown.

Figure 4 gives an overall view of the QAET area. Along the main aisle, permitting easy access and rapid delivery of test "sections," are located a group of test facilities and special testers, designed and manufactured by General Dynamics, at Pomona, California over the last two years specifically for the present missile "section-level" production quality control effort. Shown in the photograph, on the right, is one of two 4000# Unholtz-Dickie vibration facilities used in this "QAET" control effort. This is a Model #506A shaker, supported on a base common with an oil-slide table and separated from the cement plant floor by an "isolator/leveler" built by the Barry Control Company. In center foreground is the "micro-wave source" which feeds all facilities evaluating the "fuse-shroud" and ordnance sections. Just visible on the left foreground is the checkout station, at ambient conditioning for the test section. In the center background is shown the checkout programming equipment.

Possibly at this point sketches of the QAET station ground-plan might be helpful in orientating test equipment and to indicate what thought was given by Herb Holt and the QAET testing crew to advantageous positioning of all testers for minimum walking during test control, maximum overall visibility at all times, and efficient placement to provide minimum lengths of cables, "RF" plumbing, and monitoring leads to



give minimum power losses. Figure 5 shows a simplified floor plan of this QAET area.

FIGURES 6, 7, 8.

Several sectionalized views of the more complicated testers are given in Figures 6 and 7. Figure 6 indicates the vibrator supporting a "guidance" section, with nose-cone, vertically during test, so as to "boresight" at all times on the microwave horn on the compartment ceiling. This alignment must be maintained within  $1/10^\circ$  of original setup, even during vibration. Figure 7 shows the method by which several "fuse-shrouds" may be "soaked" in the temperature chamber prior to retesting. Figure 8 shows details of the 4000 lb. Unholtz-Dickie shaker (Model 506A) on its seismic mass.

Figure 9 indicates the "HI/Lo" temperature environmental test chamber ( $-100^\circ$  to  $+300^\circ$ F), with facilities for dehumidification installed. One "section" may be installed for "operation" under the temperature environment, or six "sections" soaked simultaneously during "non-operating" (as in figure 7).

Figure 10 shows an external view of the "R/F" dark room" with one main door open, showing R/F absorptive wedges installed. In the left foreground is the remote air-conditioning chamber, with ducts attached to the manifold enclosing the specimen. This air-manifold is insulated with polyurethane foam. After the specimen has stabilized in temperature, sitting upright on the 400# Unholtz-Dickie shaker within the "RF" darkroom, the external shrouding enclosure is removed for all "RF" tests. (See Figure 6.)

Figure 11 shows this same "RF" dark room, from the operator/access side, with the nose cone of the missile guidance section protruding through the absorptive wedges. Note the complete "RF" shrouding within the chamber upon closure of the front doors. Below the removable pyramid insulation, which is glued to plywood, can be seen from the shaker. A portion of the air-conditioning air manifold is seen below the insulation deck. The false floor can be removed in portions to give access for attaching or servicing the missile section.

Figure 12 is a unique low-angle camera shot to show the guidance section in position on the shaker, and at the same time to see the "RF" horns in the ceiling. During vibration, the "RF" beam input from the ceiling horn array must maintain a "boresight" angular adjustment within very close limits. This shaker base also employs a Barry air servo for automatic leveling and vibration isolation. Tight specifications, given the Unholtz-Dickie Corporation at time of purchase of this 4000# shaker, demanded

that during vibration the "guidance section" be boresighted on one of the horns within  $1/10^\circ$  degree. This operating feature has been demonstrated well within specification limits. A section of the "RF" floor has been removed to allow the reader to see the specimen. All floor sections must be in place and both doors closed tight, to obtain maximum "free-field" absorption.

Figure 13 illustrates the control console Model #MA-690 for the 4000# shakers, operated on each shaker sequentially. Thus good program planning is necessary on test specimens occupying the two shakers, to permit rapid progress of QAET specimens. This console controls sinusoidal vibration, as shown. However, random vibration is used in testing some "sections," and this equipment is to the right, just out of the picture (also indicated in Figure 5). The Unholtz-Dickie vibration system, consisting of shaker and console is known as Model #690A-40. The shaker in the "RF" dark room accommodates the guidance nose-cone section shown or a steel vertical pipe fixture on which the TLM-dorsal fin is attached. All other sections are tested on the shaker mentioned in Figures 4 and 8 outside the dark room. The vibration control console may be manually operated. All vibration levels are pre-set, prior to automatic programming. Remote programming can be made of sine vibration, sine sweep, and random tests of various distributions. Vibration tests are incorporated in the missile QAET "section-level" plan which provides automatic test programming and data retrieval.

Figure 14 shows the alternate shaker assembly on which missile sections are not requiring "RF" inputs are tested in the vertical position as shown, and in the horizontal position by gimballing the shaker and exciting the section on an oil-slide table. This shaker suspension system also employs the Barry air-servo leveler for isolation. Both sine and random tests are conducted on this shaker system.

Figure 15 shows the tester which performs functional checkout of an "autopilot/battery" section on a modified Scorsby table, under ambient conditions only. Such a test is performed before and after subjecting the "section" specimen to other environments.

Figure 16 is the electronic "heart" of the QAET test facility. This 8-1/2 bay electronic console comprises the "missile section test set." The unit is a completely automated electronic system for missile "section" testing, as well as incorporating capabilities of testing a complete missile assembly ("round"). It provides all required missile stimulus and parameter monitoring for "RF" dark room testing of specific sections and the remaining sections external to the "RF" dark room. This unit provides automatic test programming, comparison of acceptable test tolerances on all measured parameters and incorporates three methods of data retrieval; punched tape, magnetic tape and typewriter print-out.



Output test data obtained from the "section test set" of Figure 15 includes test specimen type, serial number, date, time, and test station number. Data retrieval also covers such items as individual parameter identification number, actual parametric value and acceptance status ("Go" - "No-Go") at test termination, this unit indicates an "accept/reject" condition of test specimen.

Figure 17 shows one end of the production temperature environmental test facility, capable of -50°F to +180°F imposed on an entire missile "round," to both "operating" and "non-operating" test conditions.

Figure 18 takes a side view of this same chamber, showing side and end access doors. The control console and programmer is seen at the right, where additional monitoring of "section" or "missile" specimen's critical parameters take place during the temperature environment. It will be noted that this chamber is serviced through the full-opening end door by a monorail, a segment of which swings aside to permit the door to close. With the aid of this monorail, better shown in Figure 12 with its tracking switch, a complete all-up missile "round," supported on two chain-hoists can be pushed into the temperature chamber. This box will accommodate missiles up to 20 feet in length, with tail surfaces in place.

#### QAET CONTROL

By means of the test station "operational status" charts, shown in Figure 3, and similar "QAET" status charts posted daily for information and review, a close watch is maintained on all of the five "sections" built and assembled locally on this medium-sized missile. Five samples each, of each month's production, are selected at random, of the "steering control," "fuse-shroud," "guidance," "autopilot/battery," and "TLM/dorsal" sections. Each section is then subjected to a similar QAET procedure, as follows:

1. Five "repeatability" tests (initial satisfactory performance) (ISP).
2. Low temperature test
  - a. Non-operating (storage condition)
  - b. Operating (service and flight)
3. Post-Low-temperature test - at ambient.
4. High temperature tests
  - a. Non-operating (storage condition)
  - b. Operating (service and flight)
5. Post Hi-temperature test - at ambient.
6. Sinusoidal or random vibration - (critical flight condition)
7. Final satisfactory performance tests (F.S.P.) - ambient.

In the QAET vibration phase, the random vibration distribution is based on the flight requirements of that specific section, as determined from previous flight telemetered test results.

With one QAET "missile section test set," with accessory environmental chambers and testers, indicated in Figures 2 to 18, and two such "MSTS" located at the end of the production line to provide "shake, rattles, and roll" under ambient plant conditions, the missile production is adequately controlled.

With "lot-bonding" at section-level, and section "sell-off" to the customer, maintained on a monthly basis, it is obvious that the five samples of each section must be capable of test completion each month. In fact, on a two-shift QAET operation basis, scheduling one missile section through the test sequences indicated above, in the three critical environments, takes one week with only 50 percent utilization of the station. In practice, however, simultaneous scheduling of two different sections through the station is maintained on two shifts, making possible the quality approval of five sections per month, with approximately two weeks allowed for failure diagnosis (F.D.), corrective action (CA), and retests, with a 50 percent reserve available for special "screening" tests. The third shift is reserved for test equipment maintenance and calibration.

#### PRODUCTION TESTING AND INTEGRITY CONTROL

To this point, the writer has described the QAET efforts of General Dynamics at Pomona, California primarily at "section"-level testing. However, another equally important test effort goes on simultaneously with Quality Control, and that is the production testing of "sections," made prior to "sell-off" to the customer. The sections are then mated into missile "round" level, indicating the interchangeability of "sections," and again tested by the "MST" or "MRFT" route. Appendices I and II are included to attempt to differentiate between various tests by definitions current vogue at General Dynamics Pomona Division.

Now moving into the production test areas, which is physically located along the same aisle in the main production building in Pomona, adjacent to the QAET area for convenience, we come upon a group of "testers," operating at factory ambient conditions. These "shake-rattle and roll" testers are primarily vibration facilities with parameter monitoring stations individually adapted for each missile "section."

Figure 19 gives an over "in-station" view of this "production factory missile section test set." In the foreground, to the right, are mechanical-vibrator facilities, for "autopilot" and "steering control" (tail) sections, and behind these stands, is the "autopilot" section "check-out" station, with its Scorsby table. On the left, in the foreground, is seen the mechanical vibrator on which the "fuse" and "guidance" sections can be shaken to identify and correct minor shop manufacturing problems, such as imperfect soldered or welded joints, loose wires, or improper assembly. Servicing all these stations, is the central

"programmer-monitor," in right background. This test station is identical to that used in the QAET test area, thereby providing compatibility of tests.

Figure 20 gives a close up of the steering-control section on its mechanical shaker on right, the autopilot section on its shaker in the center, and another autopilot section in ambient checkout on the Scorsby table on left. The two mechanical shakers are identical, and apply a 5 G. vibration at 32 cps. Tuned to this 32 cps resonance is a "knocker" visible under base to which each section is mounted. At resonance, this "knocker" provides a 20 G. shock pulse on specimen base measured in range from 50 to 3000 cps.

It will be noted in Figure 20, that the tail surfaces on the "steering-control" section on right are simulated by four "wheel-weights" on shafts. This was the test setup used approximately six months ago. However, on careful analysis of dynamic characteristics of the weights it became evident that the torsional compliance of this simulation did not resemble the tail surfaces. Figure 21 shows a similar vibration test on a "steering-control" section using the actual four wing surfaces. Here is another case where realistic environments were known but the "ground test" simulation failed to duplicate the exact conditions experienced by the missile in dynamic flight.

Figure 22 shows a close-up of the "knocker" on the autopilot section base, by which 20 G. shocks are generated at full-range frequencies. This "knocker" is carefully tuned by adjustment of the center nut.

Figure 23 shows the "guidance" section in place, within the "RF" dark room, on another mechanical shaker identical to those described above.

#### QAET CONTROL OF SMALL MISSILE

Figures 24 and 25 show two views of automatic test equipment, designed and built by General Dynamics, at Pomona, California to QAET control a small missile in production. In Figure 24 center is the vibration test facility which induces several motions simultaneously to the "guidance" section of a small missile. This missile spins during flight to maintain stability, therefore this tester also causes the "guidance" section to spin during QAET ambient checkout. The table top performs the function of a "rate-table" by rotating slowly during test. A vibrator is built into this tester to induce random vibration in the spinning specimen. All operations of this test table are induced from the master control panel to the left of Figure 24. It is interesting to note in this vibration test facility, emphasis has been placed upon realistic environment duplication in this QAET ground testing. Without disclosing any classified parameters on this small missile during

QAET testing, sufficient it is to say that this "combined-environment" table, can impose a "fixed frequency" vibration of 20 G. acceleration at 20 cps at an angle to the longitudinal axis of the "guidance package," and simultaneously there is applied a "superimposed" vibration of 2-1/2 G. rms "random" acceleration, from 50 to 1600 cps. ("flat" distribution). Thus Pomona Division of General Dynamics engineers attempted to realistically duplicate the most critical flight environments. Flight results from hundreds of firings made by this missile to date without one failure attributable to insufficient vibration QAET testing, indicate that the ground tests probably duplicate flight conditions closely.

In Figure 25 are shown two temperature environment tables; low temperature on left, and high temperature in center of photograph. These temperatures of the shrouded, spinning guidance sections, are closely controlled within 2°F. All missile functions on all three test tables are recorded on the master control panel.

#### CONCLUSIONS

Generalized evidence of the most beneficial method of quality controlling a missile in production is not possible, since the decision to test at "section" -level or at missile- "round" level will depend upon many factors. Both test methods must be used to some extent to produce maximum dependability. The advantages and disadvantages of both "section" and "round" levels have been presented to aid the reader in accessing his particular design, both in experimental engineering and production phases.

The new automatic "Go" - "No-Go" test equipment with records, developed at General Dynamics, Pomona, for a medium-size, and a small-size missile, has been described in detail as an adequate method of controlling "sections," both in QAET and production tests.

Finally, evidence is presented that General Dynamics has emphasized realistic environments, in these "section" -level tests, especially the application of realistic random vibration to the specimens. Only by duplicating in ground tests, on missile sections, those critical environments seen by the missile in service, can one be assured that missile reliability exists and that the target objective can be attained.

## BIBLIOGRAPHY

1. "Formulation of Realistic Environmental Test Criteria for Tactical Guided Missiles," - by George E. Padgett, General Dynamics, Pomona Division, Pomona California. pp. 441-448, Institute of Environmental Sciences - 1968 "Proceedings," as presented in session "Instrumentation - Now and Future," at 14th Annual Technical Meeting, April 29, 1968, at Chase-Park Plaza Hotel, Saint Louis, Missouri.
2. "New Development in Servo Accelerometers," by Dr. Earl D. Jacobs, Inertial Instruments Division, Endevco Corp., Santa Ana, California pp. 517-523, I.E.S. - 1968 "Proceedings," as presented in Saint Louis, Missouri, as in (1) above.
3. "Controlled Environments For Biological Research," by Guy C. Mattson, The Dow Chemical Co., Midland, Michigan (Dow Biohazards Dept.), pp. 539-542, I.E.S. - 1968 "Proceedings," as presented in Saint Louis, Missouri, as in (1) above.
4. "EMI - The Newest Environment," - by Carl Swenson, Central Electromagnetic Compatibility Group, Aerospace Division, Honeywell Inc., pp. 111-114, I.E.S. - 1968 "Proceedings," as presented in Saint Louis, Missouri, as in (1) above.
5. "Considerations in Revision of Army Climate Criteria," - by Arthur V. Dodd, Geographer, Military Applications Division, Earth Sciences Laboratory, U.S. Army Natick Labs., pp. 571-575, I.E.S. - 1968 "Proceedings," as presented in Saint Louis, Missouri, as in (1) above.
6. "Cross-Axis 'G' Control in Instrument Linear Vibration," - by Kenneth R. Jackman, General Dynamics, Pomona Division, Pomona, California Reprint of presentation at the "1965 Annual Technical Meeting," of the Institute of Environmental Sciences, "at Chicago, Illinois on April 29, 1965 and printed in I.E.S. "1965 Proceedings," pp. 369-385.
7. "Cross-Axis Vibration Test Facility Evaluation," by K. R. Jackman, General Dynamics, Pomona Division, Pomona, California as presented at U.S. Department of Commerce Trade Exposition, U.S. Trade Center, London, England, on Sept. 19, 1967.
8. "Micro-Inch Deflections and Flight Instrument Tests," by K. R. Jackman, U.S. Lecturer, as presented as slide lectures in seven European countries, Sept. 6-21, 1967. (Copies of "Abstract" available from author - no written paper.)

RESEARCH	DEVELOPMENT		ENVIRONMENTAL		EVALUATION		RELIABILITY	
	CONCEPTUAL PHASE	MATHEMATICAL MODEL	DEVELOP	CONDUCT	FLIGHT FIELD DEVELOP	CONDUCT	DEVELOP	CONDUCT
ENGINEERING	PROJECT DEFINITION PHASE	MOCKUP MODEL	ANTICIPATED OPERATING ENVIRONMENTS		BROAD PRELIMINARY PERFORMANCE REQUIREMENTS		TENTATIVE RELIABILITY REQUIREMENTS	
	DEVELOPMENT PHASE	BREADBOARD MODEL	PERIODIC ENVIRONMENTAL TEST PLAN	BREADBOARD AND STRUCTURAL TESTS	FLIGHT TEST PLAN		RELIABILITY PROGRAM PLAN	
		EXPERIMENTAL MODEL		COMPONENT, SUBSYSTEM AND SYSTEM TESTS		INITIAL FLIGHT TESTS		
		DEVELOPMENTAL MODEL		COMPLETE ENVIRONMENTAL TEST AND DESIGN QUALIFICATION		FLIGHT TESTS FOR DATA AND TO PROVE DESIGN		REPEATABILITY AND ENVIRONMENTAL TESTING
	PRODUCIBILITY EVALUATION PHASE	SERVICE TEST MODEL		FURTHER ENVIRONMENTAL TESTS		FIELD FLIGHT TEST UNDER SERVICE CONDITIONS		RELIABILITY TESTING
PRODUCTION	PRODUCTION ENGINEERING PHASE	PROTOTYPE (PRE-PROD) MODEL		QUALIFY PRODUCTION PROCESSES REQUALIFICATION AS REQUIRED		SERVICE FIELD FLIGHT TESTS TO EVALUATE PRODUCTION HARDWARE AND FOR TACTICAL TRAINING		RELIABILITY DEMONSTRATION THROUGHOUT PRODUCTION
	PRODUCTION PHASE	PRODUCTION MODEL		REQUALIFICATION OF CHANGES AND PERIODIC TESTS				

Figure 1. Correlation of Test Sequence and Functions (Typical Development/Production Program - Weapon System).

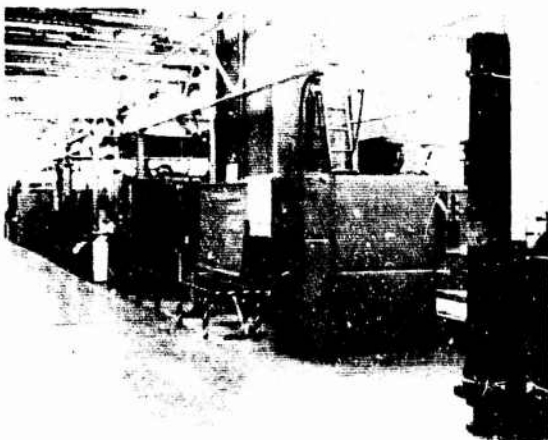


Figure 2. QAET Area of Production Factory.

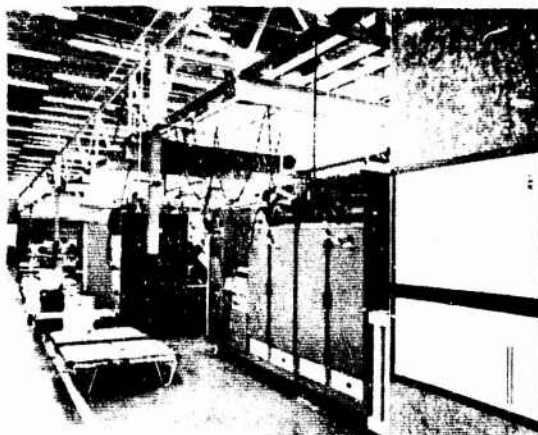


Figure 3. QAET "Operational Status" Control Charts.

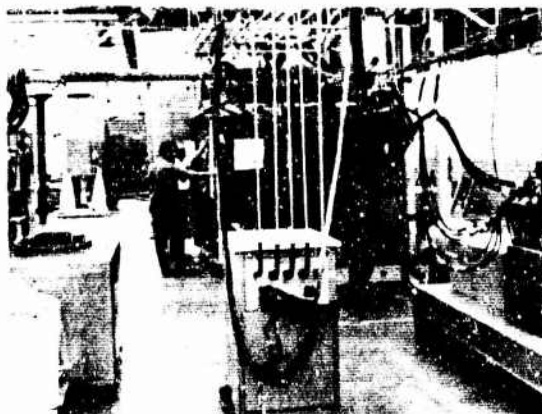


Figure 4. Operational View or Section-Level Testers.

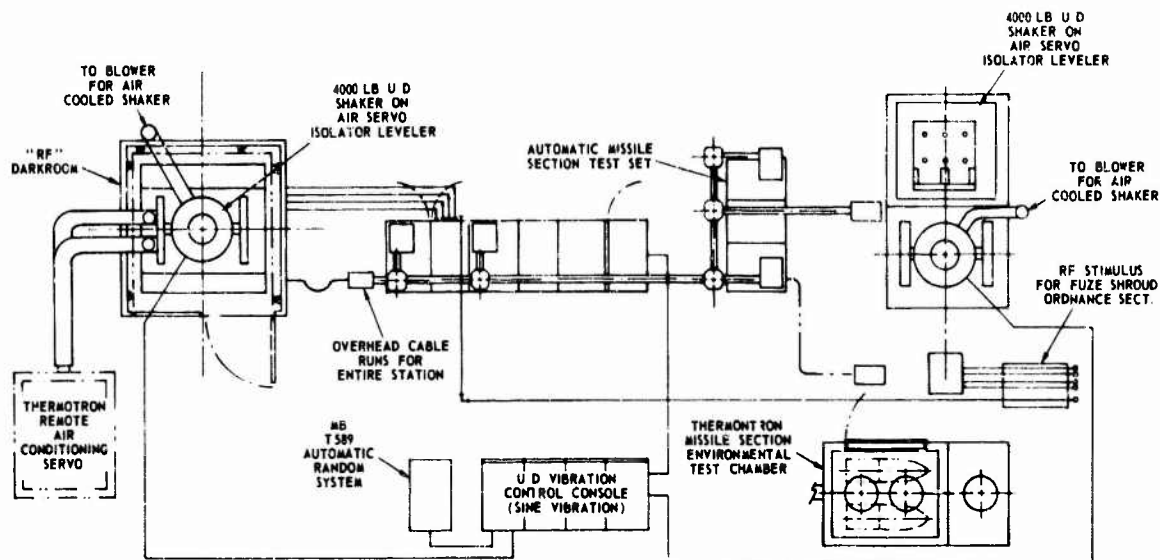


Figure 5. Floor Plan - Missile "Section-Level" Test Facilities (QAET Program).

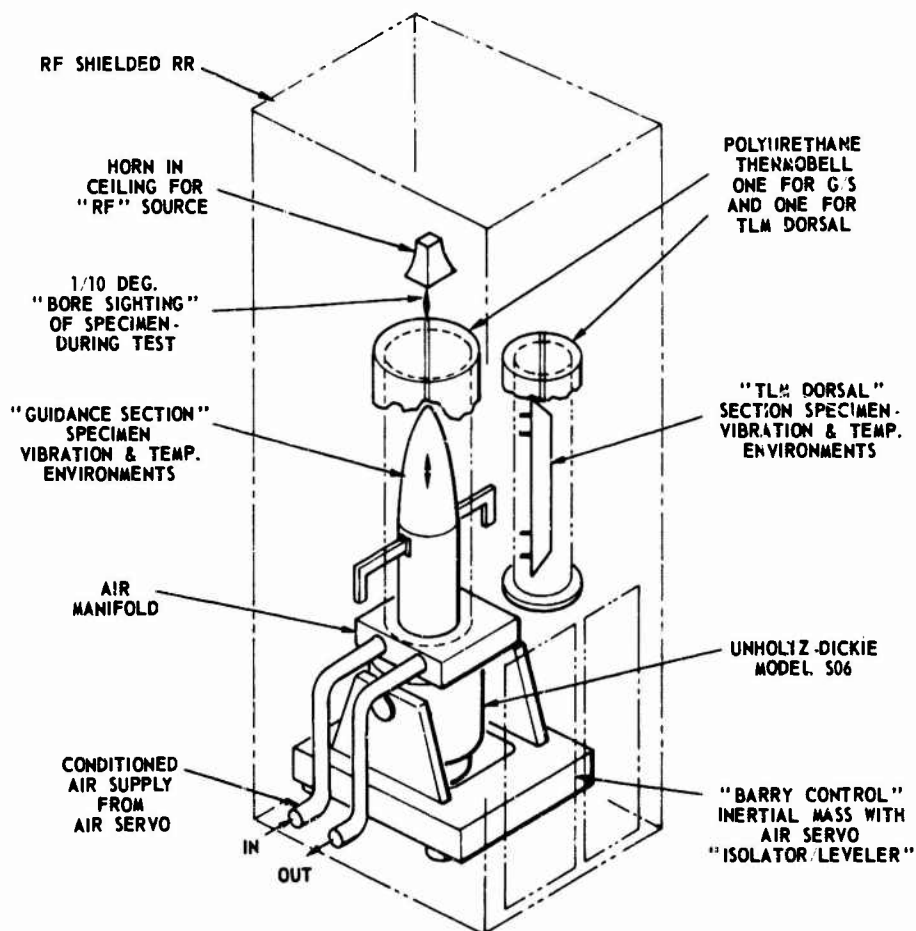


Figure 6. "RF" Darkroom - Vibration Facility (QAET Program).

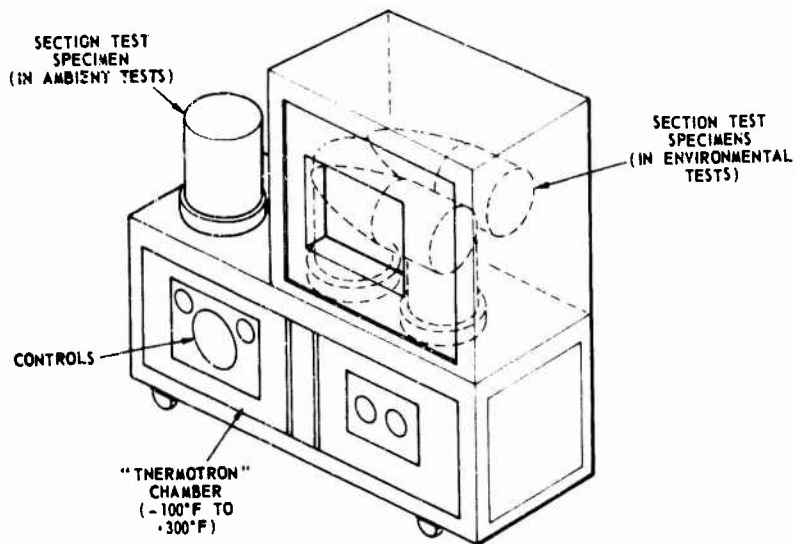


Figure 7. Missile Section Environmental Chamber (QAET Program).

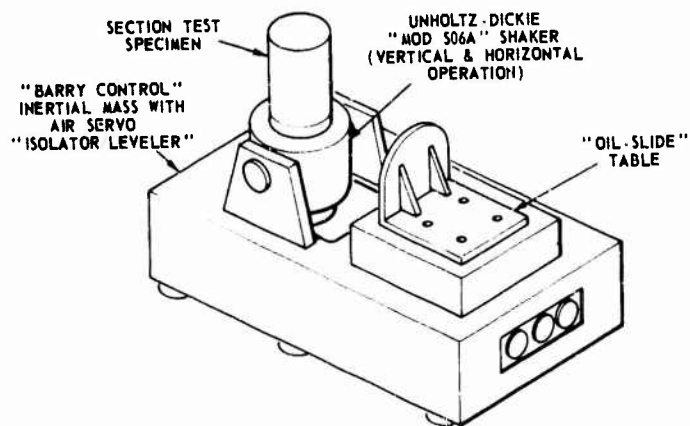


Figure 8. Missile Section Vibration Test Facility (QAET Program).



Figure 9. Environmental Chamber for Section Tests - QAET.

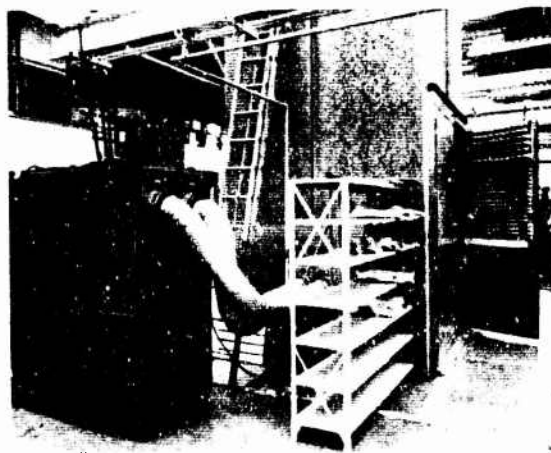


Figure 10. Temperature Conditioning Equipment on "RF" Darkroom.

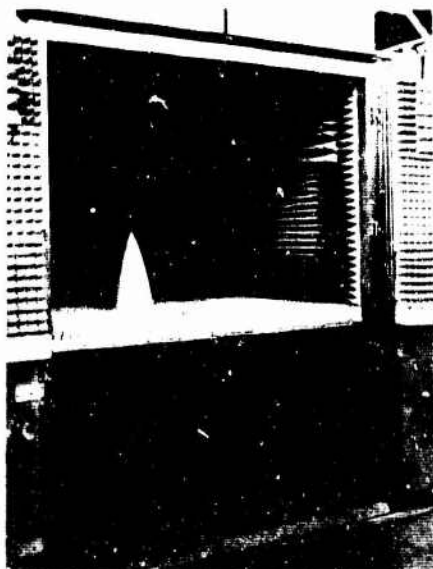


Figure 11. Front View of Open "RF" Darkroom - QAET.

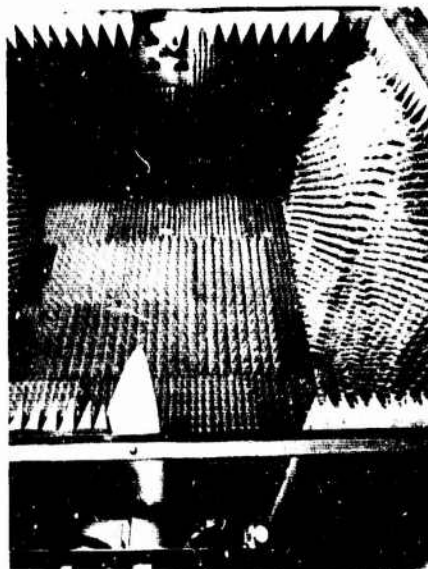


Figure 12. Vibrated Specimen Focused on "RF" Array Horns.

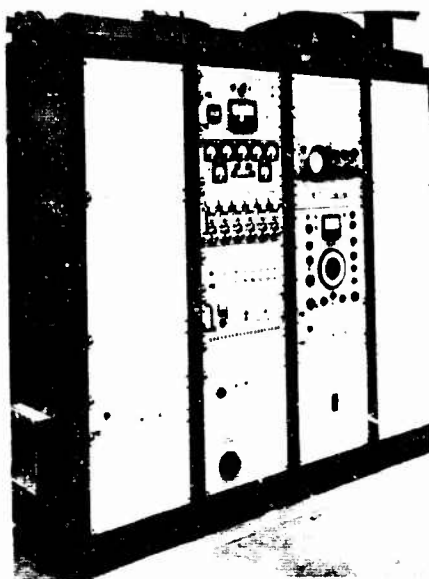


Figure 13. Unholtz-Dickie Control Console No. MA-690 - QAET.

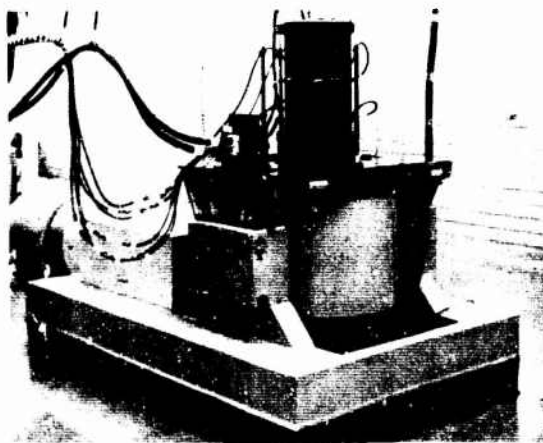


Figure 14. Unholtz-Dickie Vibrator Model No. 506A - QAET.



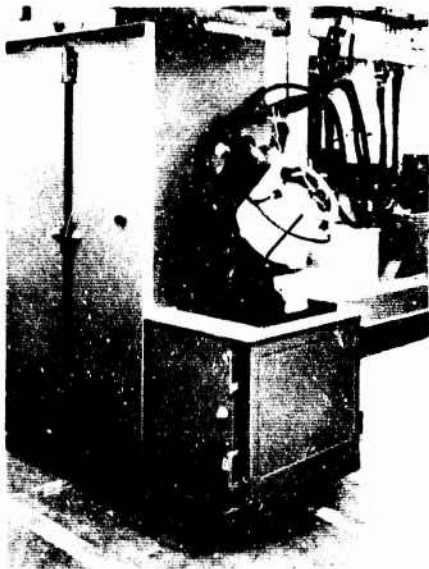


Figure 15. Autopilot Section Checkout on Scorsby Table - QAET.

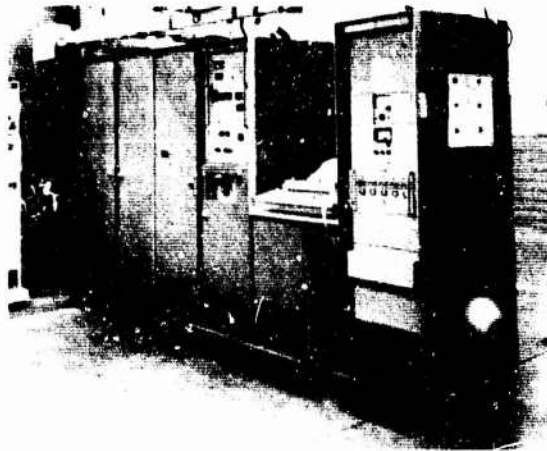


Figure 16. Missile Section Test Set - QAET.



Figure 17. Large Production Environmental Chamber - QAET.

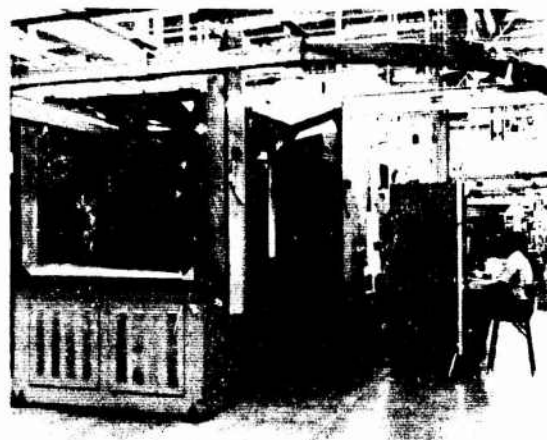


Figure 18. Three-Quarter View of Large Chamber - QAET.

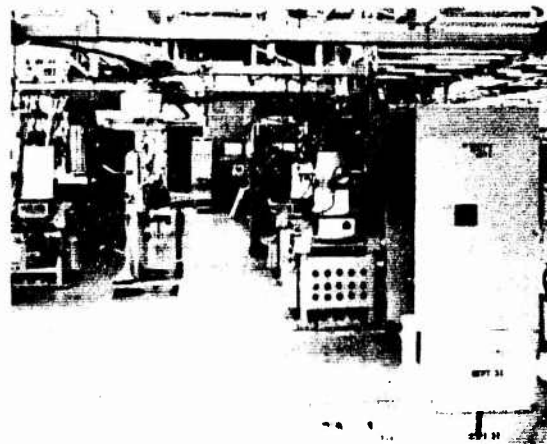


Figure 19. View of Production Control Test Area.



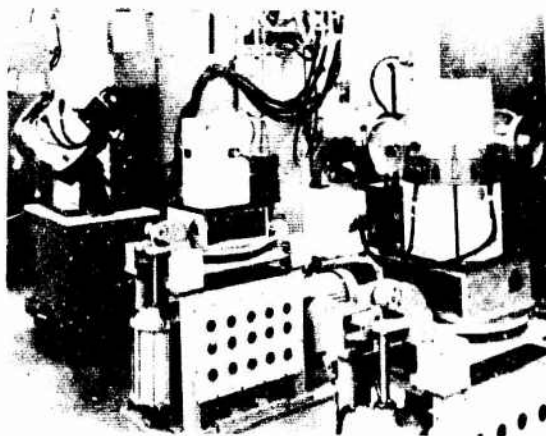


Figure 20. Mechanical Vibration of Production Sections.

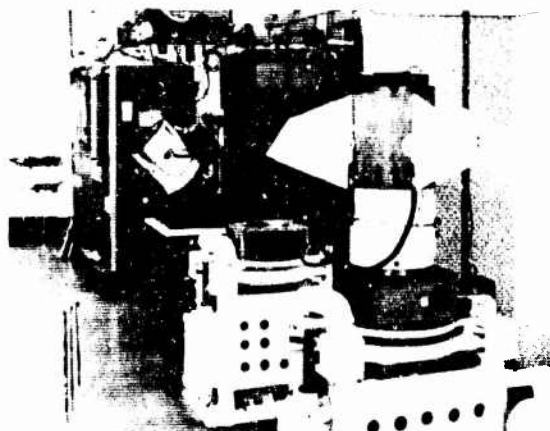


Figure 21. Recent Vibration Test of Steering Control Section, With Tail Fins.



Figure 22. Autopilot Section Being Mechanically Shaken.



Figure 23. Production Vibration Test of Guidance Section in "RF" Darkroom.

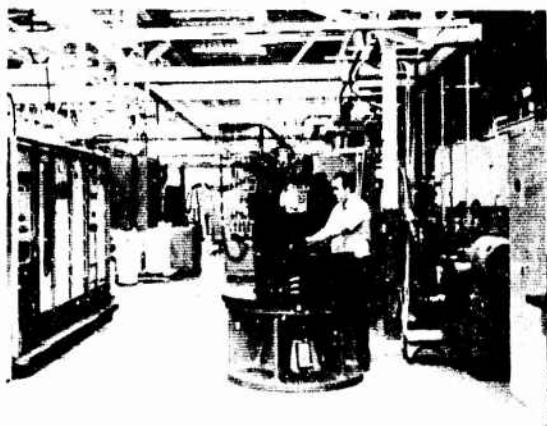


Figure 24. View of Small Missile QAET Area - Vibration Tester.

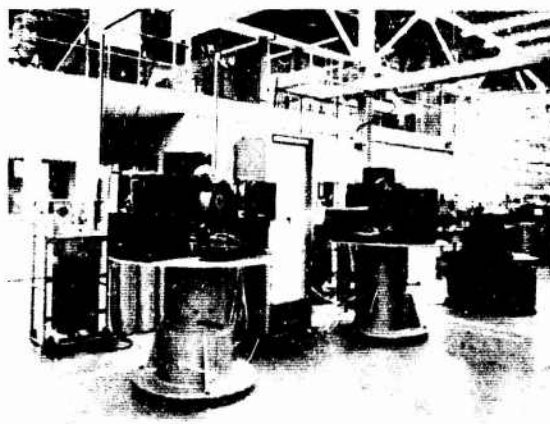


Figure 25. View of Small Missile QAET Area - Temperature Testers.

APPENDIX I  
DEFINITIONS OF TESTS CONTROLLING MISSILE INTEGRITY AND FUNCTION.  
ALPHABETICALLY ARRANGED - (Represent Several U.S. Government Services)

<u>No.</u>	<u>Designation</u>	<u>Name of Test</u>	<u>Definition</u>
1	Cat. I (AF)	Category I (Subsystem Development Test and Evaluation)	Test and evaluation to ensure that quality of components, subsystems, or systems have not been degraded by development methods and processes.
2	Cat. II (AF)	Category II (System Operational Test and Evaluation)	Testing and evaluation of the integrated system in as near an operational configuration as is practicable. Service test conducted under approximate operational system environment to assure that the system meets specifications for operational use. Tests evaluate capability and compatibility of subsystems that have been integrated into a complete system. When feasible, actual test operation and maintenance should be performed by trained military personnel.
3	Cat. III (AF)	Category III (Demonstration and Shakedown Operations)	Service conducted tests under operational environment with operating personnel and with logistic support under control and direction of operating command. Tests determine basic weapon system capabilities and limitations.
4	CET	Design Evaluation Test	DET is a series of tests performed to demonstrate performance of production hardware to specification requirements. Procedures used to conduct the tests are approved by the customer. In addition, the customer witnesses the tests. Formal reports, approved by the customer, document results of these tests.
5	EET	Engineering Evaluation Test	EET is a series of tests that are performed to evaluate breadboard and/or prototype hardware reliability, function, and performance to specifications. Engineering design groups prepare the procedures, monitor and direct evaluation of data.
6	LT	Life Test	Tests performed under logistic environments to evaluate operational reliability of the weapon system during a specified life cycle.
7	MET	Manufacturing Evaluation Test	Special Environmental type tests to provide information to demonstrate that change of manufacturing technique from development to production has not affected missile design.
8	MRFT	Missile Round Functional Tests	Ground Tests to evaluate response of a weapon system to specific stimuli for "Go", "No-Go" response to determine operational readiness.
9	MST	Missile Systems Test	Ground test operating evaluation to determine performance within parameters.

<u>No.</u>	<u>Designation</u>	<u>Name of Test</u>	<u>Definition</u>
10	PAT	Production Assurance Test	Tests to assure reliability of the production weapon system, to ensure through random sampling that the quality of the system has not been degraded in mass production, and to ensure that changes to the system have not degraded integrity of the system.
11	PCT	Periodic Conformance Test	Periodic tests to assure compliance with production sample test requirements.
12	P-DET (Navy)	Preliminary Design Evaluation Test	Pre-DET is a series of tests performed to evaluate prototype hardware design with respect to selected design evaluation test requirements. Pre-DET also provides data for parameter structure, proofing the test equipment, and establishes validity of DET test equipment. Procedures used are developed in accordance with approved specification requirements.
13	PIT	Production Improvement Test	Tests to evaluate durability, operational capability, and maintainability of modified standard items.
14	PPT	Pre-Production Test	PPT is a series of tests that are conducted to evaluate compliance of subassemblies and instruments to procurement specifications. Successful completion of these tests will provide the necessary data to permit approval for production.
15	QAET	Quality Assurance Environmental Test	Tests on production hardware to assure that quality is maintained and not degraded below acceptable limits under environments.
16	RST	Round System Test	Tests, automatically programmed and performed in triplicate to exercise missile round functional performance. Tests are based on evaluations of specific parametric values rather than "Go-no Go" check marks and usually are performed between each environmental exposure and during test operational environments.
17	ST	Storage Test	ST is a series of tests performed on each Pre-DET missile that demonstrate capability of functioning within design requirements after being subjected to expected storage environments. These tests consist of temperature, shock, and vibration.
18	VVT	Vendor Verification Tests	Special environmental type tests to provide information for assessing vendor part qualification.
19	WSGTP	Weapon System Ground Test Program	Tests to evaluate concepts of system capability in five test phases: engineering, preliminary design, pre-production, storage, and design evaluation.

APPENDIX II  
ADDITIONAL DEFINITIONS - TESTS.

PRACTICAL WORKING DEFINITION FOR PRODUCTION VIBRATION TESTS.

1. Production Tests.

Tests under fixed-frequency vibration, in automatic "section-level" test facilities, to determine ambient temperature functional testing on missile sections and "all-up" rounds and designed to eliminate problems of loose wires, partially soldered joints, poor workmanship, etc. Environments are not necessarily realistic, and do not duplicate the engineering "DET" levels.

2. Q.A.E.T. (Quality Assurance Environmental Tests).

Tests, under sequential environments ("Hi"-Temp., "Lo"-Temp. and "Fixed" or "Random" vibration), to determine at section or "all-up" rounds of missiles, the degree to which production units meet the engineering requirements set by "DET" tests. Environments are not necessarily realistic nor maximum design levels - merely arbitrary levels for repetitive testing and comparison of resulting test data over period of production time.

TYPICAL TESTS DEMANDED FOR SOME SPACE VEHICLES.

1. Qualification Tests.

Qualification tests are intended to verify design adequacy and demonstrate a minimum level of equipment capability. The qualification test conditions are generally more severe than those encountered during the lifetime of the equipment to provide better assurance of locating faults, thus compensating to some extent for the statistical limitations of the small sample size. Full qualification tests, including all applicable environments, shall be performed at the subsystem level and/or component (black box) level. In addition, space simulation and vibration qualification tests shall be performed at the satellite system level of assembly and shall account for interface connections and attachments. All qualification tests must be completed prior to the first flight. Equipment qualified on other space and missile programs will be accepted where usage indicates satisfactory operation in environments more severe than the environments to be encountered in this program. The contractor shall prepare documentation for approval of the deviation for equipment which fall into this category.

2. Acceptance Tests.

Acceptance tests are performed on each deliverable component and/or subsystem, including spares, and items used for qualification tests. The tests are performed to improve equipment quality by disclosing workmanship defects in time to permit corrections prior to end use of the equipment. The test conditions are comparable to end use environments and severe enough to detect early-life failures, but not so severe as to cause fatigue or wear-out. The minimum requirements for component and subsystem acceptance tests consist of vibration and temperature or temperature-altitude, if applicable. Additional tests shall be performed if the component or subsystem is sensitive to other environments, or if workmanship errors are not readily detected by normal inspection methods. Acceptance tests at the satellite system level of assembly may consist of space simulation and a vibration test.

3. Reliability Tests.

Plans shall be prepared in which the development, acceptance, and qualification test programs are expanded to gain additional data and information for defining the capability of the satellite system. Tests to be considered are "extended time" tests and "stress limit" tests. "Extended time" tests consist of cycling the components or subsystems through the critical environments, such as vibration, temperature, and vacuum, to determine the safety margins of the equipment with respect to time. "Stress limit" tests consist of increasing the qualification test levels until failures occur, thereby determining the margins of safety with respect to stress. The test procedures shall be based on the performance requirements of the individual subsystems and components and the environmental conditions as defined.

4. Age Tests.

All operating ground equipment shall be subjected to functional and electromagnetic interference tests. Where the equipment is believed sensitive to the ground environments defined, these tests shall also be performed. Tests on these ground environments would be performed as a part of a qualification test. All ground operating equipment shall meet the requirements of MIL-STD-883C, "Interference Test Requirements and Test Methods", as applicable. Ground handling equipment tests shall consist of the necessary structural integrity and functional tests as well as structural proof tests on each deliverable item.

THE REDUCTION OF THE VIBRATION LEVEL OF A  
CIRCULAR SHAFT MOVING TRANSVERSELY THROUGH WATER  
AT THE CRITICAL REYNOLDS NUMBER\*

by Irvin F. Gerks  
HONEYWELL  
Seattle, Washington

Instrumented tests performed on a slender, circular shaft moving transversely through water at speeds up to 8 feet per second indicated two vibrational modes: fore-and-aft, and lateral. These modes occurred at different speeds and were apparently caused by different exciting phenomena. A hypothesis was formed about these phenomena and a corrective solution was then derived. Three model shafts were tested and one whose design embodied the solution displayed very little fore-and-aft vibration throughout the entire speed range.

#### INTRODUCTION

A project was undertaken which involved towing several sonar devices about 15 feet below a ship traveling at speeds up to 8 feet per second. The accuracy of their alignment and relative positions required a rigid coupling of the devices to the ship. Retractable circular pipes were initially planned, with short wake-splitter plates on the trailing element of the pipes to reduce the anticipated vortex shedding problem. However, because extreme vibration occurred at very low speeds during the first tests, further tests were conducted in which the lower end of the shaft was instrumented with accelerometers in the fore-and-aft and lateral directions. During the next test, the instrumentation indicated that the shaft tip motion exceeded the specified maximum.

The recorded data showed that, although the vibration in each direction was coupled, the magnitude of the fore-and-aft vibration was greater at a low speed (i. e., about 2 knots) than that of the lateral vibration (Fig. 1). Conversely, at higher speeds the lateral vibration was greater than the fore-and-aft vibration, and whereas the vibration at the lower speed had been periodic this higher-speed vibration was more random in nature. The results of our initial investigation are described in the following paragraphs.

\*This paper not presented at Symposium.

#### FORE-AND-AFT VIBRATION FREQUENCY

The fore-and-aft vibration frequency was nearly constant over the speed range at 2.5 Hz. This was approximately one-half the resonance of the shaft if it were rigidly mounted, flooded with water, and accelerating an equal volume of water. Since the mounting was relatively flexible, it was concluded that this predominant frequency was the fundamental transverse resonance of the shaft and its mounting structure.

#### SECONDARY LATERAL MOTION

A similar response of lower magnitude was noticed in the lateral direction. The motion of the shaft was elliptical. Although vortex shedding may have caused this lateral motion, the large fore-and-aft motion was a necessary condition for this occurrence and, therefore, this was regarded as a secondary effect dependent upon the same exciting phenomenon as the fore-and-aft vibration.

#### MAXIMUM VIBRATION RESPONSE AT CRITICAL REYNOLDS NUMBER

It was observed that the mean velocity of the shaft, to cause the maximum fore-and-aft vibration, corresponded to a Reynolds number at which the drag coefficient of a circular shaft became discontinuous (at about  $R = 2 \times 10^5$ ). The flow pattern became separated above this velocity. Thus, it was felt that this phenom-

enon resulted in the fore-and-aft excitation.

#### VORTEX SHEDDING CONSIDERATIONS

The frequency of vibration and ship speed were considerably out of agreement with the Strouhal prediction for vortex shedding on rigid circular shafts. Since the shaft was vibrating at resonance, the regular equation could not be valid. Vortex shedding will tend to occur at the frequency of vibration when the Reynolds number is above that for flow separation on a circular shaft. At speeds of approximately 8 feet per second the fore-and-aft vibration of about 2.5 Hz had diminished to a negligible level while in the lateral direction a lower-frequency vibration of about 0.6 Hz had become significant. This was thought to be vortex shedding, although it was appearing at velocities where separated flow occurred.

The fore-and-aft vibration was felt to be more significant and detrimental to the ship and shaft-mounting structures. Since it did not appear that vortex shedding was the prime cause of vibration, no attempt was made to reduce this effect even though the initial shaft had a small wake-splitter plate on the trailing element of the shaft. A hypothesis of the exciting phenomenon was formed to find a satisfactory shaft design. This hypothesis can be demonstrated by the sequence of events during one cycle of steady-state vibration (Fig. 2).

#### FORWARD END OF THE CYCLE

At the forward end of the cycle the ship is moving near the velocity at which the critical Reynolds number occurs for flow separation. The initial conditions are that the shaft's relative velocity with respect to the ship is zero while its acceleration is to the rear. It is at the most forward point of its swing. The flow is attached and the Reynolds number is below the critical region. The elastic force accelerates the shaft to the rear, further lowering the total velocity of the shaft.

#### MIDDLE OF THE CYCLE

As the shaft swings past its normal rest position for that velocity, the total velocity stays below that at which the critical Reynolds number occurs, and the flow remains attached, resulting in a large drag force to the rear.

#### REAR END OF THE CYCLE

The shaft's elastic-restoring force limits the rearward swing, and on its return swing the velocity of the ship and shaft are in phase so that the total velocity will increase to the point where the Reynolds number will go above the critical region. The flow becomes detached with a resultant decrease in drag force which, in turn, results in a larger forward swing than would normally occur.

If the change in magnitude of these drag forces is large enough, the excitation forces will be effectively equal to the damping forces so that sustained vibration will result. It was felt that, if the shape of the shaft could be altered so that its total drag coefficient experienced a less abrupt change, the total drag force on the shaft should never become lower on the forward swing than on the rearward swing.

The conditions for this are as follows:

$$F_f \text{ (drag force, moving forward)} \leq F_r \text{ (drag force, moving rearward)}$$

$$\frac{C_{df} \times V_f^2 \times A \times \rho}{2} \leq \frac{C_{dr} \times V_r^2 \times A \times \rho}{2}$$

$$\left( \frac{V_f}{V_r} \right)^2 \leq \frac{C_{dr}}{C_{df}}$$

$$2 \log \left( \frac{V_f}{V_r} \right) \leq \log \left( \frac{C_{dr}}{C_{df}} \right)$$

$C_{df}$  - Drag coefficient during the forward moving swing of the shaft when the flow is detached.

$C_{dr}$  - Drag coefficient during the rearward moving swing of the shaft when the flow is attached.

$V_f$  - Velocity of the shaft with respect to the water during the forward moving portion of the cycle. The velocity of the boat and the shaft are in phase.

$V_r$  - Velocity of the shaft with respect to the water during the rearward moving portion of the cycle. The velocity of the boat and shaft are out of phase.

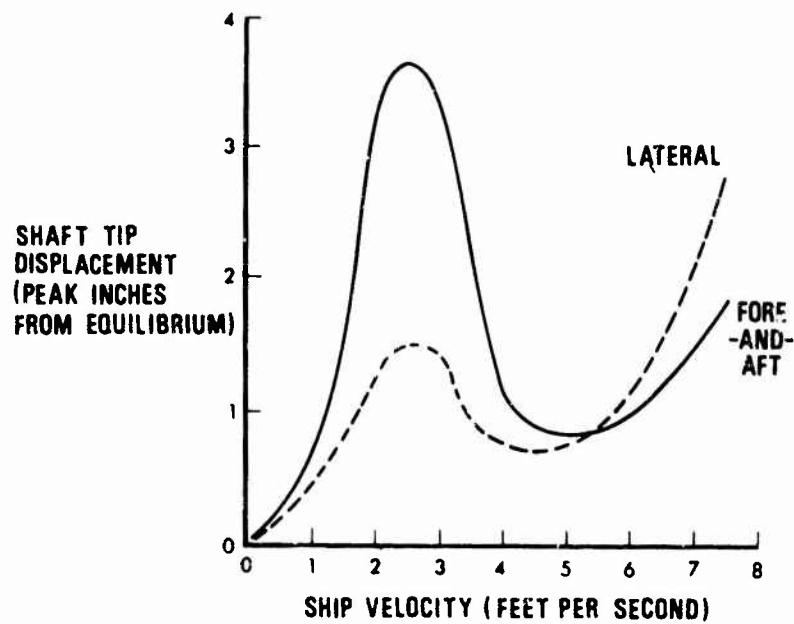


Fig. 1. Shaft Motion With Respect to Velocity

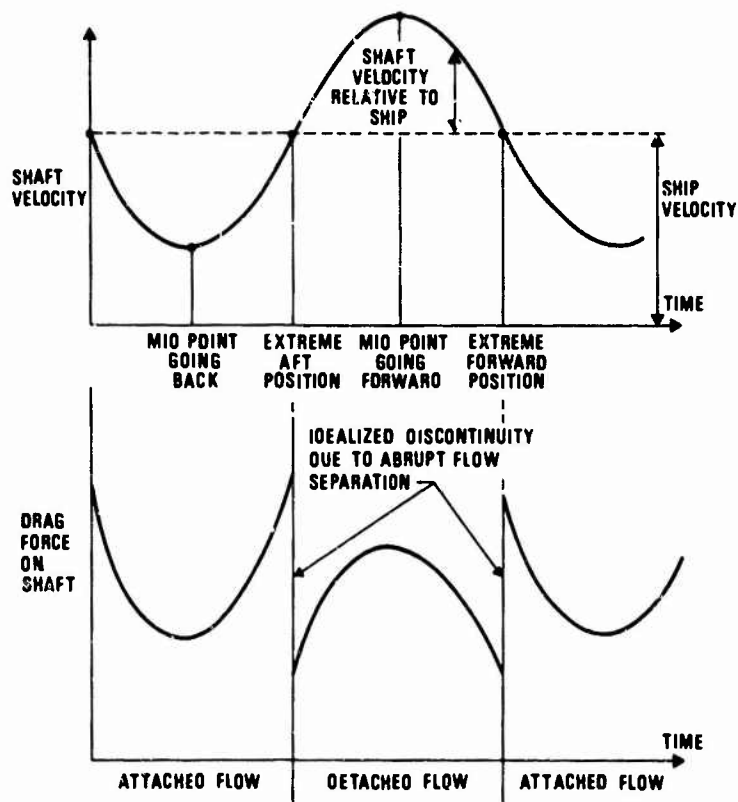


Fig. 2. Variation in Drag Force During Vibration Cycle

A - Frontal Area of the shaft

$\rho$  - Mass density of the water

A variety of shapes were available for the existing condition. Although a streamlined cross-section seemed most obvious, cost was a factor here, in addition to the potential problem of a flutter-type resonance, caused by the stalling of the streamlined shaft as it twists about its torsional axis. A tapered, circular shaft would have a continuously changing drag coefficient along the shaft so that the total drag coefficient would be a weighted mean of the sectional drag coefficients. Since the construction of such a tapered shaft was considered too expensive, we selected a shaft consisting of three straight sections. The section diameters varied over a 5-to-1 range. The section lengths were originally chosen to result in equal drag, but for the sake of appearance the below-water lengths were broken into more nearly equal lengths. The final shaft configuration is shown in Fig. 3. The total drag coefficient versus velocity is shown on a log-log plot in Fig. 4. The condition of a limiting slope of 2 is com-

plied with, but because the shape of the shaft differed from a straight shaft, other factors which were neglected could have been significant here.

This shaft was built and tested, along with a second shaft which had a varying gradient of perforated holes near the lower end to change the flow pattern to effect results similar to the stepped shaft. The results of the tests on the stepped shaft supported the hypothesis of the phenomenon on fore-and-aft vibration. The fore-and-aft vibration did not occur at the calculated critical velocity and, at the high end of the speed range, a lateral vibration of relatively low magnitude occurred. The largest deflection of the stepped shaft was about an order of magnitude less than the largest deflection of the straight shaft. The perforated shaft was apparently no improvement over the straight shaft, and it was concluded that the number and size of the perforations were insufficient. Although a solution was obtained with the stepped shaft, the complexities were such that significant factors remain unknown.

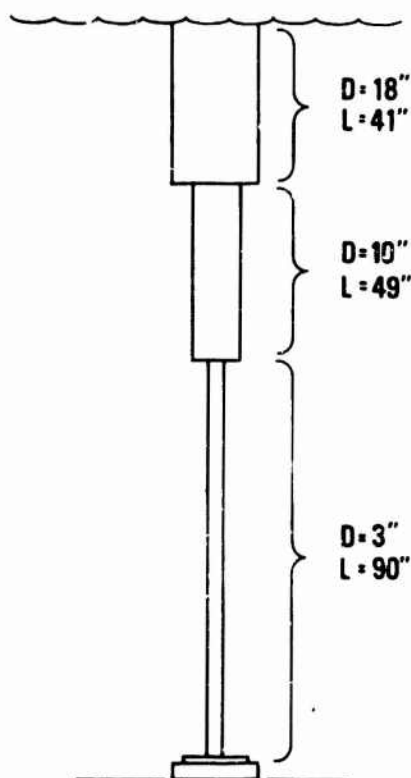


Fig. 3. Step-Shaft Configuration.

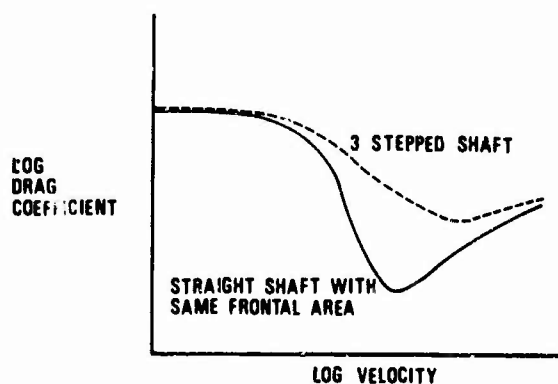


Fig. 4. Drag Coefficient Versus Velocity



## ANALYSIS AND DESIGN OF RESONANT FIXTURES TO AMPLIFY VIBRATOR OUTPUT \*

J. VERGA  
Hazeltine Corporation  
Little Neck, New York

The analysis and design of resonant fixtures to amplify vibrator output is described. When the acceleration capacity of the vibrator head output is limited, greater acceleration levels are obtainable by interposing a resonating member (designed not to fatigue) between the driving head of the vibrator and the test specimen. The resonating member, hereafter, is referred to as the resonant fixture.

General requirements, design concepts, derivation and discussion of equations and curves, and solution of a typical problem are described and conclusions presented.

### INTRODUCTION

Basically, three requirements are necessary of the resonant fixture: it must resonate at a particular frequency; it must not fatigue; and it must deliver unidirectional vibration to the test specimen. These requirements are detailed below:

1. The resonant fixture must resonate at the particular frequency band where high acceleration testing is desired. In this frequency band, the resonant fixture will serve as a mechanical amplifier to produce the desired test levels from the limited acceleration of the vibrator. This is in contrast to the more common effort in vibration fixtureization where the goal is to obtain a resonant-free fixture, so that sinusoidal vibration may be equally transmitted to the mounting points of the equipment.

Because of the head and armature weight, vibration shakers are limited (even at zero load) to the maximum G-level which they can produce. As an example, if a test specimen of 5 pounds is to be tested, using a vibrator with a force capacity of 5,000 pounds and a total weight of 95 pounds for the armature plus driving head plus the rigid supporting blocks and clamps, the maximum G-level deliverable  $G_{out}$  to the test specimen would be:

a. In the case when a rigid fixture is used, the force distribution equation is:

$$5000 \text{ lbs} = (95 + 5) \text{ lbs} \times G_{out}$$

and

$$G_{out} = 50 \text{ g}$$

b. In the case when a resonant fixture is used for which the amplification,  $Q$ , is assumed to be 20, the force distribution equation is:

$$5000 \text{ lbs} = 95 \text{ lbs} \times G_{in} + 5 \text{ lbs} \times G_{out}$$

where  $G_{in}$  is the G-level input to the resonant fixture which is equal to the level exerted by the vibrator.

$$G_{out} = 20 G_{in}$$

and solving the above relationships,

$$G_{out} = 510 \text{ g}$$

By use of the resonant fixture then, the specimen can be driven to a G-level ten times greater than without the resonant fixture.

2. The resonant fixture must be designed so as not to fatigue when vibrating at

\*This paper not presented at Symposium.

the desired levels. The fatigue endurance limit, therefore, must not be exceeded for the fixture to survive indefinitely.

3. The resonant fixture must deliver unidirectional vibration (as received from the vibrator to the test specimen). A centrally loaded beam, equally clamped at both ends, would satisfy this requirement. The vibration of its load located at the center would be at least theoretically confined to translation. On the other hand, a cantilever beam would not be appropriate because its vertical deflection is always accompanied by a rotational mode. When coupled rotational acceleration is not objectionable however, the use of a cantilever arrangement may be desired because of its greater flexibility which makes possible a more practical solution at low frequencies. The applicable formulas for the "cantilever beam" resonant fixture are also included in table A; however, this paper presents the derivation for only the centrally loaded beam equally clamped at both ends.

#### DESIGN CONCEPT

The laboratory setup of a resonant fixture employed in a recent application at Hazeltine is shown in figure 1. For convenience, especially with the calculations, the resonant fixture is confined to a plate which is clamped at both ends, and thus acts as a beam. The adaptor for mounting the test specimen is located at the center of the beam.

The end condition preferred is a simple support to produce resonances at shorter spans, thus keeping the laboratory setup small; however, a clamped end support is more practical to set up and work with. Spacer inserts within the clamp can be shifted in and out to change the length of the beam and thus control the natural frequency. In the tests conducted at Hazeltine, the movable clamp inserts were made of sheets of fiberglass and viscoelastic composites, such as used by Barry Controls for damping circuit boards.

#### DERIVATION AND DISCUSSION OF EQUATIONS AND CURVES

Derivation is limited to the "centrally loaded beam" type of resonant fixture. The applicable equations and coefficients are tabulated in table A. Table A also includes

the coefficients for the cantilever beam arrangement.

Three conditions are considered: the pure simply supported beam, the fixed end beam, and the clamped condition used in the laboratory. The latter uses viscoelastic fiberglass composites as movable inserts in the fixture clamp, as shown in figure 1. Because of the relatively soft nature of these inserts, the clamp does not behave as a pure fixed end beam. Test results, under ordinary room conditions, have shown that the natural frequency of the clamped fixture occurs at the average value between the calculated values for the fixed end and the simply supported beam. In other words, the condition can be said to have a 50% fixity.

#### Natural Frequency

For a beam having a concentrated load, the general equation for natural frequency in radians per second may be expressed as follows for the fundamental mode: (See nomenclature on page 11).

$$f_n = \sqrt{\frac{k}{M_e}} \text{ rad/sec} \quad (1)$$

Where "k" is the spring constant of the beam at the load location,

$$k = k_1 \frac{EI}{L^2} \quad (2)$$

and  $M_e$  is the effective mass located at the same point. The effective mass is expressed as follows:

$$M_e = M + \alpha m \quad (3a)$$

$$M_e = W_e/g \quad (3b)$$

$$W_e = W + \alpha w \quad (3c)$$

The beam mass or weight coefficient,  $\alpha$ , is the ratio of the effective beam weight, located at the same points as the concentrated load, divided by the actual weight of the beam. The general equation for natural frequency in a beam with uniformly distributed mass and no concentrated load is

$$f_n = a_1 \sqrt{\frac{EI}{mL^3}} \text{ rad/sec} \quad (4)$$

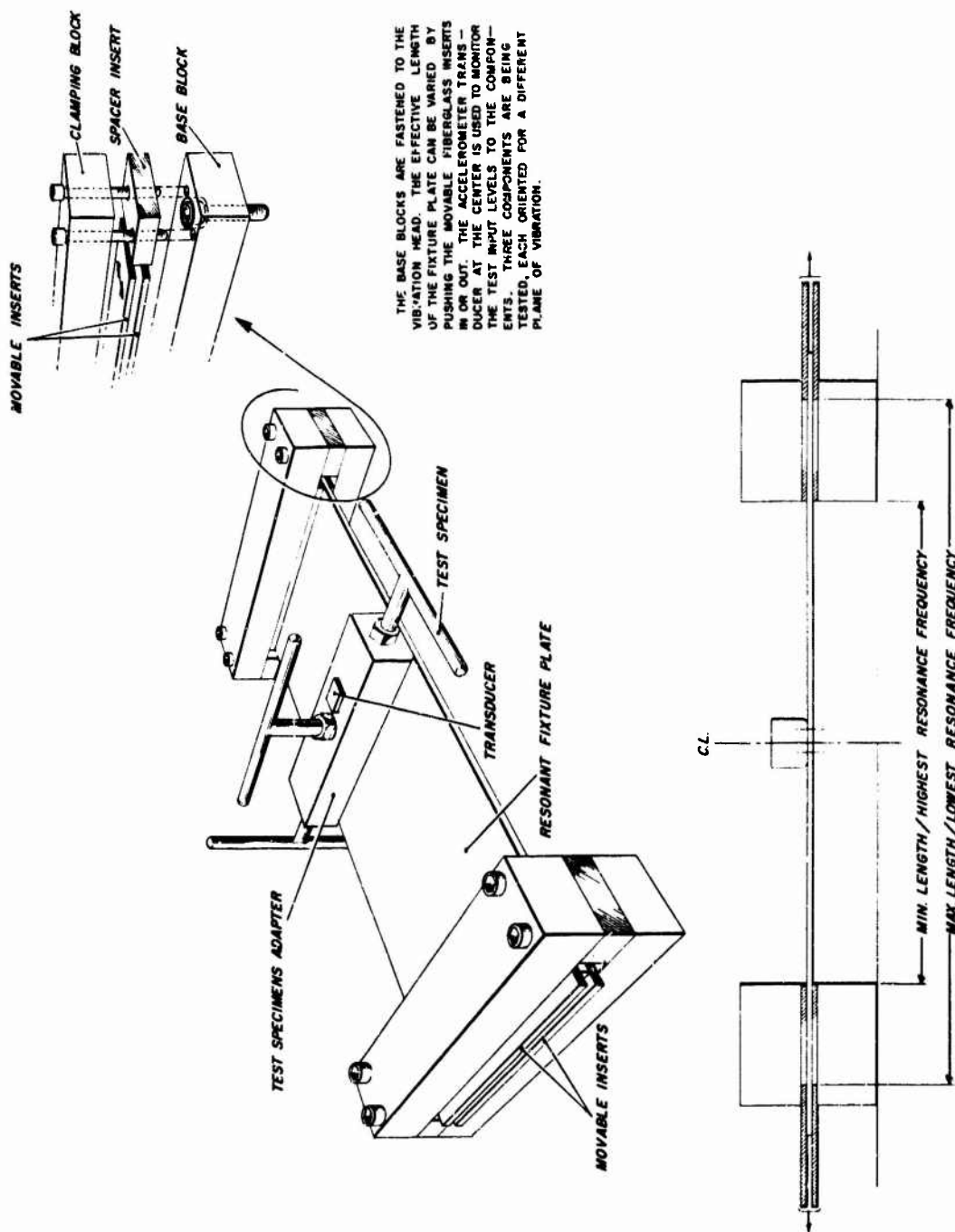
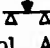

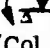



Figure 1. Typical Set-up for a Resonant Fixture

TABLE A  
EQUATIONS AND COEFFICIENTS

REF. NO.	EQUATION	COEFF	VALUES OF COEFFICIENTS			
			SIMPLE SUPPORT  (Col. A)	FIXED ENDS  (Col. B)	LAB SETUP 50% Fixity  (Col. C)	CANTILEVER  (Col. D)
		$a_1$	$\pi^2$	22	Fundamental mode	3.52
2	$k = k_1 (EI/L^3)$	$k_1$	48	192		3
3b	$W_e = W + \alpha w$	$\alpha$	.5	.4	.45, Average of Col. A & B	.23
6	$f_n = C_n \left[ \frac{E}{(W_e/b) (L/t)^3} \right]^{\frac{1}{2}}$	$C_n$	6.25	12.5	9.38, Average of Col. A & B as found from test results.	1.56
10	$K = S_{\max}/\delta_{\max}$ $= K_1 (t/L^2) E$	$K_1$	6	12		1.5
12	$S = C (t/L^2) E (G/f^2) [1 - (1/Q)]$	$C$	58.5	117	88, Average of Col. A & B	14.4
13b	$S_r = C_r (W_e/b) (L/t^2) G$	$C_r$	1.51	.75	1, Calculated from average value of C & $C_n$	5.9

The weight coefficient,  $\alpha$ , can be found by equating equations (1) and (4) with the concentrated load  $M$ , set to zero, as follows:

$$\sqrt{\frac{k}{M + \alpha m}} = a_1 \sqrt{\frac{EI}{mL^3}} \quad (5)$$

Substituting the values of " $a_1$ " and " $k$ " from table A, it is found that  $\alpha$  is 0.5 for a simply supported beam and 0.4 for a fixed-end beam. Henceforth, the location of the load will be assumed in the center. Since the test setup used in the laboratory has demonstrated an average effect between the simple and fixed support,  $\alpha = 0.45$  is assigned to the fixture. This average factor can then be assumed for this discussion. It must be noted that because of the factor  $\alpha$ , and the relatively heavy concentrated load, the effective mass contributed by the beam or fixture plate is usually found to be negligible. When such is the case, the effective mass can be considered to be independent of the length and thickness of the fixture plate.

Substituting the values of  $k$  from table A and the area moment of inertia in terms of plate thickness ( $t$ ) into equation (1), and changing from radians to cycles, the natural frequency is:

$$f_n = C_n \left[ \frac{E}{(W_e/b) (L/t)^3} \right]^{\frac{1}{2}} \text{ cps} \quad (6)$$

This equation, normalized for the material's flexure modulus,  $E$ , so that it can be used for all materials, is plotted in figure 2 for a family of curves of different effective weight ( $W_e/b = 0.0375$  through  $0.600$  lb/in). The ordinate is the "normalized natural frequency" which is defined as the resonant frequency divided by the square root of the flexure modulus, in units of cycles per second divided by the square root of pounds per square inches. The abscissa is the configuration ratio, length to thickness ( $L/t$ ), which is dimensionless.

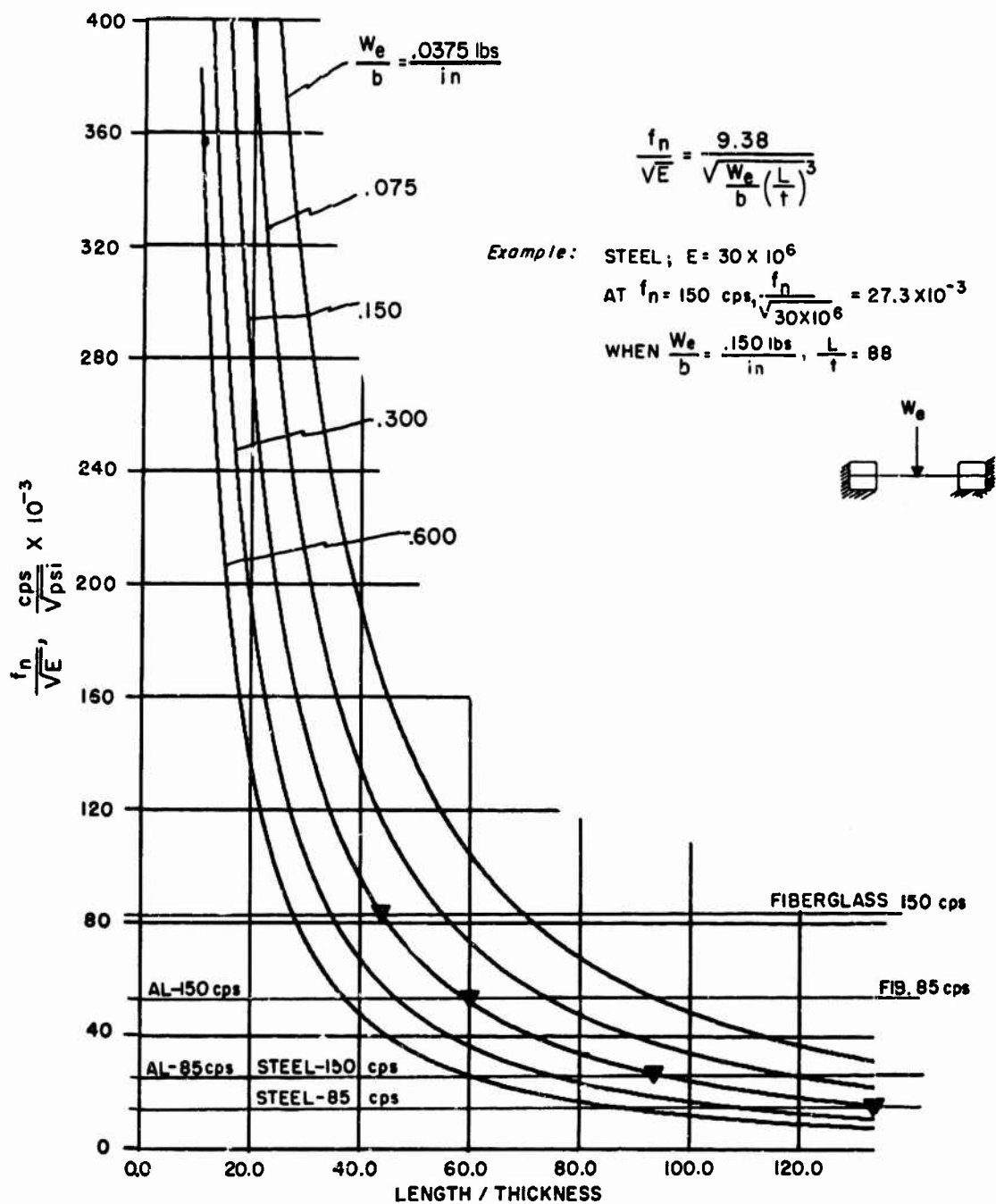


Figure 2. Normalized Natural Frequency Versus Length-to-Thickness Ratio

From this curve, one can find the ratio of  $L/t$  which is required to produce a desired natural frequency for any given effective weight per unit width and any given material whose flexure modulus is known.

#### Internal Stress in a Resonating Fixture

To produce a level of acceleration at a given frequency of sinusoidal vibration, the required amplitude may be expressed as

$$A = 9.8 \frac{G}{f^2} \quad (7)$$

In the resonant fixture, the maximum amplitude occurs at the center of the fixture span where the test specimen is mounted. Then, the maximum deflection in the fixture is the difference between the amplitude at the center and the amplitude at the support, or

$$\delta_{\max} = A_C - A_S \quad (8)$$

The amplification of the fixture is defined as

$$Q = A_C / A_S \quad (9a)$$

Therefore, substituting (9a) into (8),

$$\delta_{\max} = (1 - \frac{1}{Q}) A_C \quad (9b)$$

The maximum flexure stress in a beam can be expressed in the form

$$S_{\max} = K (\delta_{\max}) \quad (10)$$

where  $K$  is the beam stress constant which is dependent on the cross section parameters and independent of input conditions. The value for  $K$ , which can be found in any elementary text book on strength of materials, is

$$K = K_1 E \frac{t}{L^2} \quad (11)$$

Substituting (7), (9b) and (11) into (10),

$$S_{\max} = CE(t/L^2) (G/f^2) \left[ 1 - (1/Q) \right] \quad (12)$$

where "G" represents the acceleration at the center of the fixture being delivered to the test specimen.

This equation states that for a given acceleration and frequency, which is equivalent

to saying "for a given deflection amplitude," the stress increases with increasing stiffness parameters,  $E(t/L^2)$ .

The frequency may be any frequency as long as the amplification,  $Q$ , is known for the conditions. The factor,  $1 - (1/Q)$  is known as the resonance factor.

When the amplification is unity, the stress resonance factor is zero, obviously because the beam is moving in unison; it is not deflecting and, therefore, it is not stressed regardless of the G-level. On the other hand, as the amplification approaches infinity (a condition which tends to occur at the resonant frequency), the stress resonance factor approaches unity. It is generally acknowledged that the worst case for fatigue occurs when an object vibrates at its resonant frequency.

To solve for the maximum stress at the resonant condition, the equation (b) is substituted into equation (12). The result is

$$S_r = C_r (W_e/b) (L/t^2) G \left[ 1 - (1/Q) \right] \quad (13a)$$

When tuned at resonance, the resonance factor approaches unity, therefore

$$S_r = C_r (W_e/b) (L/t^2) G \quad (13b)$$

This is the maximum internal stress in the fixture plate when vibrating at its resonant frequency. This equation is only valid for the resonant condition. If the stress in the resonant fixture must not exceed the fatigue limit, the condition which must be satisfied is

$$S_r = C_r (W_e/b) (L/t^2) G \leq S_f \quad (13c)$$

It should be noted that equation (13) is independent of the material modulus of flexure. It depends only on the weight, the geometry, and the acceleration levels. However, it must be emphasized that this equation is only valid for the resonant condition; also, although the flexure modulus is not a variable, it plays its role in the determination of resonance.

A plot of equation (13b) is given in figures 3, 4, and 5. The ordinate is the resonant stress (psi) per unit G, ranging from zero to 500. The abscissa is the fixture plate thickness ranging from 0.020 to 0.22 inch. In figure 3, the curves are for a constant length

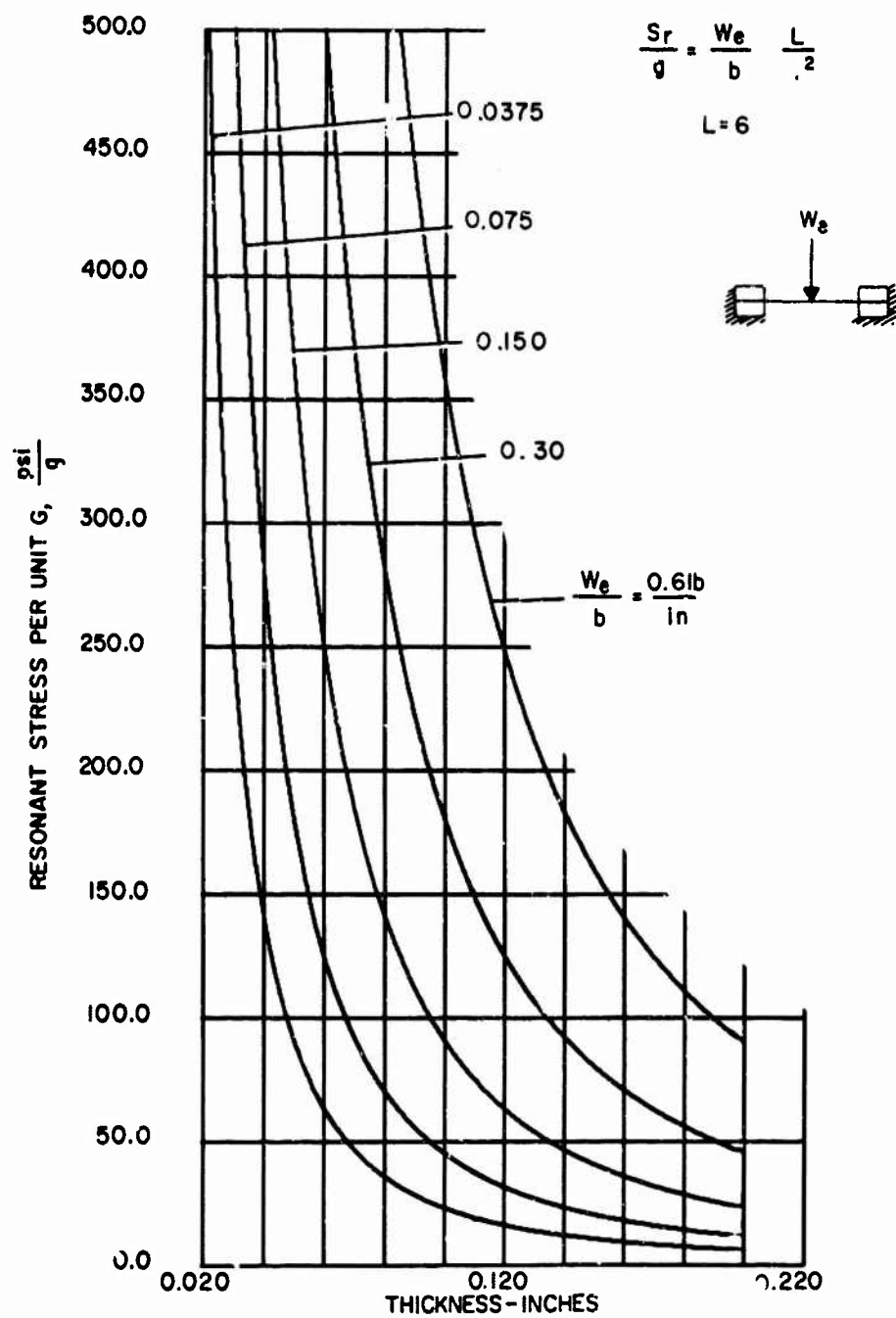


Figure 3. Stress Per Unit G Versus Thickness for the Resonant Fixture With a Span Length of 6 in.

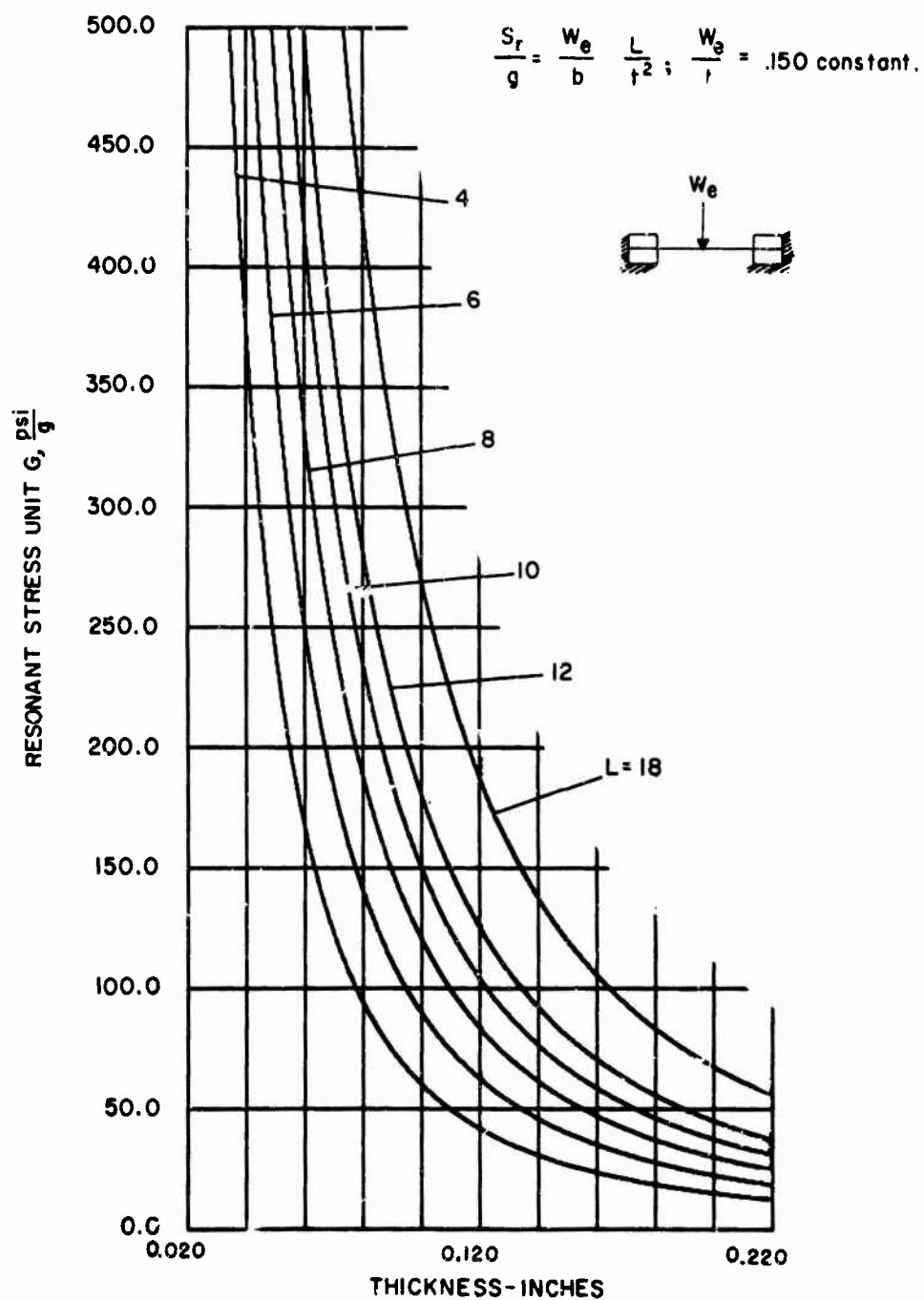


Figure 4. Stress Per Unit G Versus Thickness for the Resonant Fixture With an Effective Weight Per Unit Width of 0.150 Lb/In.



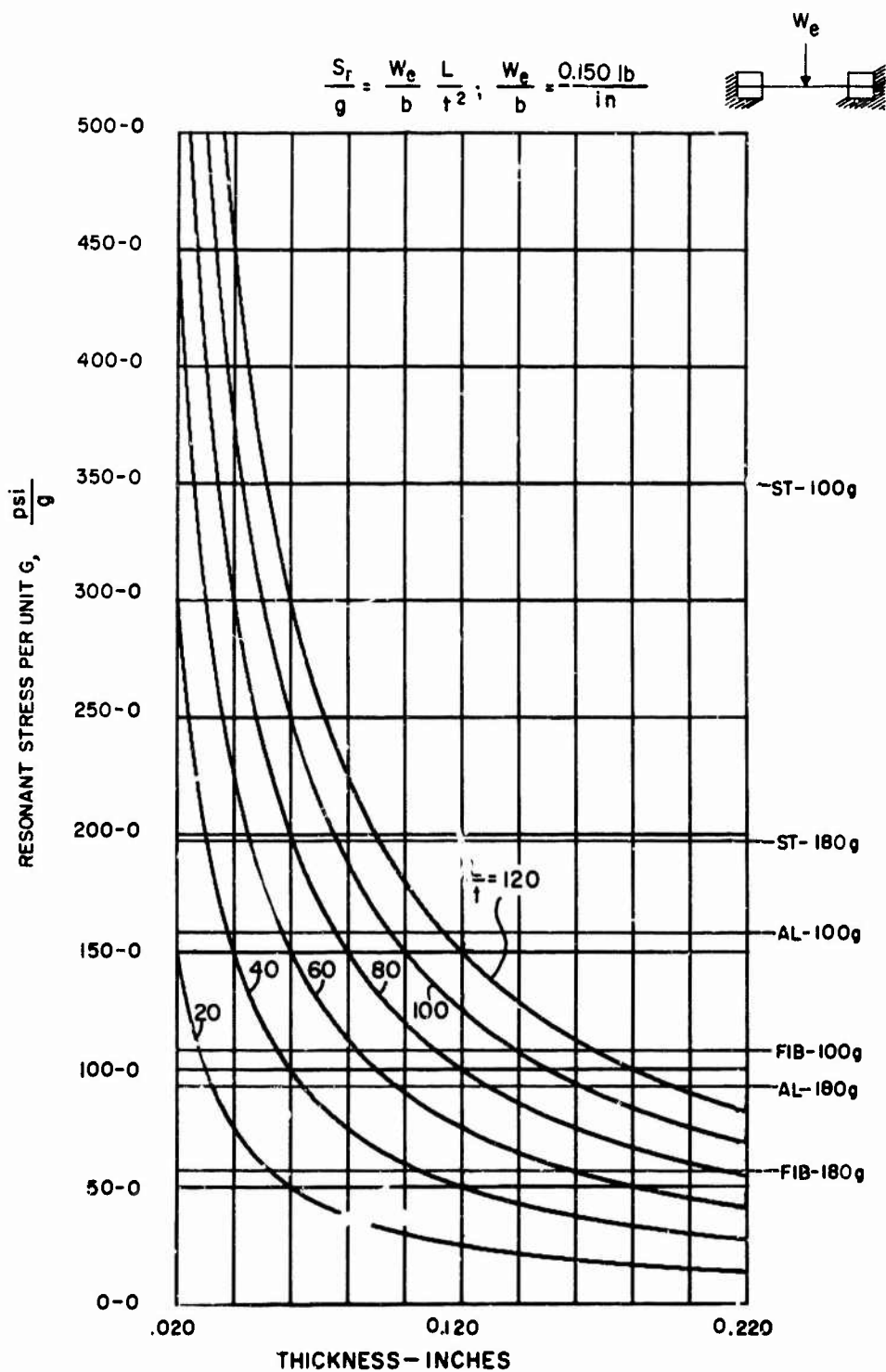


Figure 5. Resonant Stress Per Unit G Versus Thickness for the Resonant Fixture With a Constant Weight Per Unit Width of 0.150 lb/in. and Various Length-to-Thickness Ratios

( $L = 6$ ) and effective weight per unit width,  $W_e/b$ , of 0.0375, 0.075, 0.150, 0.300 and 0.600 lb/in. In figure 4, the curves are for a constant  $W_e/b = 0.150$  and lengths of 4, 6, 8, 10, 12, and 18 inches. In figure 5, the curves are for a constant  $W_e/b = 0.150$  and for length to thickness ratios of  $L/t = 20, 40, 60, 80, 100$  and 120.

The curves given are for the centrally loaded beam equally supported at both ends. The curves for the cantilever follow the same trend but are, of course, displaced in accordance with the respective equation coefficient.

## TYPICAL DESIGN PROBLEM

### Problem

Design a fixture plate which can vibrate a test specimen in each of three mutually perpendicular directions at 150 cps and 180 g's and also at 85 cps and 100 g's. A fixture with a variable length between 4 and 8 inches can be adapted to the head of the vibrator. Either fiberglass, steel, or aluminum may be used. The weight of the test specimen plus the weight of the mounting adaptor is such that the effective weight per unit width is  $W_e/b = 0.150$  lb/in.

### Solution

1. All the pertinent values for this solution are listed in table B. These values are found by following the technique outlined below:

(a) The flexure modulus and fatigue endurance limit is given for each material. These are listed in Rows 1 and 2, respectively.

(b) When the figure is delivering 180 g's at its resonant frequency, the internal stress in the fixture must not exceed the endurance limit. The endurance limit stress per unit g is found by dividing by 180 g's. This is listed in Row 3 and is marked in figure 5 for each material. The points below this stress line apply to fixtures which when delivering 180 g's at 150 cps would be stressed below the endurance limit.

(c) In figure 2, draw horizontal lines for the normalized resonant frequency of

150 cps for each material (listed in Row 5). At the intersection of this line with the curve for  $W_e/b = 0.150$ , the length to thickness ratio is found from the abscissa and listed in Row 6.

(d) For each material (Row 3), the limit stress per unit has been indicated in figure 5. By interpolating in figure 5 the required ratio of length to thickness for each material as listed in Row 6, the corresponding minimum thickness is found from the abscissa in figure 5 and listed in Row 7.

(e) Each minimum thickness has its corresponding minimum length which satisfies the required ratio of  $L/t$ . The minimum length is listed in Row 8.

The maximum thickness is that which satisfies the required ratio of  $L/t$  for the maximum length of 8 inches allowable in the machine set up. This maximum thickness is listed in Row 9.

2. In considering the condition of 85 cps and 100 g's, the same curves and techniques as above are used. The respective numbers are also listed in table B, Rows 10 through 15.

3. The results show that the design which satisfies all the conditions of the problem is a fixture made of fiberglass, 0.120 inch thick. When the length is adjusted to 5.28, it will resonate at 150 cps. When the length is adjusted to 7.2, it will resonate at 85 cps.

Aluminum and steel can satisfy the 150 cps resonant conditions at a length of 5.7 and 6 inches and a thickness of 0.095 and 0.068, respectively. However, to obtain resonance at 85 cps, they must be of a length in excess of 8 inches.

Of course, all these conditions do satisfy the stress requirement - not exceeding the fatigue endurance limit. In fact, the 0.120 thick fiberglass fixture is understressed at 85 cps and 100 g's. By proportionality, it can be seen from figure 5 that at 85 cps the acceleration can be raised to 147 g's before the fiberglass fixture starts exceeding its endurance limit of 11,000 psi.

TABLE B  
NUMERIC VALUES OF TYPICAL DESIGN FOR A RESONANT FIXTURE

ROW		EPOXY RESIN FIBERGLASS	ALUM. AL	STEEL AL	REMARKS
1	Flexure modulus, $E$ , $\text{psi} \times 10^6$	3.2	10	30	Given
2	Endurance limit, $S_f$ , $\text{psi} \times 10^3$	11	16	35	Given
3	$S_f/G = S_f/180 \text{ g}$	61	89	194	Place in Fig. 5
4	$\sqrt{E} \sqrt{\text{psi}} \times 10^3$	1.7	3.3	5.48	Given
5	$f_r / \sqrt{E} = (150 / \sqrt{E} \times 10^{-3})$	84	54	27.3	Place in Fig. 2
6	$L/t$ for $W_e/b = .150$ , $f_r = 150 \text{ cps}$	44	60	88	From Fig. 2
7	Minimum thickness, inches	0.120	.095	.068	From Fig. 5
8	Minimum length, inches	5.28	5.7	6.0	To satisfy $L/t$
9	Maximum thickness ( $L = 8 \text{ in}$ )	0.182	0.133	0.092	To satisfy $L/t$
10	$S_f/100 \text{ g}$	110	150	350	Place in Fig. 5
11	$85 / \sqrt{E} \times 10^{-3}$	54	27.3	15.6	Place in Fig. 2
12	$L/t$ for 85 cps, $W_e/b = .150$	60	88	133	From Fig. 2
13	Minimum thickness	.120	.095	.068	From above
14	Length for minimum thickness	7.2	8.3	9	To satisfy $L/t$
15	Maximum G's at 85 cps	147	$L > 8^*$	$L > 8^*$	From Fig. 5

#### CONCLUSIONS

Ideally, a resonant fixture can be designed (in terms of length, width, thickness, and material) to substantially amplify the vibrator's limited acceleration output at any desired frequency band. The design must solve equation (6) to obtain the resonant frequency desired, and must satisfy equation (13a) to obtain the stress limitation desired. Reference to the curves of the same equations can be helpful in selecting the design parameters of length, thickness, and material for a given test requirement.

#### BIBLIOGRAPHY

- (a) Don Hartog, J. P., Mechanical Vibrations, McGraw-Hill Book Company, Inc., 1956.

- (b) Church, A. A., Mechanical Vibration, John Wiley & Sons, Inc., 1957.

- (c) Harris, C. M. and Crede, C. E., Shock and Vibration Handbook, McGraw-Hill Book Company, Inc., 1961.

#### NOMENCLATURE

- A - Displacement amplitude of vibration  
b - Width of fixture beam, inch  
c - Distance from beam neutral axis to outermost fiber, inches  
E - Flexure modulus, psi  
G - Acceleration, g  
g - Acceleration of gravity = 386 in. per sec.<sup>2</sup>  
f - Frequency, cps or radians per sec.  
I - Area moment of inertia, in<sup>4</sup>  
K - Beam stress constant, psi per inch  
k - Beam spring constant, lbs per inch

\* Condition disqualified because length exceeds 8-inch limit.

L - Beam length, inch  
 M - Mass of concentrated load, lb sec<sup>2</sup> per inch  
 m - Beam mass, lb sec<sup>2</sup> per inch  
 Q - Amplification factor at any frequency  
 S - Stress, psi  
 t - Thickness of fixture plate, inch  
 W - Weight of concentrated load, lb  
 w - Weight of fixture beam, lb  
 δ - Deflection, inch

#### Subscripts

e - effective  
 n - natural frequency  
 r - resonance  
 f - fatigue  
 c - located at the center of the beam  
 s - located at the support of the beam

#### Coefficients

a<sub>1</sub> - Beam natural frequency constant - fundamental mode  
 α - Coefficient which converts actual mass of beam to the effective mass located at midspan

C - Coefficient for maximum stress at any given frequency  
 C<sub>n</sub> - Coefficient for natural frequency  
 C<sub>r</sub> - Coefficient for maximum stress at resonance  
 k<sub>1</sub> - Coefficient for the beam spring constant  
 K<sub>1</sub> - Coefficient for beam stress constant

#### LIST OF FIGURES

1. Typical Set-Up for a Resonant Fixture.
2. Normalized Natural Frequency Versus Length to Thickness Ratio.
3. Stress per Unit G Versus Thickness, for the Resonant Fixture with a Span Length of 6 Inches.
4. Stress per Unit G Versus Thickness for the Resonant Fixture With an Effective Weight per Unit Width of 0.150 lb per in.
5. Resonant Stress per Unit G Versus Thickness for the Resonant Fixture With a Constant Weight per Unit Width of 0.150 lb per in. and Various Length to Thickness Ratios.